Experimental and Numerical Investigations of Conceptual Models for Biological Clogging of Unsaturated Soils

A thesis submitted to
the Faculty of Graduate Studies and Research
in partial fulfillment of the requirements for the degree

Doctor of Philosophy

by

Mohamed Abo El-Khair Bayoumy Mostafa

M.A.Sc., Carleton University

Department of Civil and Environmental Engineering
Carleton University

Ottawa-Carleton Institute of Civil and Environmental Engineering

April 2009

© 2009, Mohamed Abo El-Khair Bayoumy Mostafa

Reproduced with permission of the copyright owner. Further reproduction prohibited without permission.

Library and Archives Canada

Published Heritage Branch

395 Wellington Street
Ottawa ON K1A 0N4
Canada

Bibliothèque et Archives Canada

Direction du Patrimoine de l'édition

395, rue Wellington
Ottawa ON K1A 0N4
Canada

Your file Votre référence
ISBN: 978-0-494-52085-7
Our file Notre référence
ISBN: 978-0-494-52085-7

NOTICE:
The author has granted a non-exclusive license allowing Library and Archives Canada to reproduce, publish, archive, preserve, conserve, communicate to the public by telecommunication or on the Internet, loan, distribute and sell theses worldwide, for commercial or non-commercial purposes, in microform, paper, electronic and/or any other formats.

The author retains copyright ownership and moral rights in this thesis. Neither the thesis nor substantial extracts from it may be printed or otherwise reproduced without the author's permission.

AVIS:
L'auteur a accordé une licence non exclusive permettant à la Bibliothèque et Archives Canada de reproduire, publier, archiver, sauvegarder, conserver, transmettre au public par télécommunication ou par l'Internet, prêter, distribuer et vendre des thèses partout dans le monde, à des fins commerciales ou autres, sur support microforme, papier, électronique et/ou autres formats.

L'auteur conserve la propriété du droit d'auteur et des droits moraux qui protège cette thèse. Ni la thèse ni des extraits substantiels de celle-ci ne doivent être imprimés ou autrement reproduits sans son autorisation.

In compliance with the Canadian Privacy Act some supporting forms may have been removed from this thesis.

While these forms may be included in the document page count, their removal does not represent any loss of content from the thesis.

Conformément à la loi canadienne sur la protection de la vie privée, quelques formulaires secondaires ont été enlevés de cette thèse.

Bien que ces formulaires aient inclus dans la pagination, il n'y aura aucun contenu manquant.

Canada

Reproduced with permission of the copyright owner. Further reproduction prohibited without permission.

ABSTRACT

Clogging in the unsaturated zone is an important issue in the field of septic systems and biofilters. Different conceptual models for clogging in the saturated zone were proposed in the literature but corresponding conceptual models for clogging in the unsaturated zone are limited.

Mostafa and Van Geel (2007) proposed three conceptual models to relate the relative permeability of unsaturated soils to microbial growth. The three models were implemented in a one-dimensional numerical code and hypothetical scenarios were simulated to verify that the equations were coded correctly. No laboratory or field data were used to validate the three conceptual models.

The objectives of this research were to further investigate and understand the processes that govern biological clogging in unsaturated soils. Through a detailed experimental study and numerical modeling, the goal was to further develop and validate these conceptual models using experimental data.

This research was divided into three stages. First stage involved an experimental study to determine the effect of different pore structures on the bioclogging process and to generate valuable data to be used in stage three. The second stage aimed to evaluate Monod kinetic parameters for the clogging process studied in stage one. The third stage aimed to improve upon and validate the three conceptual models proposed earlier by Mostafa and Van Geel (2007) using the experimental data generated in stages one and two.

Soil and Monod kinetic parameters measured/estimated in stages one and two were used to calibrate the numerical code. The calibration process revealed that a more

Reproduced with permission of the copyright owner. Further reproduction prohibited without permission.

detailed numerical model was needed to simulate the clogging process observed in stage one. Modifications were conducted on the numerical code which included the addition of new top head boundary condition to simulate ponding and a more detailed conceptual model to represent microbial growth to include EPS and an inert fraction.

After the modifications were conducted, the three conceptual models were used to simulate bioclogging process. Based on the results, a conclusion was drawn that Models #2 and #3 represent the biological clogging process in the soils used in stage one and no further modifications were needed for the models.

Reproduced with permission of the copyright owner. Further reproduction prohibited without permission.

ACKNOWLEDGMENT

I would like to express my sincere gratitude and endless thanks to the lord of the universe and the almighty ***ALLAH SWT*** for giving me strength, guidance, and patience to complete this research work.

I would like to thank my supervisor ***Prof. Paul J. Van Geel*** for his encouragement, patience, and endless support throughout the research steps. I believe this research would not have been completed this way without his sincere guidance and continuous support. I also would like to thank him for the financial support provided throughout this research.

A great endless appreciation and thanks to my parents, my brother, and my sister for their wonderful source of support, encouragement, help, guidance, and spiritual relief. Special thanks also go to ***Uncle Saaid Osman*** and his family members specially my cousin ***Karim Osman*** for his help in the numerical coding part of this research.

Special thanks to ***Prof. Roberto Narbaitz***, ***Prof. Banu Ormeci*** and ***Prof. Paul Simms*** for their helpful criticism in my proposal defense and during the course of this research.

Thanks to my colleagues in the Civil and Environmental Department for their help and support. Special thanks for all the Civil and Environmental Laboratory staff specially ***Dr. Marie Tudoret Chow*** and ***Citra Wahyudi*** for the help and support during my laboratory work.

I also would like to thank the Ontario Graduate Scholarship Program and the Department of Civil and Environmental Engineering at Carleton University for their financial support. Thanks to Premier Tech Environment for providing us with the peat soil and for the financial support and the Karson Group, Karson Kartage and Konstruction, for providing the sand soils used in this research.

Reproduced with permission of the copyright owner. Further reproduction prohibited without permission.

TABLE OF CONTENTS

ABSTRACT ..... **II**

ACKNOWLEDGMENT ..... **IV**

TABLE OF CONTENTS ..... **V**

LIST OF TABLES ..... **X**

LIST OF FIGURES ..... **XIII**

LIST OF SYMBOLS AND NOMENCLATURES ..... **XXIV**

1. INTRODUCTION **1**

1.1 OVERVIEW 1

1.2 OBJECTIVE 3

1.3 SCOPE 4

1.3.1 Stage One *4*

1.3.2 Stage Two *4*

1.3.3 Stage Three *5*

2. BACKGROUND **6**

2.1 REVIEW OF A CONVENTIONAL SEPTIC TANK SYSTEM 6

2.2 CODE REGULATIONS, ONTARIO BUILDING CODE 7

2.2.1 Peat Filter *8*

2.2.2 Biofilters with Synthetic Materials *9*

2.3 CONCEPTUAL FRAMEWORK FOR MICROBIAL GROWTH IN SATURATED SOILS 11

2.4 BIOLOGICAL CLOGGING IN SATURATED SOILS 14

2.5 BIOLOGICAL CLOGGING IN UNSATURATED SOILS 23

2.6 CONCEPTUAL MODELS FOR MICROBIAL GROWTH IN UNSATURATED SOILS 37

2.6.1 Model #1 ..... *38*

2.6.2 Model #2 ..... *41*

2.6.3 Model #3 ..... *41*

2.7 BACTERIA EXTRACTION AND COUNTING 46

Reproduced with permission of the copyright owner. Further reproduction prohibited without permission.

2.8 BIOFILM CHARACTERIZATION 49
2.8.1 Introduction *50*
2.8.2 Biofilm Structure *51*
2.8.3 Unified Model by Laspidou and Rittmann *53*
2.8.4 Biofilm Densities Reported In the Literature *56*
2.8.5 Relation between Substrate Consumption, Biomass Growth, and EPS Formation *58*
2.9 SUMMARY 63

3. STAGE ONE: EFFECT OF DIFFERENT PORE STRUCTURES ON THE CLOGGING OF UNSATURATED SOIL 65

3.1 INTRODUCTION 65
3.2 EXPERIMENTAL SETUP 69
3.2.1 Materials and Method *69*
3.2.2 Measurements during Experimental Period *74*
3.2.3 Measurements at Dismantle Time *76*
3.3 RESULTS AND DISCUSSION 78
3.3.1 Soil Properties/Parameters *78*
3.3.2 Results during the Experimental Period *82*
3.3.3 Results at Dismantle Time *97*
3.4 SUMMARY OF THE FINDINGS 112

4. STAGE TWO: DETERMINATION OF MONOD KINETIC PARAMETERS 115

4.1 INTRODUCTION 115
4.2 EXPERIMENTAL SETUP 116
4.2.1 Materials and Method *116*
4.2.2 Initial Condition for the Test Cells *118*
4.2.3 Loading Rate for the Test Cells *118*
4.2.4 Measurements at Dismantle Time *119*
4.3 RESULTS AND DISCUSSION OF THE EXPERIMENTAL PART 122

Reproduced with permission of the copyright owner. Further reproduction prohibited without permission.

4.3.1 Effluent TOC Concentration with Time *122*
4.3.2 VSS Analysis *123*
4.3.3 TOC Analysis *124*
4.3.4 Bacteria Analysis *125*
4.4 RESULTS AND DISCUSSION OF THE ESTIMATION OF THE MONOD KINETIC PARAMETERS 127
4.5 SUMMARY OF THE FINDINGS 132
5. STAGE THREE: NUMERICAL MODELING 134
5.1 INTRODUCTION 134
5.2 STEPS TAKEN IN THE NUMERICAL MODELING STAGE 135
5.3 MAIN CHANGES TO THE NUMERICAL CODE 137
5.4 COMPARISON BETWEEN THE NUMERICAL SIMULATIONS AND EXPERIMENTAL RESULTS FOR CONTROL COLUMNS 143
5.4.1 Results for Septic Bed Sand Soil *144*
5.4.2 Results for Concrete Sand Soil *147*
5.4.3 Results for Filter Media Bed Sand Soil *149*
5.4.4 Results for Compacted Peat Soil *151*
5.4.5 Results for Loose Peat Soil *153*
5.5 COMPARISON BETWEEN THE NUMERICAL SIMULATIONS AND EXPERIMENTAL RESULTS FOR THE COLUMNS LOADED WITH ORGANIC LOADING ONLY AND ORGANIC PLUS SUSPENDED LOADING 156
5.5.1 Results for Septic Bed Sand Soil *160*
5.5.2 Results for Concrete Sand Soil *167*
5.5.3 Results for Compacted Peat Soil *172*
5.5.4 Results for Filter Media Bed Sand and Loose Peat Soils *176*
5.6 SUMMARY OF THE FINDINGS 176
6. CONCLUSIONS, RECOMMENDATIONS AND SCIENTIFIC CONTRIBUTIONS 180
6.1 CONCLUSIONS 180

Reproduced with permission of the copyright owner. Further reproduction prohibited without permission.

6.2 RECOMMENDATIONS AND FUTURE WORK 183
6.3 SCIENTIFIC CONTRIBUTIONS 185

7. REFERENCES 187

APPENDIX A- STAGE ONE DATA 197

A.1 DATA COLLECTED FROM THE SEPARATE EXPERIMENTS 197
A.1.1 Particle Size Analysis Data 197
A.1.2 Fiber Content for Peat Soil 201
A.1.3 pH for Peat Soil 201
A.1.4 Saturated Hydraulic Conductivity Values for the Sand Soils 202
A.1.5 Measured Porosity Value for the Sand Soils 205
A.1.6 Soil Moisture Curves for the Soils used in Stage One 206
A.2 CALCULATION OF AVAILABLE VOID SPACE FOR EACH SOIL AT STEADY STATE.. 219
A.3 CUMULATIVE INFLUENT LOAD FOR THE EXPERIMENTAL COLUMNS WITH TIME.. 223
A.4 MEASURED WEIGHT OF THE EXPERIMENTAL COLUMNS 227
A.5 OUTFLOW FROM THE EXPERIMENTAL COLUMNS 229
A.6 VISUAL IMAGES FOR THE EXPERIMENTAL COLUMNS 237

APPENDIX B- STAGE TWO DATA 259

B.1 RAW DATA COLLECTED IN STAGE TWO FROM THE TEST CELLS 259
B.2 COMPARISON BETWEEN THE RESULTS OF THE MODEL DEVELOPED IN STAGE TWO AND THE EXPERIMENTAL DATA USING THE CALIBRATED DECAY RATE USED IN STAGE THREE 265

APPENDIX C- STAGE THREE – NUMERICAL CODE 266

C.1 FLOW EQUATION 266
C.2 CONTAMINANT TRANSPORT EQUATION 269
C.3 NUMERICAL SOLUTION 269
C.4 BOUNDARY AND INITIAL CONDITIONS 271
C.4.1 For the Flow Equation 271
C.4.2 For the Contaminant Transport Equation 272

Reproduced with permission of the copyright owner. Further reproduction prohibited without permission.

C.5 SOURCE/SINK TERMS AND MONOD KINETICS 273
C.5.1 Solution Procedure *274*
C.5.2 Operator-Splitting and Runge-Kutta Method to Solve Ordinary Differential Equations *275*

Reproduced with permission of the copyright owner. Further reproduction prohibited without permission.

LIST OF TABLES

Table 2.1- Maximum allowable concentration from sewage treatment units approved by MOE (Ontario Building Code (2006)) 7

Table 2.2- Effluent characteristics for Ecoflo and Puraflo peat biofilters, Wastewater Virtual Trade Show Technologies, United States Environmental Protection Agency 9

Table 2.3- Effluent characteristics from Waterloo biofilters (Source: http://www.nsf.org/business/water_quality_protection_center/pdf/Waterloo_Biofilter_EPAAcceptedFinalReport.pdf) 10

Table 2.4- Summary of the references used in this section and which effect on clogging they studied 14

Table 2.5- Reported biofilm thickness, density (dry mass per unit wet volume), and types, adapted from Christensen and Characklis (1990) 57

Table 2.6- k_1 and k_2 rate coefficients for Pseudomonas aeruginosa 59

Table 2.7- Parameters used in Hsieh et al. (1994) study 62

Table 3.1- Experimental columns with different soil types and different loading scenarios 72

Table 3.2- Organic only and organic plus suspended loading for the experimental columns 72

Table 3.3- Summary of the soil properties 82

Table 3.4- Weight of silica in grams added to the columns loaded with organic plus suspended loading 108

Table 3.5- Percentage of ash content in each column 108

Table 3.6- Percentage of silica removal from the loose peat columns A3 and A4 111

Table 3.7- Percentage of silica removal from the compacted peat columns B3 and B4 112

Table 4.1- Initial and estimated parameters using the developed spreadsheet model 131

Table 5.1- Total volume of loads applied to each of the twenty five columns during the experiment period 170

Table 5.2- Summary of the soil properties and Monod kinetic parameters after they were adjusted and the additional input parameters to the numerical code 178

Reproduced with permission of the copyright owner. Further reproduction prohibited without permission.

Table A.1- Particle size analysis for the filter media bed sand soil conducted in the lab197
Table A.2- Particle size analysis for the filter media bed sand soil provided by the manufacture 197
Table A.3- Particle size analysis for the concrete sand soil conducted in the lab 198
Table A.4- Particle size analysis for the concrete sand soil provided by the manufacture 198
Table A.5- Particle size analysis for the septic bed sand soil conducted in the lab..... 199
Table A.6- Particle size analysis for the septic bed sand soil provided by the manufacture 199
Table A.7- Particle size analysis for the peat soil conducted in the lab..... 200
Table A.8- Fiber content measured in the lab for the peat soil..... 201
Table A.9- pH measured in the lab for the peat soil 201
Table A.10- Saturated hydraulic conductivity for filter media bed sand soil..... 202
Table A.11- Saturated hydraulic conductivity for concrete sand soil..... 203
Table A.12- Saturated hydraulic conductivity for septic bed sand soil 204
Table A.13- Porosity test for sand soils 205
Table A.14- Comparison between soil parameters obtained using the three methods discussed in chapter three..... 218
Table A.15- Available void space for each soil at steady state 219
Table A.16- Time to reduce loading/clogging for the experimental columns..... 226
Table B.1- Data collected from test cell 12 259
Table B.2- Data collected from test cell 11 260
Table B.3- Data collected from test cell 10 260
Table B.4- Data collected from test cell 9 261
Table B.5- Data collected from test cell 8 261
Table B.6- Data collected from test cell 7 262
Table B.7- Data collected from test cell 6 262
Table B.8- Data collected from test cell 5 263
Table B.9- Data collected from test cell 4 263
Table B.10- Data collected from test cell 3 264

Reproduced with permission of the copyright owner. Further reproduction prohibited without permission.

Table B.11- Data collected from test cell 2 264
Table B.12- Data collected from test cell 1 265

Reproduced with permission of the copyright owner. Further reproduction prohibited without permission.

LIST OF FIGURES

Figure 2.1- Schematic diagram for a conventional septic tank system 6
Figure 2.2- Typical cross section for an Ecoflo ® biofilters (Source: http://www.ecofloontario.com/biofilter_files/ecoflo_biofilter.htm) 8
Figure 2.3- Foamy texture material used by Waterloo Biofilter (Source: http://www.waterloo-biofilter.com/) 10
Figure 2.4- Schematic representation for saturated soil phases, adapted from Baveye and Valocchi (1989) 11
Figure 2.5- Second conceptual framework, adapted from Baveye and Valocchi (1989). 12
Figure 2.6- Third conceptual framework, adapted from Baveye and Valocchi (1989).... 13
Figure 2.7- Visualization of Model #1 39
Figure 2.8- Visualization of Model #3 43
Figure 2.9- Schematic diagram of the unified model with all the involved components, adapted from Laspidou and Rittmann (2002a) 54
Figure 2.10- Schematic diagram for electron flow described by the unified theory, (a) original substrate and active biomass and (b) BAP and UAP utilization, adapted from Laspidou and Rittmann (2002b) 55
Figure 2.11- Schematic diagram of all the components involved in Hsieh et al. model, adapted from Hsieh et al. (1994) 60
Figure 3.1- Grain size distribution for septic bed sand with 13.8% of fines passing though sieve 0.075 mm 66
Figure 3.2- Grain size distribution for concrete sand with 1.7% of fines passing through sieve 0.075 mm 66
Figure 3.3- Grain size distribution for filter media bed sand 67
Figure 3.4- Grain size distribution for peat soil 67
Figure 3.5- Sticks, stones, and twigs found in the peat soil used 68
Figure 3.6- Buchner funnel test setup used to determine the soil moisture curves for sand soils 69
Figure 3.7- Twenty five PVC columns constructed for this experiment 70
Figure 3.8- Schematic diagram for a typical column that was built for stage one 71

Reproduced with permission of the copyright owner. Further reproduction prohibited without permission.

Figure 3.9- TDR measurement setup at five different levels; 48 cm, 37 cm, 25 cm, 15 cm, and 5 cm from the top of the lower drainage layer 74
Figure 3.10- Outflow measurement setup..... 75
Figure 3.11- Comparison between average TDR measurements for control columns during the course of the experimental period and the corresponding van Genuchten fitting curves 81
Figure 3.12- Saturation profiles for the control columns for the five soils used in this experiment..... 83
Figure 3.13- Outflow from loose peat control column A 84
Figure 3.14- Outflow from compacted peat control column B..... 85
Figure 3.15- Outflow from filter media bed sand control column C 85
Figure 3.16- Outflow from concrete sand control column D..... 86
Figure 3.17- Outflow from septic bed sand control column E 86
Figure 3.18- Saturation profiles from loose peat columns A1 and A2 88
Figure 3.19- Saturation profiles from loose peat columns A3 and A4 89
Figure 3.20- Saturation profiles from compacted peat columns B1 and B2..... 89
Figure 3.21- Saturation profiles from compacted peat columns B3 and B4..... 90
Figure 3.22- Saturation profiles from filter media bed sand columns C1 and C2..... 90
Figure 3.23- Saturation profiles from filter media bed sand columns C3 and C4..... 91
Figure 3.24- Saturation profiles from concrete sand columns D1 and D2 91
Figure 3.25- Saturation profiles from concrete sand columns D3 and D4 92
Figure 3.26- Saturation profiles from septic bed sand columns E1 and E2..... 92
Figure 3.27- Saturation profiles from septic bed sand columns E3 and E4..... 93
Figure 3.28- Outflow from loose peat column A2..... 94
Figure 3.29- Outflow from compacted peat column B3 95
Figure 3.30- Outflow from filter media bed sand column C1 95
Figure 3.31- Outflow from concrete sand column D4..... 96
Figure 3.32- Outflow from septic bed sand column E2..... 96
Figure 3.33- Bacteria count at dismantle time for columns A, A1, A2, A3, and A4..... 97
Figure 3.34- Bacteria count at dismantle time for columns B, B1, B2, B3, and B4..... 98

Reproduced with permission of the copyright owner. Further reproduction prohibited without permission.

Figure 3.35- Bacteria count at dismantle time for columns C1, C2, C3, and C4 98
Figure 3.36- Bacteria count at dismantle time for columns D, D1, D2, and D3 99
Figure 3.37- Bacteria count at dismantle time for columns E2, E3, and A4 99
Figure 3.38- Comparison between gravimetric moisture content and TDR measurements at dismantle time for loose peat columns A, A1, A2, A3, and A4 101
Figure 3.39- Comparison between gravimetric moisture content and TDR measurements at dismantle time for compacted peat columns B, B1, and B2 102
Figure 3.40- Comparison between gravimetric moisture content and TDR measurements at dismantle time for compacted peat columns B3 and B4 103
Figure 3.41- Comparison between gravimetric moisture content and TDR measurements at dismantle time for filter media bed sand columns C, C1, and C2..... 104
Figure 3.42- Comparison between gravimetric moisture content and TDR measurements at dismantle time for filter media bed sand columns C3 and C4 104
Figure 3.43- Comparison between gravimetric moisture content and TDR measurements at dismantle time for concrete sand columns D, D1, and D2..... 105
Figure 3.44- Comparison between gravimetric moisture content and TDR measurements at dismantle time for concrete sand columns D3 and D4..... 105
Figure 3.45- Comparison between gravimetric moisture content and TDR measurements at dismantle time for septic bed sand columns E, E1, and E2..... 106
Figure 3.46- Comparison between gravimetric moisture content and TDR measurements at dismantle time for septic bed sand columns E3 and E4 106
Figure 3.47- Ash content for loose peat columns 107
Figure 3.48- Ash content for compacted peat columns 108
Figure 4.1- Twelve test cells and twelve samples used for this experiment..... 117
Figure 4.2- Plan view and typical cross section for a test cell setup 117
Figure 4.3- Change in effluent and biomass concentrations versus time 121
Figure 4.4- Influent and average effluent TOC concentrations measured from the test cells..... 123
Figure 4.5- Microbial concentration in mg/L versus time using the bacteria count analysis 127

Reproduced with permission of the copyright owner. Further reproduction prohibited without permission.

Figure 4.6- Comparison between the measured effluent concentrations and the results from the spreadsheet model at time step of 1 hour 129
Figure 4.7- Comparison between the measured microbial concentrations using bacteria analysis and model prediction using a conversion factor of 1.72×10^{-10}.... 132
Figure 4.8- Comparison between the measured microbial concentrations using bacteria analysis and model prediction using a conversion factor of 3.16×10^{-11}.... 132
Figure 5.1- Comparison between saturation profiles for septic bed sand control column E versus numerical simulation 145
Figure 5.2- Comparison between outflow profiles for septic bed sand control column E versus numerical simulation 145
Figure 5.3- Comparison between saturation profiles for concrete sand control column D versus numerical simulation 147
Figure 5.4- Comparison between outflow profiles for concrete sand control column D versus numerical simulation 148
Figure 5.5- Comparison between saturation profiles for filter media bed sand control column C versus numerical simulation 149
Figure 5.6- Comparison between outflow profiles for filter media bed sand control column C versus numerical simulation 150
Figure 5.7- Comparison between saturation profiles for compacted peat control column B versus numerical simulation 152
Figure 5.8- Comparison between outflow profiles for compacted peat control column B versus numerical simulation 152
Figure 5.9- Comparison between saturation profiles for loose peat control column A versus numerical simulation 154
Figure 5.10- Comparison between outflow profiles for loose peat control column A versus numerical simulation 155
Figure 5.11- Comparison between the loose peat columns loaded with organic loading only (A1 and A2) and organic plus suspended loading (A3 and A4) 157

Reproduced with permission of the copyright owner. Further reproduction prohibited without permission.

Figure 5.12- Comparison between the compacted peat columns loaded with organic loading only (B1 and B2) and organic plus suspended loading (B3 and B4) 157
Figure 5.13- Comparison between the filter media bed sand columns loaded with organic loading only (C1 and C2) and organic plus suspended loading (C3 and C4) 158
Figure 5.14- Comparison between the concrete sand columns loaded with organic loading only (D1 and D2) and organic plus suspended loading (D3 and D4) 158
Figure 5.15- Comparison between the septic bed sand columns loaded with organic loading only (E1 and E2) and organic plus suspended loading (E3 and E4) 159
Figure 5.16- Total saturation at the top measuring location for septic bed sand columns E1 and E2 versus numerical simulation using Model #2 161
Figure 5.17- Total saturation for septic bed sand columns versus numerical simulation at 22 days using the three conceptual models 164
Figure 5.18- Total saturation for septic bed sand columns versus numerical simulation at 113 days using the three conceptual models 164
Figure 5.19- Total saturation for septic bed sand columns versus numerical simulation at 260 days using the three conceptual models 165
Figure 5.20- Total saturation at the top measuring location for concrete sand columns D1 and D2 versus numerical simulation using Model #2 168
Figure 5.21- Total saturation for concrete sand columns versus numerical simulation at 29 days using the three conceptual models 169
Figure 5.22- Total saturation for concrete sand columns versus numerical simulation at 183 days using the three conceptual models 169
Figure 5.23- Total saturation for concrete sand columns versus numerical simulation at 274 days using the three conceptual models 171
Figure 5.24- Total saturation at the top measuring location for compacted peat columns B1 and B2 versus numerical simulation using Model #2..... 172

Reproduced with permission of the copyright owner. Further reproduction prohibited without permission.

Figure 5.25- Total saturation for compacted peat columns versus numerical simulation at 8 days using Models #2 and #3 174
Figure 5.26- Total saturation for compacted peat columns versus numerical simulation at 126 days using Models #2 and #3 175
Figure 5.27- Total saturation for compacted peat columns versus numerical simulation at 253 days using Models #2 and #3 175
Figure A.1- Soil moisture curves for filter media bed sand soil using Buchner funnel apparatus 206
Figure A.2- TDR measurements recorded after filter media bed sand columns were initially saturated and then gravity drained for one day 207
Figure A.3- Soil moisture curves for concrete sand soil using Buchner funnel apparatus 208
Figure A.4- TDR measurements recorded after concrete sand columns were initially saturated and then gravity drained for one day 209
Figure A.5- Soil moisture curves for septic bed sand soil using Buchner funnel apparatus 210
Figure A.6- TDR measurements recorded after septic bed sand columns were initially saturated and then gravity drained for one day 211
Figure A.7- TDR measurements recorded after loose peat columns were initially saturated and then gravity drained for one day 212
Figure A.8- TDR measurements recorded after compacted peat columns were initially saturated and then gravity drained for one day 213
Figure A.9- Comparison between the three methods used to estimate the soil moisture curve for loose peat soil 214
Figure A.10- Comparison between three methods used to estimate the soil moisture curve for compacted peat soil 215
Figure A.11- Comparison between the three methods used to estimate the soil moisture curve for filter media bed sand soil 216
Figure A.12- Comparison between the three methods used to estimate the soil moisture curve for concrete sand soil 217

Reproduced with permission of the copyright owner. Further reproduction prohibited without permission.

Figure A.13- Comparison between the three methods used to estimate the soil moisture curve for septic bed sand soil 218
Figure A.14- Cumulative influent load for loose peat columns 223
Figure A.15- Cumulative influent load for compacted peat columns 223
Figure A.16- Cumulative influent load for filter media bed sand columns 224
Figure A.17- Cumulative influent load for concrete sand columns 224
Figure A.18- Cumulative influent load for septic bed sand columns 225
Figure A.19- COD concentration of the stock solutions; organic only and organic plus suspended 225
Figure A.20- Change in weight of the loose peat columns with time 227
Figure A.21- Change in weight of the compacted peat columns with time 227
Figure A.22- Change in weight of the filter media bed sand columns with time 228
Figure A.23- Change in weight of the concrete sand columns with time 228
Figure A.24- Change in weight of the septic bed sand columns with time 229
Figure A.25- Outflow from loose peat column A1 229
Figure A.26- Outflow from loose peat column A3 230
Figure A.27- Outflow from loose peat column A4 230
Figure A.28- Outflow from compacted peat column B1 231
Figure A.29- Outflow from compacted peat column B2 231
Figure A.30- Outflow from compacted peat column B4 232
Figure A.31- Outflow from filter media bed sand column C2 232
Figure A.32- Outflow from filter media bed sand column C3 233
Figure A.33- Outflow from filter media bed sand column C4 233
Figure A.34- Outflow from concrete sand column D1 234
Figure A.35- Outflow from concrete sand column D2 234
Figure A.36- Outflow from concrete sand column D3 235
Figure A.37- Outflow from septic bed sand column E1 235
Figure A.38- Outflow from septic bed sand column E3 236
Figure A.39- Outflow from septic bed sand column E4 236

Reproduced with permission of the copyright owner. Further reproduction prohibited without permission.

Figure A.40- Visual images of loose peat column A at dismantle time: (a) at the top surface of the column; (b) at a depth of 3 cm from the top surface; (c) at a depth of 8 cm from the top surface; and (d) at a depth of 17 cm from the top surface. 237

Figure A.41- Visual images of loose peat column A1 at dismantle time: (a) at the top surface of the column; (b) at a depth of 4.5 cm from the top surface; (c) at a depth of 10.5 cm from the top surface; and (d) at a depth of 18 cm from the top surface 238

Figure A.42- Visual images of loose peat column A2 at dismantle time: (a) at the top surface of the column; (b) at a depth of 3.5 cm from the top surface; (c) at a depth of 8.5 cm from the top surface; and (d) at a depth of 18.5 cm from the top surface 239

Figure A.43- Visual images of loose peat column A3 at dismantle time: (a) at the top surface of the column; (b) at a depth of 3 cm from the top surface; (c) at a depth of 8.5 cm from the top surface; and (d) at a depth of 17.5 cm from the top surface 240

Figure A.44- Visual images of loose peat column A4 at dismantle time: (a) at the top surface of the column; (b) at a depth of 3.5 cm from the top surface; (c) at a depth of 10 cm from the top surface; and (d) at a depth of 22 cm from the top surface 241

Figure A.45- Visual images of compacted peat column B at dismantle time: (a) at the top surface of the column; (b) at a depth of 2.5 cm from the top surface; (c) at a depth of 8 cm from the top surface; and (d) at a depth of 17 cm from the top surface 242

Figure A.46- Visual images of compacted peat column B1 at dismantle time: (a) at the top surface of the column; (b) at a depth of 2 cm from the top surface; (c) at a depth of 8.5 cm from the top surface; and (d) at a depth of 17 cm from the top surface 243

Figure A.47- Visual images of compacted peat column B2 at dismantle time: (a) at the top surface of the column; (b) at a depth of 2.5 cm from the top surface; (c) at

Reproduced with permission of the copyright owner. Further reproduction prohibited without permission.

a depth of 8.5 cm from the top surface; and (d) at a depth of 16.5 cm from the top surface 244

Figure A.48- Visual images of compacted peat column B3 at dismantle time: (a) at the top surface of the column; (b) at a depth of 2.5 cm from the top surface; (c) at a depth of 8.5 cm from the top surface; and (d) at a depth of 18.5 cm from the top surface 245

Figure A.49- Visual images of compacted peat column B4 at dismantle time: (a) at the top surface of the column; (b) at a depth of 2.5 cm from the top surface; (c) at a depth of 8 cm from the top surface; and (d) at a depth of 16.5 cm from the top surface 246

Figure A.50- Visual images of filter media bed sand column C at dismantle time: (a) at the top surface of the column; (b) at a depth of 3 cm from the top surface; (c) at a depth of 9.5 cm from the top surface; and (d) at a depth of 17 cm from the top surface 247

Figure A.51- Visual images of filter media bed sand column C1 at dismantle time: (a) at the top surface of the column; (b) at a depth of 1.5 cm from the top surface; (c) at a depth of 7.5 cm from the top surface; and (d) at a depth of 16 cm from the top surface..... 248

Figure A.52- Visual images of filter media bed sand column C2 at dismantle time: (a) at the top surface of the column; (b) at a depth of 2.5 cm from the top surface; (c) at a depth of 9 cm from the top surface; and (d) at a depth of 17 cm from the top surface 249

Figure A.53- Visual images of filter media bed sand column C3 at dismantle time: (a) at the top surface of the column; (b) at a depth of 2 cm from the top surface; (c) at a depth of 7.5 cm from the top surface; and (d) at a depth of 15.5 cm from the top surface 250

Figure A.54- Visual images of filter media bed sand column C4 at dismantle time: (a) at the top surface of the column; (b) at a depth of 2.5 cm from the top surface; (c) at a depth of 8 cm from the top surface; and (d) at a depth of 16 cm from the top surface 251

Reproduced with permission of the copyright owner. Further reproduction prohibited without permission.

Figure A.55- Visual images of concrete sand column D at dismantle time: (a) at the top surface of the column; (b) at a depth of 8.5 cm from the top surface; (c) at a depth of 16.5 cm from the top surface; and (d) at a depth of 26 cm from the top surface 252
Figure A.56- Visual images of concrete sand column D1 at dismantle time: (a) at the top surface of the column; (b) at a depth of 2 cm from the top surface; (c) at a depth of 8 cm from the top surface; and (d) at a depth of 17 cm from the top surface 253
Figure A.57- Visual images of concrete sand column D2 at dismantle time: (a) at the top surface of the column; (b) at a depth of 3 cm from the top surface; (c) at a depth of 7.5 cm from the top surface; and (d) at a depth of 15.5 cm from the top surface 254
Figure A.58- Visual image at the top surface of concrete sand column D3 at dismantle time 255
Figure A.59- Visual image at the top surface of concrete sand column D4 at dismantle time 255
Figure A.60- Visual image at the top surface of septic bed sand column E at dismantle time 256
Figure A.61- Visual image at the top surface of septic bed sand column E1 at dismantle time 256
Figure A.62- Visual image at the top surface of septic bed sand column E2 at dismantle time 257
Figure A.63- Visual image at the top surface of septic bed sand column E3 at dismantle time 257
Figure A.64- Visual image at the top surface of septic bed sand column E4 at dismantle time 258
Figure B.1- Comparison between the measured effluent concentrations from the test cells and the results from the spreadsheet model at time step of 1 hour after using the decay rate adjusted in stage three 265
Figure C.1- General layout for the modeled column 268

Reproduced with permission of the copyright owner. Further reproduction prohibited without permission.

Figure C.2- Block-centered finite difference discretization of a one-dimensional problem domain, adapted from Zheng and Bennett (1995) 270
Figure C.3- Explicit scheme 271
Figure C.4- Graphical representation for the initial and boundary concentrations..... 273
Figure C.5- Flow chart shows solution sequence of the contaminant and the microbial equations..... 275
Figure C.6- Graphical representation of one complete operator- split cycle, adapted from Odencrantz et al. (1990) 276

Reproduced with permission of the copyright owner. Further reproduction prohibited without permission.

LIST OF SYMBOLS AND NOMENCLATURES

A	active suspended biomass, Hsieh et al. (1994)
A^B	bounded/attached biomass, Hsieh et al. (1994)
BAP	Biomass-Associated Products
BOC	Bacterial Organic Carbon (mg/L)
BOD_5	Biochemical Oxygen Demand (mg/L)
b	cell decay coefficient (s^{-1})
C	substrate concentration (mg/L)
$CBOD_5$	Carbonaceous Biochemical Oxygen Demand (mg/L)
COD	Chemical Oxygen Demand (mg/L)
C_i^t	concentration at grid block (i) at time t (mg/L)
$C_i^{t+\Delta t}$	concentration at grid block (i) at time t+ Δ t (mg/L)
C_{i+1}^t	concentration at grid block (i+1) at time t (mg/L)
C_{i-1}^t	concentration at grid block (i-1) at time t (mg/L)
C_o	initial substrate concentration (mg/L)
C_{source}	pulse concentration (mg/L)
$D_{i+1/2}$	dispersion coefficient at the interface (i+1/2), Figure (C.4) (cm^2/s)
$D_{i-1/2}$	dispersion coefficient at the interface (i-1/2), Figure (C.4) (cm^2/s)
D_s	dispersion coefficient (cm^2/s)
EPS	Extracellular Polymeric Substances
f_{AP}	fraction of active cell mass "A" which is converted to cell-bound polymer "P" as active cell mass degrades
$f_{A^B P}$	fraction of attached active cell mass "A^B" which is converted to attached cell-bound polymer "P^B" as active cell mass degrades
f_d	biodegradable fraction of active biomass
g	gravitational acceleration (cm/s^2)
h	total head (cm)
$h_w(z)$	total head of water at level z (cm)

Reproduced with permission of the copyright owner. Further reproduction prohibited without permission.

$h_{w,i}$	total head for water at grid block (i) (cm)
$h_{w,i+1}$	total head for water at gird block (i+1) (cm)
$h_{w,i-1}$	total head for water at gird block (i-1) (cm)
$h_{w,1}$	prescribe total head boundary condition at the bottom of a column (cm)
$h_{w,n}$	prescribe total head boundary condition at the top of a column (cm)
IC	Inorganic Carbon (mg/L)
i	grid block index
$K(S_w)$	saturated hydraulic conductivity as a function of (S_w) (cm/s)
$K(\theta)$	unsaturated hydraulic conductivity or saturated hydraulic conductivity as a function of (θ) (cm/s)
$K(\theta)_{i+1/2}$	unsaturated hydraulic conductivity at the interface (i+1/2) (cm/s)
$K(\theta)_{i-1/2}$	unsaturated hydraulic conductivity at the interface (i-1/2) (cm/s)
$K(\theta)_{i\pm1/2}$	unsaturated hydraulic conductivity at the interface (i$\pm$ 1/2) (cm/s)
K_{AC}^{*}	half-velocity constant for growth of suspended cells
$K_{A}^{B}{}_{C}^{*}$	half-velocity constant for growth of attached cells
K_{dAC}^{*}	half-velocity constant for decomposition of suspended cells
$K_{dA}^{B}{}_{C}^{*}$	half-velocity constant for decomposition of attached cells
K_{PC}^{*}	half-velocity constant for production of polymer associated with suspended cells
$K_{P}^{B}{}_{C}^{*}$	half-velocity constant for production of polymer associated with attached cells
K_{P^*P}	half-velocity constant for production of dissolved polymer "P^*" from cell-bound polymer of suspended cells "P"
$K_{P^*P^B}$	half-velocity constant for production of dissolved polymer "P^*" from cell-bound polymer of attached cells "P^B"
K_s	half-velocity constant ($mg_{substrate}$/L)
K_{sat}	saturated hydraulic conductivity (cm/s)
k	first order rate coefficient
k_1	growth associated EPS formation coefficient in g EPS Carbon/ g biomass Carbon

Reproduced with permission of the copyright owner. Further reproduction prohibited without permission.

k_2	non-growth associated EPS formation coefficient in g EPS Carbon/ g biomass Carbon
k_r	relative permeability (cm/s)
$k_r(S_{ew})$	relative permeability as a function of effective water saturation
$k_{rw}(S_{aw})$	relative permeability as a function of actual water saturation
L	column length (cm)
L_f	biofilm thickness (μm)
M	microbial concentration (mg_{cells} /L)
MC%	moisture content in percentage
MC_{sample}	mositure content of sample
MOE	Ministry of Environment
$M_{bacteria + EPS}$	mass of bacteria and EPS (g)
M_{solids}	mass of dry solid sample (g)
M_o	initial microbial concentration (mg/L)
m	van Genuchten fitting parameter for capillary pressure-saturation relationship
N	van Genuchten fitting parameter for capillary pressure-saturation relationship or last block, Figure C.4
OBC	Ontario Building code
P	product concentration in Equation (2.22) or EPS associated with active suspended biomass in Hsieh et al. (1994)
P^B	EPS associated with bounded/attached biomass, Hsieh et al. (1994)
P^S	surface sorbed biopolymers, Hsieh et al. (1994)
P^*	dissolved biopolymers, Hsieh et al. (1994)
P_c	capillary pressure (cm)
Q	flow rate (cm^3/s) or darcy flux (cm/s)
q_l	prescribe flux boundary condition at the bottom of a column (cm/s)
q_m	maximum specific rate of substrate utilization ($mg_{substrate}$ / mg_{cell} s^{-1})
q_n	prescribe flux boundary condition at the top of a column (cm/s)
R_s	source/sink term (mg/L . s)

Reproduced with permission of the copyright owner. Further reproduction prohibited without permission.

r	radius of a capillary tube (cm)
r_i	radius at number of division (i) (cm)
S_e	effective saturation
S_{em}	effective microbial saturation
S_{et}	effective total saturation
S_{aw}	actual water saturation
S_{ew}	effective water saturation
S_o	substrate concentration, Equation (2.22)
S_{trap}	effective entrapped air
S_w	water saturation
S_{wr}	irreducible water saturation
$S_{w,i}^{t+\Delta t}$	water saturation at grid block (i) at time t+Δt
$S_{w,i}^{t}$	water saturation at grid block (i) at time t
Sat%	saturation in percentage
SMP	Soluble Microbial Products
SOC	Soluble Organic Carbon (mg/L)
TC	Total Carbon (mg/L)
TDR	Time Domain Reflectometry
TKN	Total Kjeldahl Nitrogen (mg/L)
TN	Total Nitrogen (mg/L)
TOC	Total Organic Carbon (mg/L)
TSS	Total Suspended Solids (mg/L)
t	time (seconds or days)
th	biofilm thickness (cm)
U	flow factor
UAP	Utilization-Associated Products
$U_o\|_0^{Porosity}$	constant flow factor represents the relative permeability term for Model #3 when there is no microbial activity involved

Reproduced with permission of the copyright owner. Further reproduction prohibited without permission.

$U_i\|_0^{Porosity}$	constant flow factor represents the relative permeability term for Model #3 when there is microbial activity involved
V	seepage velocity (cm/s) or volume (cm^3)
V_m	microbial volume
VS	Volatile Solids (mg/L)
VSS	Volatile Suspended Solids (%)
$V_{i+1/2}$	seepage velocity at the interface (i+1/2) (cm/s), Figure (C.4)
$V_{i-1/2}$	seepage velocity at the interface (i-1/2) (cm/s), Figure (C.4)
W	weight (g)
WC%	water content in percentage
X_a	active biomass
X_{res}	residual inert biomass
Y	cell yield coefficient (mg_{cell} / $mg_{substrate}$)
z	elevation head (cm)
α	van Genuchten fitting parameter for capillary pressure-saturation relationship (cm^{-1})
Δt	size of time step (s)
Δx	size of a grid block in x direction (cm)
Δy	size of a grid block in y direction (cm)
Δz	size of a grid block in z direction (cm)
$\partial h/\partial L$	hydraulic gradient along the flow path
ϕ	porosity
ϕ_i	porosity at block (i)
μ	dynamic viscosity (Pascal.s)
θ	volumetric moisture content
ρ	density of liquid (g/cm^3)
ρ_{bulk}	bulk soil density (g/cm^3)
ρ_{dry}	dry soil density (g/cm^3)

Reproduced with permission of the copyright owner. Further reproduction prohibited without permission.

ρ_w	water density (g/cm^3)
σ	surface tension for water/air interface (dyne/cm)
ψ	capillary pressure (cm)

Reproduced with permission of the copyright owner. Further reproduction prohibited without permission.

1. INTRODUCTION

1.1 Overview

A large number of people in North America are living in areas not serviced with sewage facilities (Jawson (1976); Hagedorn et al. (1981)). Septic tank systems are considered the most feasible way to treat wastewater in these areas (Kennedy (1998)). Septic tanks and drainage fields are located in the soil zones that are close to the ground surface. This soil zone is the unsaturated zone and will be affected by the septic tank effluent. The soil in the unsaturated zone will be responsible for treating the septic tank effluent and it may clog over time due to filtration and continuous microbial growth. Hence, clogging of unsaturated soils and how this clogging will affect the hydraulic conductivity of the soil has to be understood in order to minimize the clogging problems and to use the soil in this zone as an effective treatment system.

Researchers have looked at clogging from three aspects: chemical, physical, and biological mechanisms (Rice (1974)). Chemical clogging is caused by chemical reactions between dissolved salts in water, which result in the formation of salt particles that precipitate between soil particles and lower the permeability of the soil. Physical clogging is the result of suspended solids that physically block pores and reduce pore diameters which will lower the permeability. Biological clogging is due to growth of bacteria that attach to solid particles and block flow paths which lower the permeability (Rice (1974)).

Biological clogging, which is the focus of this research, is the most important clogging mechanism when dealing with the treatment of septic tank effluent in biofilters. Microorganisms or bacteria are already present in the soil and need a suitable

Reproduced with permission of the copyright owner. Further reproduction prohibited without permission.

environment to grow. This suitable environment can be summarized into two factors, physical and nutritional (biochemical) factors. Physical factors include moisture, hydrostatic pressure, and osmotic pressure. Nutritional factors include availability of carbon, nitrogen, sulfur, phosphorus, trace elements such as copper, iron, zinc, and cobalt and in some cases vitamins (Black (1999)). The physical factors are controlled by the design of the biofilter and the hydraulic loading. The wastewater, or septic tank effluent, provides the nutritional factors including the food source (i.e. carbon) and the required nutrients and trace elements.

Biological clogging is not a new concept. Allison (1947) started to look at the change in permeability with time due to microbial growth. Since 1949, when Monod developed his well known equation (Monod (1949)), research has advanced more rapidly in this area to try to simulate microbial growth.

Practically, the impact of biological clogging can be seen in various biofilter applications. Biofilters, such as peat filters, are one important application in this field. Peat filters are known to be a way to purify water that passes through them and they are relatively inexpensive as well (Kennedy (1998)). They have already been used in field applications such as treating septic tank effluent from small communal, residential, commercial, and public systems (e.g. Kennedy and Van Geel (2001)). In addition, a number of commercial filters for single dwelling or small communal systems are available on the market (e.g. ECOFLO ® Biofilters, Premier Tech Environment; Puraflo® Peat Biofilter, Bord na Mona US).

Although clogging of saturated soils has been studied by many researchers (e.g. Rice (1974); Okubo and Matsumoto (1979); Okubo and Matsumoto (1983); Oberdorfer and

Reproduced with permission of the copyright owner. Further reproduction prohibited without permission.

Peterson (1985); Mattison et al. (2002)), limited research has been conducted to develop a conceptual model for unsaturated zone clogging.

Mostafa and Van Geel (2007) proposed three different conceptual models to simulate biological clogging in unsaturated soils and illustrate how the microbial growth can affect the relative permeability of the soil and cause clogging. The conceptual models vary from microscopic scale to macroscopic scale and from analytically derived to empirical equations. The microscopic scale conceptual model was based on the assumption of a biofilm that covers the soil particles. The macroscopic scale models relate the growth of microbes with the relative permeability term and do not consider the distribution of the microbial growth at the microscopic scale. These models have not been validated with experimental work. Also, these conceptual models have been numerically coded to simulate one-dimensional biological clogging scenarios with different soil types (i.e. peat and sand soil) and to study the effect of continuous loading versus pulse loading with different organic and hydraulic loading (Mostafa and Van Geel (2007)). Although the pulsed versus continuous loading simulations agree conceptually with what Mostafa and Van Geel (2007) believe should occur, these conceptual models have not been validated against experimental data.

1.2 Objective

The main objective of this research was to investigate biological clogging in unsaturated soils. Testing of different soil types was conducted experimentally to study the effect of different pore structures on biological clogging due to bacterial growth. Also, valuable data were generated and used to calibrate the C++ numerical code and

Reproduced with permission of the copyright owner. Further reproduction prohibited without permission.

validate the conceptual models proposed by Mostafa (2004) and Mostafa and Van Geel (2007).

1.3 Scope

This research was divided into three main stages. In the following subsections, a brief description for these stages is provided.

1.3.1 Stage One

The purpose of this stage was to evaluate the relationship between the pore structure of unsaturated soils and biological clogging. Four different types of soils were tested to illustrate the impacts of pore size distribution (well graded versus uniform), organic/inorganic content, porosity and density on the bioclogging process.

Preliminary tests (e.g. permeability test, soil moisture curve, etc.) were conducted to characterize the soils used in this study. Also, the data generated from this stage were used to generate saturation profiles that indicated the effect of bacterial growth on moisture content. The outcomes from this stage were used to provide a better understanding of the effect of different pore structures on biological clogging processes and to provide a data set to be used later in stage three.

1.3.2 Stage Two

In this stage, Monod kinetic parameters that are needed for the Monod equation were evaluated in order to validate the proposed conceptual models. Laboratory measurements for substrate concentration versus time and microbial concentration versus time were obtained experimentally. Those measurements were used to evaluate Monod kinetic parameters; Y, cell yield coefficient in $mg_{cell}/mg_{substrate}$, q_m, maximum specific rate of substrate utilization in $mg_{substrate}/mg_{cell}\ s^{-1}$, K_s, half-velocity constant in mg/L, and b, cell

Reproduced with permission of the copyright owner. Further reproduction prohibited without permission.

decay coefficient in s^{-1} using a spreadsheet model developed for this purpose. All the estimated parameters were used in stage three in the validation of the proposed conceptual models developed earlier by Mostafa and Van Geel (2007).

1.3.3 Stage Three

A one-dimensional numerical code that calculates flow, contaminant transport, and microbial growth in unsaturated soils was developed earlier by Mostafa and Van Geel (2007) to study the relation between microbial growth and unsaturated hydraulic conductivity. Three different conceptual models put forward for this relationship and hypothetical cases were run to illustrate the differences between the three conceptual models without any laboratory data for model validation. Moreover, the Monod kinetics equation was used to simulate microbial growth and typical wastewater values were used for the Monod parameters. This stage was used to enhance the numerical code and validate the conceptual models proposed by Mostafa and Van Geel (2007) with the laboratory data obtained from stage one and the Monod parameters obtained from stage two. Soil and Monod kinetic parameters obtained from stages one and two were used to simulate flow and microbial growth. Then the conceptual representation of the bioclogging was improved to better simulate the data collected from stage one. Finally, numerous numerical simulations were conducted to establish which of the three conceptual models best simulates the bioclogging process. This stage revealed the difference between the three conceptual models and suggested which model(s) best simulates the biological clogging process shown from the experimental data.

Reproduced with permission of the copyright owner. Further reproduction prohibited without permission.

2. BACKGROUND

2.1 Review of a Conventional Septic Tank System

A conventional septic system typically consists of a septic tank, distribution box, and a network of distribution pipes. The distribution pipes are covered by a crushed stone/gravel layer, lying on a drainage bed and are sloped and perforated (Figure (2.1)). Wastewater from a home is transported to the septic tank where settling occurs. Solid particles settle, greases and oils float to form a scum layer, and the liquid (i.e. septic tank effluent) gets transported to the distribution box, by gravity, where it is distributed to the perforated pipes. In the perforated pipes, septic tank effluent percolates from the holes in the perforated pipes, into a crushed stone/gravel layer that surrounds the perforated pipes for better effluent distribution (i.e. soil absorption trench). Then the effluent percolates through the drainage bed where sand soil is typically used. Septic tank effluent is treated as it percolates through the drainage bed by different treatment mechanisms that occur within the soil (i.e. physical, chemical, and biological treatment).

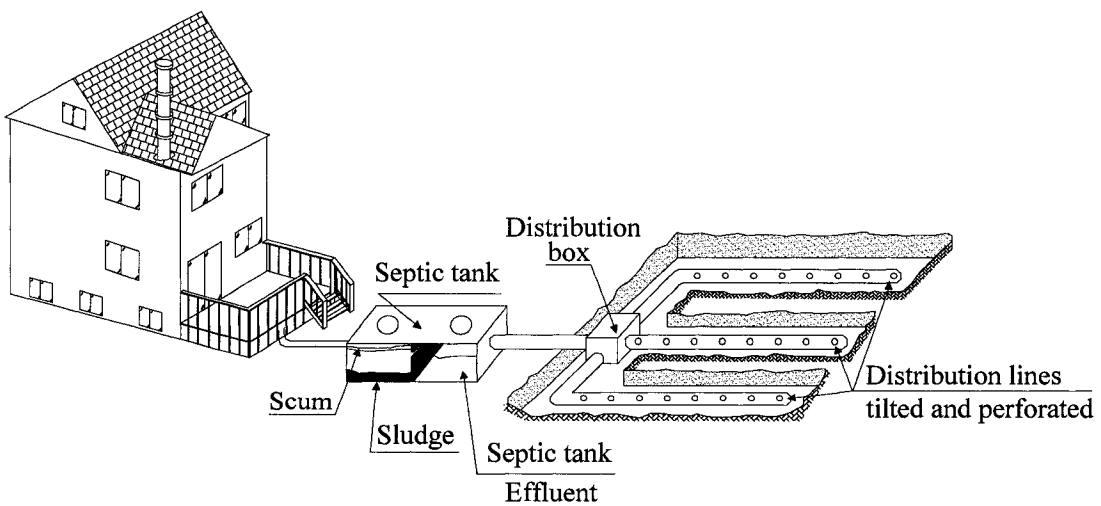

Figure 2.1- Schematic diagram for a conventional septic tank system

Reproduced with permission of the copyright owner. Further reproduction prohibited without permission.

Biological treatment is considered the dominant treatment mechanism for septic tank effluent. As discussed previously by Rice (1974) and due to the biological treatment process, bioclogging can occur and home owners may experience return flow in their septic tanks. One of the reasons for this problem is that the drainage field and/or subsurface soils clog due to microbial activity and can no longer conduct flow. The result is septic system failure.

2.2 Code Regulations, Ontario Building Code

Besides conventional septic systems, the OBC specifies other treatment units, which can be used to treat septic tank effluent, that were previously approved by the Ministry of Environment (MOE). The OBC specifies the effluent quality from those treatment units to have certain Biochemical Oxygen Demand (BOD_5), Carbonaceous Biochemical Oxygen Demand ($CBOD_5$), and Total Suspended Solids (TSS) as shown in Table (2.1).

Table 2.1- Maximum allowable concentration from sewage treatment units approved by MOE (Ontario Building Code (2006))

Effluent Characteristics	Effluent Concentration [1]
BOD_5, mg/L	15.0
$CBOD_5$, mg/L	10.0
TSS, mg/L	10.0

[1] Concentrations are based on the maximum values averaged over 30 days in mg/L

The following subsection gives two examples of two treatment units, approved by the MOE, that do not use sand soil as the treatment medium (i.e. peat soil and synthetic material) (OBC, Supplementary Standard SB-5 (2006)).

Reproduced with permission of the copyright owner. Further reproduction prohibited without permission.

2.2.1 Peat Filter

Peat is largely organic matter that consists of partially decomposed leaves, seeds, and plant roots. Ecoflo ® biofilters in Canada and Puraflo peat biofilters in the US use sphagnum peat as the filter media for their biofilters.

When septic tank effluent (STE) is distributed on the peat filter, three treatment mechanisms occur within the soil (i.e. physical filtration and adsorption, chemical adsorption and ion exchange, and biodegradation). After the effluent percolates thought the peat soil, it percolates through a crushed stone layer, as in Ecoflo ® biofilters, and then enters the native soil below. Figure (2.2) illustrates a cross section of an Ecoflo peat biofilter with typical dimensions, and Table (2.2) provides an average estimation of the effluent characteristics for both Ecoflo and Puraflo peat biofilters.

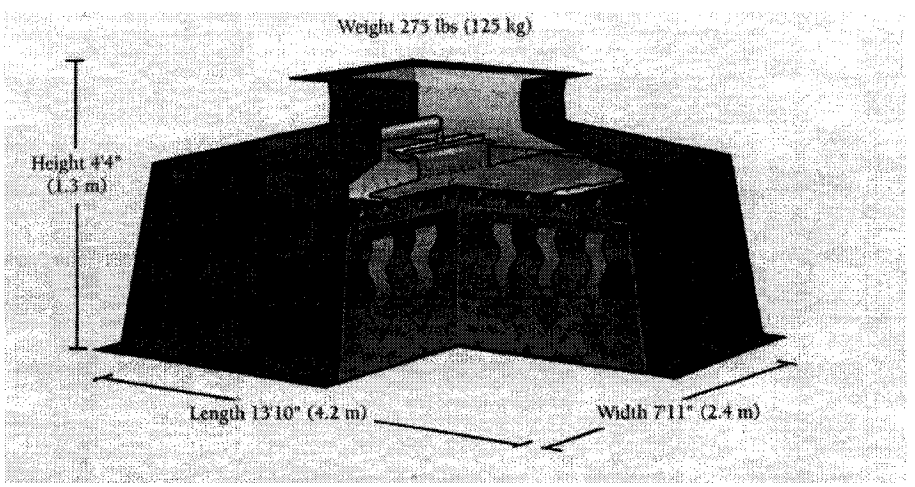

Figure 2.2- Typical cross section for an Ecoflo ® biofilters (Source: http://www.ecofloontario.com/biofilter_files/ecoflo_biofilter.htm)

Reproduced with permission of the copyright owner. Further reproduction prohibited without permission.

Table 2.2- Effluent characteristics for Ecoflo and Puraflo peat biofilters, Wastewater Virtual Trade Show Technologies, United States Environmental Protection Agency

Effluent Characteristics	Ecoflo Peat biofilter		
	Influent	Effluent	% Reduction
BOD, mg/L	≤250	≤10	95%
TSS, mg/L	≤75	≤10	90%
Fecal Coliforms, CFU/100mL	≤2,000,000	≤25,000	99%
	Puraflo Peat biofilter		
	Influent	Effluent	% Reduction
BOD, mg/L	280	<10	96%
TSS, mg/L	190	<10	95%
NH_3-N, mg/L	50	<5	90%
Total Coliforms, CFU/100mL	3,900,000	6,000	99.9%
E.Coli, CFU/100mL	910,000	760	99.9%

2.2.2 Biofilters with Synthetic Materials

One of the synthetic materials that is used as a filter media and has been used in residential biofilters is an open-cell foam material used in the Waterloo Biofilter. Figure (2.3) shows a cross section in this material.

The material of the biofilter media in the Waterloo Biofilter provides a large surface area and high porosity. Also, due to the heterogeneity of the foam particles in the filter (2"-3" cubes), it allows air flow paths that enhance the degradation by maintaining aerobic versus anaerobic conditions throughout the depth of the filter.

In a recently published report by Scherger Associates in coorperation with Barnstable County Department of Health and Environment under a cooperative agreement with the U.S. Environmental Protection Agency (Waterloo Biofilter Systems, Inc., April 2003), they reported septic tank effluent characteristics for different individual residential homes in Massachusetts, US over a thirteen month period. The tests were

Reproduced with permission of the copyright owner. Further reproduction prohibited without permission.

conducted at the Otis Air National Guard Base in Bourne, Massachusetts, US. Table (2.3) summarizes the effluent characteristics for their study.

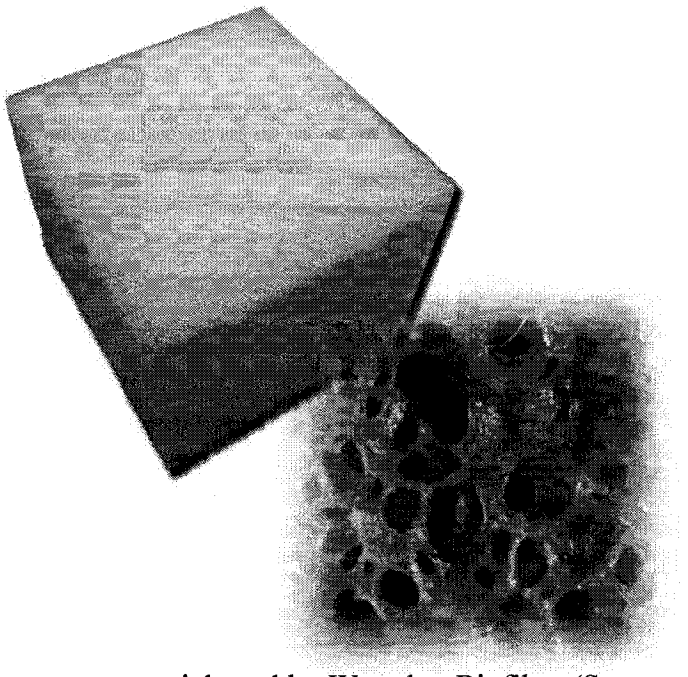

Figure 2.3- Foamy texture material used by Waterloo Biofilter (Source: http://www.waterloo-biofilter.com/)

Table 2.3- Effluent characteristics from Waterloo biofilters (Source: http://www.nsf.org/business/water_quality_protection_center/pdf/Waterloo_Biofilter_EPAAcceptedFinalReport.pdf)

Effluent Characteristics	Waterloo biofilter	
	Influent	Effluent
BOD, mg/L	210	10.0
TSS, mg/L	150	7.0
TKN, mg/L	37	3.7
NH_4, mg/L	23	2.4
TN, mg/L	37	14.0
Nitrate, mg/L	N/A	10.0
Nitrite, mg/L	N/A	0.19
Temperature, ^{o}C	N/A	15.0

Reproduced with permission of the copyright owner. Further reproduction prohibited without permission.

2.3 Conceptual Framework for Microbial Growth in Saturated Soils

Saturated soils can be represented by three phases; mobile water, immobile water, and solid phase (Figure (2.4)). In cases where bacteria are present, an additional fourth phase is present, which is the biomass layer as shown in Figure (2.4) (Baveye and Valocchi (1989)). Baveye and Valocchi (1989) present three conceptual frameworks that were developed by previous researchers to mathematically simulate the bacterial growth and the biological degradation of solutes in saturated porous media.

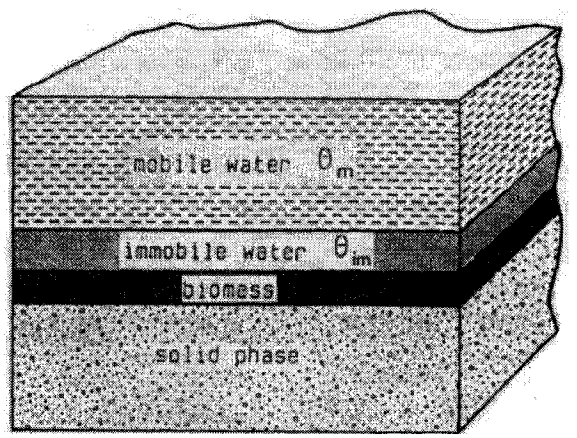

Figure 2.4- Schematic representation for saturated soil phases, adapted from Baveye and Valocchi (1989)

The first conceptual framework was based on Monod's contribution in which bacterial growth was simulated from a macroscopic point of view. It was referred to as the strictly macroscopic model by Baveye and Valocchi (1989) or Monod's model by Odencrantz et al. (1990). No assumptions related to the bacteria distribution and configurations within the pore space are made and the biodegradation kinetics are driven by the bulk concentration of the substrate added to the system (Baveye and Valocchi (1989); Odencrantz et al. (1990)). Therefore, in simple terms, this conceptual way of

Reproduced with permission of the copyright owner. Further reproduction prohibited without permission.

thinking assumes a direct relation between the bacterial growth and the macroscopic soil properties.

The second conceptual framework, which was contributed by Molz et al. (1986), assumes that the bacteria cells grow in discrete colonies, termed microcolonies, of 10 to 100 organisms attached to the solid particles (Baveye and Valocchi (1989); Odencrantz et al. (1990)).

These colonies were assumed to have a defined shape of cylinders with a defined radius and thickness. A diffusion boundary layer of certain thickness was assumed to separate the biomass from the bulk liquid (Molz et al. (1986); Baveye and Valocchi (1989); Odencrantz et al. (1990)). By assuming a number of cylindrical colonies, Molz et al. (1986) assumed that the biomass growth in a porous medium occurred by allowing the number of colonies to increase or decrease depending on the substrate concentration or mass present and the electron acceptor utilized (Baveye and Valocchi (1989), Figure (2.5)).

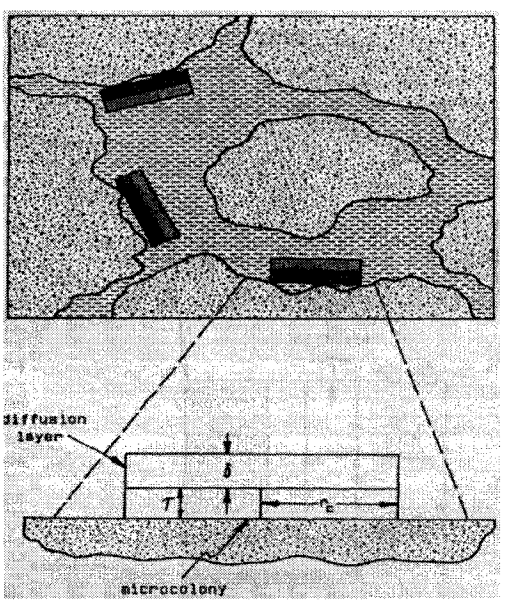

Figure 2.5- Second conceptual framework, adapted from Baveye and Valocchi (1989)

Reproduced with permission of the copyright owner. Further reproduction prohibited without permission.

The third conceptual framework, which was represented by Williamson and McCarty (1976a) and Rittmann and McCarty (1981) and named the biofilm model, assumes that the bacteria cells are covering the solid surface uniformly with a film of uniform thickness. This film is assumed to have a certain density and constant surface area per unit volume (Baveye and Valocchi (1989); Odencrantz et al. (1990)). Also, this film isolates the solid from direct contact with the bulk liquid as the bulk liquid will be only in contact with the biomass which is in contact with the solid particles (Figure (2.6)).

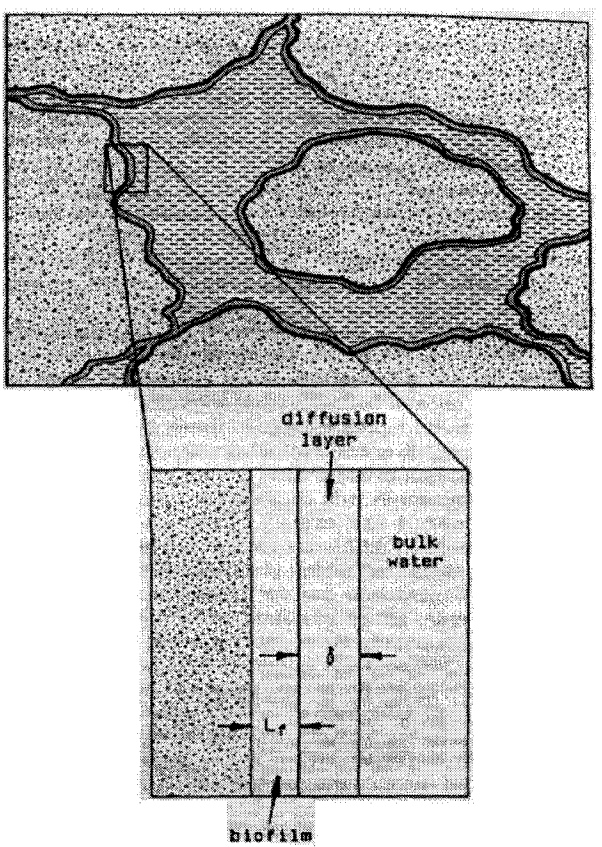

Figure 2.6- Third conceptual framework, adapted from Baveye and Valocchi (1989)

Reproduced with permission of the copyright owner. Further reproduction prohibited without permission.

2.4 Biological Clogging in Saturated Soils

Many research studies have been conducted to study the effect of clogging in saturated flow systems. This section is used to highlight some of those studies. Also, Table (2.4) summarizes those studies used in this section and the type of clogging they discussed.

Some of those studies proposed conceptual models that describe clogging in saturated soils (e.g. Okubo and Matsumoto (1979); Oberdorfer and Peterson (1985); Taylor and Jaffé (1990a); Taylor et al. (1990); Taylor and Jaffé (1990b)) while others presented experimental evidence for clogging without any theoretical explanations (i.e. Allison (1947); McCalla (1950); Frankenberger et al. (1979)).

Table 2.4- Summary of the references used in this section and which effect on clogging they studied

Effect	Reference
Biological clogging	Allison (1947); McCalla (1950); Frankenberger et al. (1979); Okubo and Matsumoto (1979); Okubo and Matsumoto (1983); Oberdorfer and Peterson (1985); Taylor and Jaffé (1990a); Taylor et al. (1990); Taylor and Jaffé (1990b); Seki et al. (1998)
Physical clogging, suspended soils	Allison (1947); McCalla (1950); Oberdorfer and Peterson (1985)
Gas generation, entrapped air	Oberdorfer and Peterson (1985); Seki et al. (1998)
Temperature	McCalla (1950)

Allison (1947) studied the causes of permeability reduction in soils under saturated conditions. A series of column experiment were conducted on three soils from different locations in California. The soils used contained organic matter (i.e. not clean). Tap water was also used to continuously submerge the experimental columns.

Reproduced with permission of the copyright owner. Further reproduction prohibited without permission.

Allison (1947) noticed a reduction in the permeability at the beginning due to swelling or the transport of particles over time. Then a noticeable increase in the permeability occurred after the entrapped air was removed. Then a large reduction in the permeability occurred until the soil clogged. Allison (1947) concluded that the clogging occurred due to microbial growth since the soils contained organic matter and the tap water was not bacteria free.

To confirm this conclusion, Allison (1947) started a second set of column experiments with sterile columns. The soils used in this column experiment were sterilized. Distilled water was also used to submerge the columns. Mercuric chloride was added to the distilled water to make sure that the water used was bacteria free.

Allison (1947) did not notice any permeability reduction compared to the first set of column experiment. The second set of column experiments proved the conclusion Allison (1947) had drawn previously that the soil clogging occurred due to microbial activity and not due to soil particle movement or any other physical causes. Allison (1947) did not give any microscopic or macroscopic explanation of how the microbial activity affects the permeability reduction of the soils.

McCalla (1950) conducted a series of column experiments to evaluate the microbial effect on saturated silty clay loam at different temperatures. Twelve columns were used in this experiment and they were kept under saturated conditions. Sucrose was used as the organic source and was added with tap water at a concentration equal to 2% by mass (i.e. 20,000 mg/L). Six columns were kept in a refrigerator at approximately 7 °C (45 °F) and the rest at room temperature. McCalla (1950) noticed that the effective hydraulic conductivity of the columns that were kept at room temperature was low due to biological

Reproduced with permission of the copyright owner. Further reproduction prohibited without permission.

clogging. However, the other six columns kept in the refrigerator maintained a higher effective hydraulic conductivity when exposed to the same organic load (McCalla (1950)). McCalla (1950) also noted that there was an increase in microbial growth in response to an increase in sucrose loading when additional sucrose was added to the columns at room temperature. McCalla (1950) concluded that the room temperature was favourable for the microbes to grow versus the refrigerator temperature. Also, there was other evidence associated with the microbial growth, which was gas generation. The results were confirmed with different types of soils and different types of organic sources. McCalla (1950) attributed the reduction in the soil conductivity caused by the bacteria to two reasons. The first reason was that the microbial products (e.g. gas, colloids, extracellular polymers, etc.) can restrict the water movement. The second reason was that microbial growth can disturb the soil structure due to decomposing or biodegrading the organic content.

Although McCalla (1950) assumed that biological clogging will occur due to the two reasons he identified, no assumption as to the shape or form of the microbial growth was given or proposed.

Frankenberger et al. (1979) conducted laboratory experiments to study the effect of microbial growth on the hydraulic conductivity of a soil under saturated conditions, to look at the effect of nutrients and energy source on clogging, and to study the relationship between bacteria population and the hydraulic conductivity of soils. Frankenberger et al. (1979) reported the same trends in permeability reduction as Allison (1947) noticed. Frankenberger et al. (1979) noticed an initial decrease in the permeability due to swelling or movement of particles followed by an increase due to removal of trapped air and a

Reproduced with permission of the copyright owner. Further reproduction prohibited without permission.

subsequent decrease in the permeability due to accumulation of microbial products. They also mentioned that the biological clogging was dependent on many factors such as the bacterial population, biological activity and nutrients, and energy sources supplied (Frankenberger et al. (1979)). Moreover, they showed, using statistical analysis, that there is a highly significant relationship between hydraulic conductivity and bacteria counts with a negative correlation (i.e. decrease in hydraulic conductivity associated with increase in bacteria count).

Okubo and Matsumoto (1979) investigated the relation between the actual infiltration rate and biological clogging under saturated conditions. They conducted an experiment on three saturated sand columns. The substrate used was added continuously during the experiment. Okubo and Matsumoto (1979) noticed that the dissolved oxygen level decreased rapidly at a depth of 2 cm from the top of the columns after the first 15 days of substrate dosing and became less than 1 mg/L. It increased again slightly after 26 days and became slightly more than 1 mg/L. At 5 cm depth, the dissolved oxygen concentration decreased rapidly as well but it increased rapidly later on from 1.4 to 5.9 mg/L during the first 15 days and it reached a constant level after 26 days. They suggest that the aerobic microbial growth was the reason for this dissolved oxygen concentration reduction at the surface layer for the first 15 days. They also noticed a variation in the infiltration rate and they explained it in four stages. In the first stage, the infiltration rate decreased rapidly with the reduction in the dissolved oxygen which was due to aerobic microbial growth in the first 10 days. In the second stage, the infiltration rate was almost constant or increased slightly as the aerobic microbial growth was limited by the limited dissolved oxygen provided between the 10th day and the 20th day. The reduction in the

Reproduced with permission of the copyright owner. Further reproduction prohibited without permission.

dissolved oxygen caused the biodegradation to decrease and the microbial population to decrease as a result. In the third stage, the infiltration rate decreased rapidly again as anaerobic microbial growth took place in the surface layer between the 20th day and the 30th day and during this period, the biological clogging developed under anaerobic conditions. The last stage started from the 30th day and they noticed a slower decrease in the infiltration rate. They recommend at that point, if the case was a real groundwater recharge system, to remove the potential clogged surface layer before the infiltration rate starts to decrease in the last stage (Okubo and Matsumoto (1979)).

Okubo and Matsumoto (1979) also developed an interesting model to simulate biological clogging. The model development was based on Hagen Poisseuille's law. They simulated the voids as bundles of straight circular capillary tubes with the same diameter. The analysis of this model was based on two assumptions. First, the capillary tube diameters will become narrow uniformly as the biological clogging develops and the second assumption is that the reduction in the porosity is proportional to the accumulative discharge (Okubo and Matsumoto (1979)). Although Okubo and Matsumoto (1979) assume that the microbial growth will be uniform in the capillary tubes; no details were given as to how the change in the capillary tube diameters can be calculated due to microbial growth. Also, their model is limited to uniform soils (i.e. based on the assumption of having capillary tubes with the same diameter).

An extension of Okubo and Matsumoto's research was conducted in 1983 when they investigated the biological clogging during artificial groundwater recharge (Okubo and Matsumoto (1983)). They divided the biological clogging into three stages. The aerobic

Reproduced with permission of the copyright owner. Further reproduction prohibited without permission.

period, the transition period, which is a transition between aerobic and anaerobic, and the anaerobic period.

Also, they divided the infiltration rate into three stages according to the changes in water quality, head losses, and hydraulic conductivity of the soil. The infiltration rate decreased rapidly during the first 10 days due to microbial growth as indicated by the rapid reduction in the dissolved oxygen. Then the infiltration rate increased slightly in the following 10 days as the microbial growth became limited by the dissolved oxygen provided (transition period). After the 21st day the infiltration rate decreased rapidly again due to microbial growth under anaerobic conditions. These three stages led to the same conclusions as their 1979 study.

Oberdorfer and Peterson (1985) reviewed the most significant causes of clogging from previous field studies conducted in aquifers. The major cause of clogging in the long term was due to the suspended solids associated with the injected substrate to the well. The second major cause of clogging is due to microbial growth at the face of the injection well and surrounding the injection area where microbes are in contact with the substrate injected. The presence of chemical processes had less impact on soil clogging. Also, clogging might occur due to entrapped air and bubbles from gas generated by the injection process.

Oberdorfer and Peterson (1985) considered those conclusions when conducting their experiment. They proved that these conclusions were less relevant for the study they proposed in the Hawaiian environment where they conducted their experiment. Oberdorfer and Peterson (1985) injected a secondary treated sewage effluent into a medium carbonate sand aquifer to study the causes of clogging. They found that the long

Reproduced with permission of the copyright owner. Further reproduction prohibited without permission.

term clogging was not due to suspended solids, which contradicts with what they found in the literature. They found that the short term reduction in permeability in the first few days of injection was due to the suspended solids. At this point, the microbial cells had not started to grow yet and thus could not biodegrade the substrate added to the environment. After a few weeks, when microbes started to grow and establish colonies, two major changes had occurred. First, a noticeable decrease in the substrate suspended solids due to replication of microbes that removed much of the clogging that took place during the first few days. Second, the denitrifying bacteria became well established and produced nitrogen gas in the zone near the injection well and fewer amounts of those bacteria were found far from the injection location. Oberdorfer and Peterson (1985) repeated the injection to support their conceptual description of the clogging scenario. However, they mentioned that this is not the only possible scenario and further investigations should be conducted.

Taylor and Jaffé (1990a) conducted an experiment on a sand column to relate the permeability reduction with biological growth. They used methanol as a substrate and assumed the biofilm conceptual framework to simulate the biomass growth. Taylor and Jaffé (1990a) suggested that one of two physical models they proposed might be the cause of the permeability reduction. The first one was the closed pore model where they allowed the biomass to grow and fill the entire pore space of the medium. By this way, water will be assumed to flow through the biomass layer itself. Using this assumption, the soil permeability is allowed to vary between a maximum value, when there is not biomass in the pores, and a minimum value, when all the pores are filled with biomass. Taylor and Jaffé (1990a) realized that if this is the case, the biofilm model that was first

Reproduced with permission of the copyright owner. Further reproduction prohibited without permission.

proposed by Williamson and McCarty (1976a) would not be applicable anymore. Taylor and Jaffé (1990a) suggested this model because it explained the measured constant permeability in the first 8 to 20 cm of their column. The second physical model suggested by Taylor and Jaffé (1990a) was the open pore model where they assumed a biofilm model in which the fluid shear stress will increase with the reduction in the medium permeability. The fluid shear stress will shear mass from the biofilm layer to keep the pore space open to conduct water. As the biofilm grows and the pore space decreases, the shear stress and velocity of the water will increase at the water-biofilm interface. When steady state is reached, a critical shear stress value will be reached as the rate of biomass removal due to shear will balance the net biofilm growth. At this point, the permeability will reach a constant level as they observed in the column experiment. Also, the biofilm will act as a second solid phase and this has to change the pore geometry and the dispersivity as well. Taylor and Jaffé (1990a) concluded that biological activities will tend to reduce the permeability of the porous medium by three orders of magnitude. They also concluded that the open pore model was a logical conceptual model to express the reduction in the permeability and that the physical models are important to conceptualize the relationship between the biomass growth and reduction in permeability.

As an extension to their work, Taylor et al. (1990) proposed an analytical estimation of the permeability reduction caused by the biofilm growth in porous media. Taylor et al. (1990) mentioned that although this was applied to saturated flow, a straightforward extension can be made for unsaturated flow. Three assumptions were made; the first assumption was that the soil was saturated with a single fluid, the second was to assume steady state flow, and the final assumption was to neglect the biofilm permeability.

Reproduced with permission of the copyright owner. Further reproduction prohibited without permission.

Taylor et al. (1990) proposed a sphere model where they assumed that the porous media consisted of spheres of equal diameter and biological clogging occurred via the biofilm model. Based on this spherical model, they concluded that this clogging model was applicable only for homogenous and unconsolidated porous media. This model also has limitations regarding the biofilm thickness as it cannot take into account the change in biofilm thickness and only limited its calculations to thin biofilms.

Taylor and Jaffé (1990b) presented a model to solve the clogging problem in aquifers during an injection period of groundwater recharge with an effluent or limiting substrate or nutrient. The model described the fate and transport of the substrate and biomass in the aquifer and it took into consideration the transport, growth, and decay in both water and biofilm phases. While the problem was multidimensional, the general phenomena may be studied in a one-dimensional form (Taylor and Jaffé (1990b)). They calibrated the model using data provided by their experimental sand columns (Taylor and Jaffé (1990a)). Taylor and Jaffé (1990b) suggested that with pulse loading, the effect of the clogging process will be limited. Also, in this study, Taylor and Jaffé (1990b) used the biofilm conceptual framework and they concluded that future research should be conducted to study filtration and adsorption of microbes by the biofilm and to study the effect of the biofilm growth on the anisotropy of the soil.

Seki et al. (1998) conducted an experiment on three columns to verify the effect of bacteria and fungi on clogging, and reducing the hydraulic conductivity and infiltration rate of the soil in experimental columns. Three 5 cm diameter by 1 cm height columns were filled with a soil consisting of 15% clay, 35% silt, and 50% sand. The column height was chosen to be very small because previous studies mentioned that biological

Reproduced with permission of the copyright owner. Further reproduction prohibited without permission.

clogging occurred within the first centimetre from the inlet of the injected substrate or nutrient (Rice (1974)). Glucose solution was used as the substrate in one of the columns. The other two columns were dosed with glucose and different solutions to kill the bacteria in the second column and kill the fungi in the third column.

Seki et al. (1998) concluded that when fungi were killed, bacteria clogged the pores and vise versa. Microbial clogging was faster than fungal clogging which suggested that the fungi grew more slowly than bacteria. The volume of biogas produced by the bacteria reached its maximum value after 103 days from the time they added the glucose. The amount of gas produced blocked the water path which results in a reduction in the hydraulic conductivity. They concluded that the main two reasons for the hydraulic conductivity reduction were biological clogging and gas generation.

As discussed previously, researchers agreed that short term clogging is due to accumulation of suspended soils (McCalla (1950); Oberdorfer and Peterson (1985)), entrapped air (Allison (1947); Oberdorfer and Peterson (1985)) and other factors, while the long term clogging is usually due to microbial growth (Allison (1947); Frankenberger et al. (1979); Okubo and Matsumoto (1979)). Also, many conceptual models were found in the literature that attempt to conceptualize the bioclogging process in saturated soils (Okubo and Matsumoto (1979); Taylor and Jaffé (1990a); Taylor et al. (1990); Taylor and Jaffé (1990b)).

2.5 Biological Clogging in Unsaturated Soils

Researchers indicated that there is a lack of understanding in the relation between biological clogging process and soil properties in unsaturated soils (e.g. Rockhold et al.

Reproduced with permission of the copyright owner. Further reproduction prohibited without permission.

(2002)). Moreover, limited research has been conducted to conceptually relate the microbial growth with the hydraulic conductivity in unsaturated soils. Mainly, researchers have focused on laboratory/field works to study the effect of septic tank effluent on filters (e.g. sand filters). Other researchers focused on the impact of the developed biomat layer on the infiltration rate in septic drainage fields (i.e. soil absorption systems) in two ways; either experimentally with no mathematical or conceptual explanations (e.g. Schwager and Boller (1997)), or conceptually with no experimental evidence (e.g. White and West (2003)).

Rockhold et al. (2002) reviewed some of the earlier research conducted on microbial growth and its impact on the hydraulic properties of porous media. They found that most of the research was focused on saturated porous media and that this issue was not fully addressed in unsaturated soil systems. Rockhold et al. (2002) discussed the characteristics of unsaturated soil systems that might be important when modeling the microbial growth. Rockhold et al. (2002) concluded that microbial growth results in the reduction of the permeability and the porosity of soils. They claimed that the characteristics of the biomass that accumulated depended on the organic substrate added to the system, the loading rate of this substrate, the type of bacteria and the flow rate of the fluid.

Rockhold et al. (2002) mentioned that unsaturated soil systems are much more complex than saturated systems as the relative permeability and the water content are nonlinear functions of the capillary pressure. More difficulties are associated with the presence of the air/water interface in unsaturated systems in comparison with saturated systems.

Reproduced with permission of the copyright owner. Further reproduction prohibited without permission.

As bacteria metabolize the substrates added to the system, gas is generated and becomes entrapped. This process noticeably reduces the hydraulic conductivity in both saturated and unsaturated soil systems (Rockhold et al. (2002)).

Kristiansen (1981a) conducted an experiment using three trench sand filters (A, B, and C) to illustrate the relationship between clogging and the physical and chemical environment of sand filters. The experiment was conducted for 17 months from July 1976 until November 1977. Trenches A and C were loaded with septic tank effluent at a rate of 4 to 6 cm/day and trench B at a rate of 12 to 18 cm/day. The temperature was between 4 °C and 16 °C for trenches B and C and between 12 °C and 15 °C for trench A. Kristiansen (1981a) found that the septic tank effluent accumulated in the sand filters as they started to clog and ponding started to occur. Pond rates, expressed as the filter area covered by ponding over time, of 0.33, 0.27, and 0.16 m^2/month were found in trenches A, B, and C respectively. After 8 months from the beginning of the loading, the septic tank effluent ponds covered about 80%, 67%, and 40% of the filter surface area in trenches A, B, and C respectively. After 15 months, the entire top surface area of the filter was covered by ponding effluent in trenches A and B but only 75% of the top surface area was covered in trench C. Kristiansen (1981a) suggested that the temperature might have different effects in different phases of clogging. Raising the temperature may have little effect on the accumulation of suspended soils in the voids but it has a major effect in causing stickiness of small particles together that may clog the smaller soil pores (Kristiansen (1981a)).

Also, and as an extention to his previous study, Kristiansen (1981b) studied the change in microbial counts due to microbial growth. He concluded that the number of

Reproduced with permission of the copyright owner. Further reproduction prohibited without permission.

microbial cells increased from an initial amount of 10^6 to $10^7 - 10^8$ per gram of dry sand due to loading with septic tank effluent. No further discussion was given by Kristiansen (1981a) or (1981b) as how the microbial growth conceptually establishes itself in the void space of the tested sand soil and resulted in the noted clogging.

Childs and Collis-George (1950) developed a permeability model that relates pore size distribution with the permeability of unsaturated soils. This permeability model, termed cut-and-random-rejoin-model, assumes that the pore structure contains pores with various radii that are distributed randomly in the medium. Clement et al. (1996) used this cut-and-random-rejoin-model along with both van Genuchten and Brooks and Corey functions to develop expressions that model the reduction in permeability due to microbial growth. The developed expressions did not assume any specific pattern for the microbial growth and just estimate the average biomass concentrations (i.e. macroscopic expressions). Clement et al. (1996) compared their expressions with the expressions developed by Taylor et al. (1990) and found good agreement in estimating the reduction in porosity, permeability and specific surface area due to microbial growth in saturated soils.

Clement et al. (1996) mentioned that in reality, bacteria will grow first in discrete colonies then gradually expand to form a continuous biofilm layer covering the solid particles (Clement et al. (1996); Rittmann (1993)). Hence, the more general macroscale approach of how bacteria will grow is more realistic than the biofilm model. Also, Darcy's law and the soil properties used in modeling the transport process were based on a continuum scale, which matched the macroscale assumptions. Clement et al. (1996) also mentioned that it was a costly process to measure the biofilm thickness of the

Reproduced with permission of the copyright owner. Further reproduction prohibited without permission.

microcolonies in reality and these processes are always associated with experimental errors.

Schwager and Boller (1997) investigated the effect of pulse loading and biomass generation on solute and gas transport in sand filters both experimentally and numerically. In the numerical simulations, they used HYDRUS-1D, a one-dimensional finite element code that simulates flow and solute transport in unsaturated soils. The solute transport equation in HYDRUS-1D includes dispersion, molecular diffusion, adsorption, and first order decay.

Schwager and Boller (1997) constructed two limestone sand filters where each filter was 90 cm in depth, 50 cm in length and 7 cm in width. The filters were initially loaded with tap water followed by septic tank effluent during their operational life. Schwager and Boller (1997) observed that the majority of the biomass growth in the filters was in the top 10 cm with less growth in the following 20 cm and almost no growth noted in the rest of the filters' depth. They also reported the results of a sodium bromide (NaBr) trace breakthrough test conducted on those filters after they had been in operation for two years. They compared the trace test results with the results reported by Boller et al. (1993) for filters that contain the same type of sand but clean and found retardation in the breakthrough point and the trace peak concentration. They concluded that this retardation was due to the biomass growth in the top layers of the filters that significantly affected the hydraulic conductivity of the top layer. Schwager and Boller (1997) did not support their experimental work with any conceptual explanation of the biomass growth behavior (e.g. biofilm, microcolonies, etc.) which resulted in the noted clogging.

Reproduced with permission of the copyright owner. Further reproduction prohibited without permission.

Or (2002) provided an overview of microbial activities in unsaturated soils at the microscale. He looked at the physical processes and criteria affecting the environment of the microbial community. Also, he studied the effect of the microbial activities on the soil structure, ability of the soil to transport fluids, and soil pore space.

Or (2002) showed that at the microscale, the position and structure of the microbial colonies within the pore diameters will affect the diffusion and adsorption processes of substrates. Or (2002) claimed, based on the literature, that in microscopic observations of biological clogging systems, studies indicated that a continuous biofilm will be formed and cover the solid phase continuously or discrete microcolonies will be developed and clog the pore diameters randomly. Also, some observations that were made in a two-dimensional glass network used for a microscale model study showed that biomass will form both a biofilm covering the solid phase and discrete microcolonies that will be randomly distributed and clog the pore throats as well. Or (2002) also reported that the transformation to a state of endogenous decay will result in partial biofilm movement and recovery in the hydraulic conductivity.

Although Or (2002) studied microbial growth on a microscale level, no mathematical or analytical derivations were given to the shape or form of the microcolonies or the biofilm formation.

Spychata and Blazejewski (2003) conducted an experiment on a series of sand columns to study the conditions and factors that affect the clogging in fine sand with septic tank effluent. Twelve columns were dosed with 82 mm/day preliminary treated septic tank effluent. The outflows from the twelve columns were connected to a main outflow exit. A reduction in the total discharge rate from the twelve columns was

Reproduced with permission of the copyright owner. Further reproduction prohibited without permission.

observed over the experiment period (from August 2000 until March 2002) at the same running temperature of 20 °C. Only six columns remained unclogged until the end of the experiment (March 2002) but the rest were clogged after 480 days in December 2001.

Spychata and Blazejewski (2003) found from the vertical distribution of the organic matter that over 40% of all organic mass was found in the top 2.5 cm of the sand columns. The main reason for clogging was the high concentration of the microbial population in this upper soil layer. The clogging process was accelerated with more suspended solids which were larger in size versus the soil pores. These suspended solids tremendously reduce the number of sand pores contributing to flow in the top layer of sand filters. The experimental data given by Spychata and Blazejewski (2003) were not supported by any conceptual model of how the microbial population developed in the clogged layer (i.e. the top 2.5 cm of the sand columns).

As mentioned previously, other researchers have focused on studying the effect of biomat formation in septic tanks drainage fields (i.e. soil absorption systems) on hydraulic conductivity of unsaturated soils either experimentally or conceptually. Beach et al. (2005) stated that limited research has been conducted in the area of quantifying the reduction in hydraulic conductivity of the infiltrative layer (i.e. biomat) in soil absorption systems due to accumulation of suspended solids and microbial growth. Based on their literature search, Beach et al. (2005) defined the infiltration rate at steady state in soil absorption systems to be governed by four main factors; thickness of the biomat layer, the hydraulic conductivity of the infiltrative surface including biomat layer, ponding height on top of the infiltrative surface, and the hydraulic conductivity of the subsoil underneath the infiltrative layer. They defined steady state to be reached when a biomat

Reproduced with permission of the copyright owner. Further reproduction prohibited without permission.

layer is fully developed which allows a certain steady state infiltration rate via the biomat layer.

Beach et al. (2005) conducted one-dimensional sand column experiments to study the hydraulic properties of a developed biomat layer under different loading rates (i.e. four loading rates were chosen for their study). Each column was 60 cm in length and 15 cm in diameter. The columns were loaded with four different loading rates for 20 weeks. A falling head test was conducted twice on the columns; before loading the columns with the wastewater, and just before dismantling the columns. The falling head test was used to estimate the final saturated hydraulic conductivity of the soil in the columns which they termed "effective saturated hydraulic conductivity". The reason for that was because the measured saturated hydraulic conductivity accounts for the heterogeneity of the soil in the columns since the infiltration rate is function of both the flow in the biomat layer and the unsaturated soil underneath.

The moisture content was also measured at three different levels in each column below the potential developed biomat layer using Time Domain Reflectometry (TDR). The measured moisture content showed that the saturation ranged from 45 to 75% during the 20 week period of the columns' operation. The measured saturations showed that the subsoil underneath the biomat layer was unsaturated even though the biomat layer was saturated given that ponding was continuous when the columns reached the steady state defined by Beach et al. (2005). Beach et al. (2005) also showed how the measured saturation range values can be explained conceptually. Conceptually, the biomat layer has more fine particles compared to the subsoil layer. These fine particles generate a capillary barrier effect since the subsoil is overlaid by a saturated biomat layer and results in

Reproduced with permission of the copyright owner. Further reproduction prohibited without permission.

generating unsaturated conditions in the subsoil just underneath the biomat layer which agrees with the numerical simulations conducted by Beach and McCary (2003) as will be discussed later in the text. Beach et al. (2005) also showed that the hydraulic conductivity of a developed biomat can be simulated by a Horton-type equation assuming that the biomat layer is very thin and fully saturated. They assumed the biomat layer has an initial saturated hydraulic conductivity value to be the same as the saturated hydraulic conductivity for the subsoil layer. This initial saturated hydraulic conductivity value exponentially declined until it reached the effective saturated hydraulic conductivity value they obtained from the falling head test just before dismantling the columns. The fitting parameter for the Horton-type equation was obtained by fitting the Horton-type equation to their experimental data.

In another research effort by Beach and McCary (2003), they numerically studied the impact of a developed biomat layer at the infiltrative surface of a soil absorption trench on the saturation, flow velocity and ponding height of the unsaturated soil zone. They used HYDRUS-2D to simulate two-dimensional trench filled with two different types of soils (i.e. sand and silt) which was assumed to have a fully developed biomat layer on their base and sidewalls. They assumed the thickness of the biomat layer to be 3 cm at the base of the trench and 2 cm thickness at the sidewalls. They treated the biomat layer as if it is a soil layer that has a hydraulic conductivity, maximum water content, irreducible water content, and van Genuchten parameters. The saturated hydraulic conductivity of the biomat layer was assumed to be significantly lower than the simulated soils (i.e. sand or silt). The unsaturated hydraulic conductivity of the biomat layer was estimated to be the saturated hydraulic conductivity multiplied by the relative permeability of this biomat

Reproduced with permission of the copyright owner. Further reproduction prohibited without permission.

layer. The relative permeability of the biomat layer was estimated by Mualem's (1976) formula multiplied by an empirical parameter "l" that they assumed to be typically 0.5 based on Simunek et al. (1999). The top boundary condition was set to be a fixed pressure head since it simulates ponding in a clogged system and the bottom boundary condition was assumed to be zero pressure head gradient. All other boundaries were assumed to have zero flux boundary conditions. They ran the simulations until steady state conditions were reached which represents constant flow passing through the fully developed biomat layers on the base and the sidewalls of the trench.

Similar to Beach et al. (2005) assumptions, Beach and McCary (2003) argued that a sand or silt layer overlaid by the biomat layer develops a capillary barrier effect. Since continuous ponding was assumed on top of the biomat layer, the biomat layer was assumed to be saturated. Thus, a coarse unsaturated soil overlaid by a fine saturated soil with ponding on top generates a high gradient across the fine layer since the top of the biomat layer has positive pressure and the bottom of the biomat layer has negative pressure. Therefore, Beach and McCary (2003) argued that a gradient higher than unity was generated and the infiltration rate via the biomat layer exceeded the assumed saturated hydraulic conductivity of the biomat layer which supported the numerical simulation results. Although Beach and McCary (2003) and Beach et al. (2005) gave a helpful conceptual explanation of how the hydraulic conductivity of soil absorption systems was affected by biomass growth, neither of them gave any conceptual explanation of how the biomass established itself in the pore space of the soil that resulted in the generation of the biomat layer that they noticed after loading the soils with septic tank effluent.

Reproduced with permission of the copyright owner. Further reproduction prohibited without permission.

Beal et al. (2006) indicated that there is a lack in understanding of the relation between long term infiltration rate of soil absorption systems and the hydraulic conductivity of unsaturated soils which is function of the pore size distribution of soils. They conducted experimental work to reach a better understanding of how the hydraulic properties of a biomat layer are affected by different soils' pore structure and to assess whether the subsurface soils' hydraulic properties are important in the evaluation of the long term infiltration rate.

In their experiment, Beal et al. (2006) conducted column experiments with three different soil types. The soils were; river sand, oxisol, and vertisol and they were loaded with septic tank effluent at three different loading rates; 50, 35, and 8 $L/m^2/d$, respectively for a 16 month period. The river sand consisted of more than 95% sand, less than 5% silt, and less than 1% clay. Oxisol, which has a clay loam texture, was 10% sand, 9% silt, and 81% clay. Vertisol, which has a medium to heavy clay texture, was 10% sand, 48% silt, and 42% clay. The experimental columns were 105 cm in height with 100 cm soil height in each column and 15 cm in diameter. The columns were loaded daily with the previously mentioned rates until ponding occurred then loaded occasionally after that (i.e. 2-3 times per week) to maintain a ponding depth of 3 cm on top of all the columns. Suction was measured at three different levels below the developed biomat layer; at 2.5 cm, 5.0 cm, and 10.5 cm. Ceramic tensiometers were located permanently at each one of those levels and connected to water manometers to measure the suction.

From the experimental results, Beal et al. (2006) showed that initial subsurface soil properties affected the rate and time at which a biomat is generated but once the biomat layer is generated; its resistance dominated the infiltration rate in the system. They also

Reproduced with permission of the copyright owner. Further reproduction prohibited without permission.

showed that river sand and oxisol soils, which are more permeable than the vertisol soil, had higher potential to accept a higher loading rate for a longer period of time. Hence they concluded that in the field, soil absorption systems constructed in soils with high saturated hydraulic conductivities will tend to be smaller in size and accept more septic tank effluent compared with soil absorption systems constructed in soils with low saturated hydraulic conductivities. Beal et al. (2006) did not give any conceptual explanation of how biomass fills in the pores of the tested soils which resulted in the biomat formation.

White and West (2003) stated that a biomat layer that has developed on infiltrative surface of a trench in soil absorption systems significantly affects the hydraulic conductivity of drainage field and affects its infiltration rate. Fines are another source which also contributes to the reduction in the hydraulic conductivity of a biomat layer. Fines can be found in gravel that is used in the construction of a conventional septic bed. They get washed out due to septic tank effluent flow and get retained at the infiltrative surface of a trench and hence lower the hydraulic conductivity.

White and West (2003) mentioned that typically a biomat layer will have saturated hydraulic conductivity lower than the saturated hydraulic conductivity of the soil underneath. If this biomat layer is saturated, it will not be able to sufficiently conduct flow to keep the soil underneath saturated. The saturation of the soil underneath will result in a hydraulic conductivity that is just enough to conduct the flow that passes through the biomat layer and hence remains at unsaturated conditions. This argument supported the discussion presented by Beach and McCary (2003) and Beach et al. (2005)

Reproduced with permission of the copyright owner. Further reproduction prohibited without permission.

where they showed an unsaturated soil zone developed underneath the biomat layer developed due to application of septic tank effluent.

Conceptually, White and West (2003) quantify the zones of conductivity in soil absorption trench systems to be five zones. From bottom to top they are 1) subsoil; 2) subsoil mixed with biomat; 3) gravel mixed with biomat and fines; 4) gravel mixed with biomat; and 5) gravel layer. Each zone of these five zones has its own properties and saturated hydraulic conductivity. White and West (2003) argued that the infiltration rate in the system is controlled by the lowest hydraulic conductivity of those layers. They assumed a hydraulic gradient of unity and assigned length and saturated hydraulic conductivity to each layer to calculate an effective saturated hydraulic conductivity which lumped all those hydraulic conductivities. They concluded that this effective saturated hydraulic conductivity was what the infiltration rate is a function of. On the other hand, Siegrist et al. (2004) argued that this method of calculating an equivalent saturated hydraulic conductivity in layered soil with vertical flow is adapted from saturated flow which is questionable when it is applied in unsaturated flow.

Siegrist et al. (2004) disagreed with White and West (2003) in the assumption they made for a unit hydraulic gradient in the five zone layers in their conceptual model. Siegrist et al. (2004) mentioned that ponding on top of a biomat layer will result in a positive pressure head at the surface of this layer and a negative pressure below it as shown by Beach and McCary (2003). They illustrated that the gradient might be greater than unity which violates the assumption made by White and West (2003). Siegrist et al. (2004) mentioned that the estimation of unsaturated hydraulic conductivity using the effective saturated hydraulic conductivity for layered system may be appropriate if the

Reproduced with permission of the copyright owner. Further reproduction prohibited without permission.

saturation of each layer is known and constant. The latter is invalid in trench systems where the saturation is discontinuous and changing with time during an infiltration event.

In his review about the evolving design of onsite soil treatment units, Siegrist (2006) defined the infiltrative zone to have three sequential/interactive processes which are related to microbial growth and hence he termed the infiltrative zone as "Biozone". At early stages and once a newly constructed drainage field is loaded with septic tank effluent, microbial growth occurs and nutrients are converted into biomass that forms biofilms. The developed biofilms might reach steady state after a certain period of time due to the stability between the biomass generation and degradation. The developed biofilms also extend to depths up to 30 cm or even further inside the soil.

As time elapses, a biomat may develop at the interface of the soil due to the increase in suspended solids filtration at the surface as well as the microbial growth which results in the formation of a biomat. The developed biomat limits the infiltration rate of the drainage field and may extend from few millimetres to few centimetres.

As shown from the previous review for biological clogging in unsaturated soils, limited research has been conducted to quantify the relation between biological clogging and hydraulic conductivity of unsaturated soils (e.g. Rockhold et al. (2002); Beach et al. (2005); Beal et al. (2006)). Researchers put forward some conceptual models at a macroscale (Clement (1996)) and microscale (Or (2002)). Also, experiment data showed that bioclogging due to microbial growth was the reason for the reduction in permeability of unsaturated soils (Kristiansen (1981a); Spychata and Blazejewski (2003)) along with other factors such as entrapped gas that was generated due to bacteria metabolism (Rockhold et al. (2002)). Researchers did not develop a complete conceptual model,

Reproduced with permission of the copyright owner. Further reproduction prohibited without permission.

which is based on mathematical derivation, for biological clogging in unsaturated soils similar to the models developed by Taylor and Jaffé (1990a), Taylor et al. (1990), and Taylor and Jaffé (1990b) for saturated soils and compared them with experimental/field data.

Mostafa and Van Geel (2007) developed three conceptual models which vary from microscopic scale to macroscopic scale and from analytically derived to empirical equations. The microscopic scale conceptual model was based on the assumption of a biofilm that covers the soil particles. The macroscopic scale models relate the growth of microbes with the relative permeability term and did not consider the distribution of the microbial growth at the microscopic scale. The three conceptual models, as described in details in the following subsection, were one of the limited attempts to relate the microbial growth with the relative permeability of unsaturated soils based on Burdine (1953) and Mualem (1976) relationships.

2.6 Conceptual Models for Microbial Growth in Unsaturated Soils

Mostafa and Van Geel (2007) proposed three conceptual models for bioclogging in unsaturated soils. The models were implemented in a one-dimensional numerical code in order to simulate the impact of the bacteria growth on flow in unsaturated soils. The proposed conceptual models varied in approach from macroscopic to microscopic and varied in form from analytical to empirical. The following subsection highlights the theory behind the models and the assumptions related to each model.

Reproduced with permission of the copyright owner. Further reproduction prohibited without permission.

2.6.1 Model #1

The voids in the unsaturated soil can be simulated as capillary tubes with different diameters; each diameter reflects a volume of void space that can be filled at a certain capillary pressure. Under unsaturated conditions, the smaller pores contribute to fluid flow. Since the biodegradable substrate will be in these smaller pores, one could assume that the microbial growth will occur in the smaller pores. Hence, when bacteria start to grow, the small diameter pores will be clogged first by the bacteria cells and the relative permeability will be reduced to compensate for the clogging of the smaller pores. As a result, the water content will increase to allow a corresponding increase in the relative permeability to conduct the same fluid flow and the flow will be displaced into the larger pores. Meanwhile, the bacteria in the larger pores will be in contact with nutrients and food and they will continue growing and displacing the flow to the larger pores. This process will take place until all the pores are filled with biomass and no more water can be conducted in the pores. Hence, the soil will be fully clogged (Figure (2.7)) (Mostafa and Van Geel (2007)).

Reproduced with permission of the copyright owner. Further reproduction prohibited without permission.

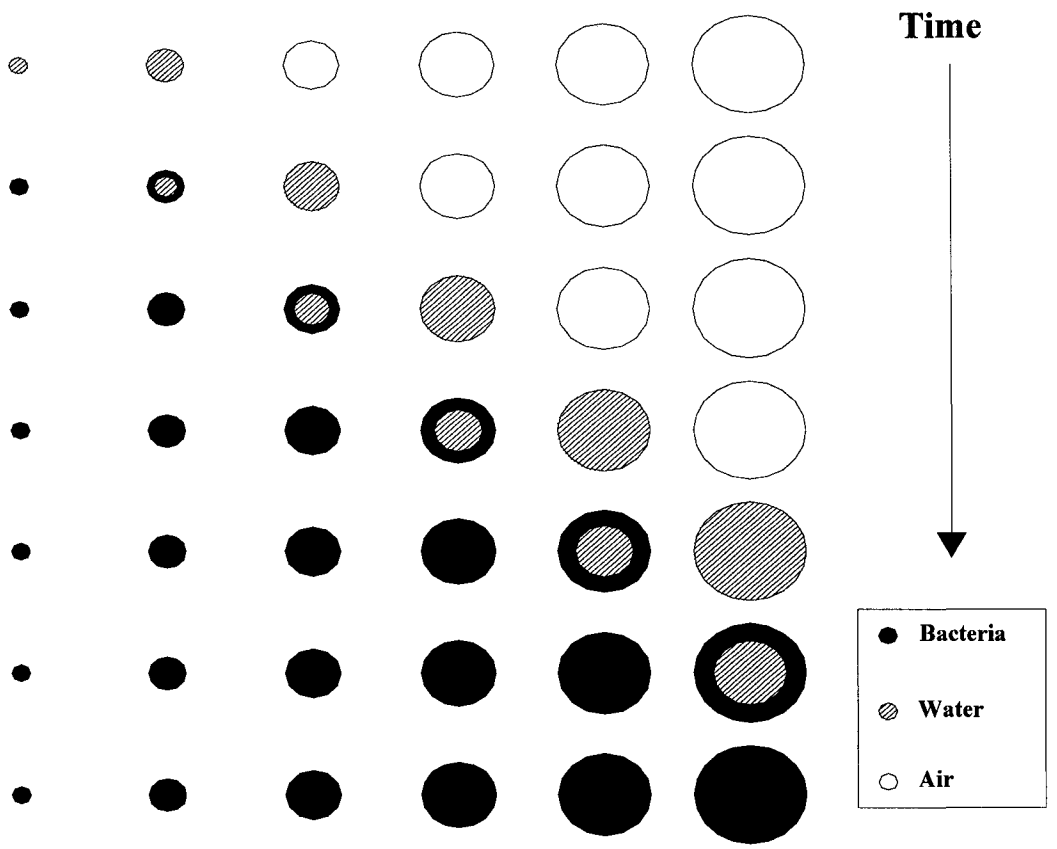

Figure 2.7- Visualization of Model #1

Based on the formulations put forward by Burdine (1953) and Mualem (1976) to estimate the relative permeability term, Lenhard and Parker (1987) proposed relative permeability terms for two-phase flow systems (e.g. water and air or non-aqueous phase liquid (NAPL) with fluid entrapment) and three-phase flow systems (water, NAPL, and air). For example, for a water-air system with air entrapment, they assumed that "*the presence of immobile air bubbles occluded by the water phase will result in an obstruction to water flow. Simultaneously, trapped air will displace water into larger pores which will tend to increase the water relative permeability at a given actual water saturation above that which would occur in the absence of air entrapment*" (Lenhard and Parker (1987)). To account for these effects they modified Mualem's equation to account

Reproduced with permission of the copyright owner. Further reproduction prohibited without permission.

for the impact of the entrapped air on the relative permeability of the water phase (k_{rw}) as follows;

$$k_{rw}(S_{aw}) = S_{aw}^{1/2}\left(\frac{\int_0^{S_{aw}} \frac{dS_{aw}}{\psi} - \int_0^{S_{trap}} \frac{dS_{trap}}{\psi}}{\int_0^1 \frac{dS_{aw}}{\psi}}\right)^2 \tag{2.1}$$

where they called S_{aw} the apparent water saturation and S_{trap} the effective entrapped air saturation.

Mostafa and Van Geel (2007) used a similar approach in Model #1 to account for microbial growth. They introduced an alternative integral form from Burdine (1953) or Mualem (1976) that takes into account the presence of a microbial saturation as follows;

For Burdine
$$k_r(S_{ew}) = S_{et}^2 \frac{\int_0^{S_{et}} \frac{dS_e}{\psi^2} - \int_0^{S_{em}} \frac{dS_e}{\psi^2}}{\int_{S_e=0}^1 \frac{dS_e}{\psi^2}} \tag{2.2}$$

For Mualem
$$k_r(S_{ew}) = S_{et}^{1/2}\left(\frac{\int_0^{S_{et}} \frac{dS_e}{\psi} - \int_0^{S_{em}} \frac{dS_e}{\psi}}{\int_{S_e=0}^1 \frac{dS_e}{\psi}}\right)^2 \tag{2.3}$$

Equations (2.2) and (2.3) express the relation between relative permeability and saturation taking into account microbial growth where the additional term $\int_0^{S_{em}} \frac{dS_e}{\psi^2}$ for Burdine and $\int_0^{S_{em}} \frac{dS_e}{\psi}$ for Mualem accounts for the effect of bacterial growth on the relative permeability term.

The closed form of the integral equations (2.2) and (2.3) are given as:

Reproduced with permission of the copyright owner. Further reproduction prohibited without permission.

For Burdine $$k_r(S_{ew}) = S_{et}^2\left(\left(1 - S_{em}^{1/m}\right)^m - \left(1 - S_{et}^{1/m}\right)^m\right) \quad (2.4)$$

For Mualem $$k_r(S_{ew}) = S_{et}^{1/2}\left(\left(1 - S_{em}^{1/m}\right)^m - \left(1 - S_{et}^{1/m}\right)^m\right)^2 \quad (2.5)$$

2.6.2 Model #2

Mostafa and Van Geel (2007) introduced a new term, (1 - S_{em}), and multiplied it by the original integration forms of Burdine and Mualem. This new term is used to reduce the relative permeability term by a factor to take into account the impact of microbial growth on relative permeability.

The new equations introduced by Mostafa and Van Geel (2007) for Model #2 were as follows;

For Burdine $$k_r(S_{ew}) = S_{ew}^2\left(1 - \left(1 - S_{ew}^{1/m}\right)^m\right).(1 - S_{em}) \quad (2.6)$$

For Mualem $$k_r(S_{ew}) = S_{ew}^{1/2}\left(1 - \left(1 - S_{ew}^{1/m}\right)^m\right)^2.(1 - S_{em}) \quad (2.7)$$

Mostafa and Van Geel (2007) stated that there was no experimental proof or theoretical derivation for this formulation. Model #2 is used to provide a quick estimation of the reduction in relative permeability due to microbial growth. Mostafa and Van Geel (2007) recommended that further experimental work needs to be done to confirm whether this second conceptual model is valid or not.

2.6.3 Model #3

The third model introduced by Mostafa and Van Geel (2007) was based on a microscale conceptual model. As discussed in Model #1, the unsaturated soil can be considered as a series of capillary tubes with different diameters. Equation (2.8) relates the capillary pressure in these tubes with the radius of the capillary tubes.

Reproduced with permission of the copyright owner. Further reproduction prohibited without permission.

$$P_c = \psi = \frac{2\sigma}{r} \tag{2.8}$$

where P_c or ψ is the capillary pressure, σ is the surface tension, and r is the radius of the capillary tube.

For unsaturated flow, the soil moisture curve is known and the pore size distribution can be inferred from this capillary pressure-saturation relationship. In Model #3, the pore distribution is determined or inferred from the soil moisture curve and the microbial growth is assumed to form a biofilm that covers the walls of the capillary tubes. For Model #3, the biofilm is assumed to form in all the pores since all the pores contain an irreducible water saturation in which the bacteria can grow. The reduction in the radii of the capillary tubes will increase the resistance to flow and reduce the permeability of those pores. Based on these assumptions, Model #3 was developed. A conceptual schematic of the model is provided in Figure (2.8) (Mostafa and Van Geel (2007)).

In developing this conceptual model, Mostafa and Van Geel (2007) used the capillary pressure-saturation relationship to determine the soil's pore size distribution. Mostafa and Van Geel (2007) rearranged the van Genuchten relationship to solve for capillary pressure as follows:

$$\psi = \frac{\left(S_e^{\frac{-1}{m}} - 1\right)^{\frac{1}{n}}}{\alpha} \tag{2.9}$$

To determine the distribution of radii for the bundle of capillary tubes representing the soil, Mostafa and Van Geel (2007) divided the saturation into a user-specified number of equal divisions. The average saturation at the midpoint of each division is then used to

Reproduced with permission of the copyright owner. Further reproduction prohibited without permission.

determine the corresponding capillary pressure. The capillary pressure is used to calculate the radius of the capillary tube.

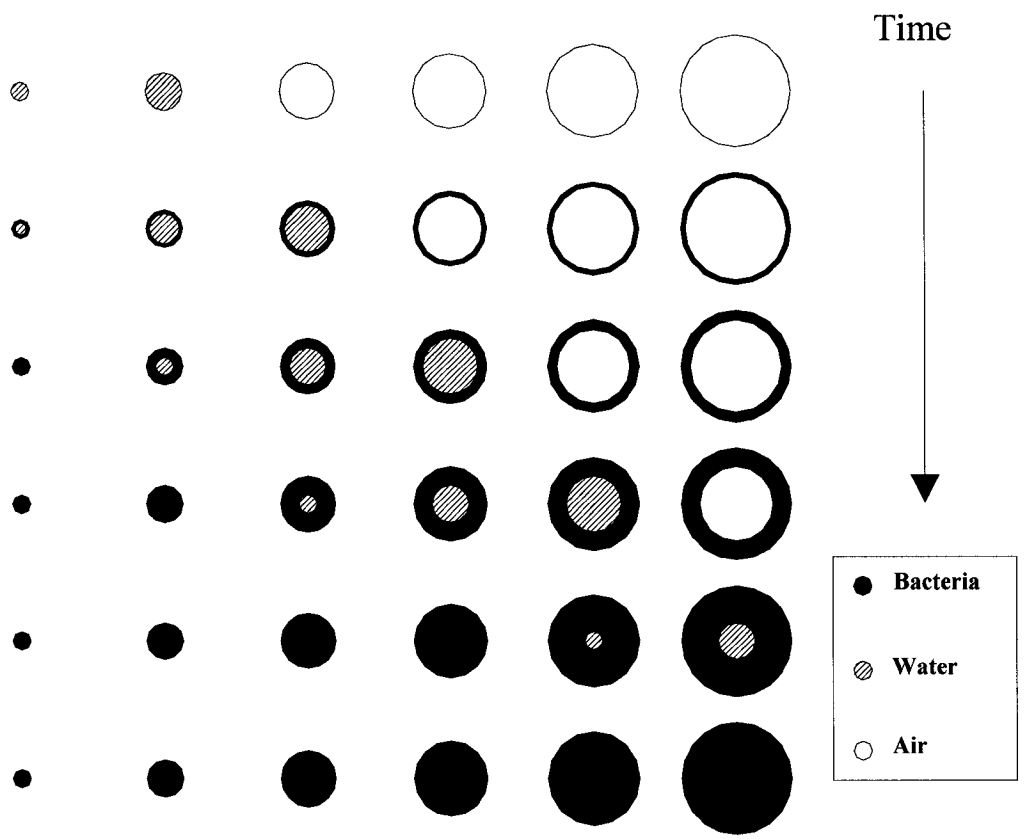

Figure 2.8- Visualization of Model #3

The number of capillary tubes within each division can be calculated by dividing the total void volume of each division (represented as a cross-sectional area) by the cross-sectional area of one capillary tube.

Once the distribution of capillary tubes is known, the microbial volume can then be distributed as a biofilm of uniform thickness, *th*, within the capillary tubes using the following equation,

$$\sum_{i=1}^{\#of\ divisions} \left(\#of\ Tubes_i .\pi .r_i^2 - \#of\ Tubes_i .\pi .(r_i - th)^2\right) = V_m \qquad (2.10)$$

Reproduced with permission of the copyright owner. Further reproduction prohibited without permission.

where V_m is the microbial volume.

Based on Hagen Poiseuille's derivation for laminar flow in a pipe and summing the flows within all the capillary tubes, Mostafa and Van Geel (2007) estimated a total flow using the following equation:

$$Q = -\frac{\sum_{i=1}^{\#of\ divisions} (\#of\ Tubes)_i\ \pi\ r_i^4}{8}\ \frac{\rho g}{\mu}\ \frac{\partial h}{\partial L} \tag{2.11}$$

as,

$$K(\theta) = K_{sat}\ k_r \cong \left(\frac{\sum_{i=1}^{\#of\ divisions} (\#of\ Tubes)_i\ \pi\ r_i^4}{8}\ \frac{\rho g}{\mu} \right) (k_r) \tag{2.12}$$

where r is the radius of the capillary tube, ρ is the density of the liquid, g is the gravitational acceleration, μ is the dynamic viscosity, θ is the volumetric water content, and ∂h/∂L is the hydraulic gradient along the flow path.

The presence of a biofilm will impact this flow and Equation (2.11) could be modified as follows:

$$Q = -\frac{\sum_{i=1}^{\#of\ divisions} (\#of\ Tubes)_i\ \pi\ (r_i - th)^4}{8}\ \frac{\rho g}{\mu}\ \frac{\partial h}{\partial L} \tag{2.13}$$

where *th* is the thickness of the biofilm layer.

Hence, to adjust the unsaturated permeability of the soil to account for the impact of the biofilm, a flow factor, U, is introduced and the ratio of the flow factors with and without the biofilm is used to reduce the relative permeability. The flow factor without the biofilm is expressed as:

Reproduced with permission of the copyright owner. Further reproduction prohibited without permission.

$$U_o\Big|_0^{Porosity} = \left(-\frac{\sum_{i=1}^{\#of\ divisions} (\#of\ Tubes)_i\ \pi\ r_i^4}{8}\ \frac{\rho g}{\mu} \right) \tag{2.14}$$

and with the biofilm, the flow factor is expressed as:

$$U_i\Big|_0^{Porosity} = \left(-\frac{\sum_{i=1}^{\#of\ divisions} (\#of\ Tubes)_i\ \pi\ (r_i - th)^4}{8}\ \frac{\rho g}{\mu} \right) \tag{2.15}$$

where $U_o\Big|_0^{Porosity}$ represents the initial flow without a biofilm for all the pores (i.e. zero through porosity) and $U_i\Big|_0^{Porosity}$ represents the reduced flow with a biofilm present in all the pores. The relative permeability term can then be reduced by a factor of $U_i\Big|_0^{Porosity}$ over $U_o\Big|_0^{Porosity}$.

Finally, the relative permeability saturation relationships that can be used to simulate this scenario for Burdine and Mualem are as follows:

For Burdine $$k_r(S_{ew}) = S_{ew}^2 \left(1 - \left(1 - S_{ew}^{1/m}\right)^m\right) . \left(\frac{U_i\Big|_0^{Porosity}}{U_o\Big|_0^{Porosity}} \right) \tag{2.16}$$

For Mualem $$k_r(S_{ew}) = S_{ew}^{1/2} \left(1 - \left(1 - S_{ew}^{1/m}\right)^m\right)^2 . \left(\frac{U_i\Big|_0^{Porosity}}{U_o\Big|_0^{Porosity}} \right) \tag{2.17}$$

Mostafa and Van Geel (2007) highlighted that at each time step, as the biofilm grows, the biofilm thickness increases. At a certain point, as shown in Figure (2.8), some radii will be filled by the bacteria and will no longer contribute to the flow. As a result, Equation (2.10) is modified with time to account for the capillary tubes which are filled.

Reproduced with permission of the copyright owner. Further reproduction prohibited without permission.

2.7 Bacteria Extraction and Counting

In granular soils, Ramsay (1984) discussed several methods that have been recommended for bacteria extraction; combination of blending, centrifuging, and ultrasonication (Balkwill et al. (1977)), shaking (Dale (1974)), and ultrasonication (Anderson and Slinger (1975); Weise and Rheinheimer (1979)).

Ramsay (1984) compared blending, shaking, and ultrasonication with the addition of Tris buffer as a dispersion agent to study bacteria removal from sandy and silt loam soils. Sand samples were collected 500 m inland from Hokio Beach in Manawatu, New Zealand, which had a pH of 6.9, organic carbon content of 1.25%, and total nitrogen of 0.09%. Also, silt loam samples were collected from Wellington, New Zealand and they had a pH of 5.7, organic carbon content of 6.2%, and total nitrogen of 0.43%.

The samples were shaken for 20 minutes on a wrist-action shaker at half of the maximum speed, or blended for 1 to 2 minutes at half of the maximum speed, or exposed to ultrasonic sound using a MSE 150 W Ultrasonic Disintergrator; probe diameter of 19 mm with different amplitude and time lengths.

Ramsay (1984) found that although ultrasonication extracted more bacteria from the sandy soil than shaking or blending (i.e. 77% bacteria removal in case of ultrasonication versus 72% in blending and 57% in shaking), there was no significant difference found between the three methods. Ramsay (1984) indicated that shaking would be more appropriate than blending where there is a large number of samples to process.

In the silt loam soil, ultrasonication was more effective in removing bacteria from the soil particles. Because silt loam tends to have small particles, shaking or blending

Reproduced with permission of the copyright owner. Further reproduction prohibited without permission.

were not able to separate bacteria cells from the small particles and hence ultrasonication gave higher counts.

Ramsay (1984) recommended that for ultrasonication, a range of amplitude of 10.5 μm for 30 seconds and 5 μm for 2 minutes should be chosen; otherwise the recovery of bacteria cells would decline. Also, using amplitude of 10.5 μm for 30 seconds was more highly recommended as 5 μm for 2 minutes will lead to greater damage of the cells. These results agree with Anderson and Slinger (1975) who used 4-6 μm for 2 minutes and they recommend that above 12 μm, cells will lyse and become damaged. Ramsay (1984) concluded that ultrasonication is a better method of extraction than shaking or blending if the amplitude and time of exposure are appropriate.

Khammar et al. (2004) studied the effect of the combination of physical and chemical methods for bacteria extraction from two biofilter packing materials, peat (Europe Environment, France) and activated carbon (IG 90, Carbio 12, France). Khammar et al. (2004) used shaking, blending, and ultrasonication along with 1% sodium-pyrophosphate (pH of 10.9), 1% sodium hexametaphosphate (pH of 6.4), and 200 mM phosphate buffer (7 mM Na_2HPO_4, 3 mM NaH_2PO_4, 0.13 M NaCl of a pH of 6.2 for the mixture).

Blending was conducted with an ultra-turrax (T25 basic, Ika) blender where three different testing scenarios were conducted with two different speeds; blending at a speed of 13000 rpm for 5 minutes with a stop of 1 second every 1 minute, blending at a speed of 13000 rpm for 1, 2, 4, and 5 minutes and blending for 5 minutes with speeds 11000, 13000, 16000, 22000, and 24000 rpm. Shaking was conducted with a vortex (Heidolph

Reproduced with permission of the copyright owner. Further reproduction prohibited without permission.

REAX 2000, Germany) with two different testing scenarios. In the first scenario, samples were shaken for 5 minutes with the maximum speed of 2400 rpm with a 1 second stop every minute and with the speed of 2400 rpm for 1, 2, 4, and 5 minutes duration. In the second scenario, ultrasonication was conducted in a sonifier bath (Branson sonifier bath, Energy). Ranges of exposure time of 0.5, 5, 30, and 60 minutes were used with the same output energy of 70 W (approximately 60 μm). In addition to the previous scenarios, Khammar et al. (2004) added glass beads (425-600 μm in diameter, G-8772, Sigma) to the three physical treatment methods to study the effect of having additional physical shearing.

Khammar et al. (2004) found that using glass beads to have additional physical shearing did not have any effect on the detachment of bacteria cells from the peat soil. They also found a difference between having a continuous and discontinuous treatment, in case of shaking and blending, but the difference was not statistically significant. Only ultrasonication showed a significant increase, close to 4 times higher in bacteria extraction between 0.5 and 60 minutes. In the case of shaking or blending, the maximum counting was found after 1 or 2 minutes and there was no significant increase in the counting after that.

Moreover, Khammar et al. (2004) found that treatment with 200 mM phosphate buffer or 1% sodium hexametaphosphate along with blending resulted in more bacteria counts versus using 1% sodium-pyrophosphate with blending. These results were in agreement with Lindahl and Bakken (1995). Lindahl and Bakken (1995) reported that as pH increases, metabolization of bacteria cells gets affected and hence cell numbering declines.

Reproduced with permission of the copyright owner. Further reproduction prohibited without permission.

Khammar et al. (2004) concluded that using either 200 mM phosphate buffer or, 1% sodium hexametaphosphate will have the same extraction efficiency versus 1% sodium-pyrophosphate but 1% sodium hexametaphosphate would be preferable because of its simplicity in preparation. They also concluded that a standard way of bacteria extraction from soil particles is difficult to define as each soil has its own properties and binding characteristics with bacteria cells.

Based on Ramsay's recommendations, shaking will be the method used in this research to separate bacteria from soils since a large number of samples will be processed, as will be discussed in the next chapter. Also, 1% sodium hexametaphosphate will be the dispersion agent that will be used in the bacteria separation process because its simplicity in preparation as discussed by Khammar et al. (2004).

2.8 Biofilm Characterization

One of the most challenging tasks of this research was to be able to model bioclogging. Bioclogging is not primarily due to the bacteria cells that occupy the pore space but due to the by-products of the bacteria that grow in the pore space. Subsection (2.2) presented a literature review on how researchers argued that bacteria cells may grow in discrete colonies or in a biofilm form. Clement et al. (1996) argued that in reality, bacteria will grow first in discrete colonies then gradually expand to form a continuous biofilm layer covering the solid particles (Clement et al. (1996); Rittmann (1993)). Moreover, some bacteria cells tend to live in cooperative interaction with each other (e.g. for substrate exchange) and the closer these cells are to each other, the easier that interaction becomes (Rittmann and McCarty (2001)). These attributes render the biofilm

Reproduced with permission of the copyright owner. Further reproduction prohibited without permission.

model most popular among contemporary researchers. This subsection presents a literature review of various researchers' characterizations of biofilm and its components.

2.8.1 Introduction

A review of the literature illustrates differences in the conceptual models developed by researchers that address the four main components of a biofilm; bacteria cells, Extracellular Polymeric Substances (EPS), inert biomass, and Soluble Microbial Products (SMP), which are defined later in the text. According to Laspidou and Rittmann's (2002a) critical literature review, two distinguishable "schools" of thought were found, the "EPS School" and the "SMP School". The SMP School considers active biomass, SMP (Soluble Microbial Products), and inert biomass but they do not consider any EPS in its analysis. The EPS School considers active biomass and EPS with no reference to SMP in its analysis. Laspidou and Rittmann (2002a) argue that each school uses terms that serve their interest. For example, the main interest of researchers that follow the SMP School is to study effluent quality and sludge production and hence they study SMP and inert biomass. On the other hand, researchers focused on EPS are more into studying the characteristics of biofilm and bacteria floc.

Due to the contradictions found in the literature, Laspidou and Rittmann (2002a) developed a unified theory that resolves the confusion between both schools and clarifies all the components that both schools used to represent biofilm components. In a series of papers, they presented the conceptual model of this unified model (Laspidou and Rittmann (2002a) and (2002b)). They formulated the unsteady state mass balance equations that describe the flow of electrons within the involved components and numerically coded the equations using a two-dimensional C++ finite difference code.

Reproduced with permission of the copyright owner. Further reproduction prohibited without permission.

Laspidou and Rittmann (2002b) and (2004a) compared their model results with experimental data published by Hsieh et al. (1994), Zhang and Bishop (1994), and Bishop et al. (1995) to validate their unified model.

2.8.2 Biofilm Structure

According to Laspidou and Rittmann (2002a), the four main components involved in a biofilm structure are active biomass, EPS, inert biomass, and SMP which is divided into Utilization-Associated Products "UAP" and Biomass-Associated Products "BAP".

Soluble microbial products (SMP), defined as soluble cellular biodegradable components that diffuse through the cell membrane, are released during cell lysis, or are lost during synthesis. SMP are important because they are present in excess and usually form the majority of the effluent biochemical oxygen demand (BOD) and chemical oxygen demand (COD) from biological treatment processes (Laspidou and Rittmann (2002a)).

Utilization-Associated Products (UAP) are produced directly during substrate metabolism as shown later in Figures (2.9) and (2.10 a&b). Biomass-Associated Products (BAP) are formed by dissolution or hydrolysis of EPS, which is the only source of generating BAP.

Dissolution of EPS from active cells occurs primarily due to sloughing. Laspidou and Rittmann (2002b) mentioned that according to Davies (1999) and Sutherland (1999), bacteria cells produce enzymes, which are responsible for dissolution of EPS, in parallel to EPS synthesis. These enzymes are produced but they do not come in contact with the synthesized EPS. If bacteria cells lyse, a "passive" release of these enzymes occurs that results in dissolution of the EPS at a steady state rate. Moreover, Davies (1999)

Reproduced with permission of the copyright owner. Further reproduction prohibited without permission.

highlighted two main reasons for an "active" release of these enzymes; first being the accumulation of CO_2/organic acids that lower pH value and the second being a cell density dependent regulation mechanism. Once bacteria cells reach a certain cell per biofilm volume density level, the cells release these enzymes. This release results in dissolution of EPS, which might result in liberating cells themselves from the EPS matrix. The active release of such enzymes is a cause of releasing EPS matrix to bulk flow without the help of fluid shear forces (Laspidou and Rittmann (2002a)).

Laspidou and Rittmann (2002a) mentioned that although EPS and SMP are not active cells, they are organic materials that contain electrons and carbon and the production of both EPS and SMP is important because the consumption of electrons and carbon affects cell yield and growth rate. The conventional thought is that electrons from electron donors are used to either generate biomass or used by electron acceptors to generate energy. If a significant portion of the electrons are used to form EPS and/or SMP, it will affect active biomass synthesis. Hsieh et al. (1994) showed that EPS production could be parallel and even exceed, as shown by Robinson et al. (1984), the production rate of new active cells. Hence if EPS and/or SMP formation is ignored, the active biomass growth will be overestimated.

Laspidou and Rittmann (2004c) found that what the SMP School called active biomass is actually a summation of active cells and bound EPS. Also, what the EPS School called soluble EPS is what the SMP School called SMP that contains UAP and BAP. This is how the unified model of Laspidou and Rittmann was able to eliminate any confusion between overlapping terms.

Reproduced with permission of the copyright owner. Further reproduction prohibited without permission.

2.8.3 Unified Model by Laspidou and Rittmann

Figure (2.9) shows a schematic diagram of the substrate fate in a biofilm system with all the involved components based on the unified model. From Figure (2.9), the following can be noted:

- Active biomass, contains active cells and bound EPS.
- Substrate utilization results in active cell synthesis, bound EPS synthesis, UAP formation, and energy production.
- Inert biomass contains part of the bound EPS and dead cell residue, which is produced as part of endogenous decay of biomass.
- All soluble EPS, or SMP, consist of UAP and BAP.
- The only way to form BAP is via hydrolysis of bound EPS.
- Both BAP and UAP are biodegradable. They are recycled and used as electron-donor substrates.

The highlighted paths on Figure (2.9) are shown again in Figure (2.10 a&b) with more details. Figure (2.10 a&b) shows in detail the eleven electron flow paths and production/decay of each component of the seven components; three solid species: bacteria, EPS, and residual inert biomass, three soluble species: organic substrate, UAP, and BAP, and an electron acceptor such as oxygen (Laspidou and Rittmann (2002b)). The eleven paths are described in brief as follows and a more detailed description is given by Laspidou and Rittmann (2002b).

Reproduced with permission of the copyright owner. Further reproduction prohibited without permission.

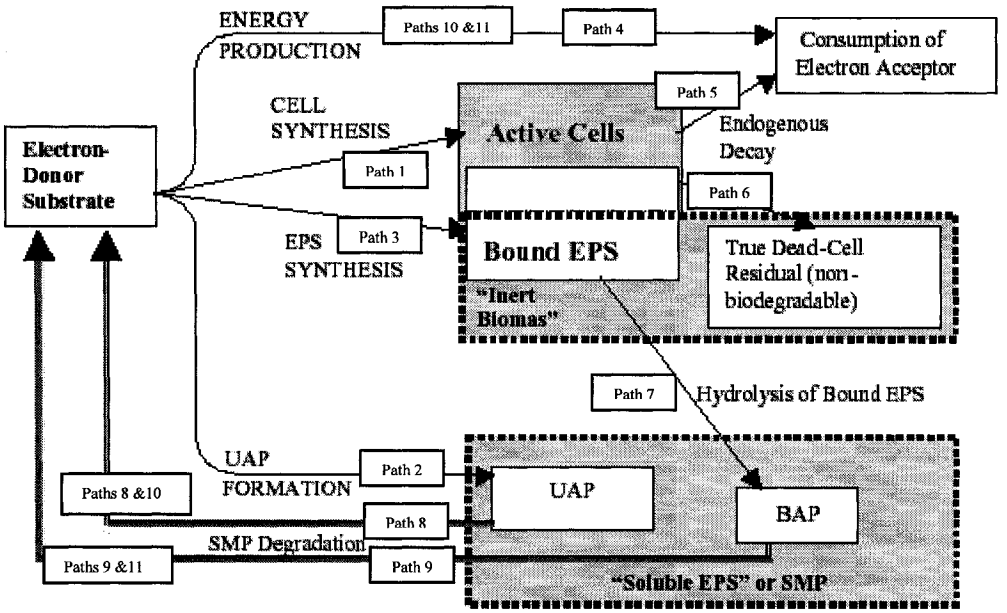

Figure 2.9- Schematic diagram of the unified model with all the involved components, adapted from Laspidou and Rittmann (2002a)

Path 1: Direct utilization of original substrate for active biomass synthesis, X_a

Path 2: Direct utilization of original substrate to generate UAP

Path 3: Direct utilization of original substrate for EPS synthesis

Path 4: Remaining electrons are used by electron acceptor to generate energy.

Path 5: Biodegradable fraction "f_d" of active biomass "X_a" is oxidized by endogenous decay to generate energy for maintenance.

Path 6: Non-biodegradable fraction of active biomass decays and produces residual inert biomass "X_{res}".

Path 7: Dissolution/hydrolysis of EPS directly generates BAP.

Paths 8 and 9: Part of UAP and BAP are recycled and become substrate to generate active biomass since UAP and BAP are biodegradable. The recycled UAP and BAP are only

Reproduced with permission of the copyright owner. Further reproduction prohibited without permission.

used to generate new active biomass and they do not result in generating new UAP and BAP.

Paths 10 and 11: The remaining part of UAP and BAP that are not recycled and are used to generate energy.

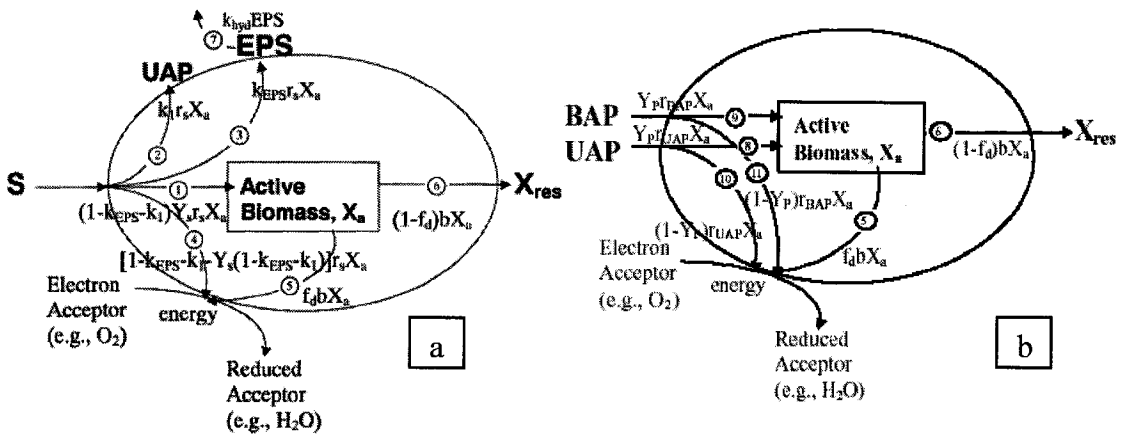

Figure 2.10- Schematic diagram for electron flow described by the unified theory, (a) original substrate and active biomass and (b) BAP and UAP utilization, adapted from Laspidou and Rittmann (2002b)

Laspidou and Rittmann (2004a) reported that most of the two and three-dimensional models currently used to model biofilms assume constant biofilm thickness. Most of those models do not take into account the three solid components of biofilm; active cells, inert biomass, and EPS.

Laspidou and Rittmann (2004a) formulated unsteady state mass balance equations that describe the flow of electrons based on the unified model and numerically coded the equations in a two-dimensional C++ finite difference model. The model simulates aerobic heterotrophic biofilms and can predict the change in density as a function of biofilm depth. The model also presented a new biofilm consolidate feature (Laspidou and

Reproduced with permission of the copyright owner. Further reproduction prohibited without permission.

Rittmann (2004b)) which provides a conceptual model to allow the biofilm density to vary with depth.

Laspidou and Rittmann (2004c) mentioned that researchers (i.e. Melo and Pinheiro (1984); Droste et al. (1990); Vieira et al. (1993)) showed that biofilm density increases if biofilm is exposed to turbulent flows and high shear stresses. Conceptually, as fluid flow passes over biofilm, it creates pressure and vibrates the biofilm structure, which causes water to be squeezed out of the biofilm and causes the biofilm to consolidate over time. This consolidation is what Laspidou and Rittmann (2004b) claim to be the reason why old biofilm layers tend to be denser than new biofilm layers, which tend to be fluffier.

Laspidou and Rittmann (2004a) compared their model results with experimental data found in the literature by Hsieh et al. (1994) who follow the EPS School and Zhang and Bishop (1994) and Bishop et al. (1995) who follow the SMP School. Laspidou and Rittmann (2004a) were able to match the trends captured by experimental results presented by both schools.

2.8.4 Biofilm Densities Reported In the Literature

A literature search revealed that biofilm density has quite a wide range of values as reported by many researchers. Christensen and Characklis (1990) reported that biofilm dry densities vary from as high as 0.130 g/cm^3(Kornegay and Andrews (1967)) to as low as 0.005 g/cm^3 (Rittmann and McCarty (1980) and (1981)). Table (2.5), adapted from Christensen and Characklis (1990), shows the wide range of densities reported by other researchers.

In their model, Laspidou and Rittmann (2004a) distinguish between the densities of the three solid components of biofilm. Density of active biomass was taken from

Reproduced with permission of the copyright owner. Further reproduction prohibited without permission.

Picioreanu et al. (1998) to be 70 g COD/L. Density of EPS was taken from Kreft and Wimpenny (2001) who used 75 g C/L as a typical value for sludge floc composition density. Laspidou and Rittmann (2004a) assumed a mole of EPS to be the same as aerobic bacteria cells found in wastewater ($C_5H_7O_2N$), Rittmann and McCarty (2001). Using this empirical formula, $C_5H_7O_2N$, the density of EPS was found to be 200 g COD/L, knowing that there is 60 g C per mole of EPS and 1.42 g COD per formula weight, Rittmann and McCarty (2001). Density of residue inert biomass was a new parameter introduced in the Laspidou and Rittmann (2004a) model. They chose 220 g COD/L to be the density of residue inert biomass. This density value was chosen to be higher than the other two solid components because it contains the residues of dead cells, inorganic precipitates and any captured suspended solids and hence it should be the highest density comparable to both active biomass and EPS densities.

Table 2.5- Reported biofilm thickness, density (dry mass per unit wet volume), and types, adapted from Christensen and Characklis (1990)

Reference	Thickness, L_f, μm	Density, kg/m^3	Biofilm[a] Type
Kornegay and Andrews (1967)	160-210	66-130	A
Hoehn and Ray (1973)	30-1300	20-105	B
Williamson and McCarty (1976b)	150-580	42-109	C
Rittmann and McCarty (1978)	100	50[b]	A
Rittmann and McCarty (1980)	119-126	5[c]	B
Rittmann and McCarty (1981)	0-125	5[c]	B
Trulear and Characklis (1982)	10-124	10-65	B
Trulear (1983)	36-47	17-47[d]	D
Bakke (1986)	0-60	27	D

[a] A, steady state, heterotrophic, mixed population; B, heterotrophic, mixed population; C, steady state, nitrifying, mixed population; D, steady state, *Pseudomonas aeruginosa*.
[b] Calculated assuming biofilm is 80% volatile solids.
[c] Calculated assuming biofilm is 50% carbon.
[d] Calculated from measured thickness corrected for refractive index of biofilm.

As can be noted in the literature, dry biofilm density has a wide range that varies between 0.005 g/cm^3 and 0.13 g/cm^3 depending on the bacteria culture involved and

Reproduced with permission of the copyright owner. Further reproduction prohibited without permission.

system conditions. Zhang and Bishop (1994) calculated the wet density of biofilm and found it to be biofilm thickness dependant. At the bottom layer of the biofilms they studied, wet density ranged between 1.01-1.02 g/cm^3. At the top layers of biofilms, the wet density was ranged between 1.001-1.003 g/cm^3 and hence an average density could be assumed to be close to the water density (i.e. 1 g/cm^3). Very few researchers distinguished between densities of biofilm components, such as Laspidou and Rittmann (2004a) because it is quite hard to measure parts of the biofilm such as residue inert biomass. The three density values for bacteria cells, EPS, and inert fraction have to be assumed when one is modeling biological clogging using the biofilm model as will be discussed later in chapter five.

2.8.5 Relation between Substrate Consumption, Biomass Growth, and EPS Formation

Laspidou and Rittmann (2002a) reported that there was a contradiction in the literature in determining the relation between substrate consumption and EPS production. Researchers such as Evans et al. (1994) and Robinson et al. (1984) showed that EPS production is inversely proportional to substrate consumption. Turakhia and Characklis (1989) showed a linear relationship between EPS production and substrate consumption while Williams (1974) showed that EPS production is independent from growth rate. Laspidou and Rittmann (2002a) concluded that this relationship is likely to depend on the microorganisms involved and the surrounding conditions.

Laspidou and Rittmann (2002a) reported values for k_1 and k_2 rate coefficients where k_1 is the growth associated EPS formation coefficient in g EPS C/ g biomass C, and k_2 is the non-growth associated EPS formation coefficient in g EPS C/ g biomass C. k_1

Reproduced with permission of the copyright owner. Further reproduction prohibited without permission.

represents how much electrons or carbon is used in EPS formation and k_2 is a first order rate of non growth EPS formation which equals the same rate of active biomass loss. Laspidou and Rittmann (2002a) mentioned that k_1 and k_2 rate coefficient values reported in the literature are not consistent and they even vary for the same bacterium. Table (2.6) shows k_1 and k_2 rate coefficient values reported in Laspidou and Rittmann (2002a) which was adapted from Christensen and Characklis (1990).

Table 2.6- k_1 and k_2 rate coefficients for Pseudomonas aeruginosa

k_1 (g EPS/g biomass)	k_2 (g EPS/g biomass)	Reference
3.3	0.1	Williams and Wimpenny (1977) and Mian et al. (1978)
2.1	0.0	Turakhia and Characklis (1989)
0.3	0.04	Robinson et al. (1984)

Laspidou and Rittmann (2002a) showed that some of the reported values such as 3.3 and 2.1 g EPS/g biomass are impossible values. Based on the following equation,

$$k_1\left(\frac{g\ EPS}{g\ biomass}\right)\times Y\left(\frac{g\ biomass}{g\ substrate}\right)=\left(\frac{g\ EPS}{g\ substrate}\right) \qquad (2.18)$$

If the yield coefficient, Y, is 0.64 g biomass C/ g substrate C, and k_1 is 3.3 and 2.1, this will result in 2.1 and 1.35 g EPS C/ g substrate C. Since it is impossible to obtain more EPS carbon mass than what is in the original substrate, Laspidou and Rittmann (2002a) concluded that the reported k_1 values are extremely high values.

Laspidou and Rittmann (2002a) discussed another way of expressing growth kinetics of EPS which was introduced by Hsieh et al. (1994). Hsieh et al. (1994), who follow the EPS School, studied the effect of growing *Pseudomonas atlantica*, a marine bacterium that is known for its ability to generate biofilms, on glass surfaces and studied how it performs under batch and continuous culture conditions. The objective was to develop a

Reproduced with permission of the copyright owner. Further reproduction prohibited without permission.

mechanistic model that simulates the bacterium growth and its polymers. Figure (2.11) shows a schematic diagram for all the components involved in the model.

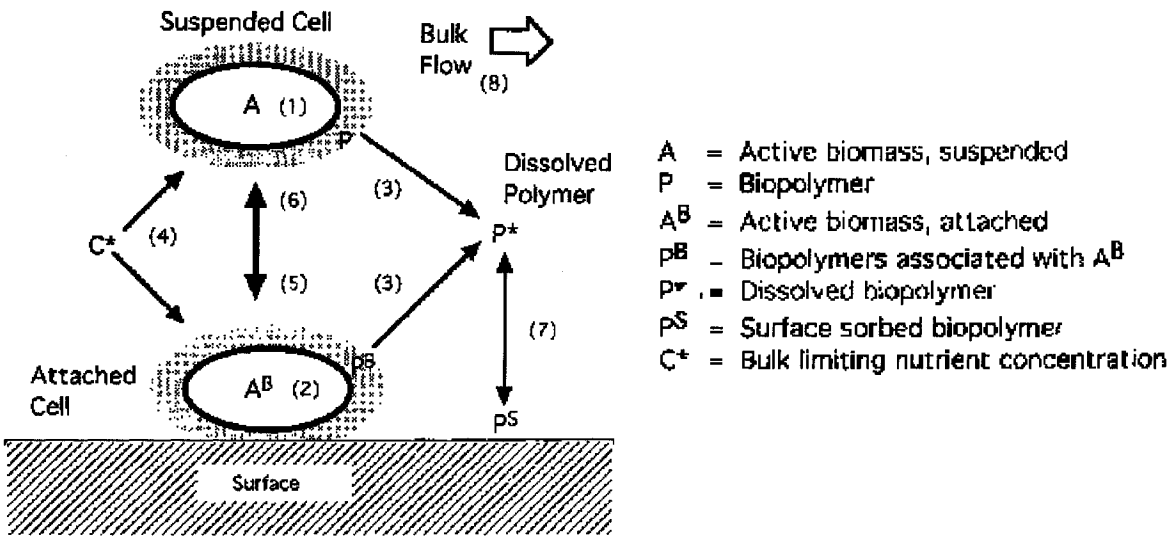

Figure 2.11- Schematic diagram of all the components involved in Hsieh et al. model, adapted from Hsieh et al. (1994)

As shown in Figure (2.11), the model introduced two different categories of biomass, suspended "A" and bounded/attached "A^B" and each category has its own EPS, EPS denoted "P" and EPS denoted "P^B", respectively. There are two other types of EPS formed, dissolved EPS "P^*" and surface sorbed EPS "P^S".

The Hsieh et al. (1994) model considered the following basic processes;

- Growth, decay, and EPS generation of suspended bacteria cells
- Growth, decay, and EPS generation of attached bacteria cells
- Growth limiting nutrient utilization by suspended and attached bacteria cells
- Release of EPS from the surface of the bacteria cells to bulk flow
- Increase/decrease of cell density due to attachment and growth/detachment and decay, and;

Reproduced with permission of the copyright owner. Further reproduction prohibited without permission.

- Detachment rate is affected by bulk flow shear on the solid surface

Based on these considerations, they define the following seven microbial components in their model;

- Active suspended biomass "A" which represents suspended polymer-free cells
- Active bound biomass "A^B" which represents cells that are attached to the solid surface
- EPS biopolymers "P" which are associated with suspended
- EPS biopolymers "P^B" associated with A^B
- Dissolved biopolymers "P^*" which are cell-free polymers present in the bulk flow
- Surface sorbed biopolymers "P^S" which represents cell-free polymers attached to the solid surface, and
- Bulk limiting nutrients "C" which is carbon in glucose in this experiment.

Hsieh et al. (1994) formulated equations that represent the previously described microbial components. Table (2.7) lists the parameters they used in the equations and the corresponding numerical values they used in the model.

As can be noted from Table (2.7), Hsieh et al. (1994) treated the parameters for attached cells to have the same values as the suspended cells. K_{PC}^* and K_{dAC}^* are parameters that were found in the literature while K_{AC}^*, $K_P^*{}_P$, and f_{AP} were estimated by Hsieh et al. (1994).

Hsieh et al. (1994) assumed that the net rate of bound EPS formation from suspended biomass has three terms; the first being a growth term for growth–associated EPS formation based on Monod kinetics. The second term is a non-growth associated EPS formation where a fraction of electrons and carbon in the decayed suspended active

Reproduced with permission of the copyright owner. Further reproduction prohibited without permission.

biomass, $f_A{}^B{}_P$, is considered as a source term for the non-growth associated EPS. The third term is a decay term for the EPS formed.

Table 2.7- Parameters used in Hsieh et al. (1994) study

Parameter	Description	Value	Units
$K_{AC}{}^*$	Half-velocity constant for growth of suspended cells	4.7×10^{-4}	g/L
$K_{PC}{}^*$	Half-velocity constant for production of polymer associated with suspended cells	4.4×10^{-3}	g/L
$K_A{}^B{}_C{}^*$	Half-velocity constant for growth of attached cells	4.7×10^{-4}	g/L
$K_P{}^B{}_C{}^*$	Half-velocity constant for production of polymer associated with attached cells	4.4×10^{-3}	g/L
f_{AP}	Fraction of active cell mass "A" which is converted to cell-bound polymer "P" as active cell mass degrades	0.95	gP/gA
$f_A{}^B{}_P$	fraction of attached active cell mass "A^B" which is converted to attached cell-bound polymer "P^B" as active cell mass degrades	0.95	gP^B/gA^B
$K_P{}^*{}_P$	Half-velocity constant for production of dissolved polymer "P^*" from cell-bound polymer of suspended cells "P"	0.1	gP/gA
$K_P{}^*{}_P{}^B$	Half-velocity constant for production of dissolved polymer "P^*" from cell-bound polymer of attached cells "P^B"	0.1	gP^B/gA^B
$K_{dAC}{}^*$	Half-velocity constant for decomposition of suspended cells	0.01	g/L
$K_{dA}{}^B{}_C{}^*$	Half-velocity constant for decomposition of attached cells	0.01	g/L

In their unified model, Laspidou and Rittmann (2002b) adapted the same concept used by Hsieh et al. (1994) to estimate EPS generation. The values of the model parameters used by Laspidou and Rittmann (2002b) where the same as those used by Hsieh et al. (1994) except for a few parameters. For example, Hsieh et al. (1994) used a value of 0.27 mg COD_x/ mg COD_s to represent the percentage of substrate used to generate active biomass. They also used 0.59 mg COD_p/ mg COD_s to represent the percentage of substrate used to generate EPS. Laspidou and Rittmann (2002b) argued that the latter value is quite high because, and based on the unified model, the remaining portion of the substrate used to generate energy will be relatively small. Instead, Laspidou and Rittmann (2002b) used a value 0.18 mg COD_p/ mg COD_s in their model.

Reproduced with permission of the copyright owner. Further reproduction prohibited without permission.

Laspidou and Rittmann (2002b) also used a value of is 0.17/d to represent the first order hydrolysis coefficient rate for dissolution of EPS to BAP. This is a typical value for biological solids (Rittmann and McCarty (2001)). Hsieh et al. (1994) used 0.96/d but their kinetic approach was different from what Laspidou and Rittmann (2002b) are presenting.

In stage three of this research work, to simulate biological clogging based on a biofilm model, relations between the generated active biomass, EPS, and inert fraction have to be assumed. From the previous discussion, a value of 0.27 mg COD_x/ mg COD_s and 0.59 mg COD_p/ mg COD_s will be used to relate the percentage of substrate used to the generated active biomass and EPS, respectively. Also, a value of 0.8 will be used to calculate the inert fraction of the active biomass in the biofilm structure.

2.9 Summary

Different conceptual models for clogging in the saturated zone were proposed in the literature but corresponding conceptual models for clogging in the unsaturated zone are limited. Mostafa and Van Geel (2007) proposed different conceptual models that relate the relative permeability to the microbial growth in unsaturated soils. The models were implemented in a one-dimensional numerical code and hypothetical cases were simulated to illustrate the differences between the three conceptual models without any laboratory or field data validation.

This research provides experimental and numerical works that were used to calibrate the numerical code and validate the three conceptual models presented earlier by Mostafa and Van Geel (2007). The research work is divided into three stages which are discussed

Reproduced with permission of the copyright owner. Further reproduction prohibited without permission.

sequentially in the following chapters. The following chapter, chapter three, discusses stage one which was used to generate data sets that demonstrate the clogging behavior in different pore structures. Chapter four discusses stage two, which was used to estimate the Monod kinetic parameters that demonstrate the growth behavior of the bacteria cultures that caused the clogging process in stage one. Chapter five discusses stage three which was used to validate the three conceptual models proposed by Mostafa and Van Geel (2007) using the generated data sets in stages one and two, which aimed to increase our understanding of the relationship between microbial growth and the macroscopic soil properties.

Reproduced with permission of the copyright owner. Further reproduction prohibited without permission.

3. STAGE ONE: EFFECT OF DIFFERENT PORE STRUCTURES ON THE CLOGGING OF UNSATURATED SOIL

This chapter presents the results from stage one of this research. Stage one of this research aimed to highlight the effect of different pore structures on the bioclogging process in unsaturated soils. The chapter consists of four main sections; an introduction to the type of soils used in this stage and preliminary tests, experimental setup, analysis of results and discussion, and a summary of the findings from this stage.

3.1 Introduction

The purpose of this stage was to study the relationship between the pore structure of unsaturated soils and biological clogging in the laboratory. Four different types of soils were tested to represent various pore size distributions, porosities, densities, as well as organic versus inorganic soils. Septic bed sand, concrete sand, and filter media bed sand were used to represent inorganic soils and peat, compacted at two different densities, was used as an organic soil. Septic bed sand and concrete sand represent well graded soils as opposed to filter media bed sand, which represents a uniform soil. Also, septic bed sand has a higher percentage of fines (i.e. 13.8% fines passing through sieve 0.075 mm) versus the concrete sand (i.e. 1.7% fines passing through sieve 0.075 mm). Sieve analysis tests were conducted at Carleton University's Civil Engineering laboratory and were compared with sieve analyses provided by the supplier. A comparison is provided Figures (3.1) through (3.4).

Reproduced with permission of the copyright owner. Further reproduction prohibited without permission.

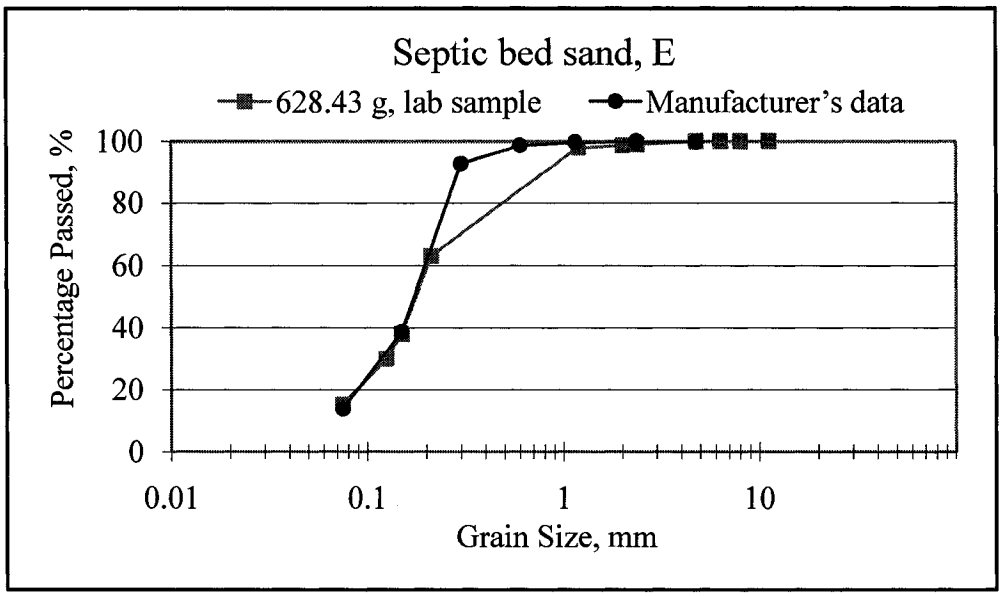

Figure 3.1- Grain size distribution for septic bed sand with 13.8% of fines passing though sieve 0.075 mm

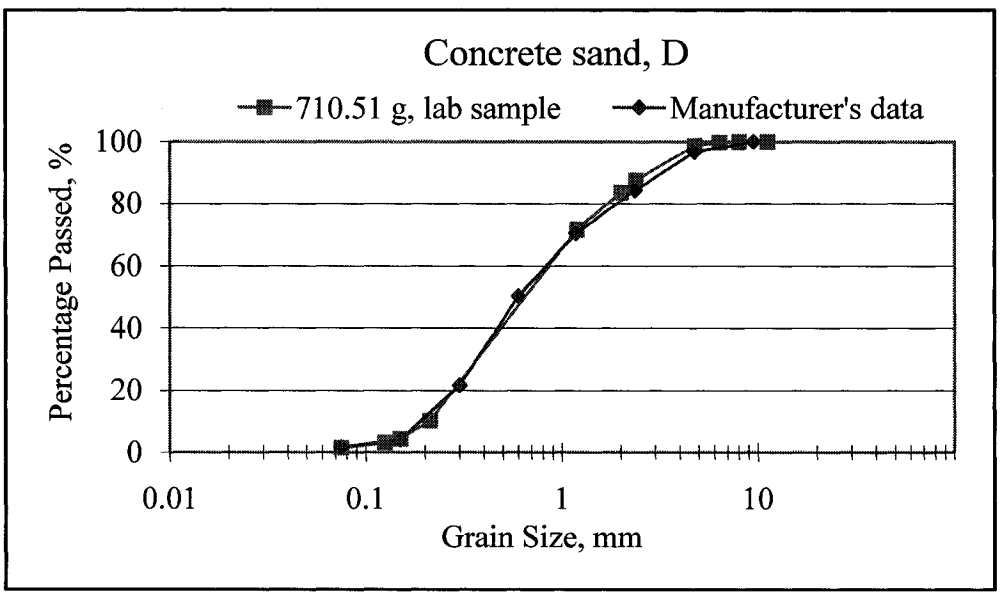

Figure 3.2- Grain size distribution for concrete sand with 1.7% of fines passing through sieve 0.075 mm

Reproduced with permission of the copyright owner. Further reproduction prohibited without permission.

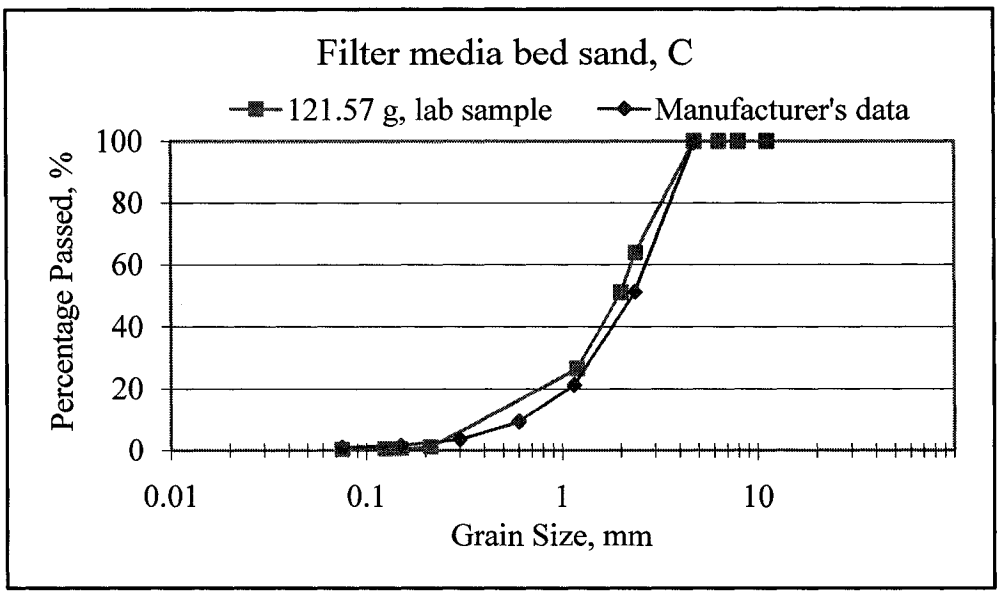

Figure 3.3- Grain size distribution for filter media bed sand

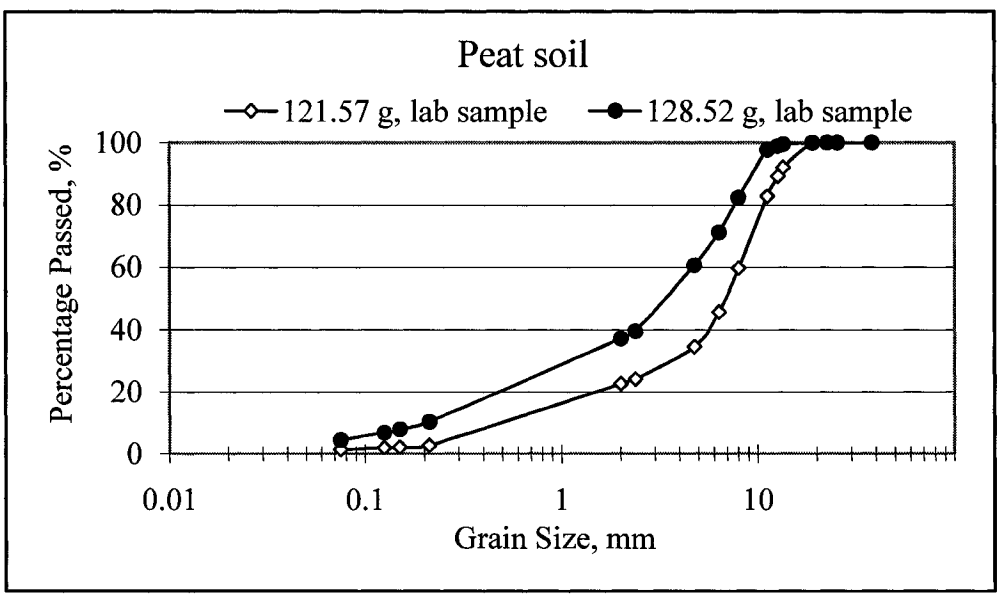

Figure 3.4- Grain size distribution for peat soil

The septic bed sand, concrete sand, and filter media bed sand were provided by Karson Kartage and Konstruction from pits west of Ottawa and the peat soil was provided by Premier Tech/Ecoflo® Biofilters.

Reproduced with permission of the copyright owner. Further reproduction prohibited without permission.

It should be noted from Figure (3.4) that all peat particles had sizes less than 3 cm in diameter. The peat that was used in this experiment went through a preprocessing stage to remove peat clods that had a diameter larger than 3 cm (e.g. sticks, stones, and twigs as shown in Figure (3.5)). The reason for this preprocessing stage is that the larger particles may create heterogeneities and may cause channeling within the laboratory column experiments proposed here. This preprocessing step was used by other researchers to avoid this potential problem (Shibchurn (2001)).

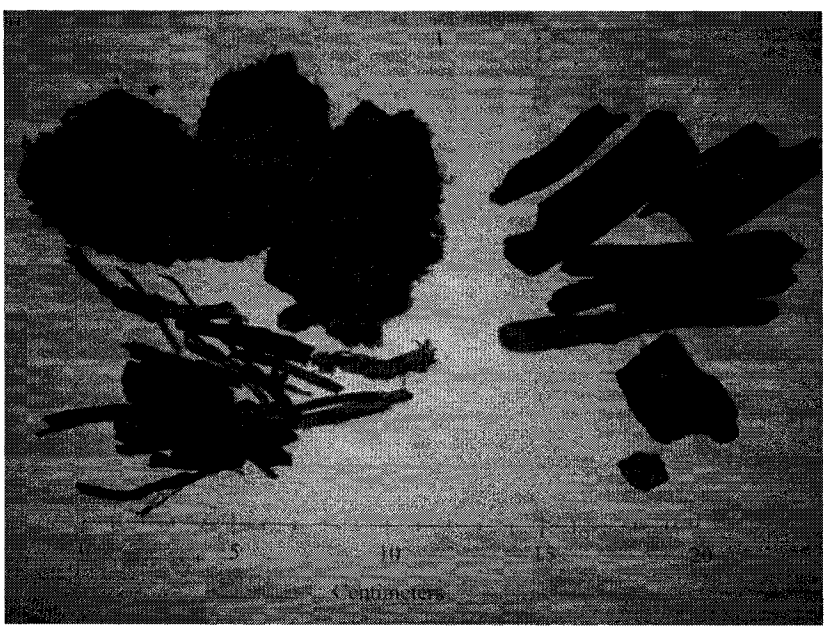

Figure 3.5- Sticks, stones, and twigs found in the peat soil used

In addition to the sieve analysis test, permeability tests using the constant head test method were conducted on the sand soils to determine their saturated hydraulic conductivities, K_{sat}. Moreover, soil moisture curve parameters (i.e. van Genuchten parameters, n and α) were measured for the three inorganic soils using a Buchner funnel apparatus. Figure (3.6) shows a typical test setup for the Buchner funnel that was used to

Reproduced with permission of the copyright owner. Further reproduction prohibited without permission.

determine soil moisture curves for the three sand soils. The soil moisture curve and hydraulic conductivity, as a function of density, for the peat was determined from a previous study by Shibchurn et al. (2005).

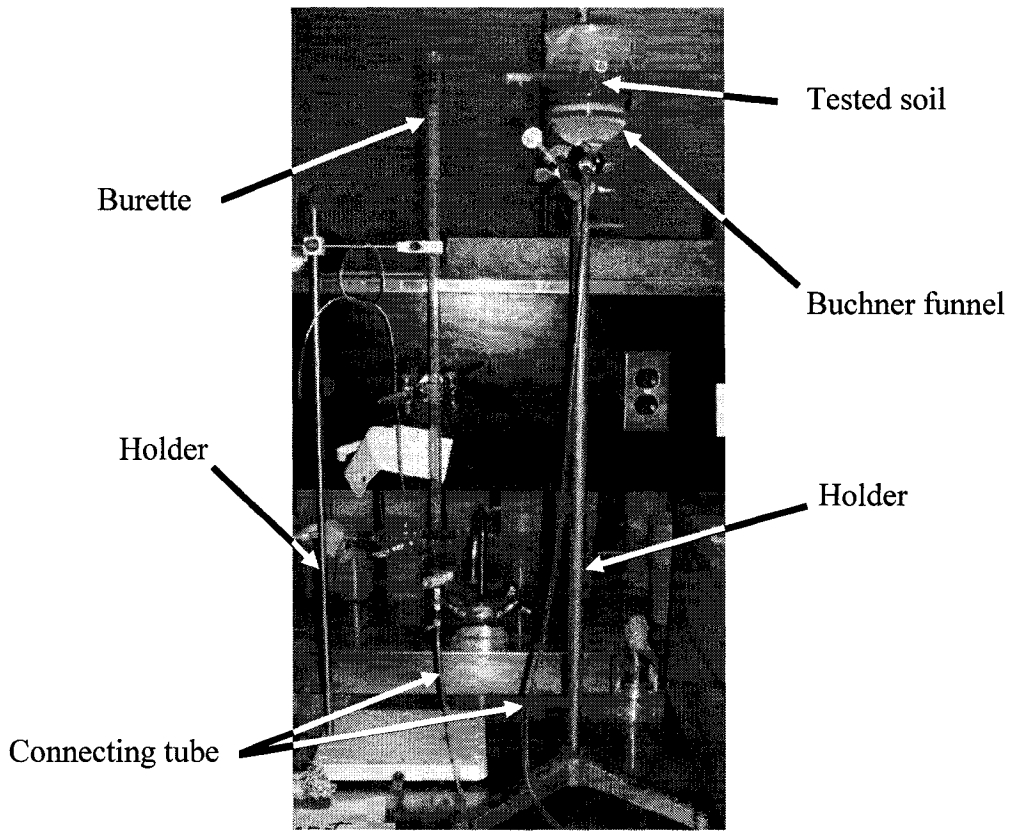

Figure 3.6- Buchner funnel test setup used to determine the soil moisture curves for sand soils

3.2 Experimental Setup

3.2.1 Materials and Method

To illustrate the impact of biological clogging on unsaturated soils, experimental columns were prepared using the soils mentioned earlier and were pulsed daily with synthetic feeding solutions until the columns clogged. A total of twenty five columns, as shown in Figure (3.7), were built for this experiment. Figure (3.8) provides a schematic

Reproduced with permission of the copyright owner. Further reproduction prohibited without permission.

diagram for a typical column that was built for this purpose. For each soil type as shown in Table (3.1), five columns were constructed; one column was loaded with tap water as a control, two columns were loaded with organic loading only, and two columns were loaded with organic plus suspended loading. Table (3.1) also illustrates the loading scenario for each column of the experimental columns built for this experiment. The chemical constituents used to prepare the organic only and organic plus suspended feeding solutions are listed in Table (3.2).

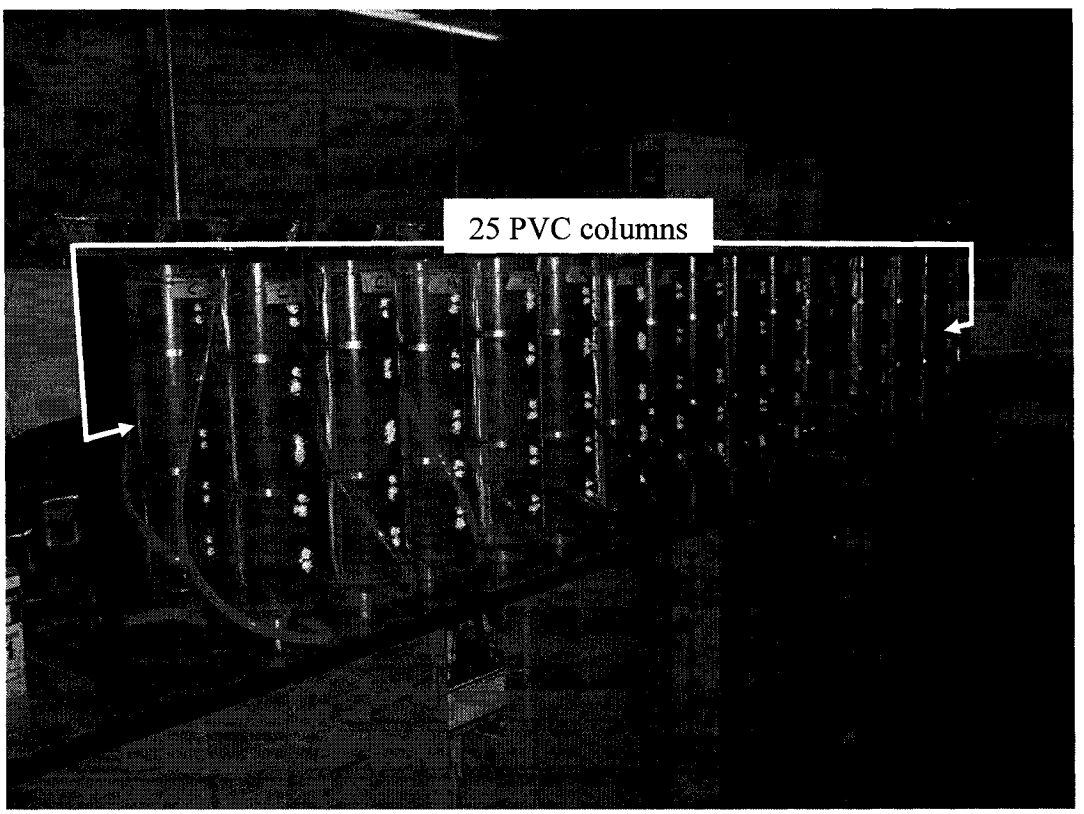

Figure 3.7- Twenty five PVC columns constructed for this experiment

Reproduced with permission of the copyright owner. Further reproduction prohibited without permission.

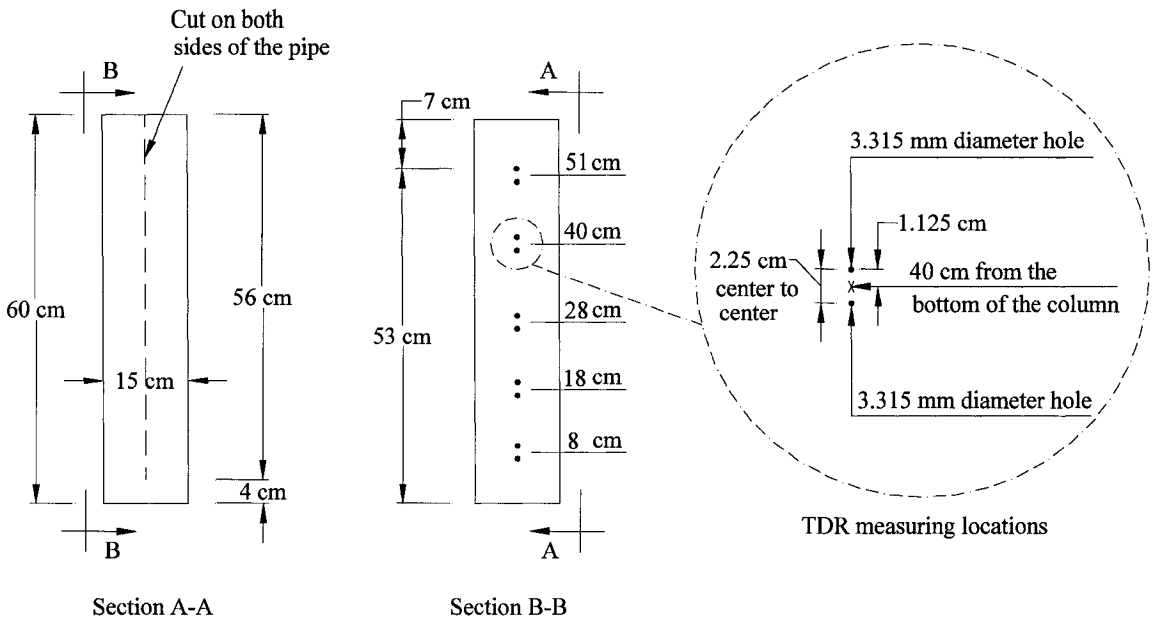

Figure 3.8- Schematic diagram for a typical column that was built for stage one

As shown in Figure (3.8), each column was 60 cm in height and 15 cm in diameter (i.e. 6-inch commercial plastic pipe bought from CANAS Plastic in a 20-foot length). Each pipe had two side slits along the length of the column. The slits were approximately 1 mm in thickness (i.e. thickness of the cutting blade) and were filled with silicon and covered with duct tape to prevent leakage. The reason for these slits was to be able to dismantle the columns to obtain undisturbed samples after the columns clog. Also, two holes 2.25 cm apart were drilled at five different elevations on each column for two 15 cm long stainless steel rods that were used to measure moisture content using Time Domain Reflectometry (TDR).

Reproduced with permission of the copyright owner. Further reproduction prohibited without permission.

Table 3.1- Experimental columns with different soil types and different loading scenarios

Soil type	Loading type	Column label	Comments
Loose peat	Tap water	A	Control
	Organic loading	A1 and A2	Duplicate
	Organic + suspended loading	A3 and A4	Duplicate
Compacted peat	Tap water	B	Control
	Organic loading	B1 and B2	Duplicate
	Organic + suspended loading	B3 and B4	Duplicate
Filter media bed sand	Tap water	C	Control
	Organic loading	C1 and C2	Duplicate
	Organic + suspended loading	C3 and C4	Duplicate
Concrete sand	Tap water	D	Control
	Organic loading	D1 and D2	Duplicate
	Organic + suspended loading	D3 and D4	Duplicate
Septic bed sand	Tap water	E	Control
	Organic loading	E1 and E2	Duplicate
	Organic + suspended loading	E3 and E4	Duplicate

Table 3.2- Organic only and organic plus suspended loading for the experimental columns

Constituents	To make 1.0 L of stock	Loading Type	
Water	1.0 L	To prepare organic loading only	To prepare organic + suspended loading
Glucose	13.75 g		
Ammonium Bicarbonate	4.167 g		
Potassium Phosphate (mono)	0.25 g		
Potassium Phosphate (di)	0.167 g		
Yeast Extract	0.15 g		
Silica	2.0 g		

A drainage layer was placed at the bottom of each column. The bottom drainage layer consists of a geotextile sheet under a 3 cm thick gravel layer (average particle size diameter is approximately 1 cm), overlain by a second geotextile sheet. A 50 cm soil layer was packed in each column and a top drainage layer consisting of large crushed stones (average particle size diameter is approximately 3 cm) was placed on top of the soils in the remaining 7 cm that acted as a distribution layer. The stone layer also helped to hold the peat in place. Each column had a drainage port at the bottom.

Reproduced with permission of the copyright owner. Further reproduction prohibited without permission.

Since twenty five columns were loaded daily, 18 L stock solution was prepared in a 20 L plastic bucket and was stored in the refrigerator at a temperature of approximately 4 ^{o}C to prevent any bacterial growth. Chemical oxygen demand, COD, test was conducted on the stock solutions (i.e. organic only and organic plus suspended) to determine the substrate concentration of the influent. The COD test was conducted occasionally on the stored feed stock to ensure that the concentration did not change during storage. Data for the COD tests are provided in Figure (A.19), Appendix A. The average concentration of the feed stock was approximately 26010 mg COD/L.

To load a column, two liters of feed solution was generated by combining 100 mL of stock solution with 1.9 L of tap water (temperature of tap water was approximately 10 ^{o}C). Each column was loaded twice a day (i.e. morning load at approximately 8:00 am and afternoon load at approximately 4:00 pm), five consecutive days (i.e. Monday through Friday) a week, with 2 L (i.e. average substrate concentration was approximately 1369 mgCOD/L) and each column was loaded as described previously in Table (3.1). The number of pulses per week was reduced as ponding occurred. The time when the loading was reduced to below 20 L per week, to below 4 L per week, and the time the columns were dismantled are provided in Table (A.16), Appendix A. It should be noted that both the hydraulic and organic loading used in this experiment were selected such that clogging process occurs fast and hence, both were substantially higher than what could be found in a typical residential septic system (Tchobanoglous and Burton (1991)).

Reproduced with permission of the copyright owner. Further reproduction prohibited without permission.

3.2.2 Measurements during Experimental Period

3.2.2.1 Moisture Content Using TDR

During this stage, moisture content measurements were taken using TDR as shown in Figure (3.9). The moisture content was measured at five different levels for each column (i.e. 51 cm, 40 cm, 28 cm, 18 cm, and 8 cm from the bottom of the columns) and this provided a vertical saturation profile in the 50 cm soil column at depths of 48 cm, 37 cm, 25 cm, 15 cm, and 5 cm from the top of the lower drainage layer. These measurements were taken twice a day, one day a week (Monday), before the two loading events.

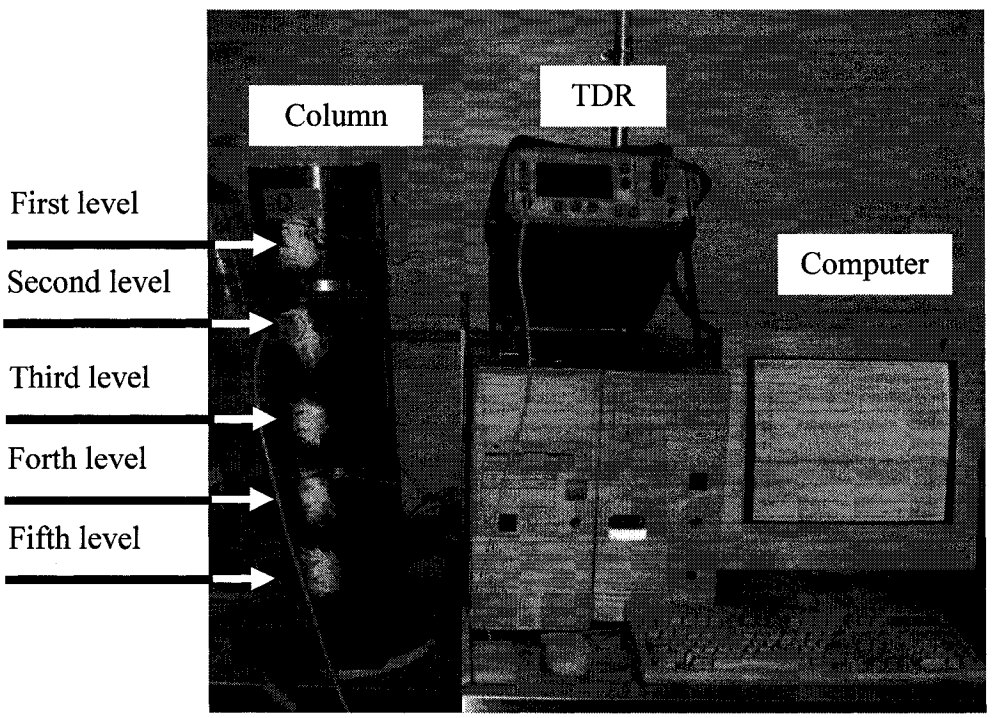

Figure 3.9- TDR measurement setup at five different levels; 48 cm, 37 cm, 25 cm, 15 cm, and 5 cm from the top of the lower drainage layer

Reproduced with permission of the copyright owner. Further reproduction prohibited without permission.

3.2.2.2 Flow and Weight Measurements

Each day, flow measurements were taken for one column immediately after each loading using a 30-kg balance connected to a computer to record the data as shown in Figure (3.10). The balance was moved each day to the next column and hence the flows from each column were recorded approximately every fifth week (twenty five columns and loading five days per week). In addition to the weekly TDR measurements and flow measurements, weight measurements for all the columns were taken every month (i.e. at the beginning of each month) to be able to track the weight increase of each column as microbial growth occurred (data provided in Figures (A.20) through (A.24), Appendix A).

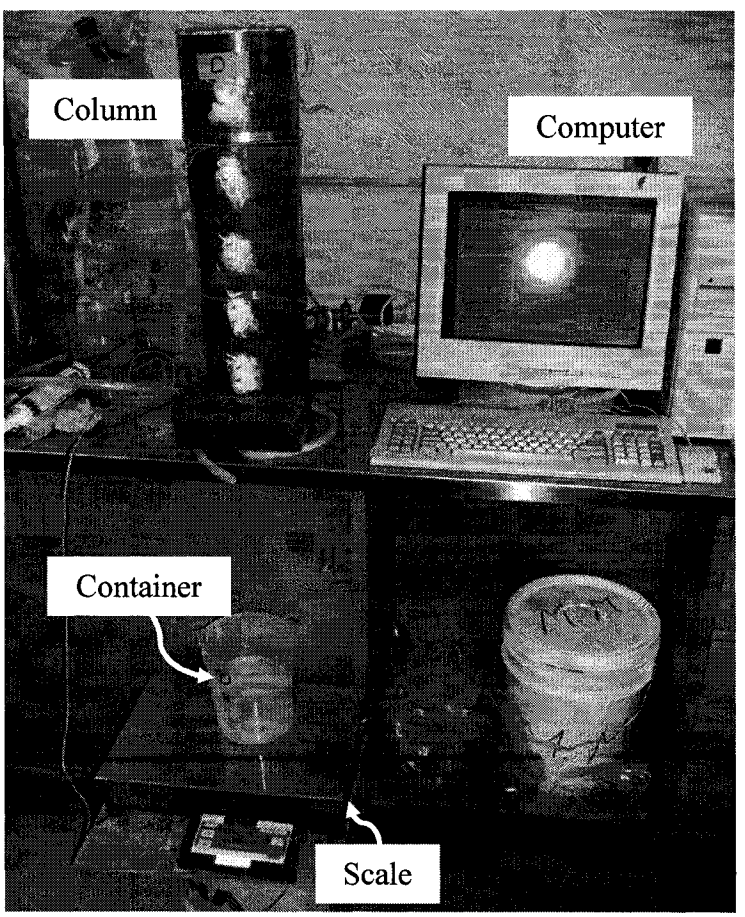

Figure 3.10- Outflow measurement setup

Reproduced with permission of the copyright owner. Further reproduction prohibited without permission.

3.2.3 Measurements at Dismantle Time

At the end of the column experiments and after the columns clogged, each column was dismantled into six layers and three types of measurements/analyses were conducted on those layers (i.e. bacterial count analysis, gravimetric moisture content measurement, and ash content measurement). The average length from the top of the columns to the top of each layer was 6.5 cm, 9.0 cm, 15.0 cm, 23.5 cm, 33.0 cm, and 44.0 cm. The bottom of the last layer was at 56.0 cm from the top of the columns. The six layers were extracted by hand from the top of the column and placed into six aluminum trays pre-dried in the oven. It should be noted that the slits pre-made in each column were not used in dismantling the columns as initially planned. The extraction process by hand was suitable for the type of analyses that were conducted in this stage and hence undisturbed samples were not needed.

3.2.3.1 Bacteria Culturing

Eight soil samples were collected from the dismantled layers (i.e. two samples from each of the first two layers and one sample from each of the remaining layers). Each sample consisted of two to three smaller samples selected randomly from the tray for a total weight of approximately 4.0 grams and was placed into a sterilized 50 mL centrifugal plastic tube and capped. For each centrifugal tube, 40 mL of a 1% solution of sodium hexametaphosphate was added as a dispersion agent. The samples were shaken on a mechanical shaker at the highest speed (10,000 rpm) for 2 minutes. The reason for this shaking process was to separate bacteria from the solid phase so that they became suspended in the liquid phase. To obtain a series of dilutions to be able to measure the

Reproduced with permission of the copyright owner. Further reproduction prohibited without permission.

microbial concentration, first, a 10^0 dilution was obtained by filtering the liquid into another sterilized 50 mL centrifugal plastic tube using a sterilized strainer to remove the solids. Then, a series of sterilized 50 mL centrifugal plastic tubes were labeled from 10^1 to 10^8 and were filled with 45 mL of buffer water for the dilution process. A 5 mL sample was taken from the 10^0 centrifugal tube with a pipet that had a sterilized pipet tip and was deposited in the centrifugal tube labeled 10^1 and shaken on the mechanical shaker for few seconds for homogenization. Then, a 5 mL sample was taken from the 10^1 centrifugal tube and was deposited in the centrifugal tube labeled 10^2 and shaken. The same procedure was used for the rest of the dilutions.

After dilutions were prepared, bacteria culturing took place using the membrane filtration method (9215 D, Eaton et al. (2005)). Duplicate agar plates for each dilution were prepared and stored in the fridge for not more than 24 hours. The agar media used in this process was R2A type of agar that is used to culture heterotrophic bacteria. The reason for using R2A was to be able to culture most of the bacteria types that are culturable in the soil media using the bacteria count method. To culture the bacteria on the agar plate, a vacuum pump and 0.45 μm filter papers were used. Filter paper was placed on a sterilized funnel and suction was applied on the funnel using the vacuum pump while pouring a 5 mL sample of the dilution collected using a pipet. The filter paper was then placed on an agar plate and incubated in an incubator for an average of three days at 35 °C. After three days, bacterial counts were conducted for the plates to obtain an average number for bacteria for each sample.

Reproduced with permission of the copyright owner. Further reproduction prohibited without permission.

3.2.3.2 Gravimetric Moisture Content and Ash Content Measurements

After obtaining the eight samples for bacterial culturing, the six trays were weighted and placed in the oven at 105 °C for 24 hours to calculate the gravimetric moisture content (ASTM D 2974-87, ASTM (1995)). After 24 hours, triplicate samples were obtained from the trays and were burned in a furnace at 450 °C for 2 hours (ASTM D 2974-87, ASTM (1995)) to calculate the ash content. The gravimetric moisture content was compared with the TDR measurements taken for the columns just before dismantling them. This comparison was used to verify the accuracy of the TDR measurements that have been taken during the experiment. Also, the ash content measurements were used to determine the distribution of the suspended solids (i.e. silica) with depth in the columns pulse loaded with organic plus suspended loading.

3.3 Results and Discussion

3.3.1 Soil Properties/Parameters

This experiment started with columns at saturated conditions. The columns then were allowed to gravity drain for one day and followed by TDR measurements to record the initial steady state saturation profiles. Three different methods could be used, and theoretically should be the same, to calculate van Genuchten parameters for the soil moisture curves; using the TDR measurements recorded after the columns were initially saturated and then gravity drained for one day, using Buchner funnel experiment, and by averaging all the saturation profiles recorded using TDR for the control columns during the experiment period. The latter should give the best estimation for van Genuchten

Reproduced with permission of the copyright owner. Further reproduction prohibited without permission.

parameters because it is estimated from the actual columns under study and hence will be the most accurate.

A comparison between the three previously mentioned methods did not result in a good match. Initial saturation profiles measured for the columns after gravity drainage were higher than the saturation profiles measured during the course of the experiment for the control columns. This leads to the conclusion that the columns did not drain to their steady state profiles after one day of gravity drainage and hence should not be used to calculate the van Genuchten parameters. Also, the soil moisture curves obtained from the Buchner funnel experiment were different from the averaging profiles measured during the course of the experiment. The differences may be due to the different packing techniques used to fill the Buchner funnels versus the columns which resulted in different soil densities and hence different soil moisture curves. This difference may also be due to potential suction at the bottom of the columns as a slight decrease in saturation due to evaporation at the bottom of the columns may have led to an increase in the suction at the base to a value between zero and the air entry pressure for that soil as shown from the Buchner funnel results (see Figures (A.3) and (A.5), Appendix A).

One can argue that TDR measurements were not accurate and hence soil moisture curves using the Buchner funnels should be used to estimate the van Genuchten parameters. A comparison of the TDR and gravimetric moisture contents, which is presented later in this chapter, indicated that the TDR measurements were reasonably accurate and hence this argument is not valid. Thus, it was concluded that the best method to estimate van Genuchten parameters was by fitting van Genuchten equation to the average of all the saturation profiles measured in the control columns during the

Reproduced with permission of the copyright owner. Further reproduction prohibited without permission.

course of the experiment because this presents the most accurate estimation of van Genuchten parameters for the soils used.

Figure (3.11) presents the soil moisture curves obtained by averaging all the saturation profiles for the control columns during the course of the experiment and the corresponding soil moisture curves estimated by fitting the van Genuchten equation to the averaged saturation profiles. The soil moisture curves from the Buchner funnel experiments and the saturation profiles measured using TDR after gravity drainage for one day are provided in subsection (A.16), Appendix A.

Saturated hydraulic conductivities for the sand soils were determined by a constant head permeability test and for the peat soils, were calculated based on the study carried by Shibchurn (2001). The porosity of the sand soils were estimated using porosity test and were found to be consistent with the average moisture content value obtained by averaging the five measured values obtained for each column by the TDR when the soil columns were saturated. It should be noted that TDR measures the moisture content and if the soil is saturated, any measured TDR value should theoretically be equal to the porosity of the soil if there is no entrapped air. For peat soils, TDR measurements for the five levels were averaged when the columns were at saturated conditions and used as the porosity values for the two peat soils. Raw data for porosity tests are provided in Table (A.13), Appendix A.

Reproduced with permission of the copyright owner. Further reproduction prohibited without permission.

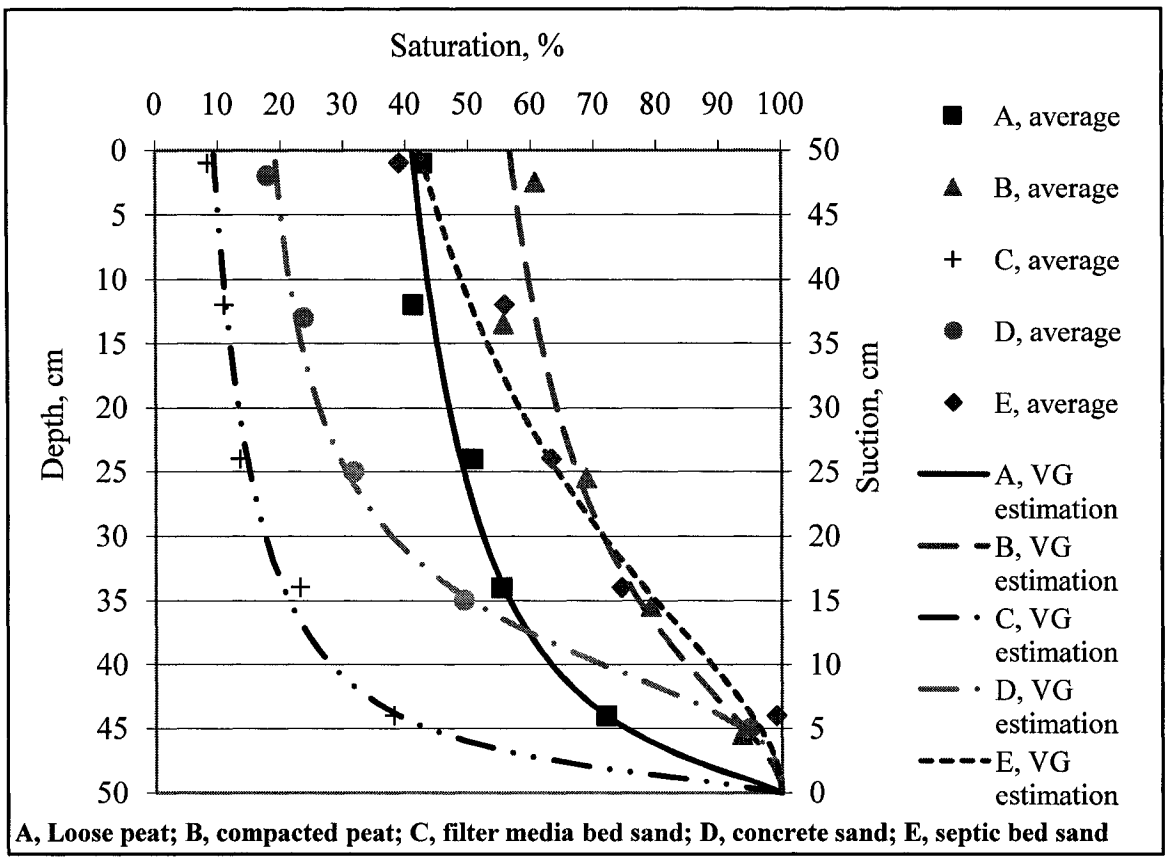

Figure 3.11- Comparison between average TDR measurements for control columns during the course of the experimental period and the corresponding van Genuchten fitting curves

Table (3.3) summarizes all the soil properties for the five soils. All the parameters shown in Table (3.3) are the measured or calculated parameters using the separate experiments (e.g. permeability test, porosity test, Buchner funnel test, etc). Irreducible saturations, van Genuchten parameters, K_{sat}, and porosities were the soil parameters used later during the numerical simulations in stage three. It should be noted that the italic/underlined numbers are values that were adjusted later while conducting the numerical simulations and a table with the final soil properties is provided later in the discussion of stage three in chapter five.

Reproduced with permission of the copyright owner. Further reproduction prohibited without permission.

Table 3.3- Summary of the soil properties

Soil Type	Irreducible saturation S_{wr}, %	van Genuchten parameters		K_{sat}, cm/s	Porosity	ρ_{dry}, g/cm^3	ρ_{bulk}, g/cm^3
		n	α, cm^{-1}				
Filter media bed sand, C	*10.99*	*3.562*	*0.281*	*0.212*	0.450	1.631	1.638
Concrete sand, D	*18.22*	*4.128*	*0.039*	*0.00206*	0.387	1.753	1.820
Septic bed sand, E	6.89	*4.134*	*0.014*	*0.00124*	0.366	1.352	1.617
Peat, loose density, A	*27.02*	*1.499*	*0.841*	*0.631*	0.878	0.084	0.588
Peat, compacted density, B	37.36	*1.369*	*0.076*	0.035	0.824	0.150	0.763

3.3.2 Results during the Experimental Period

This subsection presents the results of the data collected in this stage. Saturation profiles for the control columns are presented followed by their outflow profiles. Then the saturation profiles for the columns loaded with organic loading only and organic plus suspended are presented followed by their outflow profiles.

3.3.2.1 Saturation Profiles from Control Columns

Figure (3.12) shows the saturation profiles for the control columns for the five soils used in this stage. Since the control columns were pulsed twice daily with water without any food source, the saturation profiles prior to a pulse did not change over time due to microbial growth. Figure (3.12) shows the saturation profiles at different times (i.e. 50 days, 141 days, and 260 days) all clustered at a consistent saturation profile prior to pulsing.

Reproduced with permission of the copyright owner. Further reproduction prohibited without permission.

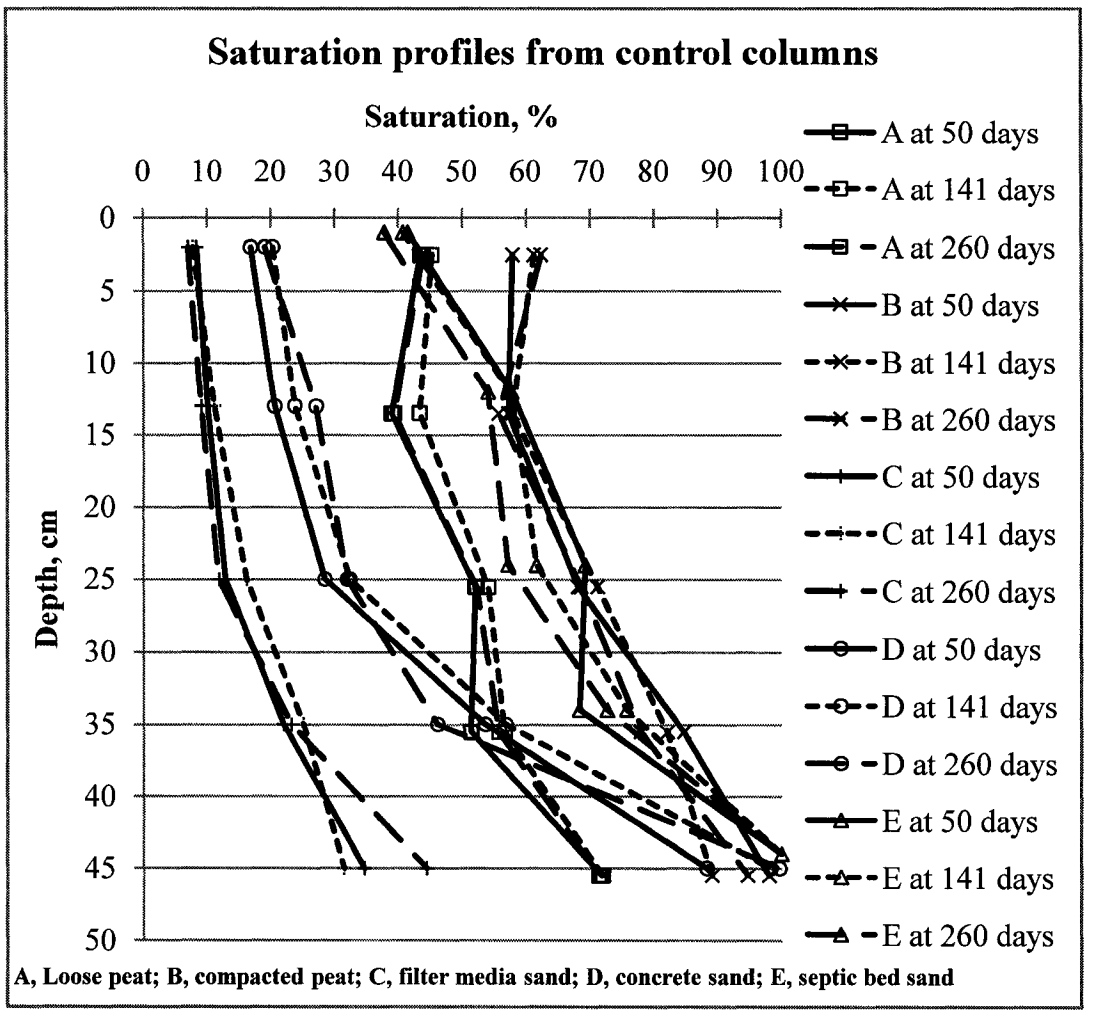

Figure 3.12- Saturation profiles for the control columns for the five soils used in this experiment

Since the soil moisture curves for all the soils were obtained by fitting van Genuchten equation to the average of all the saturation profiles measurements for the control columns during the course of the experiment, the saturation profiles shown in Figure (3.12) fit the soil moisture curves very well (Figure (3.11)).

3.3.2.2 Outflow Profiles for Control Columns

Figures (3.13) through (3.17) show the recorded outflow data for loose peat "A", compacted peat "B", filter media bed sand "C", concrete sand "D", and septic bed sand

Reproduced with permission of the copyright owner. Further reproduction prohibited without permission.

"E". Since the flows from each column was recorded approximately every fifth week, only four to five outflow profiles for each column were recorded.

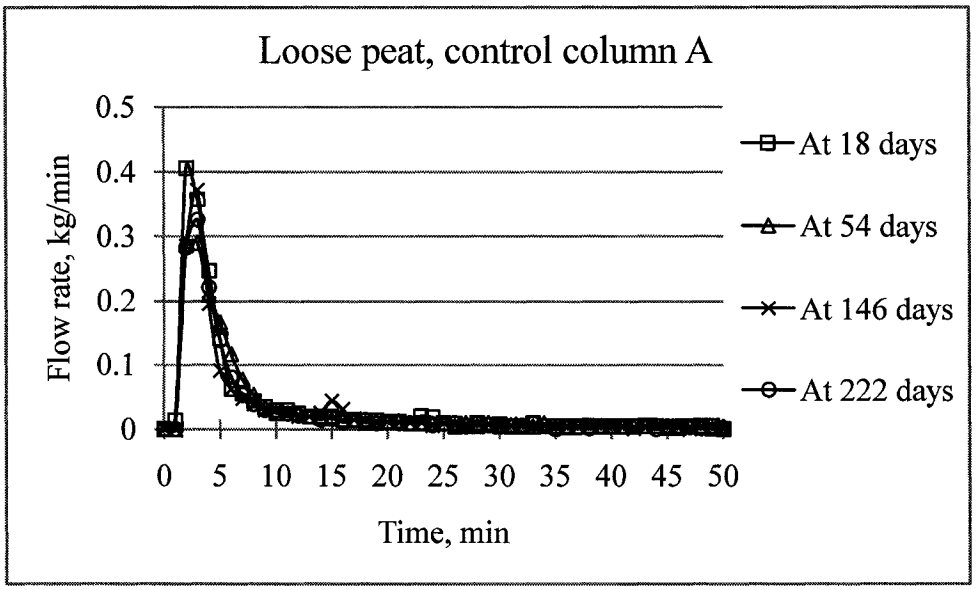

Figure 3.13- Outflow from loose peat control column A

Outflow profiles show different distinguishable peaks for each soil type. For the two peat soils, the peak flow for the loose peat soil exited the column before 5 minutes after loading the column with the 2 L of water. On the other hand, compacted peat soil showed the peak flow around 10 minutes. The delay in the peak flow is due to the much lower K_{sat} for the compacted peat soil versus the loose peat soil.

For the sand soils, the peak flow for the filter media bed sand column was approximately 2.5 minutes after loading the column with the 2 L of water, approximately 10 minutes for the concrete sand soil, and there was no distinguishable peak flow for the septic bed sand soil due to the relatively very low K_{sat} value of the septic bed sand soil. The variation in the outflow profiles shown in Figures (3.14) and (3.17) for the compacted peat and the septic bed sand control columns, respectively, may be attributed

Reproduced with permission of the copyright owner. Further reproduction prohibited without permission.

to the hydraulic loading provided to these columns prior to the time where the outflow measurements were recorded. It should be noted that the time axes for soils A, B, C, and D are consistent at 50 min; where outflow for the septic bed sand is plotted to 200 min due to the slower outflow.

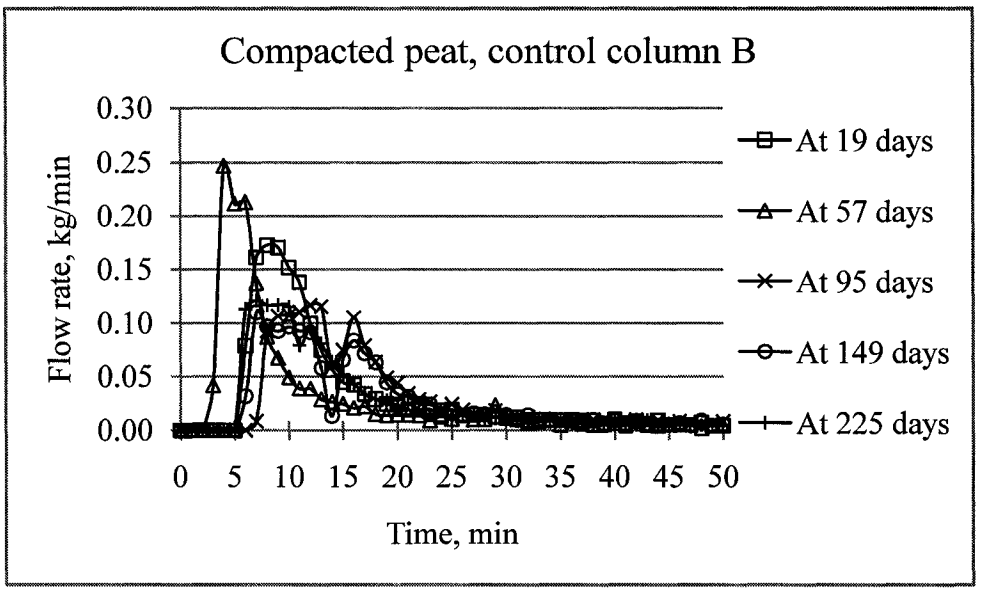

Figure 3.14- Outflow from compacted peat control column B

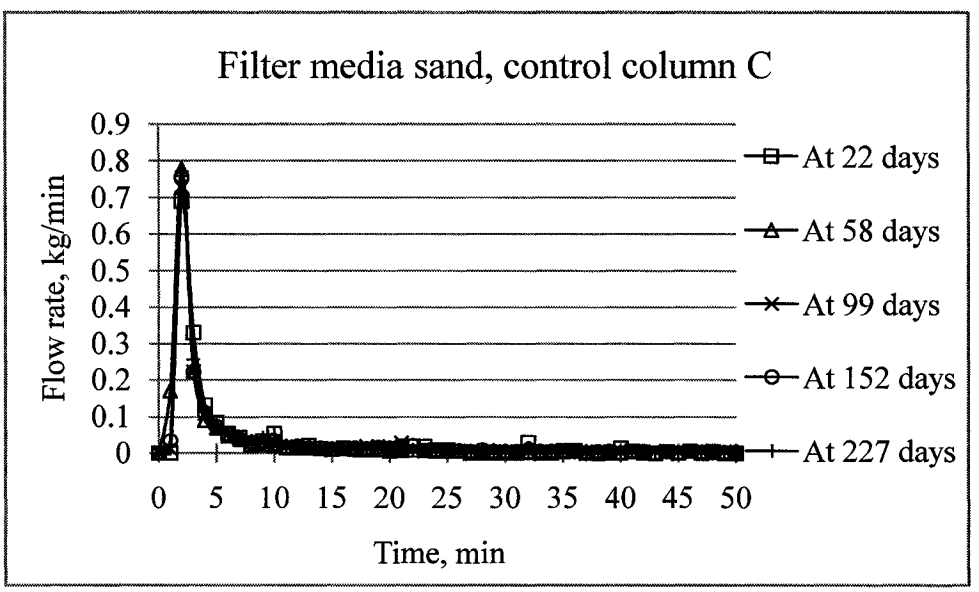

Figure 3.15- Outflow from filter media bed sand control column C

Reproduced with permission of the copyright owner. Further reproduction prohibited without permission.

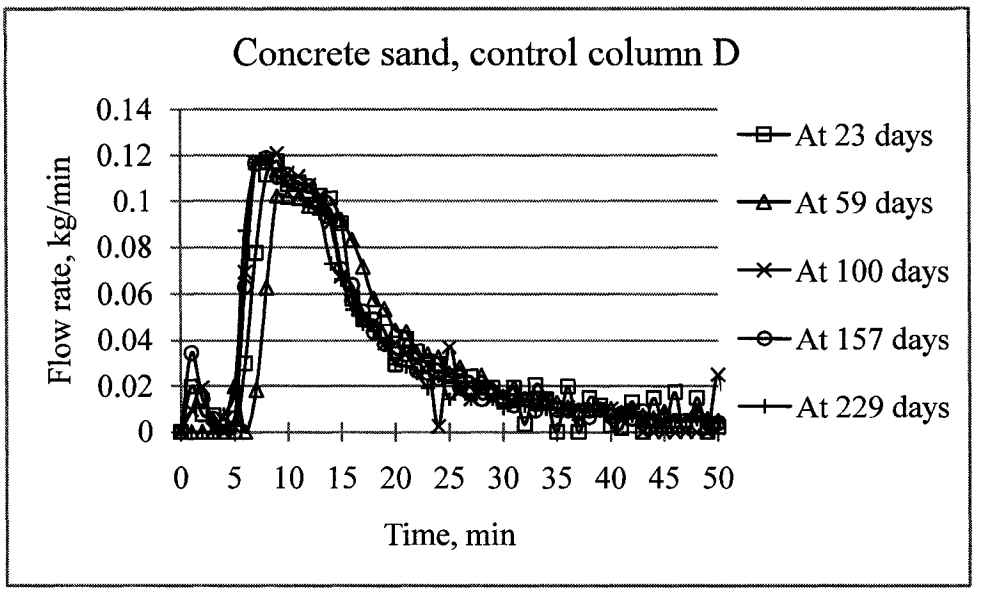

Figure 3.16- Outflow from concrete sand control column D

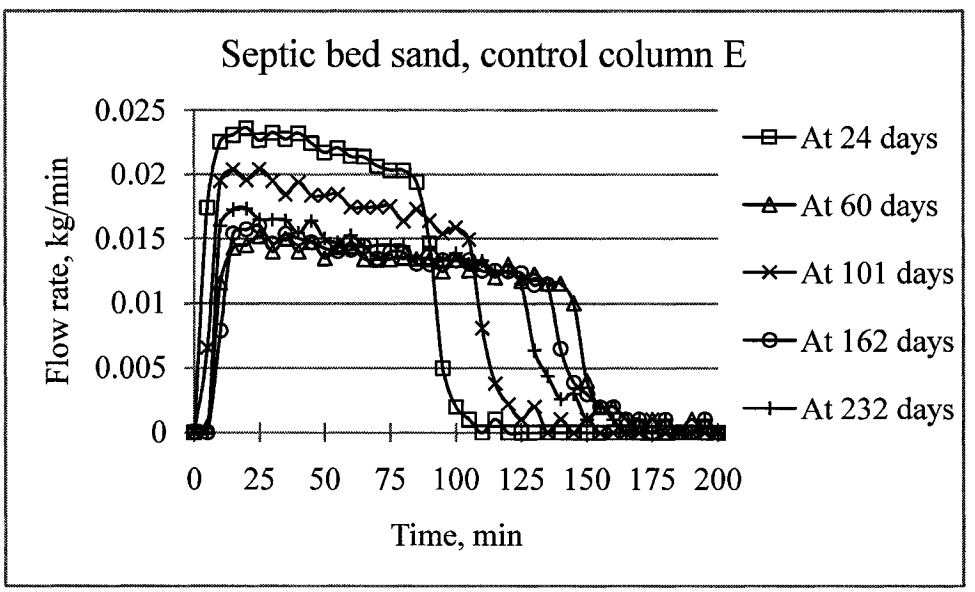

Figure 3.17- Outflow from septic bed sand control column E

Reproduced with permission of the copyright owner. Further reproduction prohibited without permission.

3.3.2.3 Saturation Profiles for Columns Loaded With Organic and Loaded With Organic plus Suspended Loading

Figures (3.18) through (3.27) present the TDR measurements for duplicate columns pulsed with and without suspended solids. The figures illustrate that duplicate columns show no visual appreciable differences in the measured saturation profiles. Also, comparing the columns loaded with organic loading only and organic plus suspended loading did not result in any differences either. The addition of silica power to the loading did not impact clogging because the amount of silica added was not sufficient to impact the overall clogging process in the soils. It is believed that if the amount of silica added at each pulse was greater than the amount used, physical clogging might also have been considered and significantly affected the time to clog for the columns loaded with organic plus suspended loading as reported in the literature.

If one compares the changes in the saturation profiles for the peat soils with the sand soils, different trends will be noticed. The saturation profiles for the peat tended to shift to higher saturations with time over the entire depth of the peat columns. However, the saturation profiles for the septic and concrete sands demonstrated a sharp increase in saturation at the top of the columns over time.

One explanation for the different responses from the peats versus sand soils may be attributed to the porosity. For example, both the filter media bed sand and loose peat have initial high K_{sat} values which allow a pulse to move through the columns quickly (approximately 10 minutes, Figures (3.13) and (3.15)). In addition, the peat soils have a much greater porosity and hence an increase in microbial growth, assuming both the soils generate similar volumes of biomass, will have less impact on the overall porosity

Reproduced with permission of the copyright owner. Further reproduction prohibited without permission.

contributing to flow. Hence, the impacts of the microbial growth may be more significant in the sand soils and result in a greater decrease in permeability at the top of the column. This will reduce the flow rate at the top of the column, reducing the rate of flow though this section of the column and causing the biomass to concentrate in this section. In contrast, the impacts of the microbial growth on the permeability of the peat are lower due to the greater porosity and a pulse is allowed to migrate further into the column. This impact can be seen in the outflow rates presented in the next section.

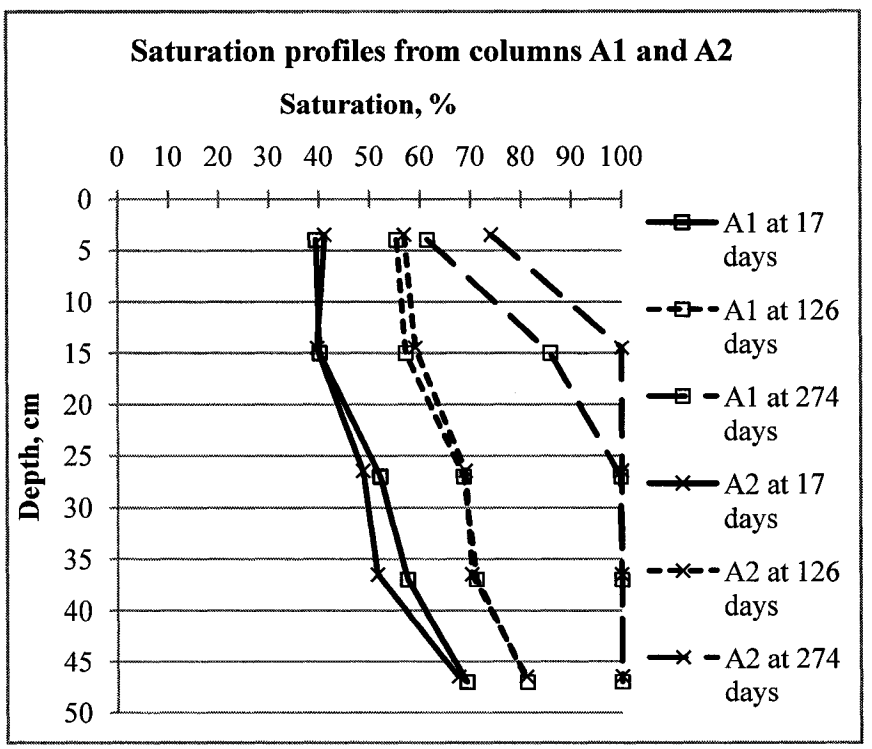

Figure 3.18- Saturation profiles from loose peat columns A1 and A2

Reproduced with permission of the copyright owner. Further reproduction prohibited without permission.

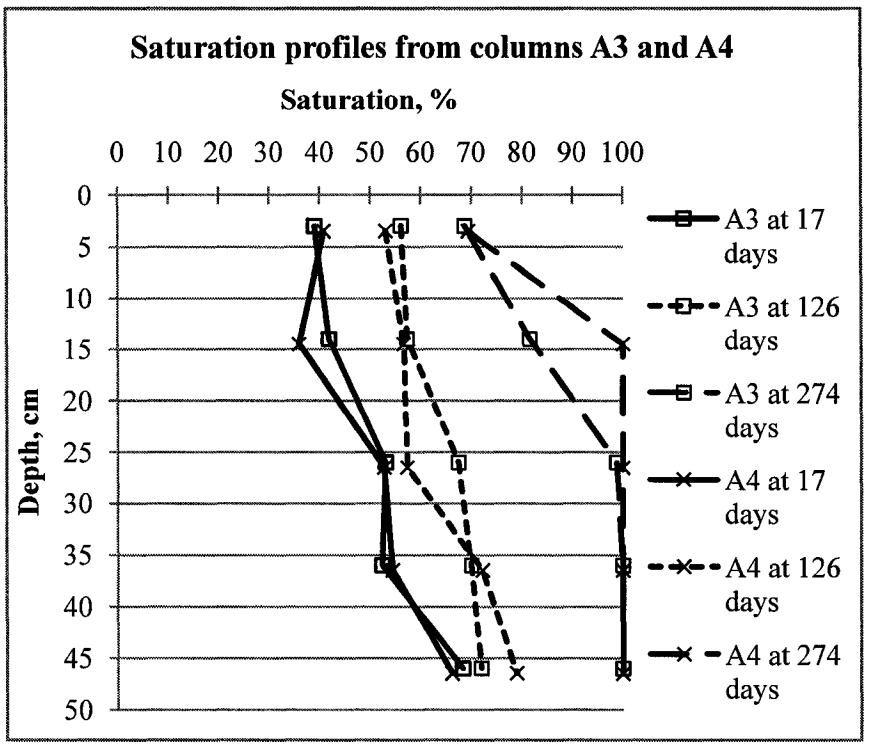

Figure 3.19- Saturation profiles from loose peat columns A3 and A4

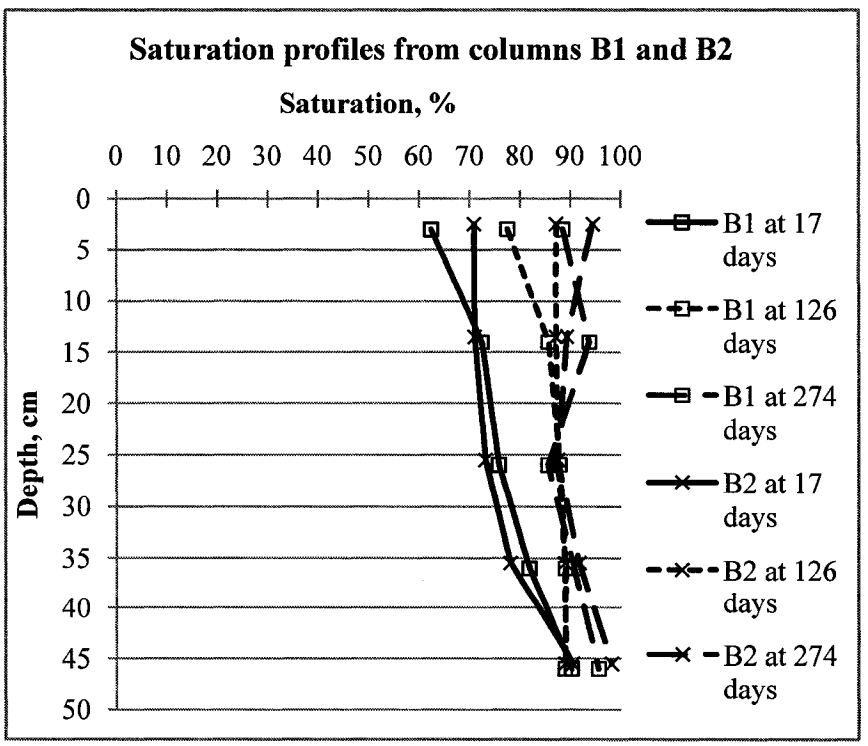

Figure 3.20- Saturation profiles from compacted peat columns B1 and B2

Reproduced with permission of the copyright owner. Further reproduction prohibited without permission.

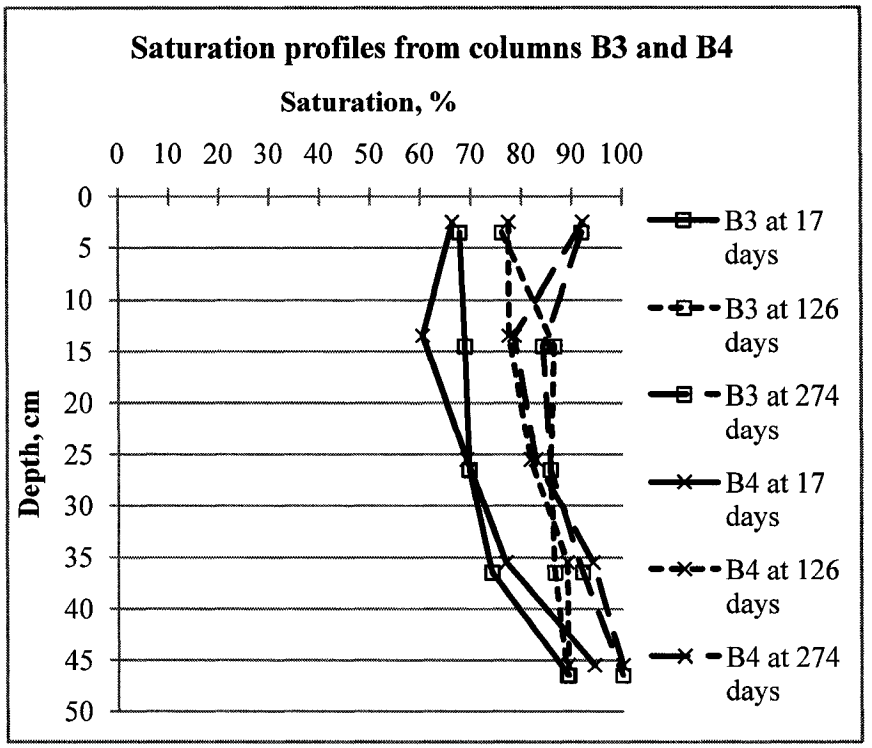

Figure 3.21- Saturation profiles from compacted peat columns B3 and B4

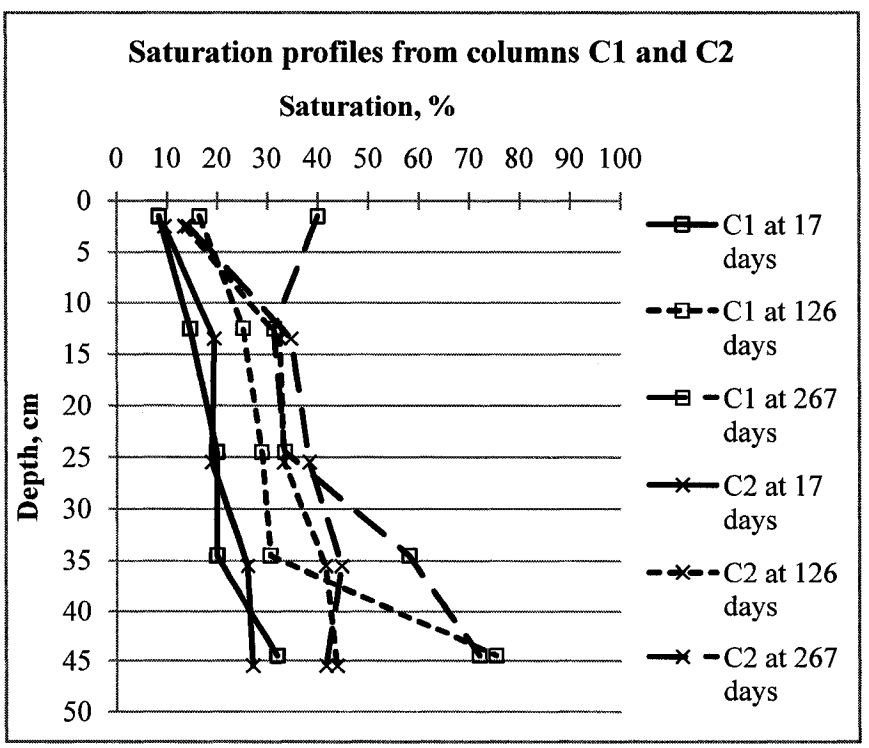

Figure 3.22- Saturation profiles from filter media bed sand columns C1 and C2

Reproduced with permission of the copyright owner. Further reproduction prohibited without permission.

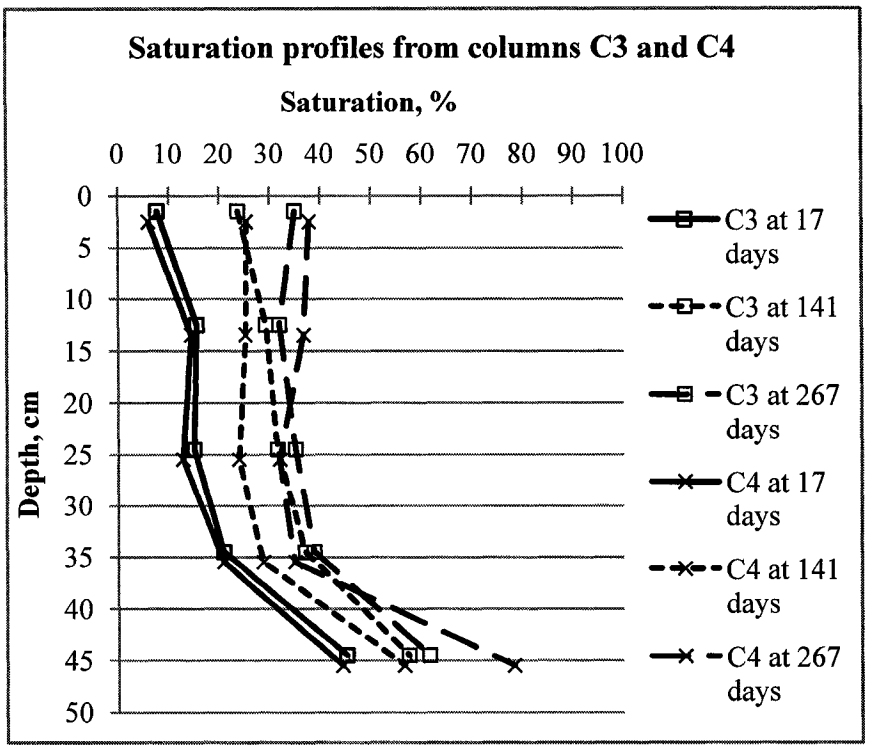

Figure 3.23- Saturation profiles from filter media bed sand columns C3 and C4

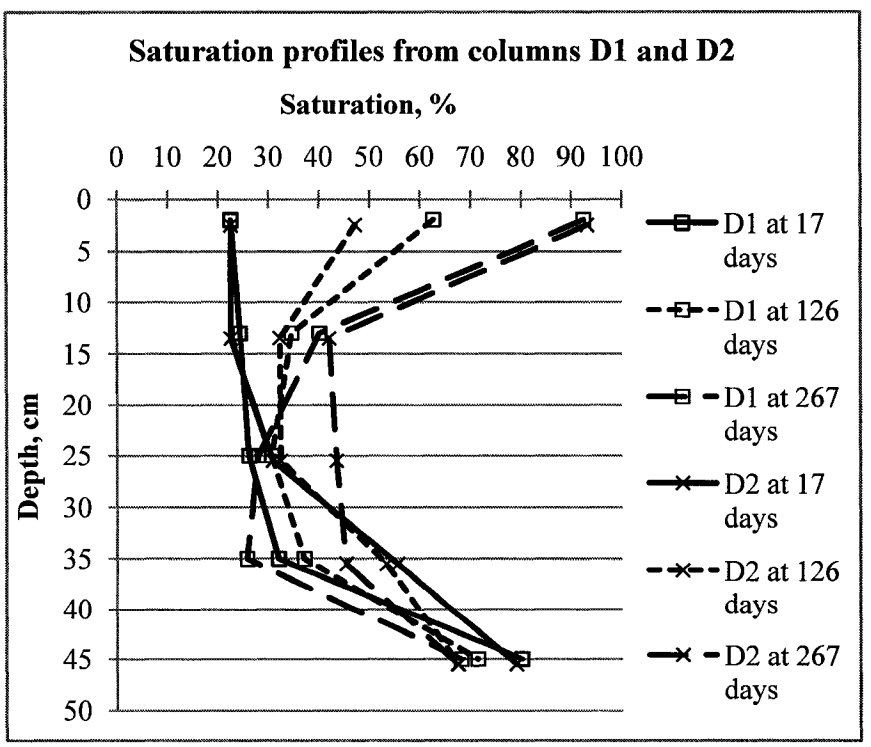

Figure 3.24- Saturation profiles from concrete sand columns D1 and D2

Reproduced with permission of the copyright owner. Further reproduction prohibited without permission.

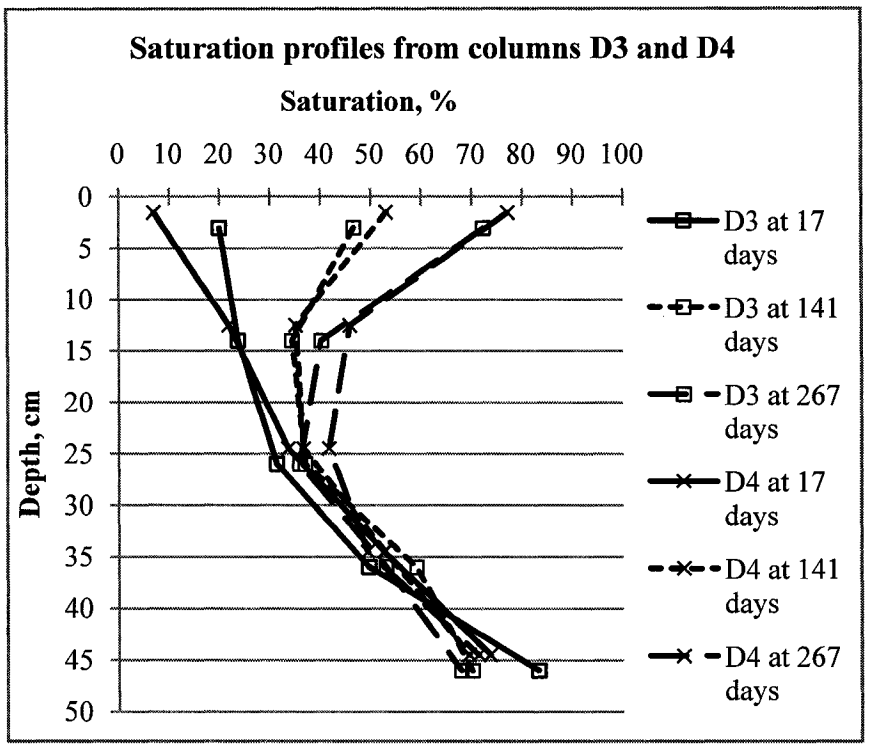

Figure 3.25- Saturation profiles from concrete sand columns D3 and D4

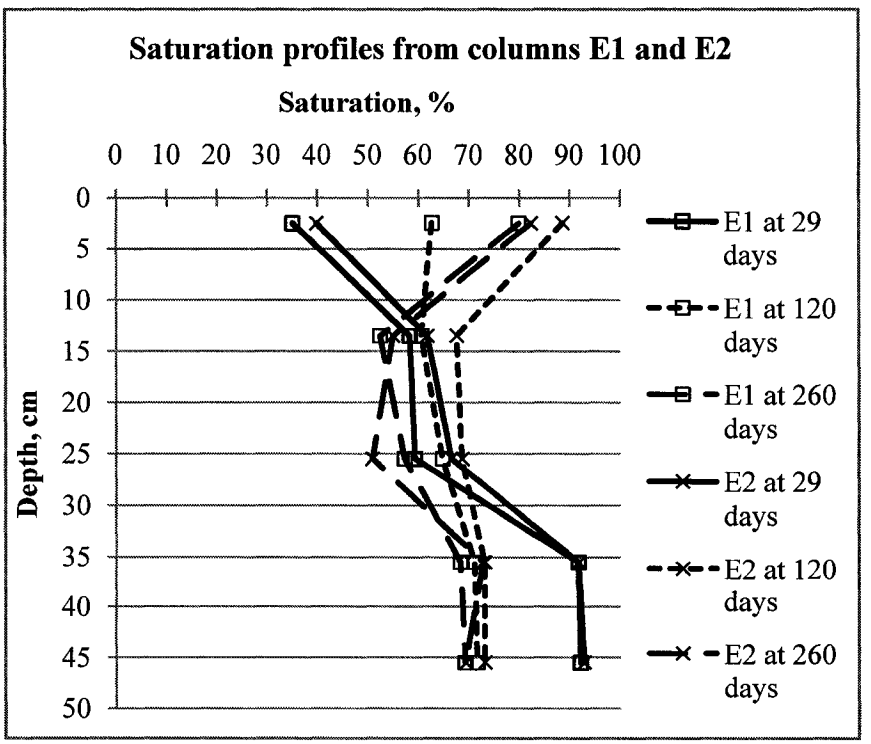

Figure 3.26- Saturation profiles from septic bed sand columns E1 and E2

Reproduced with permission of the copyright owner. Further reproduction prohibited without permission.

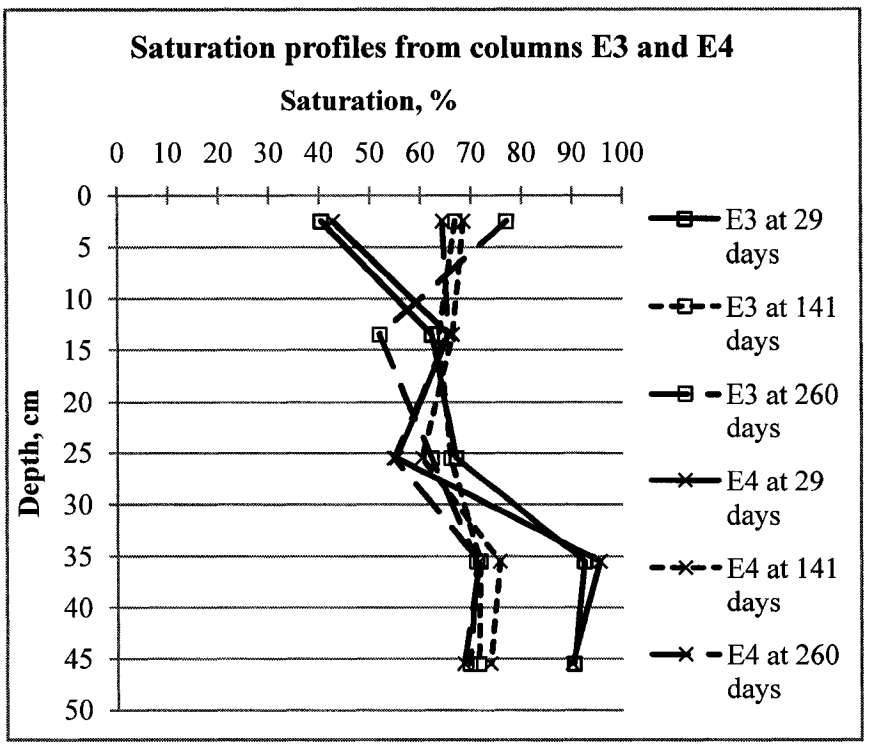

Figure 3.27- Saturation profiles from septic bed sand columns E3 and E4

3.3.2.4 Outflow Profiles for Columns Loaded With Organic and Loaded With Organic plus Suspended Loading

As mentioned previously, since the flows from each column were recorded approximately every fifth week, only four to five outflows for each column were recorded. For the columns loaded with organic loading only and organic plus suspended, it was challenging to capture the reduction and delay in the peak flow from the columns. For a number of columns, by the time that column was scheduled to record the outflow, the relative permeability was significantly reduced and there was no distinguishable peak.

Figures (3.28) through (3.32) show examples of the outflow data recorded for columns with the five types of soil used in this experiment (see section (A.5), Appendix

Reproduced with permission of the copyright owner. Further reproduction prohibited without permission.

A, for the rest of the outflow data). The figures show a reduction and a delay in the peak flow as time elapsed. As microbial mass established in the columns, relative permeability is reduced and this reduction resulted in a delay and reduction to the peak flow compared to the control columns.

Peat soils show gradual reduction in the outflow with time compared to rapid reduction for the sand soils. As discussed previously, the impact on the permeability due to microbial growth was lower in peats versus sand soils. The increase in biomass growth has less impact on the peats due to high porosity values which resulted in gradual reduction and delay of the peak flow compared with sand soils.

It is interesting to note that the saturation profiles for the filter media bed sand did not show a sharp increase in saturation at the top of the columns as the septic bed and concrete sands did. However, the reduction in the outflow rate over time for the filter media bed sand was rapid and consistent with the sharp reductions witnessed for the septic and concrete sands.

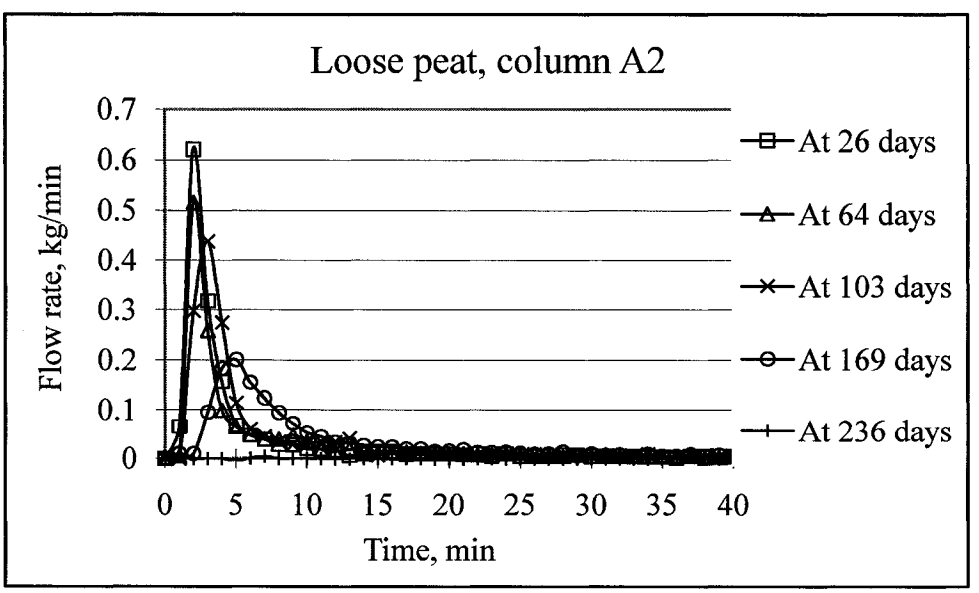

Figure 3.28- Outflow from loose peat column A2

Reproduced with permission of the copyright owner. Further reproduction prohibited without permission.

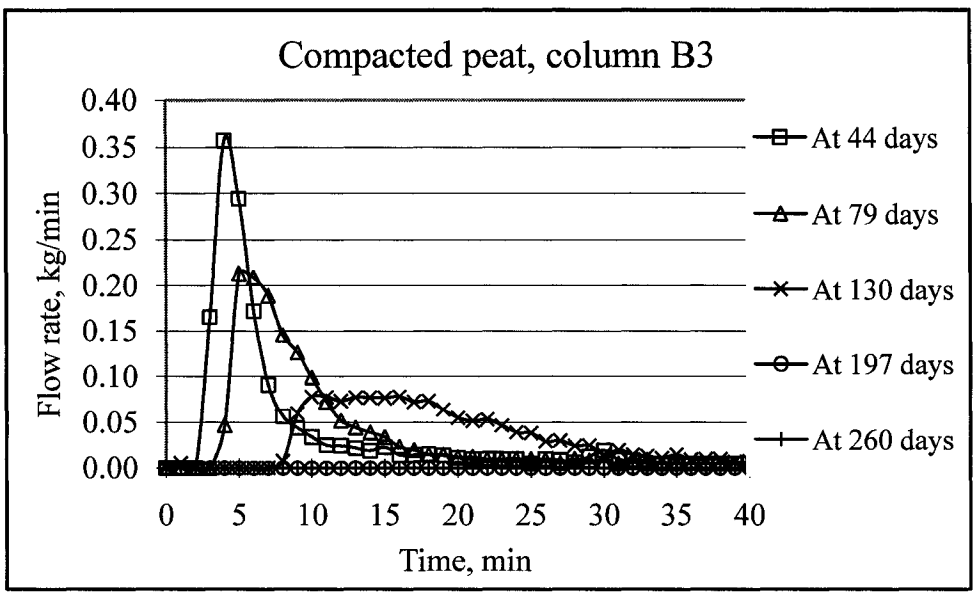

Figure 3.29- Outflow from compacted peat column B3

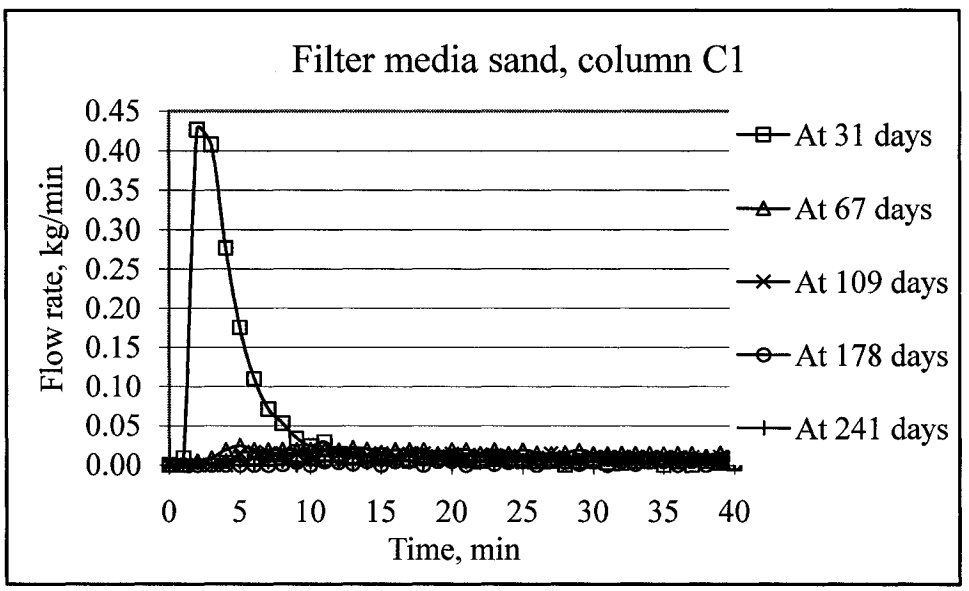

Figure 3.30- Outflow from filter media bed sand column C1

Reproduced with permission of the copyright owner. Further reproduction prohibited without permission.

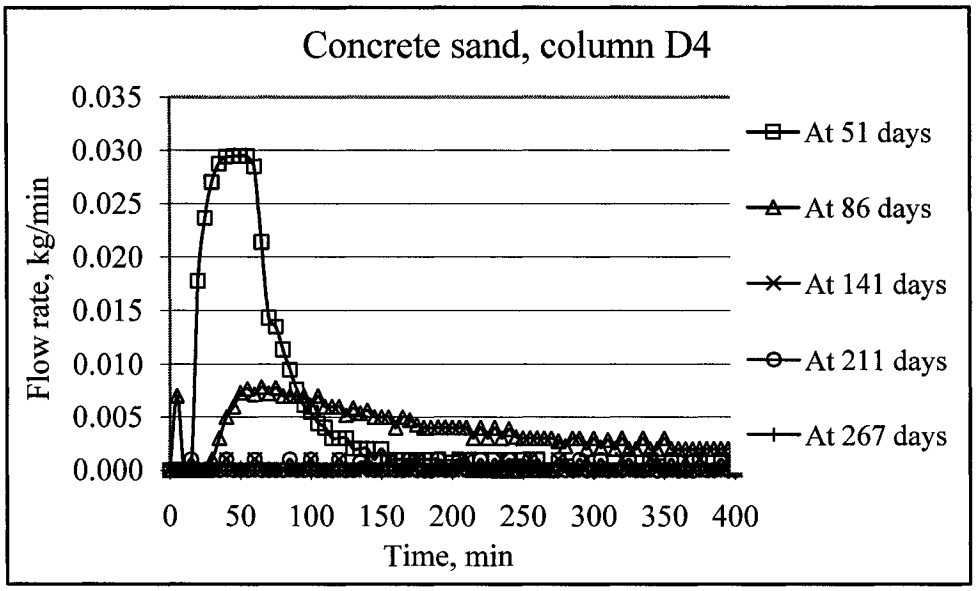

Figure 3.31- Outflow from concrete sand column D4

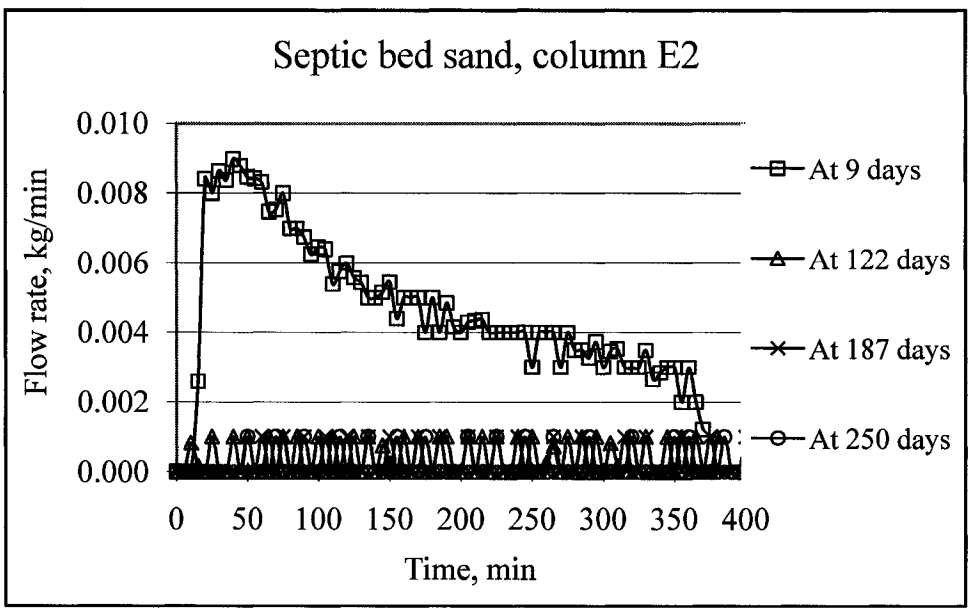

Figure 3.32- Outflow from septic bed sand column E2

Reproduced with permission of the copyright owner. Further reproduction prohibited without permission.

3.3.3 Results at Dismantle Time

As mentioned earlier, at dismantle time, each column was divided into six layers and three types of analyses were conducted on each layer; bacteria count, gravimetric moisture content, and ash content. Bacteria count analysis was conducted to illustrate the microbial distribution with the depth in the column. In addition, TDR measurements were taken just before the columns were dismantled.

3.3.3.1 Results of Bacteria Count

Bacteria counts were conducted on the experimental columns to study the microbial distribution with depth in each column. Figures (3.33) through (3.37) show the bacteria count results. Some of the samples resulted in over grown colonies on the agar plates. The latter is due to contamination during the preparation of the samples and/or culturing the bacteria. Those data points are not shown in the figures.

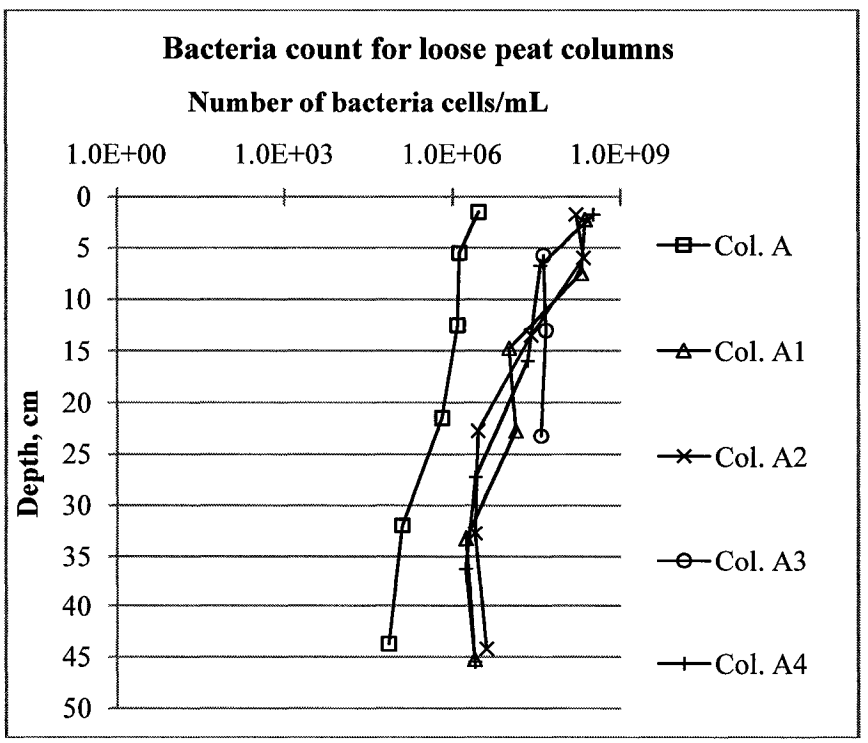

Figure 3.33- Bacteria count at dismantle time for columns A, A1, A2, A3, and A4

Reproduced with permission of the copyright owner. Further reproduction prohibited without permission.

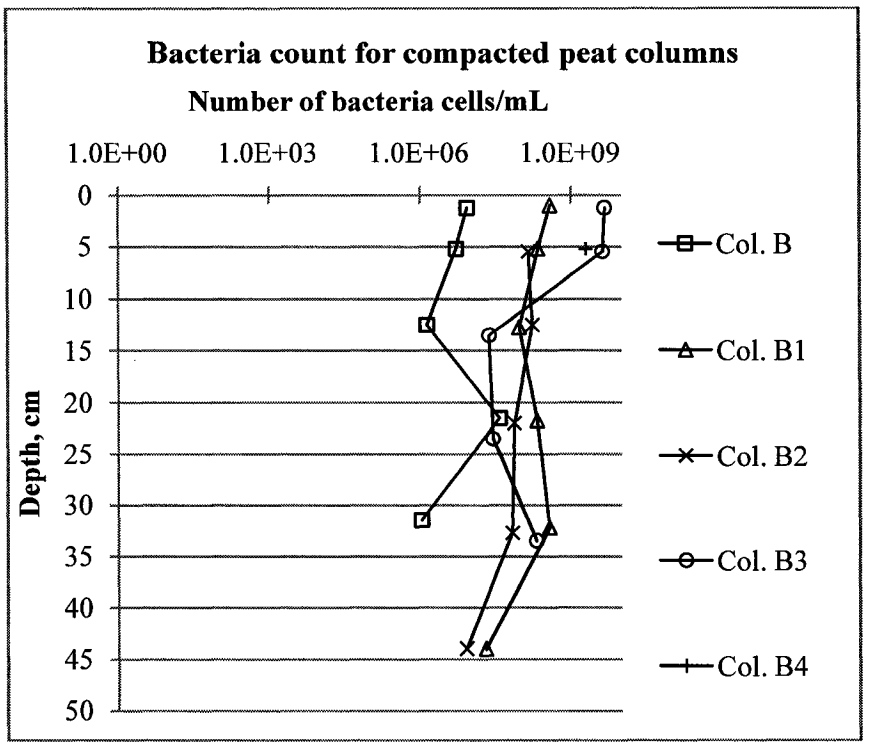

Figure 3.34- Bacteria count at dismantle time for columns B, B1, B2, B3, and B4

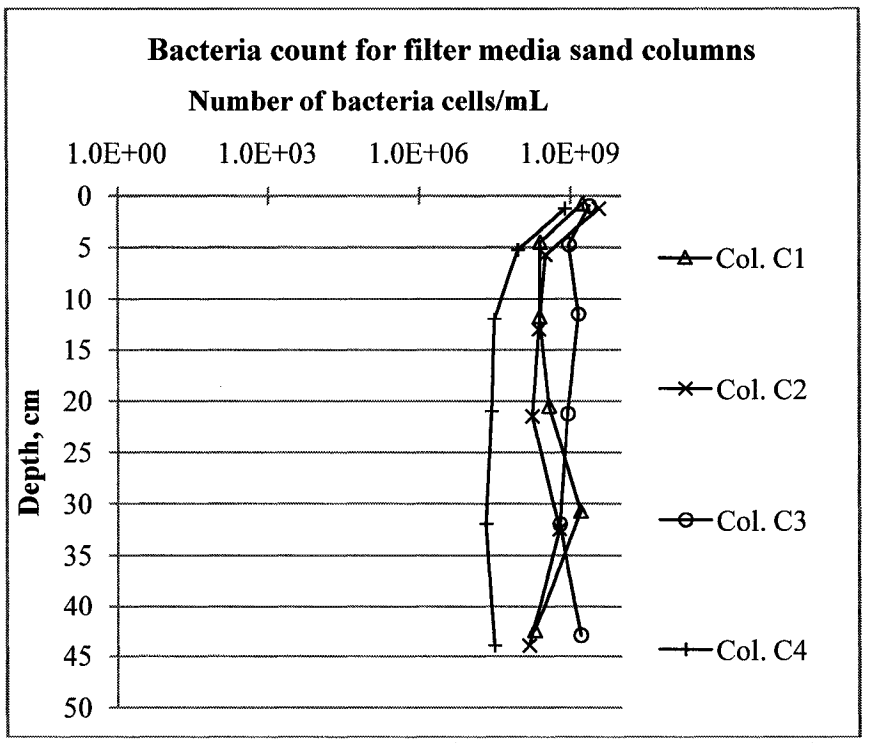

Figure 3.35- Bacteria count at dismantle time for columns C1, C2, C3, and C4

Reproduced with permission of the copyright owner. Further reproduction prohibited without permission.

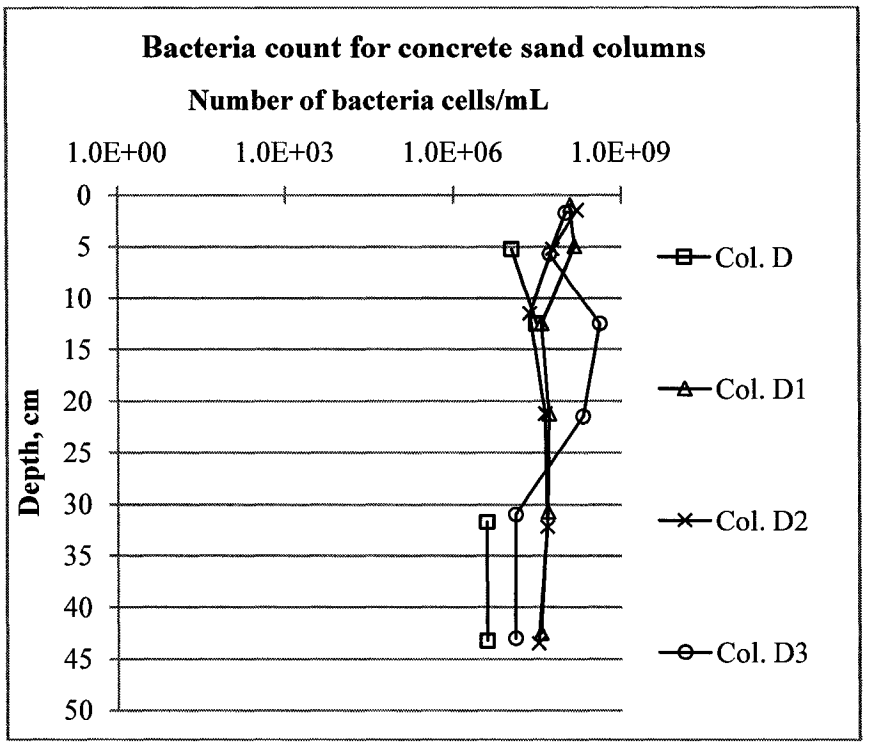

Figure 3.36- Bacteria count at dismantle time for columns D, D1, D2, and D3

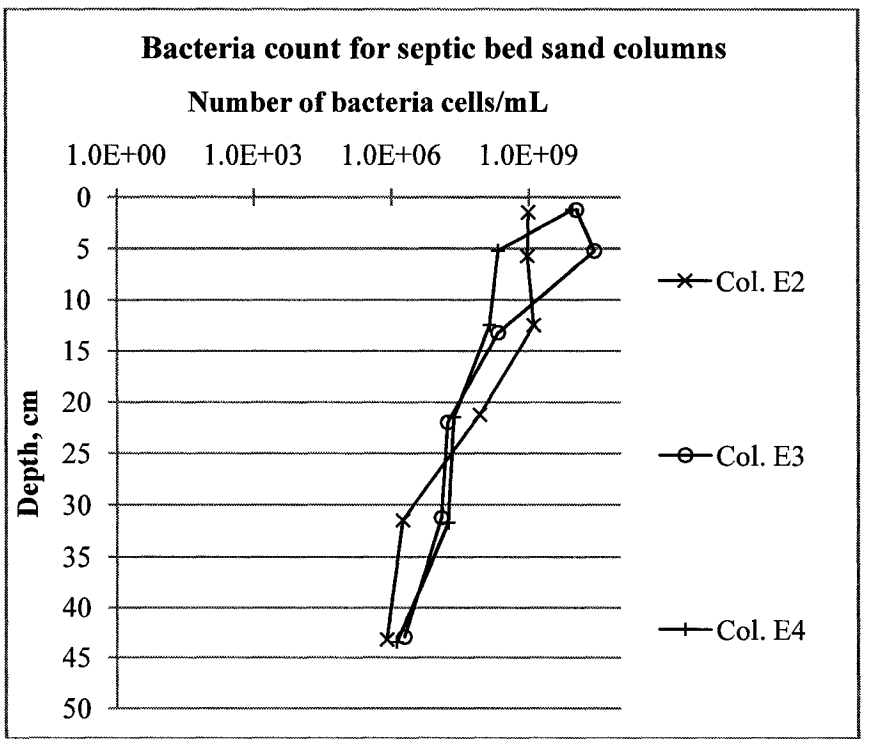

Figure 3.37- Bacteria count at dismantle time for columns E2, E3, and A4

Reproduced with permission of the copyright owner. Further reproduction prohibited without permission.

As expected and as shown in Figure (3.33), columns A1, A2, A3, and A4 show higher bacteria counts than the control column A due to microbial growth. Also, all the bacteria count profiles show high counts at the top of the columns versus the bottom. A higher bacteria count at the top of the columns indicates that most of the food source added to the columns was degraded within the top layer. If most of the food source is degraded within the top layer, the top layer will be severely clogged which was noticed during the visual inspection of the columns while dismantling them. Visual images are provided in section (A.6), Appendix A, for illustration.

3.3.3.2 Comparison between Gravimetric Moisture Content and TDR Measurements at Dismantle Time

The six layers of each column were placed in a clean oven dried aluminum tray. Weight of each tray was recorded after placing the soil layers in the trays and then placed in the oven to dry for 24 hours at 105 °C. The weight of each tray was then recorded and the gravimetric moisture content for each layer was calculated. Figure (3.38) shows the results of the recorded TDR measurements and the corresponding gravimetric moisture content values for loose peat columns A, A1, A2, A3, and A4. It is obvious that TDR measurements for all the recorded data points were always greater than the corresponding gravimetric moisture content value. This difference can be partially attributed to the dismantling process and the difficulty in removing the loosely packed peat. While excavating the six layers from each of the loose peat soil columns, there was always excess water as each layer was removed and this water was dripping from the peat as the soil was moved to the aluminum tray. TDR captured this excess water in its measurements but this water was released and lost while placing the soil in each tray and

Reproduced with permission of the copyright owner. Further reproduction prohibited without permission.

hence was not accounted for in the gravimetric moisture content measurements. For this reason, all the TDR measurements for the loose peat columns, which are presented in Figure (3.38), were always greater than the corresponding gravimetric moisture content values. Also, it should be noted that the TDR measurements agree with the weight measurements at the time that the columns were dismantled which indicates that the TDR measurements were more accurate than the gravimetric moisture content values.

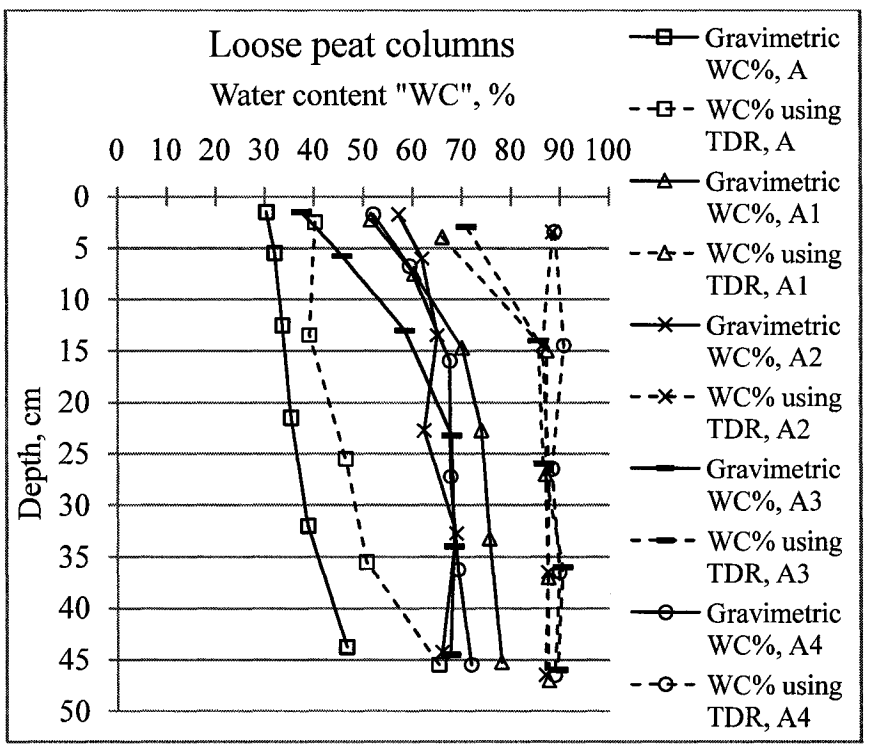

Figure 3.38- Comparison between gravimetric moisture content and TDR measurements at dismantle time for loose peat columns A, A1, A2, A3, and A4

Figures (3.39) and (3.40) show the results for the compacted peat columns. Compacted peat soil did not have the same excess water problem as the loose peat soil. There was no significant difference between the TDR measurements and the corresponding gravimetric moisture content values based on a paired t-test with a 95%

Reproduced with permission of the copyright owner. Further reproduction prohibited without permission.

confidence level. Only for column B4 there was a significant difference due to errors made while taking the TDR measurements for this column.

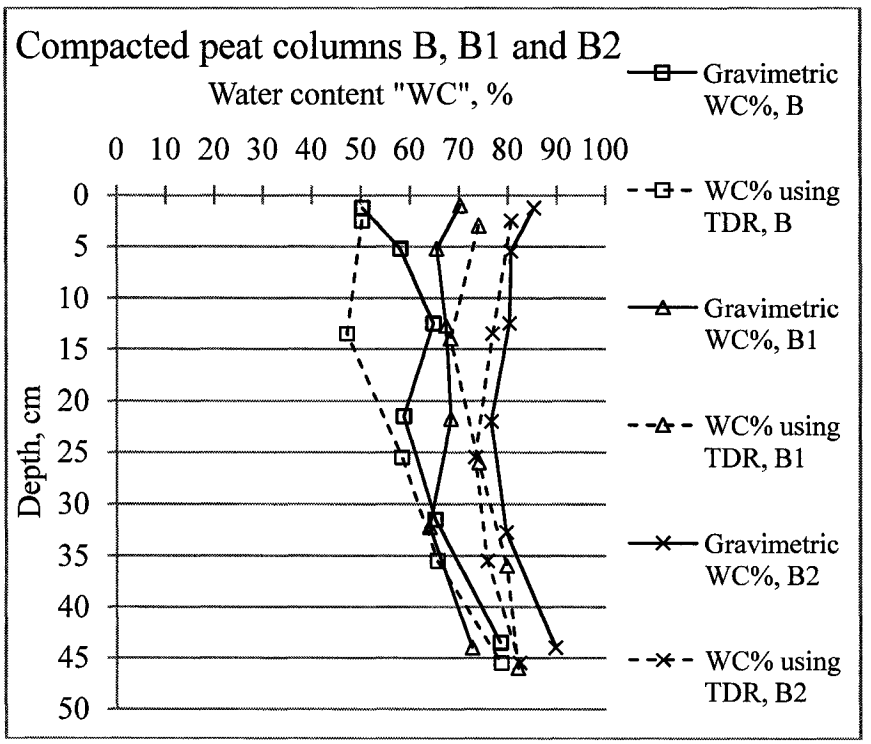

Figure 3.39- Comparison between gravimetric moisture content and TDR measurements at dismantle time for compacted peat columns B, B1, and B2

Figures (3.41) through (3.46) shows the TDR measurements and the corresponding gravimetric moisture content values for filter media bed sand, concrete sand, and septic bed sand. The excess water problem in the loose peat soil was not found in the sand soils and hence the comparison between the moisture contents resulted in a good match with no significant difference between the TDR measurements and the corresponding gravimetric moisture content values based on a paired t-test with a 95% confidence level. The high gravimetric moisture content values measured at the top layers and shown in Figures (3.43) through (3.46) are attributed to a saturated biofilm layer that grew on top

Reproduced with permission of the copyright owner. Further reproduction prohibited without permission.

of the soil surfaces which caused the measured gravimetric moisture content values to be higher than the corresponding porosity values for those soils.

It should be noted that the comparison between the TDR measurements and the corresponding gravimetric moisture content values supports the argument discussed earlier in subsection (3.3.1) regarding the selection of the proper soil moisture curves to represent the sand soils. The reader can argue, as mentioned in subsection (3.3.1), that TDR measurements are not accurate which resulted in having differences between the measured values from the Buchner funnel and the TDR values measured for the saturation profiles during the course of the experiment. This subsection verifies that the TDR measurements represent the saturation in the tested soils reasonably well.

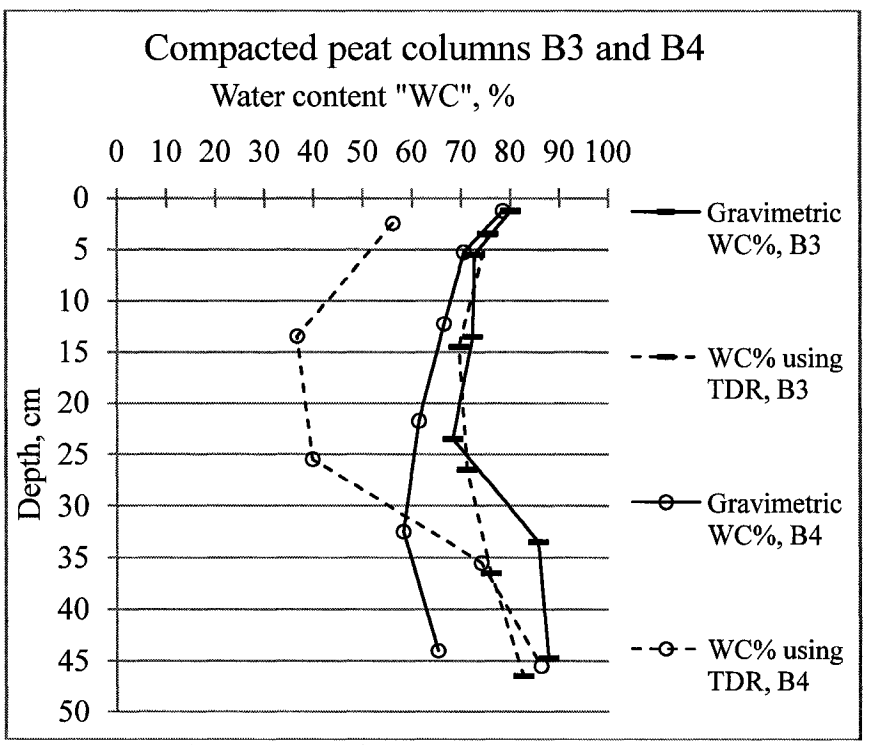

Figure 3.40- Comparison between gravimetric moisture content and TDR measurements at dismantle time for compacted peat columns B3 and B4

Reproduced with permission of the copyright owner. Further reproduction prohibited without permission.

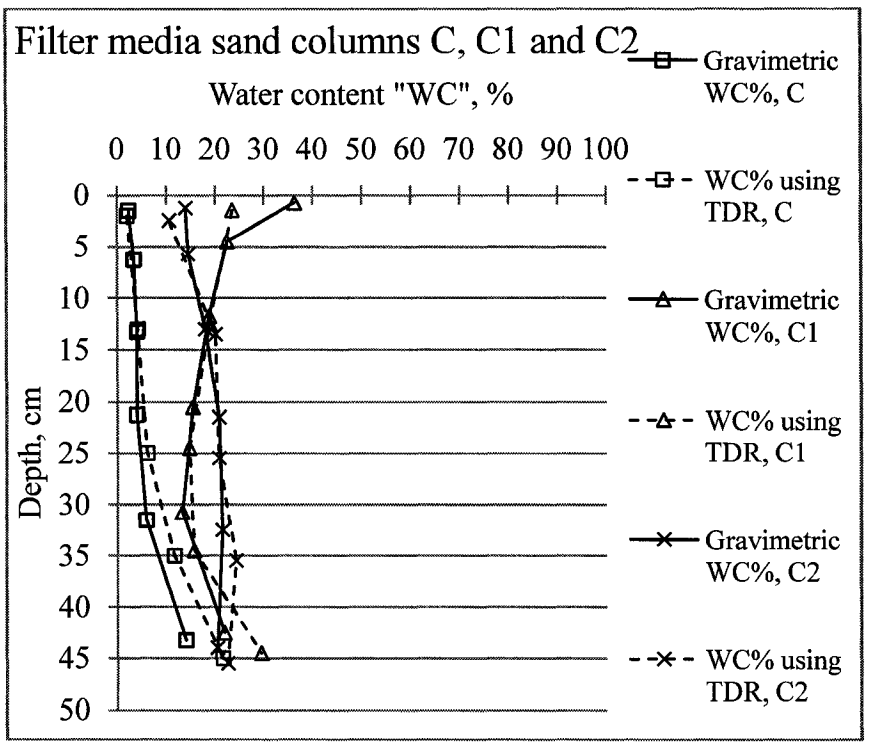

Figure 3.41- Comparison between gravimetric moisture content and TDR measurements at dismantle time for filter media bed sand columns C, C1, and C2

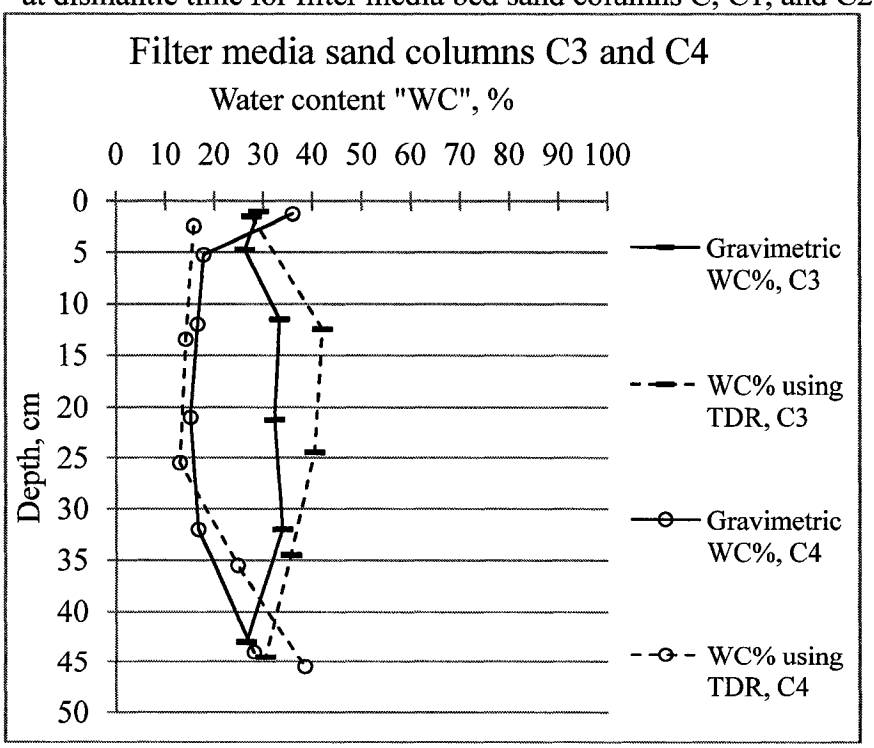

Figure 3.42- Comparison between gravimetric moisture content and TDR measurements at dismantle time for filter media bed sand columns C3 and C4

Reproduced with permission of the copyright owner. Further reproduction prohibited without permission.

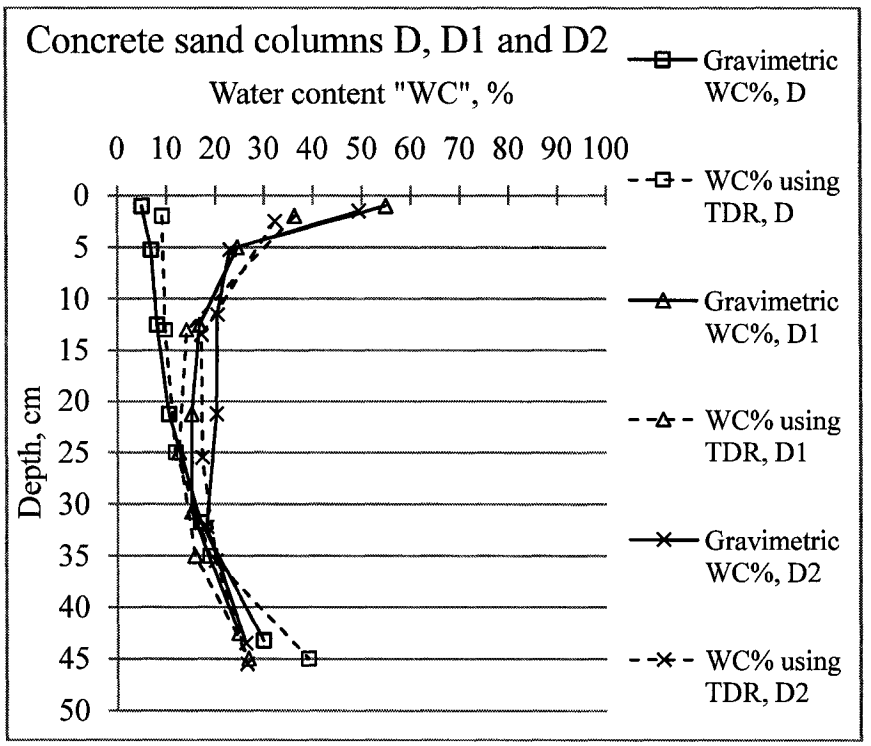

Figure 3.43- Comparison between gravimetric moisture content and TDR measurements at dismantle time for concrete sand columns D, D1, and D2

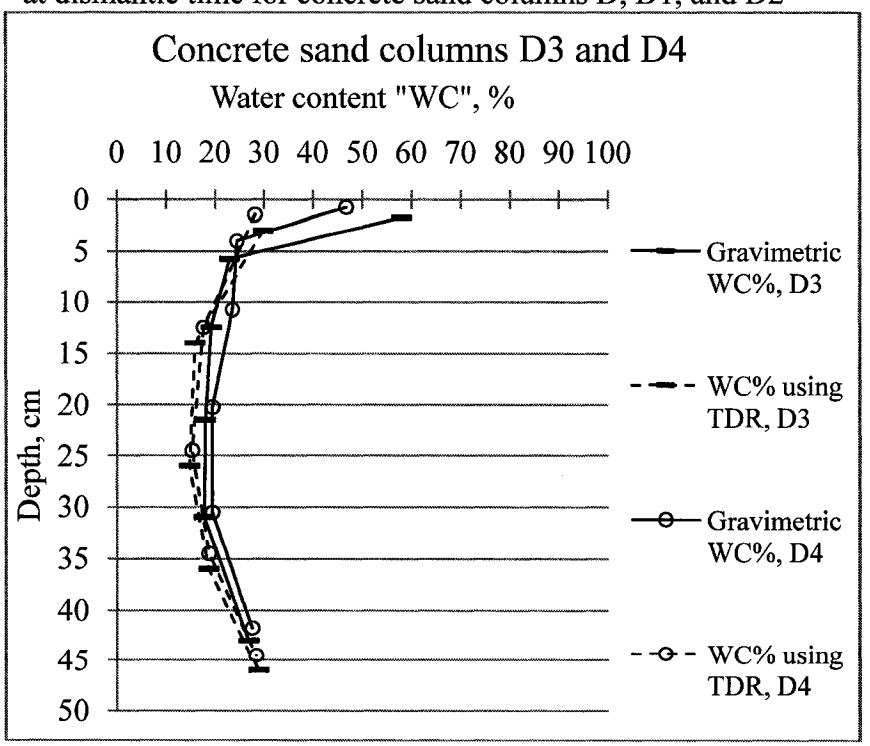

Figure 3.44- Comparison between gravimetric moisture content and TDR measurements at dismantle time for concrete sand columns D3 and D4

Reproduced with permission of the copyright owner. Further reproduction prohibited without permission.

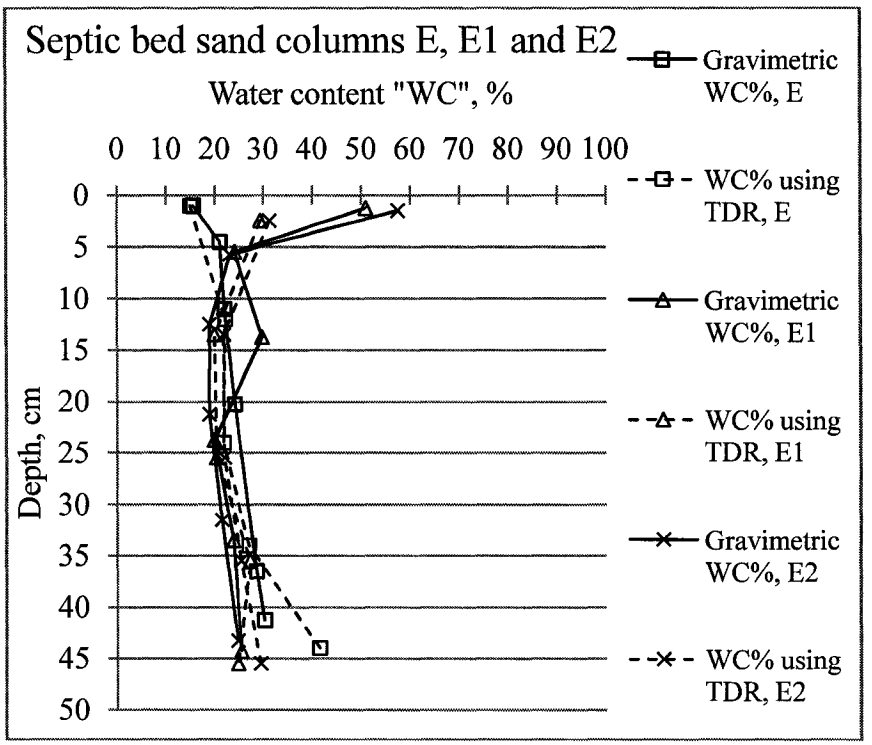

Figure 3.45- Comparison between gravimetric moisture content and TDR measurements at dismantle time for septic bed sand columns E, E1, and E2

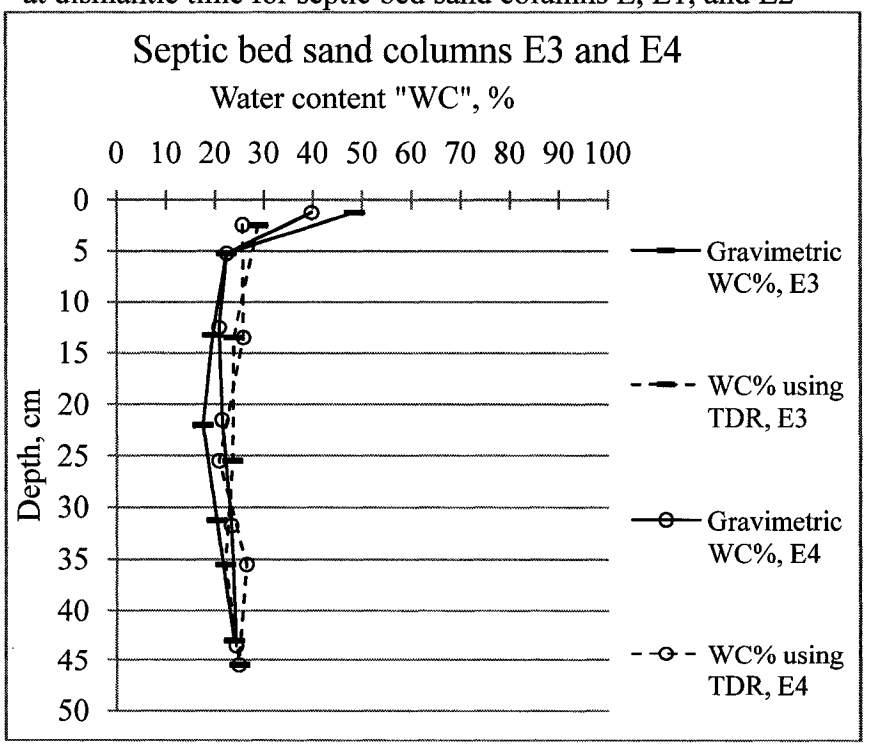

Figure 3.46- Comparison between gravimetric moisture content and TDR measurements at dismantle time for septic bed sand columns E3 and E4

Reproduced with permission of the copyright owner. Further reproduction prohibited without permission.

3.3.3.3 Results of Ash Content

Ash content tests were conducted to check the silica distribution in the columns and to determine whether the columns were able to filter the suspended solids added with the pulse loading. Triplicate samples were taken from each of the six layers from each column and the percentage of ash content was calculated based on the average of the triplicate sample. Figures (3.47) and (3.48) illustrate the percentage of ash content for the two peat soils. Table (3.4) provides the total amount of silica added to the columns loaded with the organic plus suspended loading during the experiment period and Table (3.5) illustrates the percentage of ash content for the three sand soils.

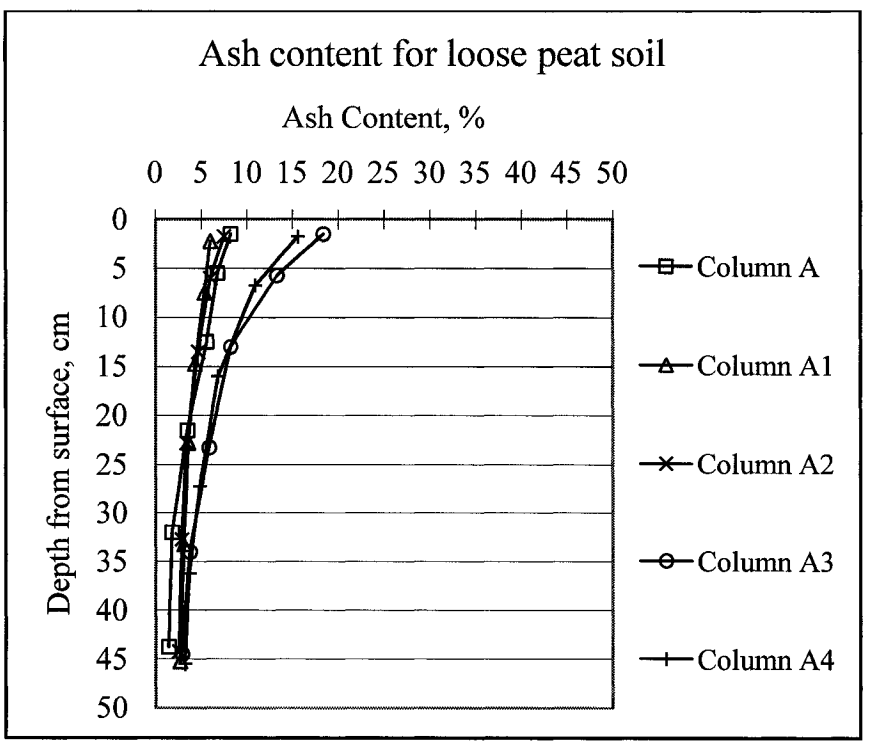

Figure 3.47- Ash content for loose peat columns

Reproduced with permission of the copyright owner. Further reproduction prohibited without permission.

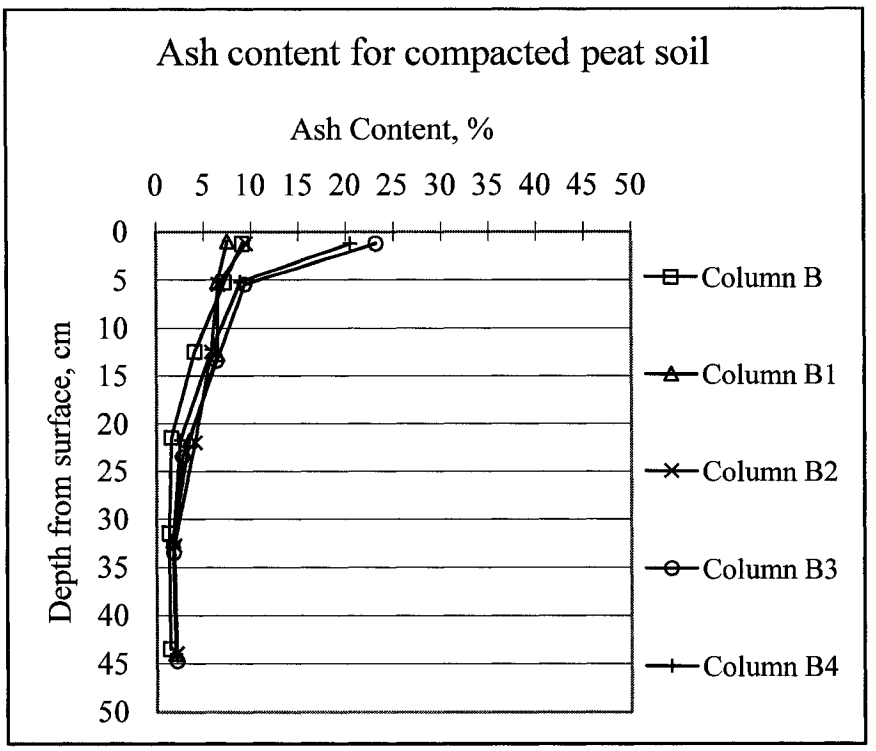

Figure 3.48- Ash content for compacted peat columns

Table 3.4- Weight of silica in grams added to the columns loaded with organic plus suspended loading

Soil type	Loose peat		Compacted peat		Filter media bed sand		Concrete sand		Septic bed sand	
Column	A3	A4	B3	B4	C3	C4	D3	D4	E3	E4
Silica, g	51.85	54.60	43.75	42.90	67.60	46.40	32.95	37.70	25.30	26.15

Table 3.5- Percentage of ash content in each column

Soil type	Col.	Ash Content, %	Soil type	Col.	Ash Content, %	Soil type	Col.	Ash Content, %
Filter media bed sand	C	99.554	Concrete sand	D	99.538	Septic bed sand	E	99.622
	C1	99.102		D1	99.308		E1	99.509
	C2	98.518		D2	99.442		E2	99.491
	C3	98.501		D3	99.408		E3	99.405
	C4	99.217		D4	99.390		E4	99.272

Reproduced with permission of the copyright owner. Further reproduction prohibited without permission.

Except for the filter media bed sand columns C3 and C4, Table (3.4) shows that both of the duplicate columns approximately received the same amount of silica during the experimental period.

As shown in Table (3.5), the control sand columns show approximately 100% ash content. The columns loaded with organic loading and organic plus suspended loading show slightly less percentage of ash content values as these samples contain microbial mass which will lower ash content measured in the samples extracted from those columns.

For the sand soils loaded with and without suspended silica, there was no visual appreciable difference in the ash content given that they are mineral soils. On the other hand, peat is an organic soil and the measured ash content is significantly lower than the sand soils. Figures (3.47) and (3.48) illustrate the ash content distribution in the peat soils. The effect of the silica added is clearly shown in the figures because the weight of the silica added was relatively high compared to the weight of the ash in the clean peat soil.

Most of the silica added to the peat soils was filtered in the top layers. Silica was distributed over a greater depth in the loose peat versus the compacted peat. In the compacted peat soil, soil particles were much denser which resulted in greater physical straining (filtration) and a much steeper silica distribution with depth.

A check was conducted to calculate the percentage removal of silica in the peat soils. Tables (3.6) and (3.7) illustrate the calculation of silica removal from the loose peat columns A3 and A4 and compacted peat columns B3 and B4, respectively.

Reproduced with permission of the copyright owner. Further reproduction prohibited without permission.

The percentage of ash content measured in the control columns are due to the soil's solid particles. In the columns loaded with organic loading only, a second source is presented, which is ash content from the microbial mass that resulted in clogging the soils. In the columns loaded with organic plus suspended loading, silica is the third source that contributes to the ash content. Figures (3.47) and (3.48) show greater ash content profiles for A3, A4, B3, and B4 than the rest of the columns which is clearly from the silica added with the loading. To check the percentage removal of silica, a background value for the ash content has to be calculated. This background value takes into account the ash resulted from the actual peat soil particles and the ash resulted from the microbial mass. The difference between the background ash content value and the measured values for columns A3, A4, B3, and B4 are the ash content due to the silica added. The percentage removal of silica in the two peat soils can then be calculated by comparing the difference between the measured ash content values and the background value with the total silica mass added to the columns during the experiment period.

Tables (3.6) and (3.7) show the calculations of the background ash content which is 39.45 g from columns A1 and A2 and 58.27 g from columns B1 and B2. Background ash content value is higher in the compacted peat columns than the loose peat soil because it has higher density than the loose peat soil which results in more mass of peat soil in a column and hence higher ash content if it was averaged over the column depth.

Reproduced with permission of the copyright owner. Further reproduction prohibited without permission.

Table 3.6- Percentage of silica removal from the loose peat columns A3 and A4

	Ash content for A1, %	Ash content for A2, %		Mass of dry soil in A1, g	Mass of dry soil in A2, g
	5.98	7.48		91.50	72.40
	5.33	5.96		119.30	98.30
	4.30	4.64		125.80	167.70
	3.57	3.37		170.40	153.80
	3.09	2.86		195.80	179.50
	2.68	2.54		224.50	228.60
Average	4.16	4.48	Sum	927.30	900.30

Average mass of ash in A1 and A2 = 4.32 %

Average mass of dry soil in A1 and A2 = 913.8 g

Background ash content = 39.45 g

Col. A3	Ash content for A3, %		Mass of dry soil in A3, g
	18.42		80.40
	13.30		116.40
	8.21		174.70
	5.83		199.10
	3.74		176.20
	2.89		189.60
Average	8.73 %	Sum	936.40 g

Col. A4	Ash content for A4, %		Mass of dry soil in A4, g
	15.62		72.40
	10.93		141.80
	6.83		205.00
	4.81		197.90
	3.70		124.30
	3.21		188.00
Average	7.52 %	Sum	929.40 g

Total mass of ash in A3, g	81.76	Total mass of ash in A4, g	69.86
Background ash content, g	39.45	Background ash content, g	39.45
Total mass of silica added, g	51.82	Total mass of silica added, g	54.60
Total mass of silica left the col., g	9.51	Total mass of silica left the col., g	24.20
Percentage removal of silica, %	81.64	Percentage removal of silica, %	55.69

Average silica removal from columns A3 and A4 = 68.66%

The total mass of ash in column A3 is 81.76 g and the total mass of silica added in this column during the experiment period is 51.82 g as shown in Table (3.4). The total mass of silica which existed the column during the experiment period will be (51.82-(81.76-39.45)) = 9.51 g which indicates approximately 81.64% percentage removal. The percentage removal for column A4 equals 55.69% which results in average percentage removal of silica in the loose peat soil to be 68.66%. The average percentage removal of

Reproduced with permission of the copyright owner. Further reproduction prohibited without permission.

silica in the compacted peat soil is 76.32% which is slightly higher than what was found in the loose peat because of the density difference.

Table 3.7- Percentage of silica removal from the compacted peat columns B3 and B4

	Ash content for B1, %	Ash content for B2, %		Mass of dry soil in B1, g	Mass of dry soil in B2, g
	7.50	9.48		63.70	66.30
	6.44	6.51		178.60	144.00
	6.45	5.79		186.60	192.00
	3.46	4.05		235.40	264.60
	1.74	1.88		290.00	239.40
	1.98	2.11		319.90	257.00
Average	4.59	4.97	Sum	1274.20	1163.30

Average mass of ash in B1 and B2 = 4.78 % Average mass of dry soil in B1 and B2 = 1218.75 g

Background ash content = 58.27 g

Col. B3	Ash content for B3, %		Mass of dry soil in B3, g	Col. B4	Ash content for B4, %		Mass of dry soil in B4, g
	23.17		58.30		20.48		68.30
	9.36		143.00		8.90		150.40
	6.34		254.50		5.85		214.10
	2.76		237.50		2.50		287.50
	1.80		183.80		1.73		328.10
	2.14		295.40		2.02		304.80
Average	7.60 %	Sum	1172.50 g	Average	6.91 %	Sum	1353.20 g

Total mass of ash in B3, g	89.06	Total mass of ash in B4, g	93.57
Background ash content, g	58.27	Background ash content, g	58.27
Total mass of silica added, g	43.75	Total mass of silica added, g	42.90
Total mass of silica left the col., g	12.97	Total mass of silica left the col., g	7.60
Percentage removal of silica, %	70.36	Percentage removal of silica, %	82.28

Average silica removal from columns B3 and B4 = 76.32%

3.4 Summary of the Findings

The objective of stage one was to study the effect of different pore structures on the clogging of soils. Experimental columns were constructed with five different soil types; three different sand soil types and one peat soil type with two different densities. Saturation profiles measured using TDR indicate an overall shift in the saturation profile

Reproduced with permission of the copyright owner. Further reproduction prohibited without permission.

with time for the peat columns while the sand columns experienced a pronounced increase in saturation at the top of the column. This was attributed to the differences in porosity and will be discussed further in the discussion of stage three.

Microbial growth was the main clogging mechanism in this experiment. The silica added to represent a suspended load did not have any significant impact on the clogging process. The straining or filtration of suspended solids is a physical clogging mechanism that occurs as stated in the literature; but in this experiment, the amount of silica added with each pulse was not large enough to cause any noticeable physical clogging.

Outflow profiles recorded for the twenty five columns showed a reduction and lag in the peak flow due to a pulse as clogging progressed. As microbial mass occupies the pores, a reduction in the relative permeability occurs. This reduction was shown in the outflow profiles presented. Consistent with the saturation profiles, the reduction and lag in the peak flow for the peats were more gradual with time indicating less impact due to microbial growth as the microbial growth distributed itself over a greater depth in the peat soils.

Comparison between TDR measurements and gravimetric moisture content at dismantling provided confidence in the TDR measurements. Also, bacteria counts completed at dismantling showed higher counts at the top layers as opposed to bottom layers. Higher bacteria counts support the argument that most of the food source was degraded within the top layer.

It was difficult to track the percentage of silica removal in sand soils using the ash content test results. Peat soils, on the other hand, indicated that a fraction of the silica was

Reproduced with permission of the copyright owner. Further reproduction prohibited without permission.

retained in the peat columns. The amount retained was greatest in the top layer and decreased with depth.

Data recorded and calculated in this stage will be used in stage three to calibrate the numerical code developed to model clogging in unsaturated soils and to validate the three conceptual models put forward by Mostafa and Van Geel (2007) that relate microbial growth with the reduction in permeability in the unsaturated soils.

Reproduced with permission of the copyright owner. Further reproduction prohibited without permission.

4. STAGE TWO: DETERMINATION OF MONOD KINETIC PARAMETERS

This chapter investigates stage two of this research. Stage two of this research aimed to determine the Monod kinetic parameters that are needed for calibrating the numerical code and the validation of the three conceptual models in stage three. The chapter consists of five main sections; an introduction to stage two, experimental setup, results and discussion of the experimental part of this stage, analysis of results and discussion of the estimation of the Monod kinetic parameters, and a summary of the findings from this stage.

4.1 Introduction

The objective of this stage was to evaluate the Monod kinetics parameters. The first part of this evaluation was conducted experimentally by constructing a series of batch reactor test cells to measure the reduction in the Total Organic Carbon (TOC) with time due to microbial growth. In the second part, a spreadsheet model was developed using Microsoft Excel. This spreadsheet model used the measured TOC data with time from the first part to estimate the Monod kinetic parameters. More details are provided in the following subsections of this chapter.

Reproduced with permission of the copyright owner. Further reproduction prohibited without permission.

4.2 Experimental Setup

4.2.1 Materials and Method

The origin of the microbial population that grew in the experimental columns in stage one was not known since the columns were not inoculated with septic tank effluent. Hence, the population that developed may have originated in the soil, from the air (Seki et al. (1996); Seki et al. (2002)), or from the stock solution during preparation. Given this, the samples for the batch experiment presented here were not inoculated and the experiment was conducted in the same manner as the stage one column experiments with the hope that a similar microbial population would develop.

Concrete sand soil was the soil chosen to be used in this stage. It is believed that the growth behavior in all the five soils used in stage one should be the same but the initial microbial mass might be different since three soils were inorganic (i.e. mostly clean soils) but the other two were organic (i.e. might have some initial inactive microbial mass). The Monod kinetic parameters estimated from this stage were used later in stage three to calibrate the numerical code. If the same Monod kinetics parameters could simulate all the soils, it will support the hypothesis that a similar microbial population was established. In this experiment, a series of batch test cells (i.e. twelve test cells) were pulse loaded twice a day, 5 days a week for approximately 47 days (Figure (4.1)). The same organic feed concentration as what was used in the column experiments in stage one was used to feed the test cells. The test cells were treated as batch reactors (i.e. loaded once every 12 hours) and maintained under unsaturated conditions (i.e. saturation was controlled to ensure saturation less than 100% in each test cell). A more detailed

Reproduced with permission of the copyright owner. Further reproduction prohibited without permission.

explanation is provided in the following sections. Figure (4.2) shows a schematic diagram for a test cell setup.

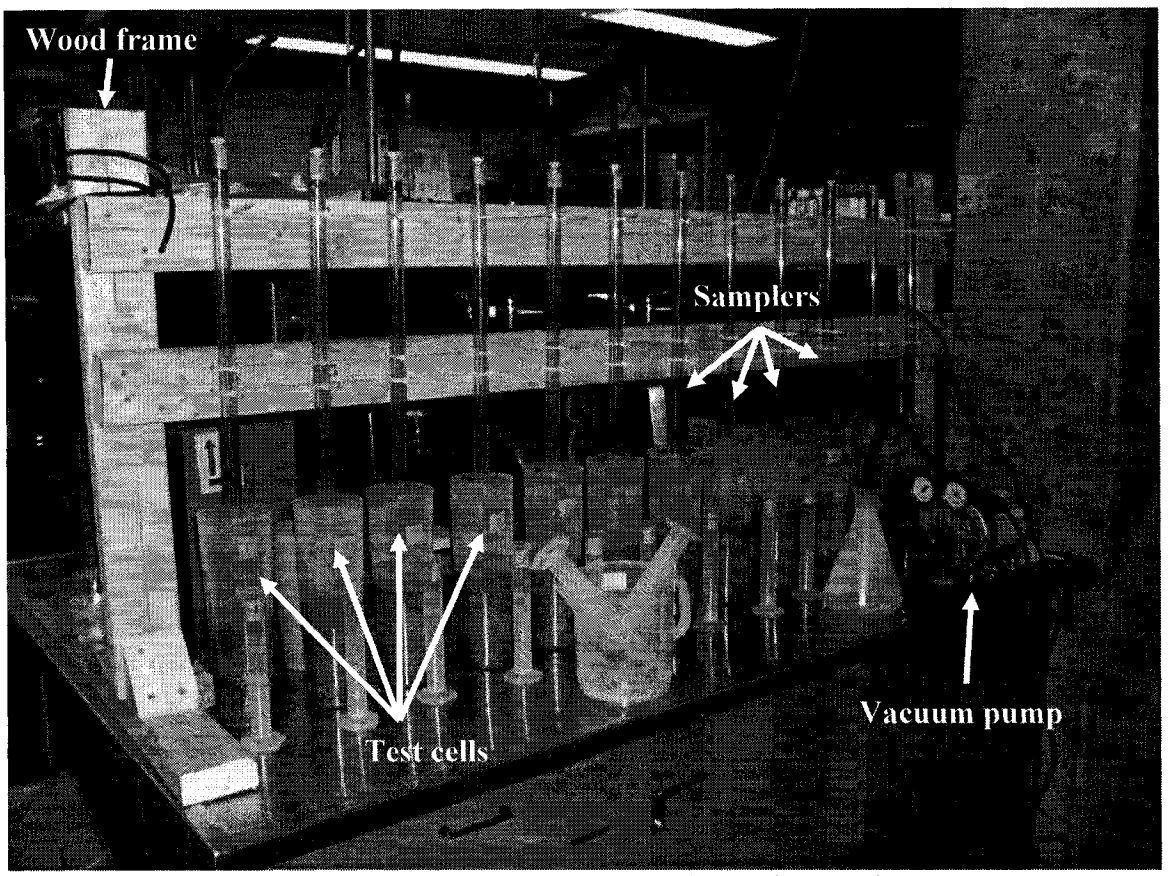

Figure 4.1- Twelve test cells and twelve samples used for this experiment

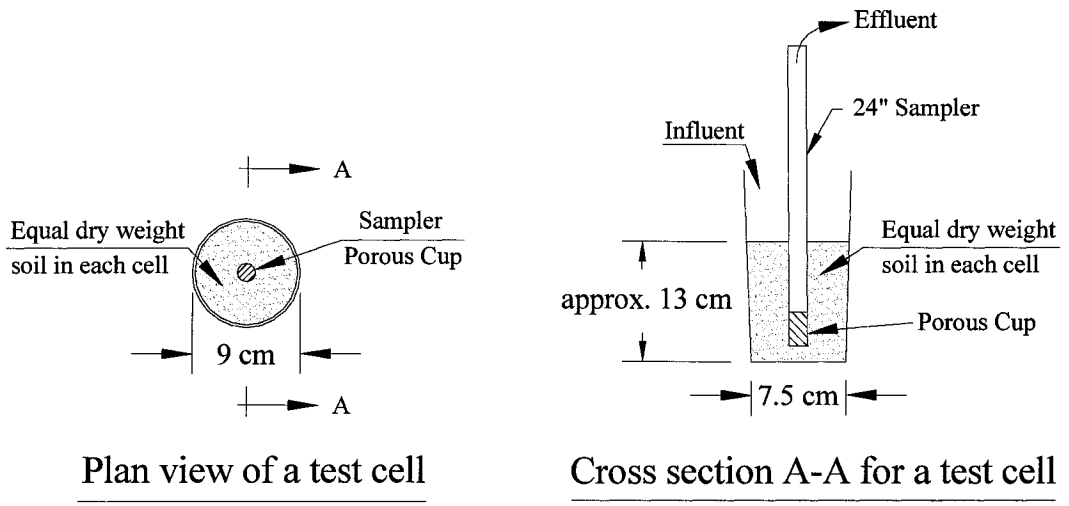

Figure 4.2- Plan view and typical cross section for a test cell setup

Reproduced with permission of the copyright owner. Further reproduction prohibited without permission.

4.2.2 Initial Condition for the Test Cells

As shown in Figure (4.2), each test cell contained soil in a form of a cylinder, 8 cm average diameter by approximately 13 cm in height which was maintained under unsaturated conditions during the experimental period. To ensure unsaturated conditions in each test cell at the beginning of the experiment, test cells were packed after the soil was air dried for 24 hours (approximately 20% saturation). Then the saturation was increased to 50% by adding a calculated volume of water. The 50% saturation was the lowest saturation any test cell would reach during the experimental period.

4.2.3 Loading Rate for the Test Cells

The concentration of the influent added to the cells was equal to the influent concentration for stage one pulsing. The test cells were pulsed twice per day. The difference between the two pulse events per day was approximately 12 hours which created a hydraulic residence time of approximately 32 hours (i.e. batch system).

To ensure sufficient oxygen for aerobic degradation, unsaturated conditions were maintained throughout the experiment. The saturation was maintained at 80%. The hydraulic load for each pulse was equivalent to 30% saturation of the test cell sample.

Prior to each loading, suction was applied using a porous cup connected to a sampler which is connected to a vacuum pump, as shown in Figure (4.1), to withdraw a volume of liquid equivalent to 30% saturation (i.e. same volume added in the previous loading, approximately 70 mL). The pulse load was then added such that the test cells were maintained at a saturation of 80% after each pulse and were treated as a continuously fed batch system.

Reproduced with permission of the copyright owner. Further reproduction prohibited without permission.

At the beginning of every week, the test cells were weighed and water was added to bring the weight of each test cell to a level corresponding to 80% saturation. The water added was to compensate for the water lost due to evaporation.

4.2.4 Measurements at Dismantle Time

Two main measurements were conducted in this experiment; the first was liquid TOC measurements on the influent and effluent from the test cells every 2-3 days using a Total Organic Carbon Analyzer (TOC-V_{CPN}, Shimadzu Corporation). The liquid TOC measurements were used in the second part of this stage to estimate Monod kinetics parameters using the developed spreadsheet model. The second was biomass concentration analysis conducted on the test cells each time a test cell was dismantled.

All the test cells were loaded twice per day, 5 days per week. After the 6th day, two test cells were dismantled every week until all the test cells were dismantled. On the days a test cell was scheduled to be dismantled, a suction was applied on the sampler in this test cell to lower the saturation to approximately 40% and the effluent pumped was used to determine the final liquid TOC for this test cell. Then the soil in the test cell was emptied into a clean aluminum tray pre-dried in the oven. Three different types of analyses were conducted on the soil; Volatile Suspended Solids analysis (VSS), TOC analysis, and bacteria count. The three different analysis types were used to estimate the biomass concentration and compare it with the results of the spreadsheet model.

Bacteria count was conducted in triplicate soil samples (approximately 4.0 g each) using the same procedures explained in stage one. Bacteria counts were converted into microbial concentration using reported conversion factors in the literature. Alvarez et al. (1991) observed bacteria size of 1 μm^3 in a sand aquifer. By assuming a bacteria density

Reproduced with permission of the copyright owner. Further reproduction prohibited without permission.

similar to water (1.04 g/cm^3), they assumed a conversion factor of 10^{-9} mg/bacteria cell to convert a bacteria count into a microbial concentration (in mg/L). It should be noted that the bulk density of the soil has to be known in order to complete the conversion.

Schirmer et al. (1999) used the same value reported by Balkwill et al. (1988) as a conversion factor in a sandy aquifer soil to convert the bacteria count into microbial concentration. A value of 1.72×10^{-10} mg/bacteria cell was assumed with a bacteria size of 1.07 ± 0.71 μm^3.

For the VSS analysis, another set of triplicate samples were chosen randomly from the tray. Each sample was placed in a crucible and the weight was recorded before they were oven dried at 105 °C. Then the samples were placed in the oven at 105 °C for 2 hours or until the weight was constant (i.e. water had evaporated). Then the samples were placed in the furnace at 550 °C for 2 hours and transferred to a desiccator for cooling before the weight was recorded. The cycle of placing the crucibles in the furnace, then a desiccator, and recording the weight was repeated until the weight was constant or the weight change was less than 4% (Eaton et al. (2005)). Knowing the mass lost after weighing the samples before and after placing them in the furnace, %VS removal could be estimated.

The third way to estimate the biomass concentration was by measuring the total TOC in the soil samples. Taylor and Jaffe (1990a) reported microbial concentration directly in terms of Bacterial Organic Carbon (BOC) in mg/L. Bacterial Organic Carbon was calculated by measuring the total TOC in mg/L and subtracting from it the Soluble Organic Carbon (SOC) in mg/L. In order to adopt this method in this stage, triplicate soil samples were extracted from a dismantled test cell and analyzed with the solid TOC analyzer to obtain the total TOC. To calculate the SOC, triplicate soil samples of

Reproduced with permission of the copyright owner. Further reproduction prohibited without permission.

approximately 4.0 grams each were chosen randomly from the tray. Each sample was placed in a 50 mL centrifugal tube with 40 mL of the same dispersion agent used in stage one. The centrifugal tubes were shaken for 2 minutes to separate the biomass from the solid phase and then were filtered on a 0.45 μm membrane filter. The filtered liquids were analyzed for liquid TOC which represents the SOC. The difference between the total TOC and SOC values was the Bacterial Organic Carbon (BOC) (i.e. biomass concentration) as shown by Taylor and Jaffe (1990a).

From the previous measurements, two sets of data were obtained; increase in biomass concentration (M, mg/L) versus time (t, day) and reduction in substrate concentration (C, mg/L) versus time. Figure (4.3) illustrates the expected relationships for a batch system with an initial effluent concentration and biomass concentration of C_o and M_o, respectively.

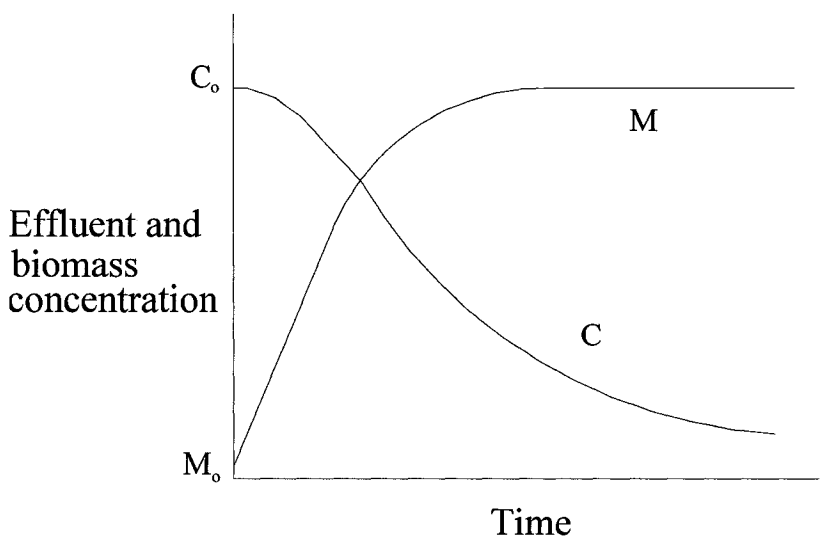

Figure 4.3- Change in effluent and biomass concentrations versus time

Reproduced with permission of the copyright owner. Further reproduction prohibited without permission.

4.3 Results and Discussion of the Experimental Part

4.3.1 Effluent TOC Concentration with Time

Figure (4.4) shows the TOC concentration measured for the influent and the average effluent from the test cells. The average influent concentration was approximately 350 mg/L. This average value was used in the estimation of the Monod kinetic parameters.

For the latter stages, the average effluent concentration had an expected weekly trend as showed in Figure (4.3). Loading of the test cells resumed each Monday morning and a reduction in substrate concentration was noted during the week as biomass grew. When loading stopped over the weekend, the biomass experienced a period of decay prior to resuming the loading on Monday. As a result, the effluent concentrations measured after the first pulse period on Monday increased in comparison to the effluent concentration from the previous Friday. The peak concentration at the beginning of each week decreased with time as more biomass established in the soil pore space. The trend is clearly evident during the final three weeks of sampling (day 30- day 47). The loading history and effluent data were used later in the spreadsheet model to estimate the Monod kinetic parameters.

Reproduced with permission of the copyright owner. Further reproduction prohibited without permission.

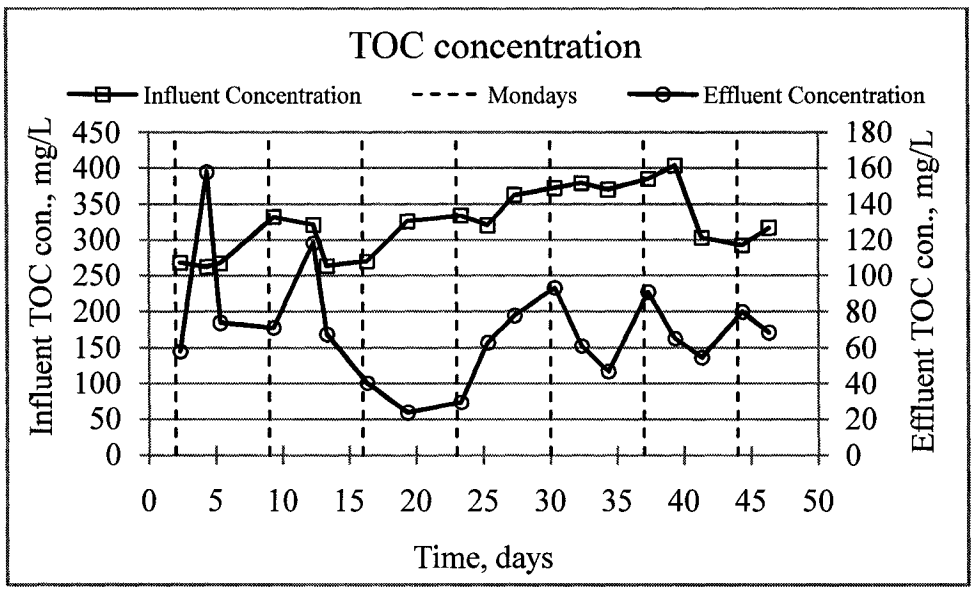

Figure 4.4- Influent and average effluent TOC concentrations measured from the test cells

It should be noted that at day 11, an error occurred in the calculations of the concentration of the feed solution which resulted in feeding the test cells with double the regular concentration. This error was accounted for in the modeling process using the developed spreadsheet model.

4.3.2 VSS Analysis

Although the data measured for the VSS analysis resulted in the same trend noted in Figure (4.3) and agree with the range of values reported by Rittmann and McCarty (2001) (i.e. ranges from 5×10^3 mg VS/L for aerobic biofilm up to 2×10^5 mg VS/L for anaerobic biofilms), the calculated biomass concentrations were considerably higher than what one would expect to be present in the test cells given the carbon loading. A mass balance of the carbon added to the test cells was calculated and found to be significantly less than the biomass concentrations calculated using the data measured for the VSS analysis. This

Reproduced with permission of the copyright owner. Further reproduction prohibited without permission.

difference could be attributed to errors in the weighting technique since the weight of the generated biomass was very small and hence error in the weight measurements could be significant. Therefore, results from the VSS analysis are not shown since they are not realistic and significantly higher than what should be expected from carbon mass balance in the test cells.

4.3.3 TOC Analysis

Using the TOC analysis and as discussed previously, biomass concentration (BOC) can be calculated by subtracting the liquid TOC from the total TOC. The liquid TOC measurements, which represent SOC, were significantly higher than the TOC concentration in the influent feeding solution (i.e. 350 mg/L). The shaking process may have disturbed the EPS structure and resulted in the release of the carbon from the EPS structure into the liquid phase. After filtration, the measured liquid TOC would represent the carbon that was present originally in the liquid phase plus the additional carbon released from EPS structure into the liquid phase due to the shaking process. This additional carbon may be the reason for obtaining higher liquid TOC in the TOC analysis than the TOC concentration in the influent feeding solution. Hence, the liquid TOC used in the TOC analysis to calculate the biomass concentration were the liquid TOC values measured from the liquid samples obtained before each cell was dismantled.

A Solid TOC Analyzer (Solid Sample Module, SSM-5000A, Shimadzu Corporation) was used to determine the total TOC of a sample. The sample was divided into two samples where the Total Carbon (TC) and Inorganic Carbon (IC) were determined separately to estimate the Total Organic Carbon (TOC). Unfortunately, the solid TOC analyzer was not accurate and resulted in discrepancies in the measured TOC values.

Reproduced with permission of the copyright owner. Further reproduction prohibited without permission.

Moreover, the calculated biomass concentrations in the TOC analysis were significantly higher than the calculated biomass concentrations using the VSS analysis. One would expect the biomass concentrations from the VSS analysis to be greater than the biomass concentrations from the BOC analysis by a factor of two given that the carbon content of a typical aerobic bacteria cell is approximately 50% by mass based on an empirical structure of $C_5H_7O_2N$ (Rittmann and McCarty (2001)). Hence, the results from the TOC analysis are not shown in this discussion.

4.3.4 Bacteria Analysis

As discussed in chapter three, bacteria analysis was conducted using a membrane filtration method. In this stage, triplicate samples were collected from a dismantled cell. Each sample was approximately 4.0 grams and was placed into a sterilized 50 mL centrifugal plastic tube. For each centrifugal tube, 40 mL of a 1% solution of sodium hexametaphosphate was added as a dispersion agent. The samples were shaken on a mechanical shaker at the highest speed (10,000 rpm) for 2 minutes to separate bacteria from the solid phase to the liquid phase.

To obtain a series of dilutions to be able to measure the microbial concentration, first, a 10^0 dilution was obtained by filtering the liquid into another sterilized 50 mL centrifugal plastic tube using a sterilized strainer to remove the solids. Then, a series of sterilized 50 mL centrifugal plastic tubes were labeled from 10^1 to 10^8 and were filled with 45 mL of buffer water for the dilution process. A 5 mL sample was taken from the 10^0 centrifugal tube with a pipet that had a sterilized pipet tip and was deposited in the centrifugal tube labeled 10^1 and shaken on the mechanical shaker for few seconds for homogenization. Then, a 5 mL sample was taken from the 10^1 centrifugal tube and was

Reproduced with permission of the copyright owner. Further reproduction prohibited without permission.

deposited in the centrifugal tube labeled 10^2 and shaken. The same procedure was used for the rest of the dilutions.

After dilutions were prepared, bacteria culturing took place using the membrane filtration method (9215 D, Eaton et al. (2005)). Duplicate agar plates for each dilution were prepared and stored in the fridge for not more than 24 hours. To culture the bacteria on the agar plate, a vacuum pump and 0.45 μm filter papers were used. Filter paper was placed on a sterilized funnel and suction was applied on the funnel using the vacuum pump while pouring a 5 mL sample of the dilution collected using a pipet. The filter paper was then placed on an agar plate and incubated in an incubator for an average of three days at 35 °C. After three days, bacterial counts were conducted for the plates to obtain an average number for bacteria for each sample.

The following equations illustrate the calculations used to estimate the increase in microbial concentration due to microbial growth using the bacteria count analysis. Also, Figure (4.5) illustrates the relationship between microbial concentration in mg/L and time.

The microbial concentration is calculated as follows,

$$\text{Volume of water in the sample, mL} = \text{W}_{\text{solids}} \times MC_{sample} \tag{4.1}$$

$$\text{Average \# of cells} = \text{Average \# of counts} \times \text{dilution} \tag{4.2}$$

$$\text{\# cells/mL} = \frac{Average\ \#\ of\ cells \times 40_{\ dispersion\ agent\ volume}\ (mL)}{5_{\ sample\ volume}\ (mL) \times Volume\ of\ water\ in\ the\ sample\ (mL)} \tag{4.3}$$

Conversions factor, mg/cell = 1.72×10^{-10}

$$\text{Microbial concentration, mg/L} = \text{Conversion factor}\left(\frac{\text{mg}}{\text{cell}}\right) \times \frac{\text{\# cells}}{\text{mL}} \times \left(\frac{1000\,\text{mL}}{\text{L}}\right) \tag{4.4}$$

Reproduced with permission of the copyright owner. Further reproduction prohibited without permission.

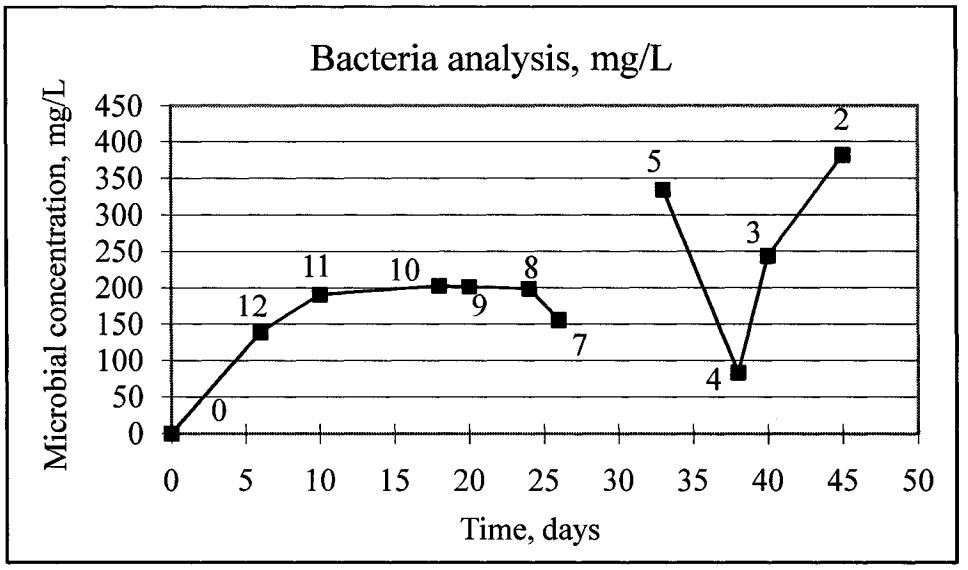

Figure 4.5- Microbial concentration in mg/L versus time using the bacteria count analysis

Although the microbial concentration measured using the bacteria count analysis was not directly comparable to the results measured in the VSS or TOC analyses, Figure (4.5) shows the same trend assumed previously in Figure (4.3). The reason for the difference is that bacteria count analysis only takes into account the bacteria cells and disregards any EPS or inert fraction presented as parts of the biofilm generated. Both EPS and inert fraction are considered in both VSS and TOC analyses.

4.4 Results and Discussion of the Estimation of the Monod Kinetic Parameters

As mentioned previously in subsection (4.2.4), the effluent liquid TOC was measured every 2-3 days to track the reduction in the substrate concentration with time. The data set obtained was used in a spreadsheet model to estimate the Monod kinetics parameters. The model assumed the system to be complete mix reactor and solved for

Reproduced with permission of the copyright owner. Further reproduction prohibited without permission.

both substrate and microbial concentrations using an explicit scheme with time step of one hour.

In developing the model, Monod equation (equation (4.5)) was used to calculate the substrate concentration based on the mixing occurred to the added substrate during each pulse (i.e. removing 30% saturation prior to a pulse then adding the influent substrate to increase the saturation by 30%). Then equation (4.6) was used to calculate the microbial concentration at the current time step. The Monod equation and the equation used to calculate the microbial concentrations are as follows;

$$\frac{\partial C}{\partial t} = -\frac{q_{\max}\, M\, C}{K_S + C} \tag{4.5}$$

$$\overbrace{\frac{\partial M}{\partial t}}^{\text{Change in microbial concentraion with time}} = \overbrace{(Y)\left(\frac{q_m\, M\, C}{K_s + C}\right)}^{\text{Growth rate}} - \overbrace{(b)(M)}^{\text{Decay rate}} \tag{4.6}$$

where C is the substrate concentration (mg/L), q_m is the maximum specific rate of substrate utilization ($mg_{substrate}/mg_{cell}\ s^{-1}$), M is the microbial concentration (mg/L), K_s is the half-velocity constant (mg/L), Y is the cell yield coefficient (mg cell / mg substrate), and b is the cell decay coefficient (s^{-1}).

After simulating the total time which corresponds to 47 days, solver in Excel was used to minimize the sum of the square errors between the measured data and the corresponding developed model prediction by allowing the Monod kinetic parameters (i.e. q_m, K_s, Y, and b) to change. Figure (4.6) shows the measured liquid TOC concentrations presented earlier in Figure (4.4) and the developed spreadsheet model results at time steps of 1 hour after minimizing the sum of the square errors between the measured data and the corresponding developed model prediction.

Reproduced with permission of the copyright owner. Further reproduction prohibited without permission.

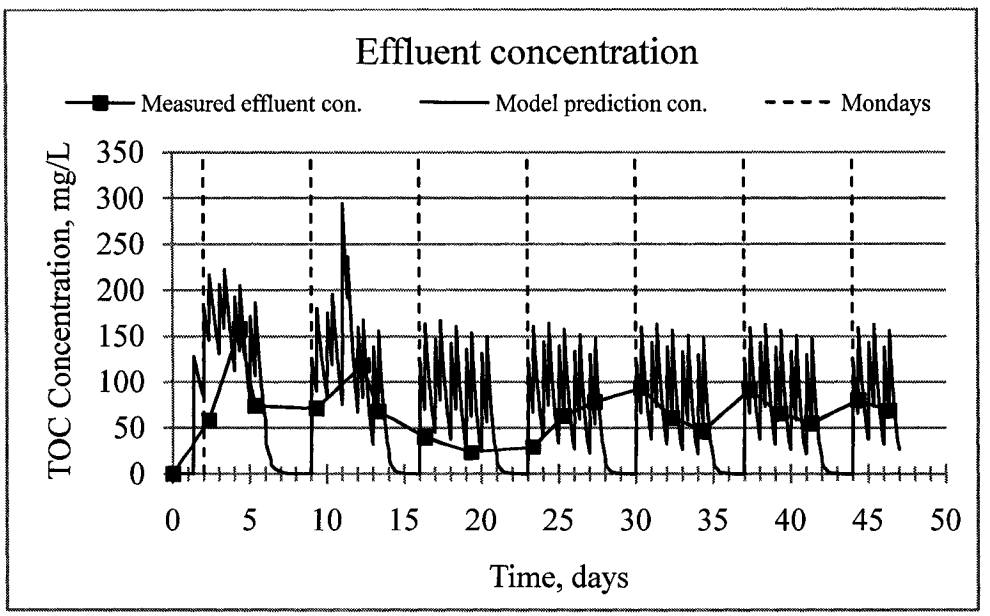

Figure 4.6- Comparison between the measured effluent concentrations and the results from the spreadsheet model at time step of 1 hour

Figure (4.6) shows a weekly model prediction concentration trend which corresponds to the hydraulic loading scenario provided to the test cells. On any given Monday, the TOC concentration started at a certain value which corresponds to the substrate concentration after the morning pulse on Monday. Then the substrate concentration decreased, due to microbial activity, until the afternoon pulse where the substrate concentration increased again due to the afternoon pulse event. Then the microbial activity reduced the substrate concentration until the morning pulse of the next day. This daily cycle was repeated 5 time per week (i.e. Monday to Friday) and followed by two days of no loading (i.e. weekend) where the model showed approximately zero TOC concentration for these two days. The weekly cycle/oscillation was repeated until the model was terminated at 47 days.

Reproduced with permission of the copyright owner. Further reproduction prohibited without permission.

In the spreadsheet model, the initial microbial concentration was assumed to be a very small value (i.e. 10 mg/L). This small value was assumed to initiate the microbial growth in the spreadsheet model. The initial substrate concentration was zero mg/L and each pulse added 350 mg/L as a source of substrate. The maximum and minimum saturations were fixed at 80% and 50%, respectively to simulate the upper and lower limits of the saturation conditions in the test cells. Monod kinetic parameters (i.e. q_m, K_s, Y, and b) were all initialized with assumed values to obtain an initial data set for the change in the substrate concentration versus time. The sum of the square difference between the obtained data set and the measured effluent concentrations from the test cells was calculated and solver in Excel was used to minimize this summation by allowing the assumed Monod kinetic parameters to change. Table (4.1) presents Monod kinetic parameters estimated using solver in Excel. These parameters were used later in stage three to calibrate the numerical model. It should be noted that the error made at day 11 in calculating the feed concentration was taken into account in the model which is shown as a spike in Figure (4.6) that has an approximate concentration equal to 300 mg/L. Also, it should be noted that the Monod kinetic parameters presented in Table (4.1) reflect the high hydraulic and organic loading for the influent substrate used in this experiment which is relatively higher than what is expected in a typical residential septic system.

Reproduced with permission of the copyright owner. Further reproduction prohibited without permission.

Table 4.1- Initial and estimated parameters using the developed spreadsheet model

Parameter	Units	Values				
		This research work	Typical waste water	Molz et al. (1986)	Taylor and Jaffé (1990b)	Clement et al. (1996)
Initial substrate concentration, C_o	mg/L	0.0	N/A	N/A	N/A	N/A
Pulse concentration, C_{source}	mg/L	350.0	N/A	N/A	N/A	N/A
Initial microbial concentration, M_o	mg/L	10.0	1500.0	3.5	1.0	1.5
Yield coefficient, Y		0.0508	0.50	0.278	0.0975	0.0006
Half-velocity constant, K_s	mg/L	540.18	100.0	120.0	0.8	40.33
Maximum specific rate of substrate utilization, q_m	s^{-1}	5.22×10^{-4}	5.0×10^{-6}	1.8×10^{-4}	8.9×10^{-5}	8.14×10^{-3}
Decay coefficient, b	s^{-1}	2.32×10^{-6}	5.8×10^{-7}	2.3×10^{-7}	3.2×10^{-7}	5.8×10^{-7}
Saturation range						
Maximum saturation	%	80				
Minimum saturation	%	50				
Replaced saturation	%	30				

Figure (4.7) presents a comparison between bacteria analysis and the corresponding model microbial concentration prediction since the bacteria analysis provides a direct comparison with the model microbial concentration prediction. The figure shows that biomass concentration calculated using the bacteria analysis is approximately one order of magnitude higher than the model prediction. This could be attributed to the conversion factor that was used to convert bacteria counts into mass. A conversion factor of 1.72×10^{-10} mg/bacteria cell (Schirmer et al. (1999)) was used to plot Figure (4.7). The conversion factor was then allowed to change to allow the bacteria analysis results to better fit the model prediction. An average conversion factor of 3.16×10^{-11} mg/bacteria cell was found which resulted in a better match between bacteria analysis results and the model prediction as can be seen in Figure (4.8).

Reproduced with permission of the copyright owner. Further reproduction prohibited without permission.

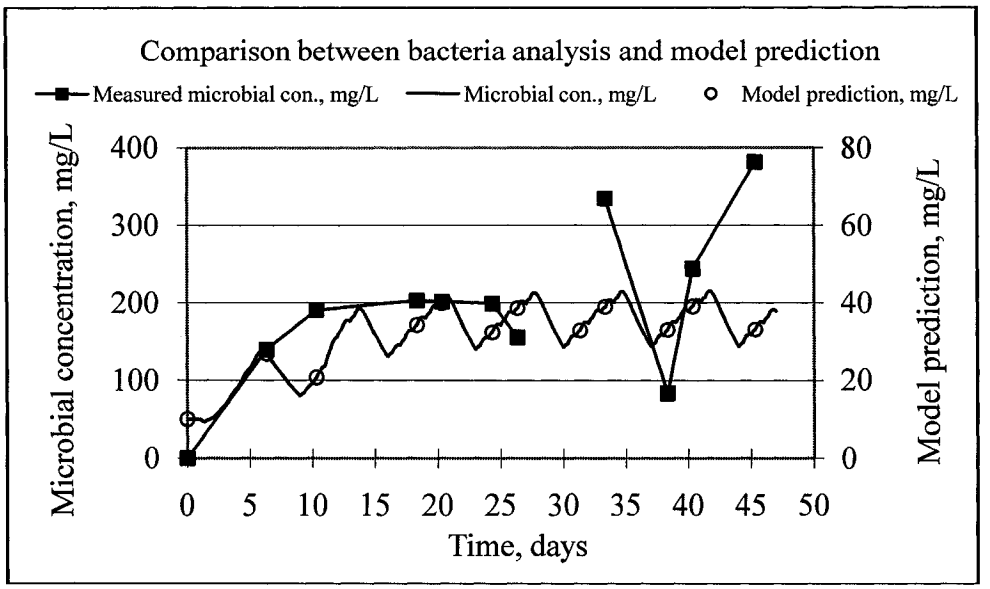

Figure 4.7- Comparison between the measured microbial concentrations using bacteria analysis and model prediction using a conversion factor of 1.72×10^{-10}

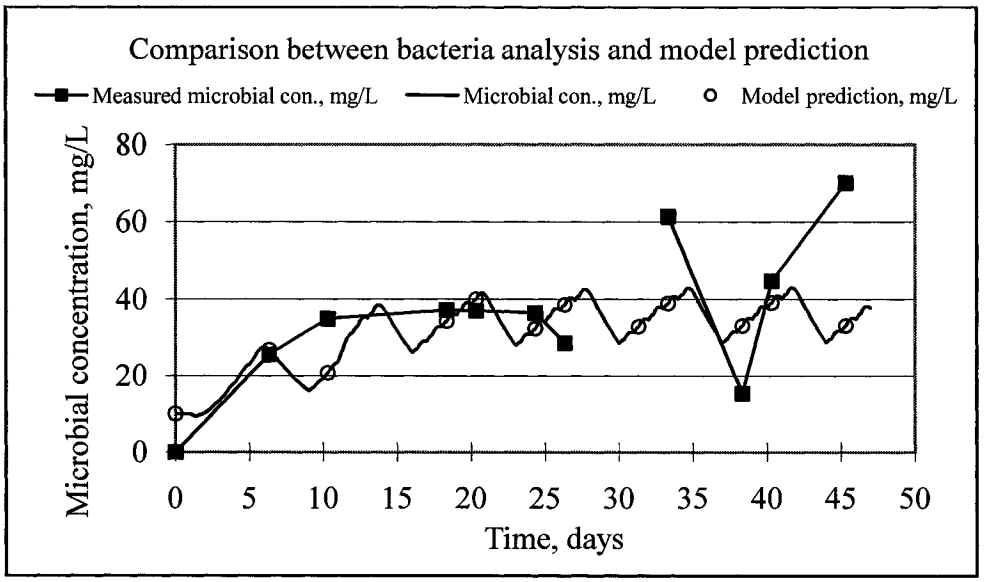

Figure 4.8- Comparison between the measured microbial concentrations using bacteria analysis and model prediction using a conversion factor of 3.16×10^{-11}

4.5 Summary of the Findings

The objective of stage two was to estimate the Monod kinetic parameters needed to simulate the biological clogging experiments conducted in stage one. Experimental test

Reproduced with permission of the copyright owner. Further reproduction prohibited without permission.

cells were constructed with concrete sand. The test cells were maintained under unsaturated conditions by controlling the maximum and minimum saturations to be between 80% and 50%, respectively. The effluent liquid TOC concentration was measured approximately every 2-3 days to track the reduction in substrate concentration with time as microbial population was building up and degrading the substrate. Two test cells were dismantled every week and biomass concentrations were measured by conducting three types of analyses; VSS analysis, TOC analysis, and bacteria counts. Although all the three types of analyses showed the same trend in biomass concentration which agreed with what was expected from the conceptual understanding of a batch system pulse-fed twice per day, both the VSS and TOC analysis measurements were significantly higher than what should be expected to be present in the soil based on a mass balance of carbon in the test cells.

The effluent substrate concentrations with time were compared to data simulated using a spreadsheet model developed for this stage to estimate the Monod kinetic parameters. Solver in Excel was used to minimize the sum of the square differences between the predicted substrate concentrations from the developed model and the measured effluent substrate concentrations from the test cells. Monod kinetic parameters obtained in this stage fell within the range of values found in the literature and were used later in stage three to calibrate the numerical code and validate the three conceptual models presented by Mostafa and Van Geel (2007).

Next chapter discusses stage three, which deals with the numerical modeling part of this research using the numerical code developed earlier by Mostafa and Van Geel (2007).

Reproduced with permission of the copyright owner. Further reproduction prohibited without permission.

5. STAGE THREE: NUMERICAL MODELING

This chapter investigates stage three of this research. Stage three aimed to model bioclogging using the one-dimensional numerical developed earlier by Mostafa and Van Geel (2007). The chapter consists of six main sections; an introduction to the stage, discussion of the steps taken in the modeling process, the main changes made to the original numerical code developed by Mostafa and Van Geel (2007), comparison between the numerical simulations and experimental data for control columns, comparison between the numerical simulations and experimental data for the bioclogging columns and summary of the findings from this stage.

5.1 Introduction

As discussed previously, Mostafa and Van Geel (2007) developed a one-dimensional numerical code that solves for flow, contaminant transport, and microbial growth in unsaturated soils. For the flow equation, the numerical code used a control volume approach to solve for total heads using the unsaturated flow equation. Then saturations were calculated based on van Genuchten relationship. The numerical code also solved for substrate concentration by coupling the Monod equation with the one-dimensional advection-dispersion equation where explicit finite difference scheme was used to solve the advection-dispersion equation. Appendix C provides more details about the equations used and the numerical methods used in solving these equations.

Three different conceptual models, proposed by Mostafa and Van Geel (2007), were implemented in the code to study the relation between the relative permeability of unsaturated soils and microbial growth. Hypothetical scenarios were also simulated to

Reproduced with permission of the copyright owner. Further reproduction prohibited without permission.

illustrate the differences between the three conceptual models. However, experimental data was needed to calibrate the code, by adjusting the input parameters, and validate the three conceptual models.

In this stage, the code developed by Mostafa and Van Geel (2007) was modified to address several issues that arose when simulating the experiments conducted in stage one of this research. These changes are discussed in detail in the following sections and include changes related to:

- The top boundary condition to better reflect conditions seen in the experiments
- The representation of the biofilm as a multi-component biofilm as discussed in chapter two
- The permeability when the pore space is filled with biomass
- The relative permeability calculation at the block interface
- The determination of time step size for the contaminant transport equation

The main objective of this stage was to calibrate the numerical code to simulate the experimental data obtained from the column experiments in stage one by adjusting the parameters measured and estimated from stages one and two. This stage was also used to validate the three conceptual models proposed earlier by Mostafa and Van Geel (2007) and select the model(s) which best simulated the experimental data.

5.2 Steps Taken in the Numerical Modeling Stage

The numerical modeling in this stage was divided into two main sequential steps. The first step dealt with the flow portion of the code, and the second step dealt with the microbial growth and bioclogging portion of the code.

Reproduced with permission of the copyright owner. Further reproduction prohibited without permission.

In the first step, the soil parameters obtained from stage one, and listed in Table (3.3), were used as the first attempt to model the flow in the five control columns. Since the five control columns were only pulsed with water during the experimental period, the results from these columns could be used to calibrate the flow predicted by the numerical code by adjusting the soils' hydraulic parameters measured in the laboratory in the separate experiments (e.g. permeability tests, porosity tests, soil moisture curves using the Buchner funnel, etc.). Thus, the parameters listed in Table (3.3) were adjusted, if needed, to simulate the saturation and outflow profiles from the five control columns.

After adjusting the flow parameters in the first step, step two was initiated. Numerous simulations were conducted with the original numerical code presented by Mostafa and Van Geel (2007) and the Monod kinetic parameters obtained from stage two. Many changes were implemented to attempt to fit the model simulations to the results obtained from stage one but the simulations still failed to produce meaningful results. As a result, it was determined that a more detailed conceptual model was needed to relate the microbial concentration, estimated using the Monod equation, to the biomass volume and corresponding biomass saturation, which was incorporated in the relative permeability relationships proposed by Mostafa and Van Geel (2007). The literature was revisited and the unified model presented by Laspidou and Rittmann (2002a) was incorporated in the model. In addition, a minimum relative permeability term was introduced as proposed by Beach and McCary (2003) in simulating a biomat.

After implementing numerous changes to the original numerical code presented by Mostafa and Van Geel (2007) and adjusting the Monod kinetic parameters, the

Reproduced with permission of the copyright owner. Further reproduction prohibited without permission.

appropriate conceptual model was chosen from the three conceptual models proposed by Mostafa and Van Geel (2007).

5.3 Main Changes to the Numerical Code

The first significant modification to the code related to the top boundary condition. The original code allowed for two types of boundary conditions at the top of the simulated domain; prescribed head or flux boundary conditions. Neither reflected the boundary conditions witnessed in the lab. In the laboratory experiments, 2 L of water were added to the top of the columns. During the early stages, the columns would allow this water to enter over a relatively short period of time. During the later stages, the 2 L pulse would generate ponding and it took some time for the pulse to enter. Neither a prescribed head nor prescribed flux boundary condition could simulate these boundary conditions. Hence, a head dependant flux boundary condition was implemented. The 2 L pulse provides a hydraulic load of 10.96 cm of water column per pulse. Hence, an initial total head equivalent to 10.96 cm of water column (pressure) was prescribed. During the initial time step, the flow which enters the column under this condition is simulated. Then the total head at the top block is recalculated to account for the flow that enters the column at the top block. This process is repeated for each time step. The flux that enters the column is a function of the permeability of the top grid blocks which reflects its clogging status. A pulse may pond for a long period of time if the permeability of the grid blocks is severely affected by biomass. The pressure head at the top block may or may not reach zero water column before the following pulse event.

Reproduced with permission of the copyright owner. Further reproduction prohibited without permission.

During the course of the experiments and as the ponding persisted, the hydraulic loading was reduced to avoid excess ponding. The new boundary condition provided a more reasonable top boundary condition that reflected what was happening over time during the column experiments. It also helped to calibrate the minimum hydraulic conductivity of the biomat layer, which will be discussed in later paragraphs in this chapter.

The second significant modification related to the conceptual representation of the biomass and its volume within the void space. The original code accounts for water saturation and microbial saturation. Both saturations contribute to the total saturation. The microbial saturation was calculated by converting the microbial concentration simulated using the Monod equation into a microbial volume using an assumed bacteria density adapted from the literature (Baek et al. (1989); van Veen and Paul (1979); Robertson et al. (1998)). The microbial volume only accounted for the microbial mass but did not account for any by-products that the microorganisms produce to generate a biofilm. Hence, the only way the original model could simulate bioclogging over a reasonable period of time was to artificially decrease the microbial density to indirectly account for the production of EPS and inert biomass that form as part of the biofilm. This approach may have worked; however, it does not properly account for decay and hence cannot simulate clogging at later stages when the hydraulic load is reduced. Hence, there was a need to more accurately represent the development of the biomass within the void space. Therefore, the modified code incorporates a biofilm saturation, which replaces the microbial saturation presented in the original code, and this biofilm saturation accounts for three different components; microbial mass, EPS, and inert fraction.

Reproduced with permission of the copyright owner. Further reproduction prohibited without permission.

In the modified code, a microbial mass was calculated using the Monod equation. Then using the relations provided by Hsieh et al. (1994), the fraction of substrate used to generate active biomass, EPS, and the inert fraction were determined. Hsieh et al. (1994) used 0.27 mg COD_x/ mg COD_s to represent the percentage of substrate used to generate active biomass and 0.59 mg COD_p/ mg COD_s to represent the percentage of substrate used to generate EPS. The mass of EPS generated was calculated (i.e. for every 1.0 mg of active biomass generated, approximately 2.0 mg of EPS are generated based on the relations provided by Hsieh et al. (1994)). Also, 20% was the percentage adapted from Laspidou and Rittmann (2002b) to calculate the fraction of biomass that is converted to inert biomass (i.e. for every 1.0 mg of active biomass generated, 0.2 mg of inert biomass is generated). After calculating the three different masses of the biofilm structure, each mass was converted to volume using assumed density values adapted from Laspidou and Rittmann (2002b). In their model, Laspidou and Rittmann (2002b) used 0.07 $gCOD/cm^3$, 0.2 $gCOD/cm^3$, and 0.22 $gCOD/cm^3$ to represent active biomass, EPS, and inert density values, respectively. These density values were converted to TOC because all the data measured in the experiments in this research were based on TOC. Since the ratio of BOD to COD is between 0.4 and 0.8 and the ratio of BOD to TOC is between 1.0 and 1.6 (Tchobanoglous and Burton (1991)), the TOC to COD ratio can vary between 0.25 and 0.8. Based on the TOC to COD ratio, the density values given by Laspidou and Rittmann (2002b) can be rewritten in terms of TOC and the upper limits for those density values are 0.056 $gTOC/cm^3$, 0.16 $gTOC/cm^3$, and 0.176 $gTOC/cm^3$ for active biomass, EPS, and inert, respectively. The lower limits for the density values are 0.0175 $gTOC/cm^3$, 0.05 $gTOC/cm^3$, and 0.055 $gTOC/cm^3$ for active biomass, EPS, and inert, respectively. Since

Reproduced with permission of the copyright owner. Further reproduction prohibited without permission.

the upper limit of the total biofilm density is 0.392 gTOC/cm^3 which is higher than what was reported in the literature, Table (2.5), the lower limits of the density values were used as assumed density values for the biofilm structure components. After calculating the volume of the three components, the sum of the three volumes was used to estimate the biofilm saturation which replaces the microbial saturation in the original code.

The third significant modification related to the hydraulic conductivity of the biomat when a clogged state was reached. The original code defined clogging to occur when the total saturation at any given block reaches 100%. When this occurs, the microbial saturation is assumed to reach its maximum value and as a result, the code exits the simulation. Clogging mostly occurs at the top grid block as illustrated in the results presented by Mostafa and Van Geel (2007). In reality, and based on the closed pore model suggested by Taylor and Jaffé (1990a) in saturated soils, which was discussed earlier, flow can be assumed to occur through the biomass layer itself. Using this assumption, Taylor and Jaffé (1990a) allowed the soil permeability to vary between a maximum value, when there is no biomass in the pores, and a minimum value, when all the pores are filled with biomass. The same concept can be adapted in unsaturated soils, the focus of this research. It was noticed during stage one that a pulse may pond on top of a column for a few days and it slowly enters the column. Assuming a minimum relative permeability when all the pore space at the top layer is filled with biomass can explain why this ponded pulse enters the column over a relatively long time. The original code presented by Mostafa and Van Geel (2007) cannot simulate this situation as the code will stop once the total saturation reaches 100%. A modification was added to the code to allow a maximum relative permeability value when biomass is at its initial condition and

Reproduced with permission of the copyright owner. Further reproduction prohibited without permission.

a minimum relative permeability value when biomass fills all the pores within a grid block.

When the biofilm saturation approaches 100% at the top grid block, the relative permeability reaches the minimum relative permeability value specified for this grid block. Biomass continues to build up at the top grid block but when all the pores are filled with biomass, the excess biomass cannot remain within this grid block and is assumed to migrate to the downstream block. Based on this new total biomass, the biofilm saturation is calculated at the downstream block. If the biofilm saturation is such that not all the pores are filled, the code precedes and calculates the new biofilm saturations for the rest of the domain but if the calculated biofilm saturation were to fill all the pores in this downstream block, the excess biomass is again calculated and assumed to migrate to the next downstream grid block and the cycle repeated. This cycle of rechecking the volume available for biomass growth and adding the excess biomass to the downstream block is done every time step to allow the biomass to continue to grow and to form a biomat. As a result, 100% total saturation might be seen in the top few centimetres below the soil surface. A scenario like this could not be simulated using the original code presented by Mostafa and Van Geel (2007).

Another modification was made to the code which is related to the relative permeability term calculation. The modified code alternates between two ways of calculating the relative permeability term; the first is used if only flow is being simulated, and the second is used if the code is simulating clogging. During any given pulse event, if the code is simulating only flow, the relative permeability at the upstream interface of the top grid block is assumed to be equal to 1.0 otherwise it is assumed to be equivalent to

Reproduced with permission of the copyright owner. Further reproduction prohibited without permission.

the relative permeability at the center of the top grid block. This assumption is valid since the upstream interface of the top grid block will be saturated (i.e. relative permeability equals 1.0) during any pulse event given that no microbial growth is being simulated. The rest of the relative permeability values throughout the domain are calculated based on the moving saturation front (i.e. upstream weighting for a wetting front and downstream weighting for a drainage front). Alternating between upstream and downstream weighting eliminates the sharp front problem generated due to the moving wetting or drainage saturation fronts. It was found that this modification to the calculation of the relative permeability term helped in best representing the outflow profiles from the five control columns which are illustrated later in this chapter.

The second alternate way of calculating the relative permeability term is used when the code is simulating a clogging scenario. In this case, Equation (C.5) is used to calculate the relative permeability for all the grid blocks. During any given pulse, all the grid blocks will have an initial maximum relative permeability, which is lower than 1.0, since an initial biomass concentration is initially assumed to be present to initiate biomass growth. At early times in the simulation, Equation (C.5) is used to calculate the relative permeability for all the grid blocks. At later times in the simulations and when grid blocks are totally filled with biomass, they are assigned a minimum relative permeability value that guarantees a minimum flow in these grid blocks to stimulate flow through a developed biomat layer. When the biomass develops to an even greater depth with a column, all the grid blocks that have 100% total saturation are assigned the minimum relative permeability to guarantee minimum flow through the developed biomat in these grid blocks.

Reproduced with permission of the copyright owner. Further reproduction prohibited without permission.

The final major modification added to the solution of the contaminant transport equation is the variable time step. The original code by Mostafa and Van Geel (2007) used a fixed time step for the entire simulation. Mostafa and Van Geel (2007) showed that for the chosen time step they used, no instability was found in the solution of the contaminant transport equation for the soils they simulated. When attempting to simulate the five soils under study with the original code, oscillations in the solution to the contaminant transport equation occurred. The oscillations were due to the fixed time step used by the original code. The code was modified to reduce the time step for the contaminant transport equation used every time an oscillation occurred. In different occasions, the time step needed to be reduced up to 7 orders of magnitude less than the assigned time step for the entire simulation so that oscillations do not occur. The time step modification to the contaminant transport solution added great benefit to the solution and eliminated the oscillation problem.

5.4 Comparison between the Numerical Simulations and Experimental Results for Control Columns

As discussed earlier in this chapter, the first step in the numerical simulation was to adjust the soil parameters using the saturation and outflow profiles from the control columns to calibrate the numerical code. This subsection presents a comparison between the experimental results for the control columns and the corresponding model results.

Table (3.3) listed the parameters obtained using the separate experiments. Irreducible saturation, van Genuchten parameters, saturated hydraulic conductivity, and porosity values were the input soil parameters to the code. As discussed in chapter three, the

Reproduced with permission of the copyright owner. Further reproduction prohibited without permission.

irreducible saturation and van Genuchten parameters obtained using the Buchner funnel did not represent the initial saturation profiles measured during the course of the experiment. An average of all the saturation profiles measured using TDR for each column during the experiment period was obtained. Then this average profile was fit using the van Genuchten equation and the irreducible saturation and van Genuchten parameters were obtained. The obtained parameters were used as input soil parameters for the code. The saturated hydraulic conductivity obtained using the permeability test was also adjusted by trial and error to be able to model the outflow profile measured in the lab.

5.4.1 Results for Septic Bed Sand Soil

Figure (5.1) presents the saturation profile measured in the lab and the comparable numerical simulation result after adjusting the parameters for the septic bed sand control column. Figure (5.2) also shows the outflow profiles measured in the lab and the corresponding numerical simulation result.

Reproduced with permission of the copyright owner. Further reproduction prohibited without permission.

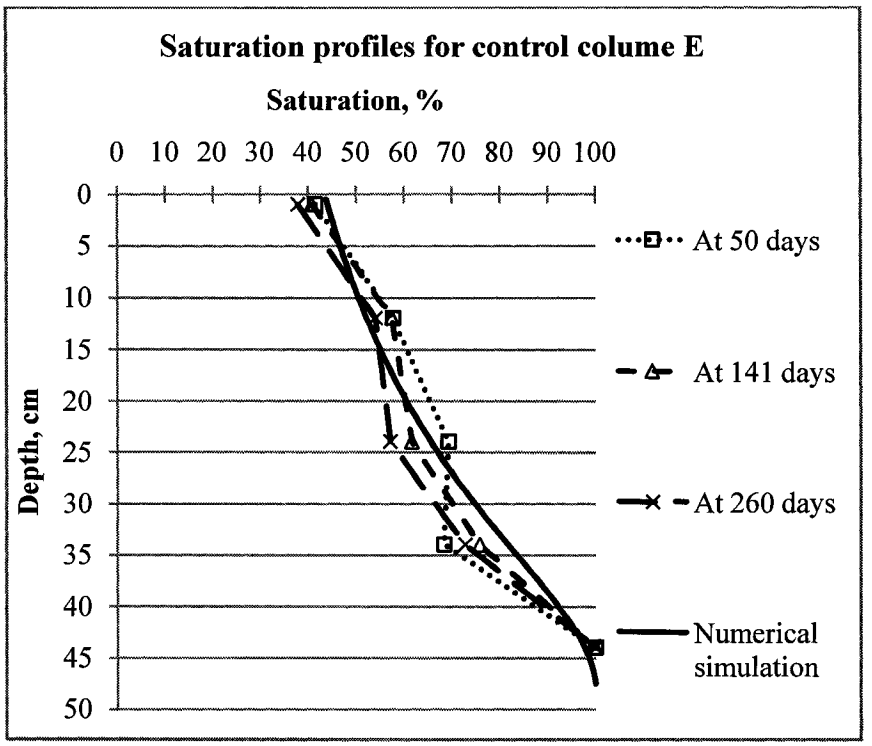

Figure 5.1- Comparison between saturation profiles for septic bed sand control column E versus numerical simulation

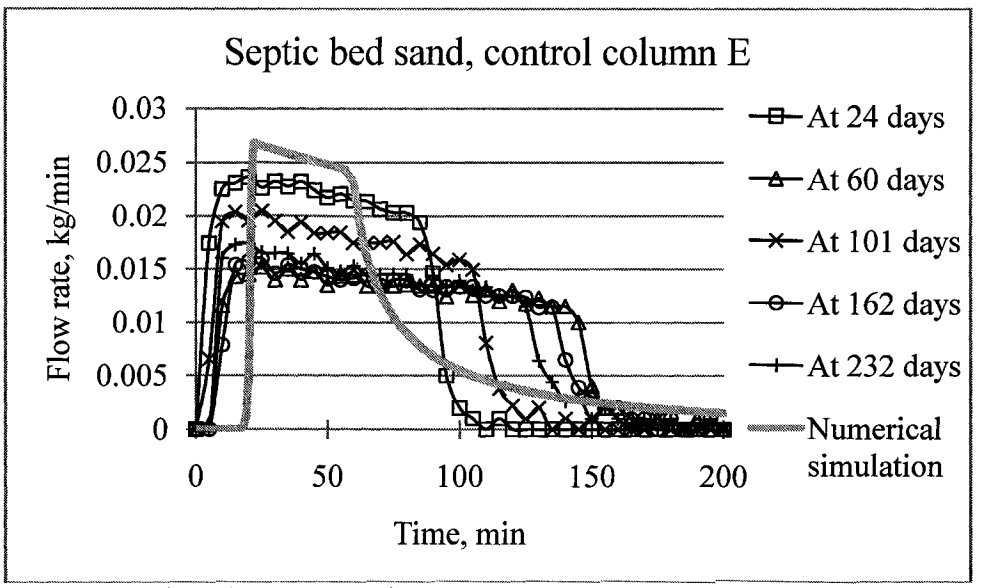

Figure 5.2- Comparison between outflow profiles for septic bed sand control column E versus numerical simulation

Reproduced with permission of the copyright owner. Further reproduction prohibited without permission.

The numerical simulation profiles for both saturation and outflow were approximately the same for all the times and hence only one profile is shown, denoted numerical simulation, to represent the numerical simulation results. Figure (5.2) illustrates how well the numerical simulation result fits the experimental data. It should be noted that the saturated hydraulic conductivity used to obtain the numerical simulation result presented here (i.e. 0.00225 cm/s) was approximately twice what was determined via the permeability tests (i.e. 0.00124 cm/s) conducted in the lab. The van Genuchten parameters n and α used to model the saturation profile in Figure (5.1) were 1.906 and 0.054 cm^{-1}, respectively. Both van Genuchten parameters obtained from the Buchner funnel experiment and by averaging the initial saturation profiles for the five septic bed sand columns were used in the model and both resulted in saturation profiles higher than what was recorded during the experiment period (data provided in subsection (A.1.6), Appendix A). Van Genuchten parameters used in the simulation presented in Figure (5.1) resulted in a good match with experimental data and were from averaging all the saturation profiles recorded for the septic bed sand control column during the experiment period.

Flow in the septic bed sand soil was lower than the flow in the other two sand soils due to its lower saturated hydraulic conductivity. Having a lower saturated hydraulic conductivity impacts how fast the peak flow exits the column if the column was pulse loaded. Figure (5.2) shows that the peak flow exited the column and extended to approximately 100 minutes with a maximum peak value of approximately 0.025 kg/min. Also, it was relatively easy to select a time size and grid block size to model the flow

Reproduced with permission of the copyright owner. Further reproduction prohibited without permission.

since the flow was relatively slow. A time step equal to 1 second and block size equal to 1 cm was used for the septic bed sand simulation.

5.4.2 Results for Concrete Sand Soil

Figure (5.3) presents the saturation profile measured in the lab and the comparable model result after adjusting the parameters for the concrete sand control column. Figure (5.4) also shows the outflow profiles measured in the lab and the corresponding model result.

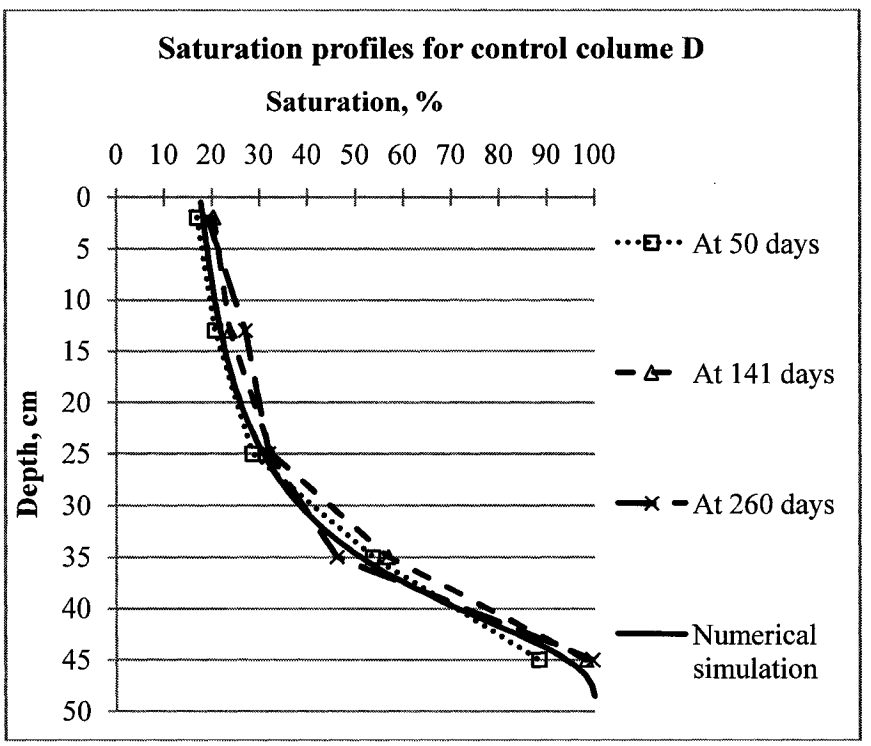

Figure 5.3- Comparison between saturation profiles for concrete sand control column D versus numerical simulation

The van Genuchten parameters n and α used to model the saturation profile in Figure (5.3) were 2.485 and 0.106 cm^{-1}, respectively. The van Genuchten parameters for this soil were obtained from averaging the initial saturation profiles for the five concrete sand columns after gravity drainage for one day which was found to be approximately similar

Reproduced with permission of the copyright owner. Further reproduction prohibited without permission.

to the van Genuchten parameters obtained from the average of all the saturation profiles recorded for the compacted peat control column during the experiment period. The saturated hydraulic conductivity was also adjusted (i.e. 0.012 cm/s) and found to be six times greater than the value measured in the permeability test (i.e. 0.00206 cm/s).

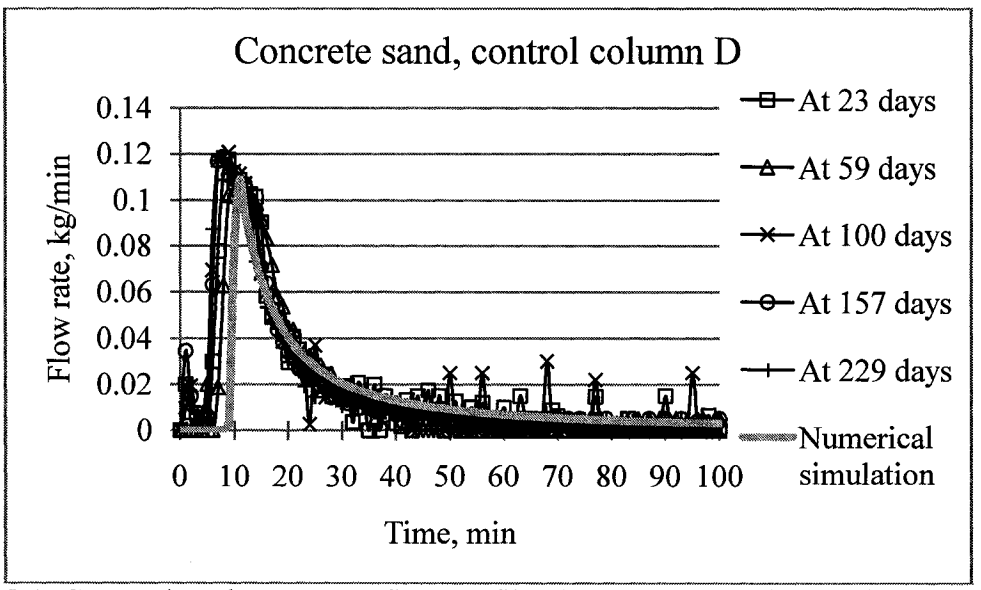

Figure 5.4- Comparison between outflow profiles for concrete sand control column D versus numerical simulation

Saturated hydraulic conductivity for the concrete sand was higher than the septic bed sand. Hence the peak flow measured for the concrete sand soil is expected to be higher and sharper than what was found in the septic bed sand. Figure (5.4) shows that the peak flow exited the column sooner (i.e. approximately 10 minutes) and the maximum peak flow recorded was approximately 0.12 kg/min. The experimental data presented in Figure (5.4) also indicate what appears to be a small peak flow that exited the column during the first 2-3 minutes. This initial flow maybe a slug of water that was held in the soil due to capillary barrier effects generated from the geotextile layer located in the bottom drainage

Reproduced with permission of the copyright owner. Further reproduction prohibited without permission.

layer. Once a pulse was added at the top of the column, head increased and resulted in releasing this slug that created this small peak flow noted in Figure (5.4).

Although the flow in the concrete sand was faster than the septic bed sand, the code managed to simulate the flow with the same time and spatial discretizations used for the septic bed sand soil (i.e. Δt equal to 1 second and Δx equal to 1 cm).

5.4.3 Results for Filter Media Bed Sand Soil

Figure (5.5) presents the saturation profile measured in the lab and the comparable model result after adjusting the parameters for the filter media bed sand control column. Figure (5.6) also shows the outflow profiles measured in the lab and the corresponding model result.

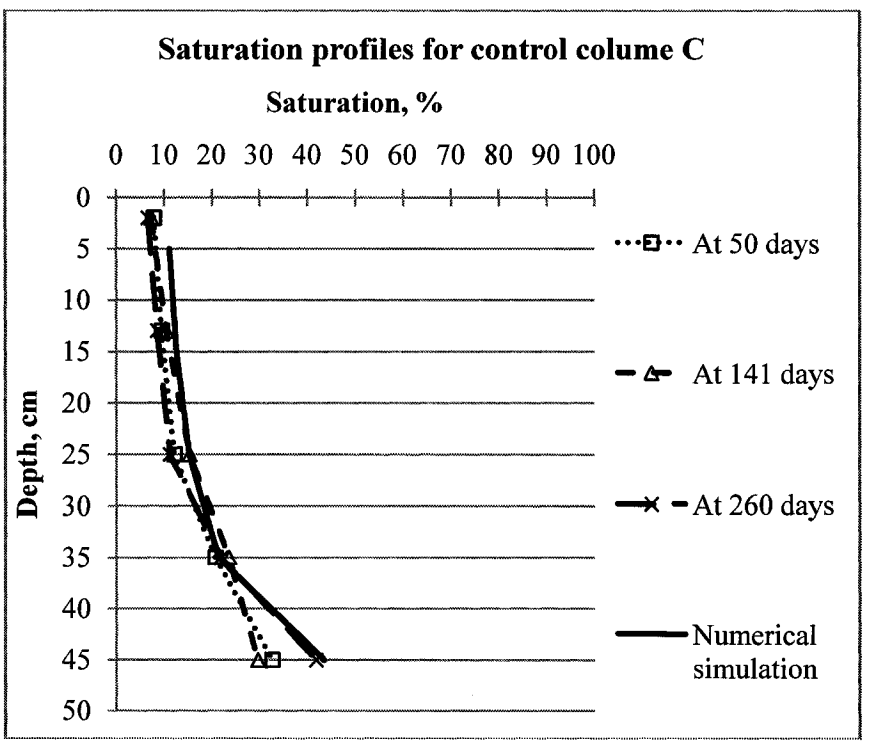

Figure 5.5- Comparison between saturation profiles for filter media bed sand control column C versus numerical simulation

Reproduced with permission of the copyright owner. Further reproduction prohibited without permission.

The van Genuchten parameters n and α used to model the saturation profile in Figure (5.5) were 1.691 and 0.617 cm^{-1}, respectively. The van Genuchten parameters for this soil were obtained from the average of all the saturation profiles recorded for the filter media bed sand control column during the experiment period. The saturated hydraulic conductivity was adjusted (i.e. 0.427 cm/s) and found to be twice what was measured in the permeability test (i.e. 0.212 cm/s).

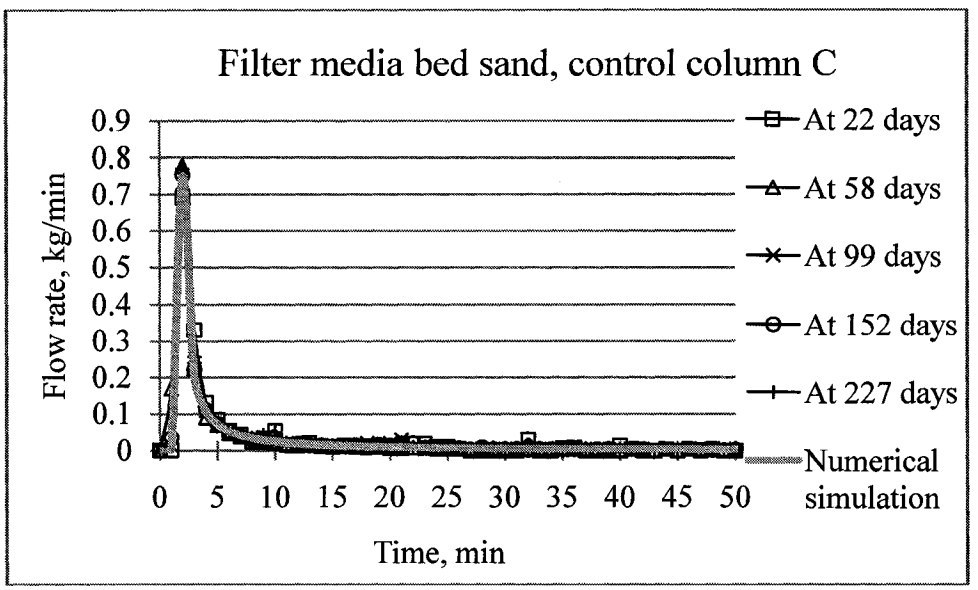

Figure 5.6- Comparison between outflow profiles for filter media bed sand control column C versus numerical simulation

Saturated hydraulic conductivity for the filter media bed sand was much higher in value than the other two sand soils. Figure (5.6) shows that the peak flow exited the column at approximately 2 minutes and the maximum peak flow recorded was approximately 0.75 kg/min.

Due to the high hydraulic conductivity of the filter media bed sand, the temporal and spatial discretizations needed to be modified. Using the same discretizations that were used for the previous sands resulted in the wetting front travelling through more than one

Reproduced with permission of the copyright owner. Further reproduction prohibited without permission.

grid block during a time step which caused the code to crash. In such cases, a smaller time step and larger grid size should be used to capture the moving front. The solution presented in Figures (5.5) and (5.6) used Δt equal to 0.1 seconds and Δx equal to 10 cm. Using this spatial discretization, the whole soil column was only simulated by 5 grid blocks (i.e. approximately 50 cm soil high and Δx equals 10 cm). A much finer spatial discretization is needed to accurately simulate the clogging behavior expected in the first few centimeters at the top layer. This would increase the simulation time by orders of magnitude and hence it was not feasible to simulate the bioclogging is the filter media bed sand.

5.4.4 Results for Compacted Peat Soil

Figure (5.7) presents the saturation profile measured in the lab and the comparable model result after adjusting the parameters for the compacted peat control column. Figure (5.8) also shows the outflow profiles measured in the lab and the corresponding model result.

Reproduced with permission of the copyright owner. Further reproduction prohibited without permission.

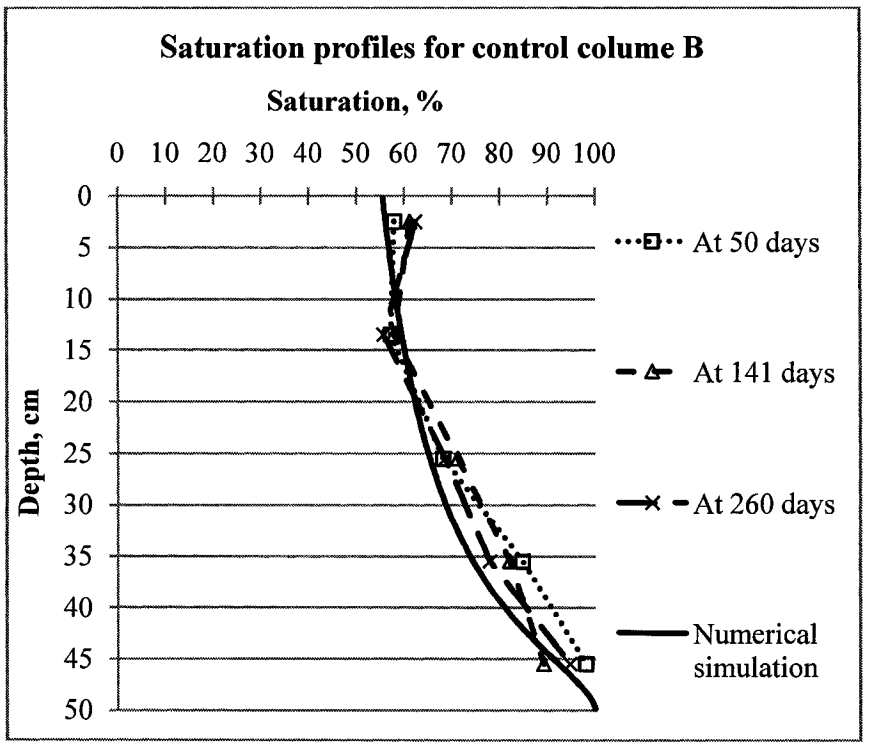

Figure 5.7- Comparison between saturation profiles for compacted peat control column B versus numerical simulation

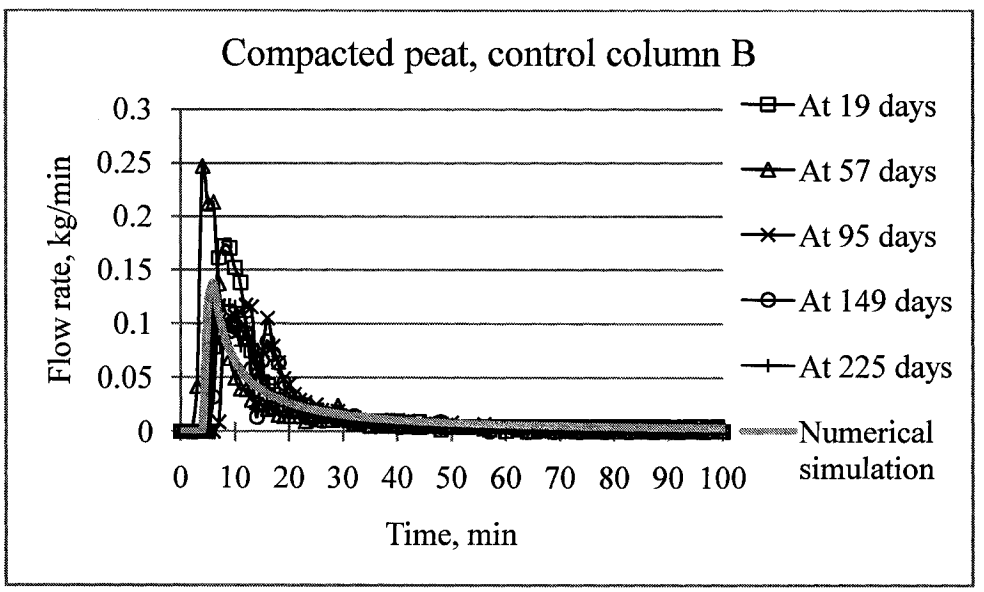

Figure 5.8- Comparison between outflow profiles for compacted peat control column B versus numerical simulation

Reproduced with permission of the copyright owner. Further reproduction prohibited without permission.

The van Genuchten parameters n and α used to model the saturation profile in Figure (5.7) were 1.659 and 0.127 cm^{-1}, respectively. The van Genuchten parameters for this soil were obtained from averaging the initial saturation profiles for the five compacted peat columns after gravity drainage for one day which was found to be approximately similar to the van Genuchten parameters obtained from the average of all the saturation profiles recorded for the compacted peat control column during the experiment period. The same saturated hydraulic conductivity obtained by Shibchurn et al. (2005) was used to model the flow in the compacted peat soil and no adjustments were required.

The results presented in Figures (5.7) and (5.8) used time and spatial discretizations of 5 seconds and 0.25 cm, respectively. Using the same time and spatial discretizations as the concrete sand and septic bed sand resulted in the code crashing.

5.4.5 Results for Loose Peat Soil

Figure (5.9) presents the saturation profile measured in the lab and the comparable model result after adjusting the parameters for the loose peat control column. Figure (5.10) also shows the outflow profiles measured in the lab and the corresponding model result.

Reproduced with permission of the copyright owner. Further reproduction prohibited without permission.

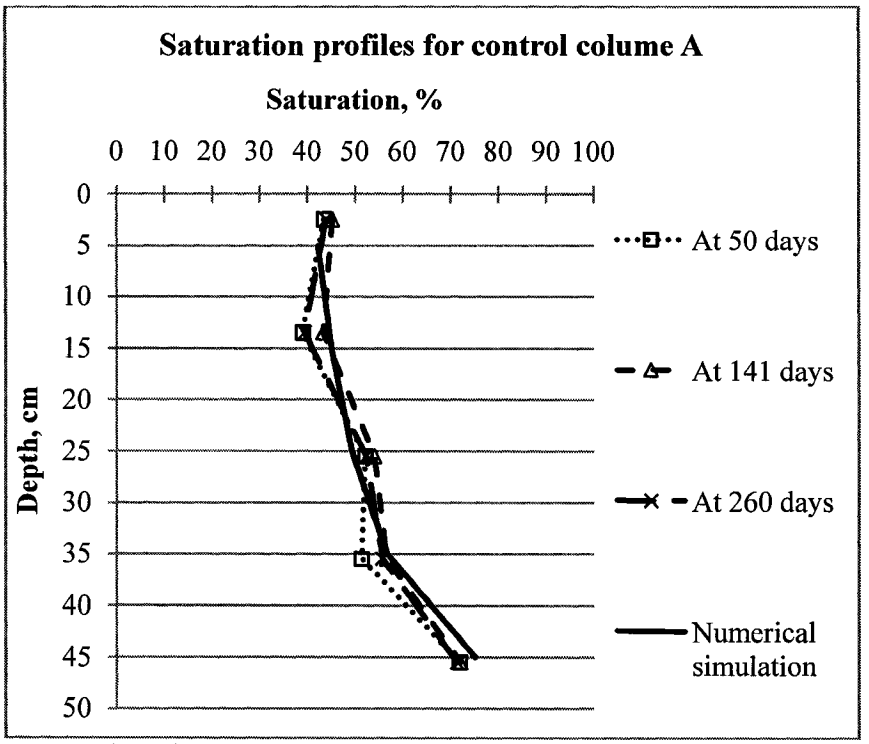

Figure 5.9- Comparison between saturation profiles for loose peat control column A versus numerical simulation

The van Genuchten parameters n and α used to model the saturation profile in Figure (5.9) were 1.405 and 0.366 cm^{-1}, respectively. The van Genuchten parameters for this soil were obtained from the average of all the saturation profiles recorded for the control column during the experiment period. The saturated hydraulic conductivity was adjusted (i.e. 1.25 cm/s) and found to be approximately twice the value determined by Shibchurn et al. (2005) (i.e. 0.631 cm/s). It should be noted that the relationship reported by Shibchurn et al. (2005) which relates the dry density to the saturated hydraulic conductivity was obtained for peat soil with dry density values between 88 kg/m^3 and 153 kg/m^3. The dry density for the loose peat soil was approximately 84 kg/m^3 and hence extrapolation was made to obtain the saturated hydraulic conductivity for the loose peat soil (i.e. 0.631 cm/s from Shibchurn et al. (2005)).

Reproduced with permission of the copyright owner. Further reproduction prohibited without permission.

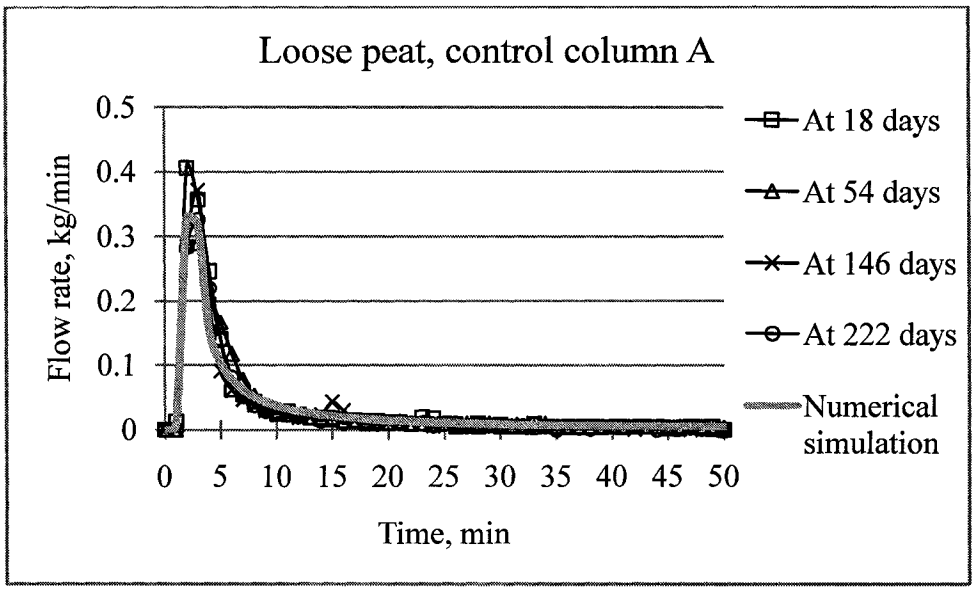

Figure 5.10- Comparison between outflow profiles for loose peat control column A versus numerical simulation

Saturated hydraulic conductivity for the loose peat soil was much higher than the other four soils. Figure (5.10) shows that the peak flow exits the column at approximately 2 minutes and the maximum peak flow recorded was approximately 0.35 kg/min. Although the saturated hydraulic conductivity for the loose peat soil was 2.5 times higher than the filter media bed sand, the peak flow was almost half the value estimated for the filter media bed sand (Figure (5.6)). The reason for this difference is the difference in the relative permeability relationships and the maximum saturations reached during a pulse.

Since the flow in the loose peat is fast and similar to the filter media bed sand, time and spatial discretizations similar to what was used to model the filter media bed sand were used. A Δt equal to 0.1 seconds and Δx equal to 10 cm were used which resulted in representing the soil column with only 5 grid blocks.

Reproduced with permission of the copyright owner. Further reproduction prohibited without permission.

As discussed with the filter media bed sand, larger grid size and smaller time step would increase the simulation time by orders of magnitude and hence it was not feasible to simulate the bioclogging in the loose peat.

5.5 Comparison between the Numerical Simulations and Experimental Results for the Columns Loaded With Organic Loading Only and Organic plus Suspended Loading

Two loading types were used in this research as illustrated in Table (3.2); organic loading only and organic plus suspended loading. Silica powder was the suspended material used with the organic plus suspended loading to study the effect of suspended solids on the soil clogging. It is well documented in the literature that suspended solids cause physical clogging and hence the columns loaded with organic plus suspended loading were expected to clog faster (i.e. due to both physical and biological clogging) compared to the columns loaded with organic loading only (i.e. due to biological clogging only). The amount of silica added with each pulse was not enough to cause physical clogging as anticipated and the behavior/clogging time for the columns loaded with and without silica was approximately the same. Figures (5.11) through (5.15) illustrate examples from columns loaded with organic loading only and organic plus suspended loading. The figures show similar saturation profile behavior for each soil type. For the latter reason, simulations with the hydraulic loading scenario from compacted peat column B1, concrete sand column D1 and septic bed sand column E1 were used in the following discussion for the comparison between the numerical simulations and the experimental data.

Reproduced with permission of the copyright owner. Further reproduction prohibited without permission.

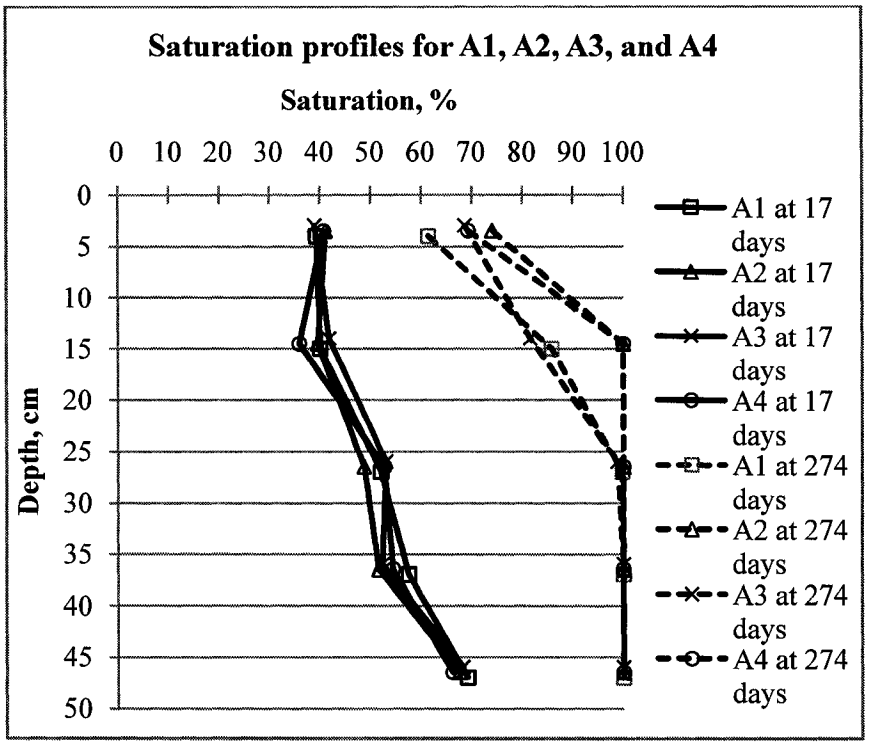

Figure 5.11- Comparison between the loose peat columns loaded with organic loading only (A1 and A2) and organic plus suspended loading (A3 and A4)

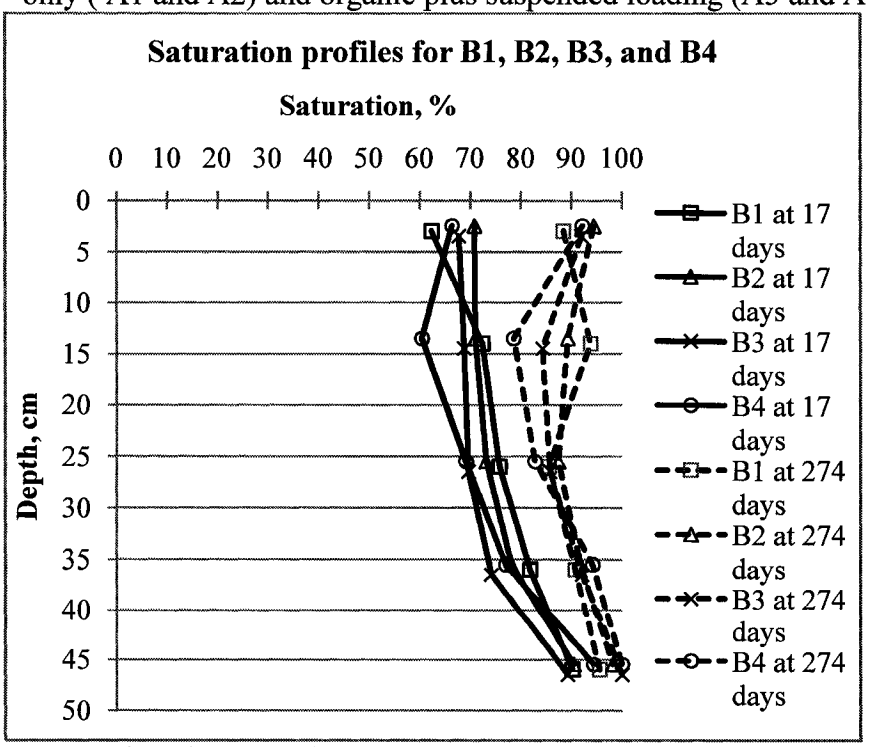

Figure 5.12- Comparison between the compacted peat columns loaded with organic loading only (B1 and B2) and organic plus suspended loading (B3 and B4)

Reproduced with permission of the copyright owner. Further reproduction prohibited without permission.

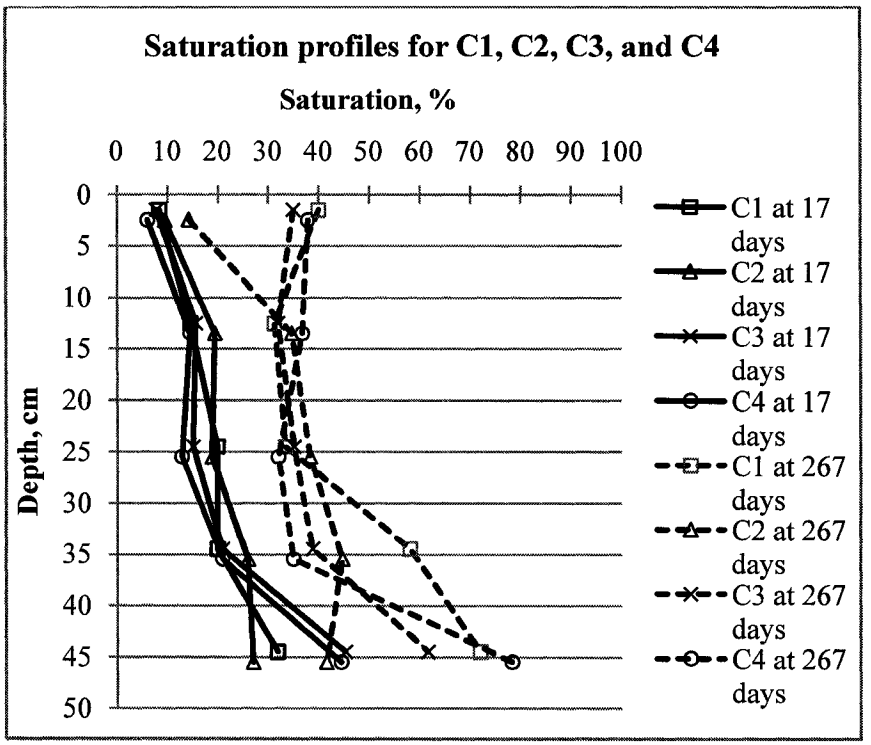

Figure 5.13- Comparison between the filter media bed sand columns loaded with organic loading only (C1 and C2) and organic plus suspended loading (C3 and C4)

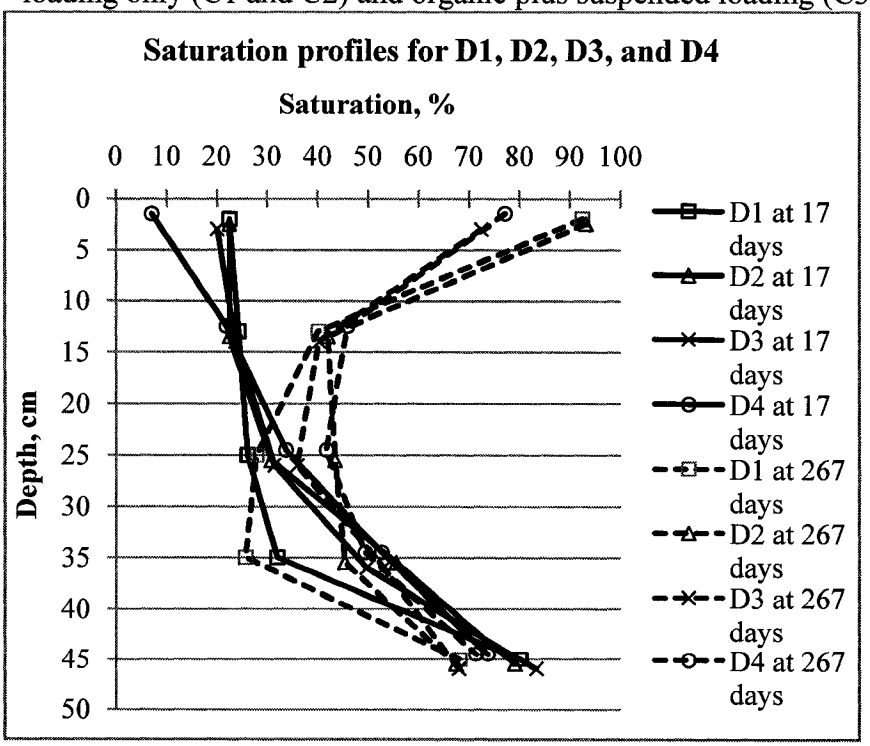

Figure 5.14- Comparison between the concrete sand columns loaded with organic loading only (D1 and D2) and organic plus suspended loading (D3 and D4)

Reproduced with permission of the copyright owner. Further reproduction prohibited without permission.

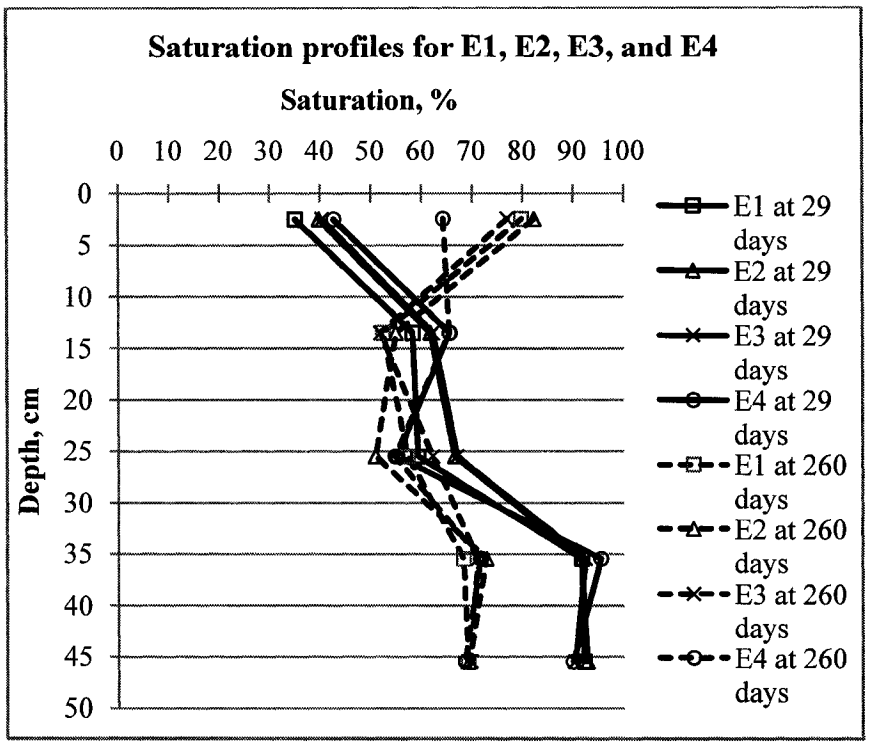

Figure 5.15- Comparison between the septic bed sand columns loaded with organic loading only (E1 and E2) and organic plus suspended loading (E3 and E4)

As discussed earlier, the soils were initially assumed to have limited to no bacteria present and the source of microbial growth was assumed to be from the bacteria that were picked up from the air or might have been present in the soil or in the water used to prepare the stock solution. The initial biomass concentration is an input parameter to the code and was assumed to be very small just to initiate microbial growth once a pulse is added. Also, maximum and minimum relative permeability values were assigned as input parameters to the code. A summary of the initial biomass concentration and the maximum and minimum relative permeability values for each soil is provided in a summary table at the end of this chapter.

In this subsection, a discussion of the bioclogging results from the numerical simulations is provided. Also, this subsection highlights the difference between the three

Reproduced with permission of the copyright owner. Further reproduction prohibited without permission.

conceptual models proposed by Mostafa and Van Geel (2007). A selection of the best fitting model(s) is made with a conceptual discussion.

It should be noted that the bioclogging simulations presented in the following subsections were conducted using a Pentium 4 machine with a 3.2 GHz processor and 2 GB of RAM. It took approximately 7 hours to run a complete bioclogging simulation using Models #1 or #2 and approximately 10 hours to run a complete bioclogging simulation using Model #3.

5.5.1 Results for Septic Bed Sand Soil

Biological clogging simulations using the modified numerical code started with numerous trials conducted to adjust the Monod kinetic parameters obtained from stage two to calibrate the clogging portion of the numerical code. In this calibration process, a plot of the TDR measurements with time at the top measurement point was prepared for septic bed sand columns E1 and E2 as shown in Figure (5.16). This plot was used to illustrate the progressive clogging over time within the top few centimeters of the column. Knowing the location and approximate depth over which the TDR probe measures the average saturation, the corresponding simulation data was also averaged over this depth (4 cm) to allow direct comparison with the TDR results. Using this plot, the best trial was selected and a check on the rest of the saturation profile at different times was made to ensure that the code simulates all TDR measuring points reasonably well.

It was found that all the Monod kinetic parameters obtained from stage two, except for the decay rate coefficient, led to a reasonable match between the measured saturation profiles from stage one and the numerical simulations. The decay rate coefficient

Reproduced with permission of the copyright owner. Further reproduction prohibited without permission.

estimated in stage two had a high value and the simulations using this estimated value did not result in any significant microbial growth and significantly underestimated the clogging over time. The calibrated decay rate coefficient and the rest of Monod kinetic parameters used to obtain the successful simulation are summarized in a table at the end of this chapter. The calibrated decay rate was then assigned in the developed spreadsheet model in stage two that was used to estimate Monod kinetic parameters. A comparison between the experimental data from stage two and the developed spreadsheet model results, after using the calibrated decay rate, is provided in Figure (B.1), Appendix B.

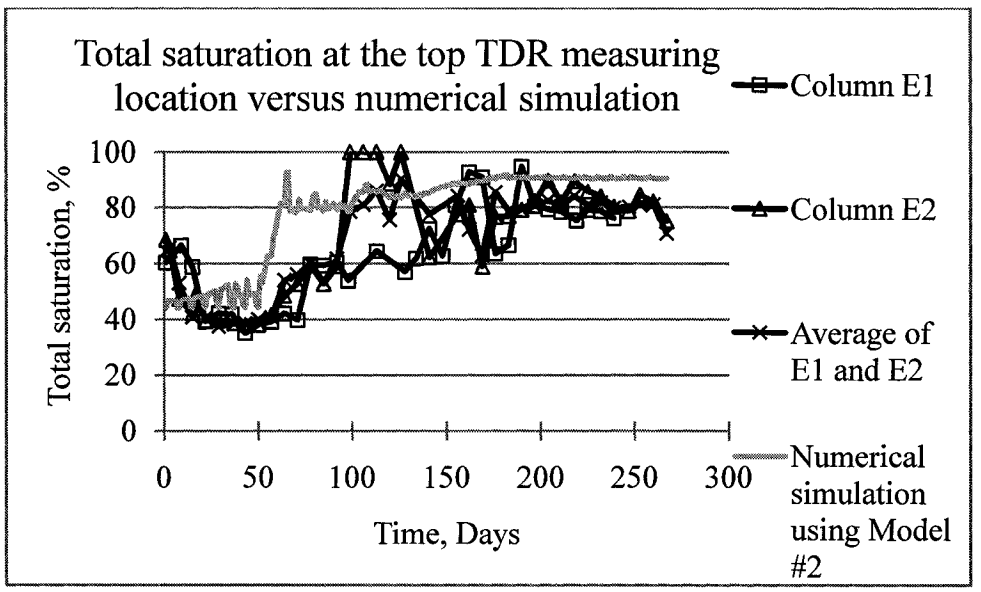

Figure 5.16- Total saturation at the top measuring location for septic bed sand columns E1 and E2 versus numerical simulation using Model #2

The initial biomass concentration was also calibrated using Figure (5.16). Initial biomass concentration affects how early the total saturation at the top TDR measuring location increases with time. Conceptually, a high initial biomass concentration will correspond to an early increase in the total saturation as opposed to a lower initial

Reproduced with permission of the copyright owner. Further reproduction prohibited without permission.

biomass concentration. Figure (5.16) was used to calibrate the initial biomass concentration used to model the clogging process in the septic bed sand and the value used in the modeling process is listed in the summary table provided at the end of this chapter.

A maximum relative permeability was assigned as an input parameter to the code. This maximum relative permeability value corresponded to the initial biomass volume presented in the soil. The maximum relative permeability value was obtained by assuming a 1% biofilm saturation initially occupying the void space. Then Mualem's equation was used to estimate the maximum relative permeability value. This maximum relative permeability value was assigned to the top block only at the beginning of a simulation when a column is to be pulsed and the pores contain the initial biomass concentration. As time elapsed, biomass increased and the relative permeability at the top block was calculated or assigned a minimum relative permeability when a biomat was developed in that block. A minimum relative permeability value is also an input parameter to the code. This minimum relative permeability value was calibrated based on the hydraulic loading scenario noted from the column experiments in stage one. At later times as the top blocks reached an apparent total saturation of 100%, the pressure head at the surface of the simulated column was compared with the hydraulic loading scenario of that column and trials were conducted to match the pressure head at the top block from numerical simulations with the corresponding hydraulic loading scenario. A minimum relative permeability value was then chosen based on the best match. Both the calculated and calibrated maximum and minimum relative permeabilities are listed in the summary table at the end of this chapter.

Reproduced with permission of the copyright owner. Further reproduction prohibited without permission.

Figures (5.17), (5.18), and (5.19) illustrate the experimental saturation profiles measured for septic bed sand columns E1 and E2 and the corresponding numerical simulations using the three conceptual models. There was a distinguishable difference between the results of Model #1 and Models #2 and #3. The model results for Models #2 and #3 almost lie on top of each other in Figures (5.17) through (5.19). Based on the discussion presented by Mostafa and Van Geel (2007), Model #1 assumes that smaller pores will fill first with biomass. Since these smaller pores contribute the least to the flow, Model #1 predicts the lowest reduction in relative permeability at early times and hence the least impact on the total saturation. At early times (e.g. 22 days as shown in Figure (5.17)), the three models predict approximately the same total saturation because the developed biomass was not enough to impact the relative permeability term in any of the three models. Once enough biomass occupied the void space, an increase in the total saturation is noted from the experiment results which both Models #2 and #3 managed to simulate reasonably well (e.g. at 113 days as shown in Figure (5.18)). At this time, the increase in biomass volume did not impact the relative permeability estimated by Model #1 and hence Model #1 did not predict any increase in the total saturation at 113 days. At later times, and when enough biomass is present in the void space to significantly reduce the relative permeability term, Model #1 predicted an increase in the total saturation. Model #1 may have only predicted the increase in the total saturation at the top of the column reasonably well, but only Models #2 and #3 successfully predicted the increase in the entire saturation profile.

Reproduced with permission of the copyright owner. Further reproduction prohibited without permission.

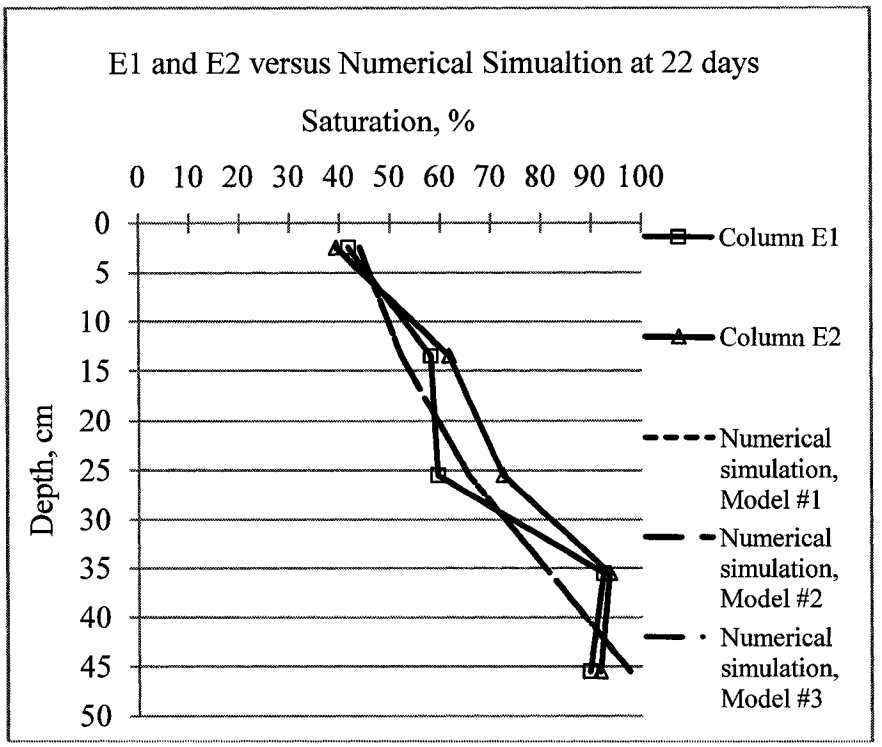

Figure 5.17- Total saturation for septic bed sand columns versus numerical simulation at 22 days using the three conceptual models

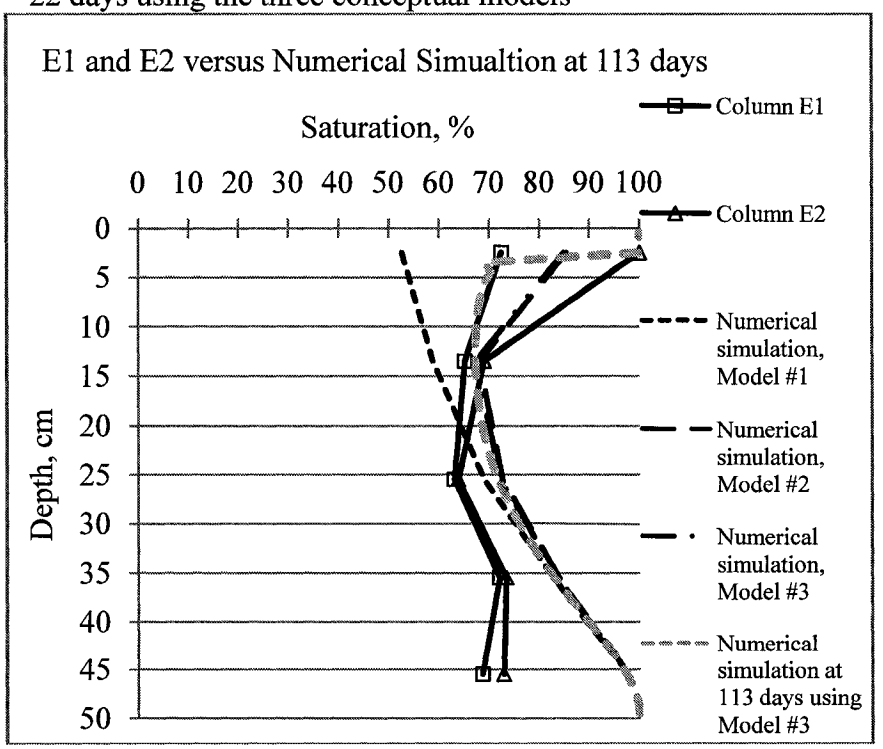

Figure 5.18- Total saturation for septic bed sand columns versus numerical simulation at 113 days using the three conceptual models

Reproduced with permission of the copyright owner. Further reproduction prohibited without permission.

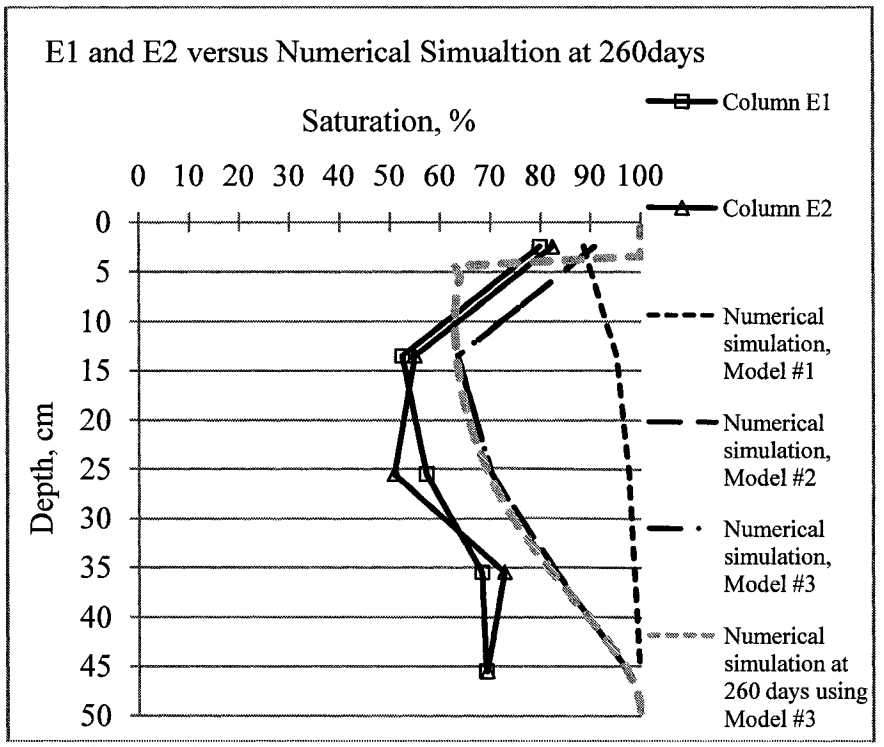

Figure 5.19- Total saturation for septic bed sand columns versus numerical simulation at 260 days using the three conceptual models

Ponding was experienced with the columns loaded with organic loading only and organic plus suspended loading due to biomass growth. As discussed earlier, at early times, the columns were loaded twice per day, five days per week. As time elapsed, a reduction in the relative permeability occurred due to microbial growth and hence the columns could no longer conduct the same flow and the pulses ponded and took longer to enter the columns. One might question why the columns could not conduct the flow and ponding occurred while Figure (5.19) shows approximately 80% total saturation at later times.

As discussed before, TDR measures the average saturation over a certain depth. The 80% total saturation measured by the TDR is the average saturation over the top 4 cm. Since at later times the column could not handle the ten pulses per week and ponding

Reproduced with permission of the copyright owner. Further reproduction prohibited without permission.

occurred, the surface of the soil must have been clogged with biomass that formed a biomat but the TDR cannot capture this because it averages the saturation over a depth greater than the biomat thickness. Hence TDR measurements will only reach 100% saturation if the biomat thickness equals or exceeds the depth over which TDR measures the saturation. To clarify this hypothesis, the entire simulated saturation profiles based on Model #3 at 113 days, denoted numerical simulation at 113 days using Model #3, and at 260 days, denoted numerical simulation at 260 days using Model #3, were plotted on Figures (5.18) and (5.19), respectively. At 113 days, it is clearly shown that the top 2.5 cm reached 100% total saturation (i.e. void space filled with the generated biofilm) followed by a sharp reduction in the saturation to approximately 70% immediately below the biomat. From the simulated saturation profile, the average saturation over the depth of the TDR measurement is approximately 80% even though the code still predicts 100% total saturation at the surface and a biomat has formed in the column. Also at 260 days, the top 3.5 cm has reached 100% saturation and a sharp reduction to approximately 63% was simulated immediately below the biomat. The average saturation over the depth measured by the TDR probe is still approximately 80%. Hence, the TDR may not have captured the biomat generated at the surface of the soil but the code managed to show that a biomat was established at the surface.

Another critical point is how the ponded pulse managed to enter the column even though a biomat was formed. The only logical explanation is that flow occurred through the generated biofilm layer with a minimum relative permeability. This may explain why the ponded pulse took a long time to enter the column when only 1 to 2 cm of the top surface was clogged with biofilm.

Reproduced with permission of the copyright owner. Further reproduction prohibited without permission.

The previous discussion and the experimental data showed that in reality, a pulse can pond for few days as it slowly enters the soil and even though the soil maybe clogged, minimum flow may still occur via the generated biofilm layer. The two major modifications; adding a new top head boundary condition that allows a pulse to pond and allowing a minimum relative permeability value in the grid blocks clogged with biomass, significantly enhanced the code performance to simulate the behaviors noted from the experimental data. The original code developed by Mostafa and Van Geel (2007) would not have simulated these results without these modifications.

5.5.2 Results for Concrete Sand Soil

The same Monod kinetic parameters used to simulate the clogging process in the septic bed sand soil were used with the concrete sand soil. Figure (5.20) shows a plot of the TDR measurements at the top measurement point prepared for concrete sand columns D1 and D2 and the successful numerical simulation using Model #2. Similar to the discussion with the septic bed sand soil, initial biomass concentration and maximum/minimum relative permeabilities were calibrated in a similar manner as discussed earlier with the septic bed sand soil. The calibrated parameters are listed in the summary table at the end of this chapter.

Figure (5.20) shows what appeared to be a sudden increase in the saturation from the numerical simulation between days 152 and 156. This sudden increase is an artifact with the code which did not allow the pulse at day 152 to move through the column due to the water saturation reaching the irreducible saturation at the top block. This artifact is corrected when the next pulse was added.

Reproduced with permission of the copyright owner. Further reproduction prohibited without permission.

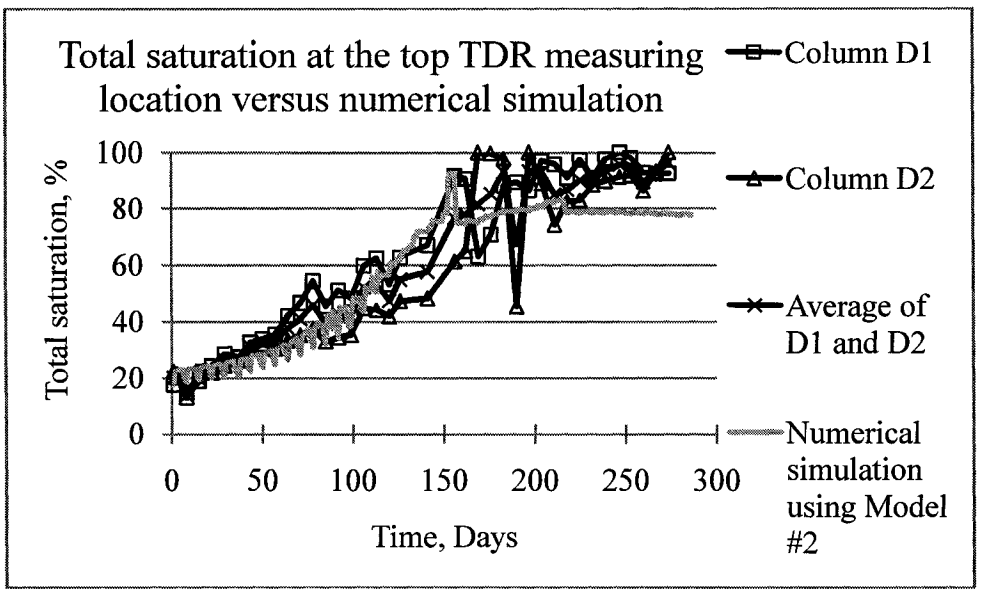

Figure 5.20- Total saturation at the top measuring location for concrete sand columns D1 and D2 versus numerical simulation using Model #2

Figures (5.21), (5.22), and (5.23) illustrate the experimental saturation profiles measured for columns D1 and D2 and the corresponding numerical simulations using the three conceptual models. The same distinguishable difference between the results of Model #1 and Models #2 and #3 was noted with the concrete sand soil. Comparisons between Model #1 results and experimental results in Figures (5.21), (5.22), and (5.23) show that Model #1 did not predict any increase in the total saturation because not enough biomass was established to impact the relative permeability term. Both Models #2 and #3 predicted the increase in total saturation noted from the experimental data. The latter supports the argument that both Models #2 and #3 better simulate reality.

Reproduced with permission of the copyright owner. Further reproduction prohibited without permission.

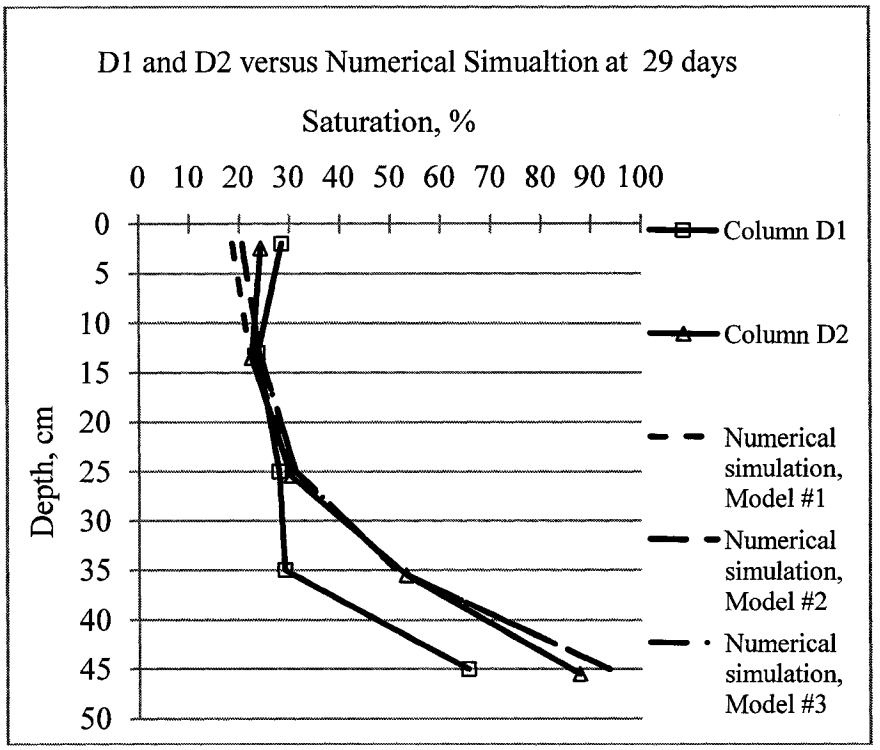

Figure 5.21- Total saturation for concrete sand columns versus numerical simulation at 29 days using the three conceptual models

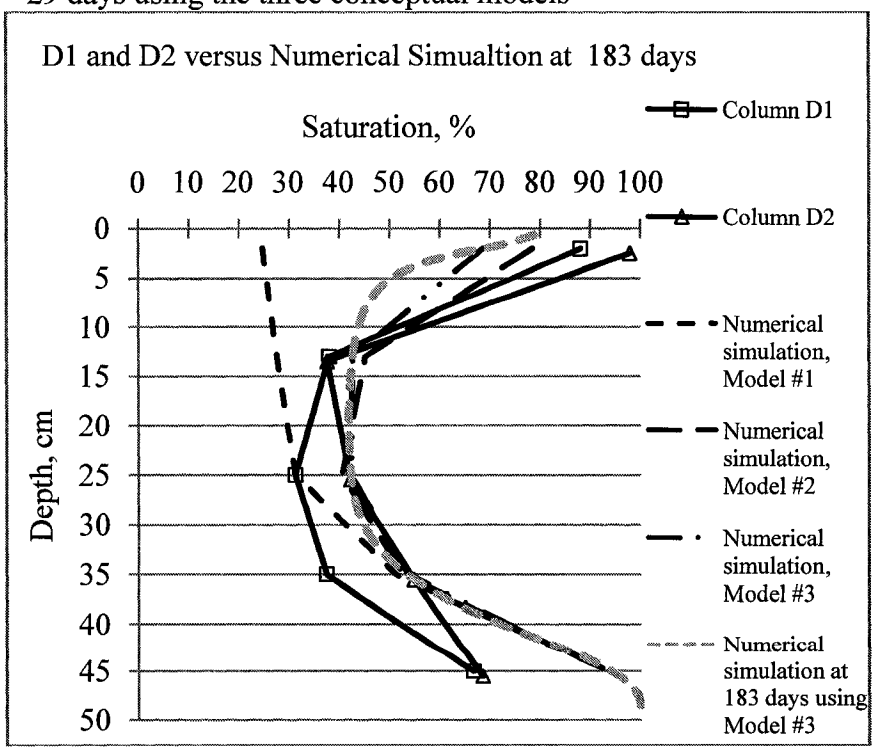

Figure 5.22- Total saturation for concrete sand columns versus numerical simulation at 183 days using the three conceptual models

Reproduced with permission of the copyright owner. Further reproduction prohibited without permission.

The concrete sand columns were able to sustain the flow and not clog as fast as the septic bed sand columns. Table (5.1) list the total volume of loads or total hydraulic loading added to the twenty five experimental columns. This table illustrates that the concrete sand columns were loaded more than the septic sand columns which means that septic bed sand columns took less time to clog versus the concrete sand columns. The number of loads per day was reduced for the concrete sand soil at a later time compared with the septic sand soil (data provided in Table (A.15), Appendix A). Figure (5.20) illustrates how the total saturation kept increasing until it reached a threshold at approximately 200 days while the septic bed sand soil reached this total saturation threshold at approximately 100 days (Figure (5.16)).

Table 5.1- Total volume of loads applied to each of the twenty five columns during the experiment period

Soil type	Column/Total volume of loads, L				
Septic bed sand soil	E	E1	E2	E3	E4
Total volume of loads, L	586.0	274.5	313.0	253.0	240.5
Concrete sand columns	D	D1	D2	D3	D4
Total volume of loads, L	642.0	351.5	372.0	329.5	356.0
Filter media bed sand soil	C	C1	C2	C3	C4
Total volume of loads, L	690.0	569.5	676.0	676.0	443.0
Compacted peat columns	B	B1	B2	B3	B4
Total volume of loads, L	662.0	442.5	419.5	437.5	429.0
Loose peat columns	A	A1	A2	A3	A4
Total volume of loads, L	668.0	549.5	520.0	518.5	546.0

Reproduced with permission of the copyright owner. Further reproduction prohibited without permission.

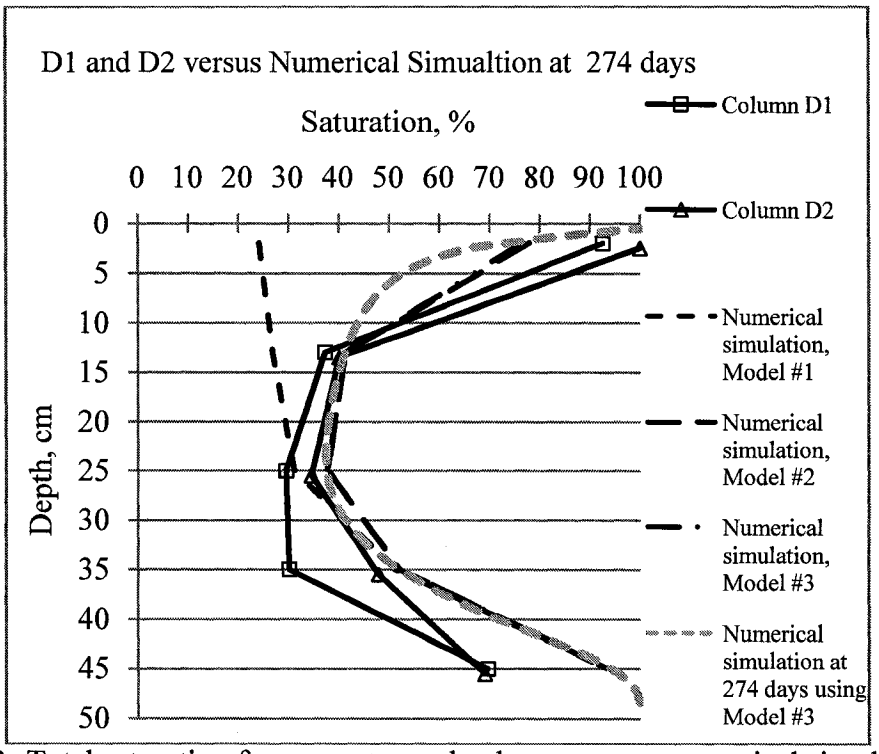

Figure 5.23- Total saturation for concrete sand columns versus numerical simulation at 274 days using the three conceptual models

Figures (5.22) and (5.23) show the total saturation profiles obtained from the numerical simulation denoted numerical simulations at 183 days and 274 days using Model #3, respectively. The saturation profile in Figure (5.22) shows that the total saturation at the surface of the soil at 183 days was only at approximately 80% and this is why the concrete sand columns was able to handle more pulses. At 274 days, numerical simulation predicts 100% total saturation at the first grid block but the total saturation fell off gradually below the first grid block and that was why the TDR measured an approximate saturation of 90%. Conceptually, if the loading of the concrete sand columns was continued, the top TDR measuring location would have eventually recorded 100% saturation and the numerical simulation would have simulated the increase in biomat layer thickness similar to what was noted for the septic bed sand soil.

Reproduced with permission of the copyright owner. Further reproduction prohibited without permission.

5.5.3 Results for Compacted Peat Soil

The same Monod kinetic parameters used to simulate the clogging process in the previous soils were used with the compacted peat soil. Figure (5.24) shows a plot of the TDR measurements at the top measurement point prepared for compacted peat columns and the simulated saturation using Model #2. Also, Figures (5.25), (5.26), and (5.27) illustrate the experimental saturation profiles measured for columns B1 and B2 and the corresponding numerical simulations using Models #2 and #3. The initial biomass concentration and maximum/minimum relative permeabilities were calibrated with the same manner discussed with the sand soils. The calibrated parameters are listed in Table (5.2)

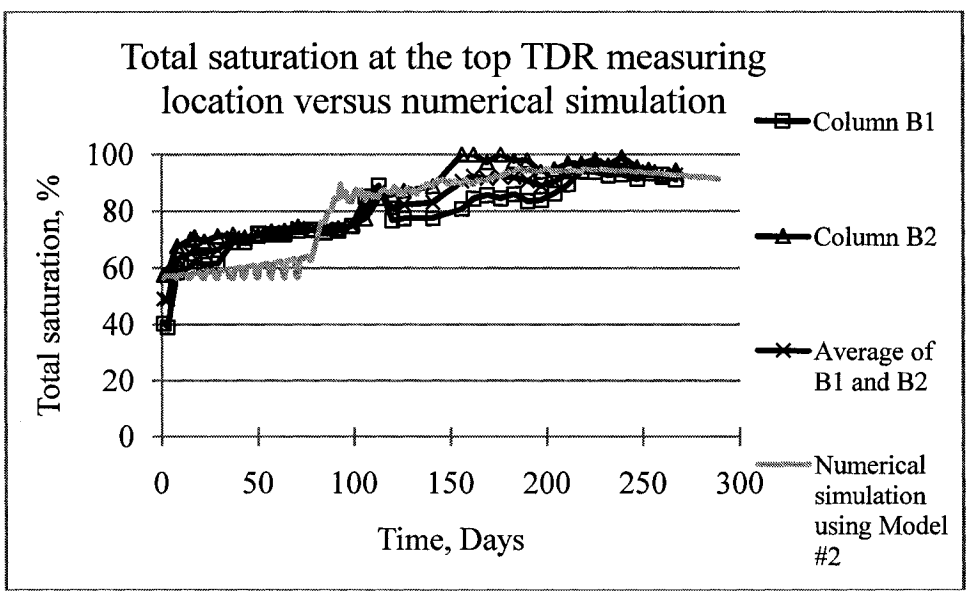

Figure 5.24- Total saturation at the top measuring location for compacted peat columns B1 and B2 versus numerical simulation using Model #2

Although the simulated average saturations at the top few centimeters indicated good agreement with the experiment data, Figures (5.26) and (5.27) show that only the top measurement location agreed well with the saturation profiles measured from the

Reproduced with permission of the copyright owner. Further reproduction prohibited without permission.

experimental columns. A large number of trials were conducted to try to match the other four TDR measuring locations by changing the Monod kinetic parameters. Unfortunatly, no set of parameters could be found to allow the saturation profiles to shift to match the other four TDR measuring locations. The inability of the model to simulate the shift in the saturation profile may be partially attributed to the hydraulic component of the model. As noted in chapter three for the peat soils, the saturation profiles shifted and the changes in the outflow with time in response to a pulse are gradual as the system clogs. These trends are opposite to what was observed in the sand soils which indicated a sharp increase in saturation at the top of the column and this coincided with a rapid decrease in the outflow rate from the base of the column in response to a pulse. The responses observed in the peat columns indicate that the influent was able to migrate further into the column, due to a high hydraulic conductivity, and hence the biomass formed over a greater depth causing the entire saturation profile to shift and causing less impact on the outflow rate in response to a pulse. However, this scenario could not be simulated for the peat soils using the parameters considered.

Reproduced with permission of the copyright owner. Further reproduction prohibited without permission.

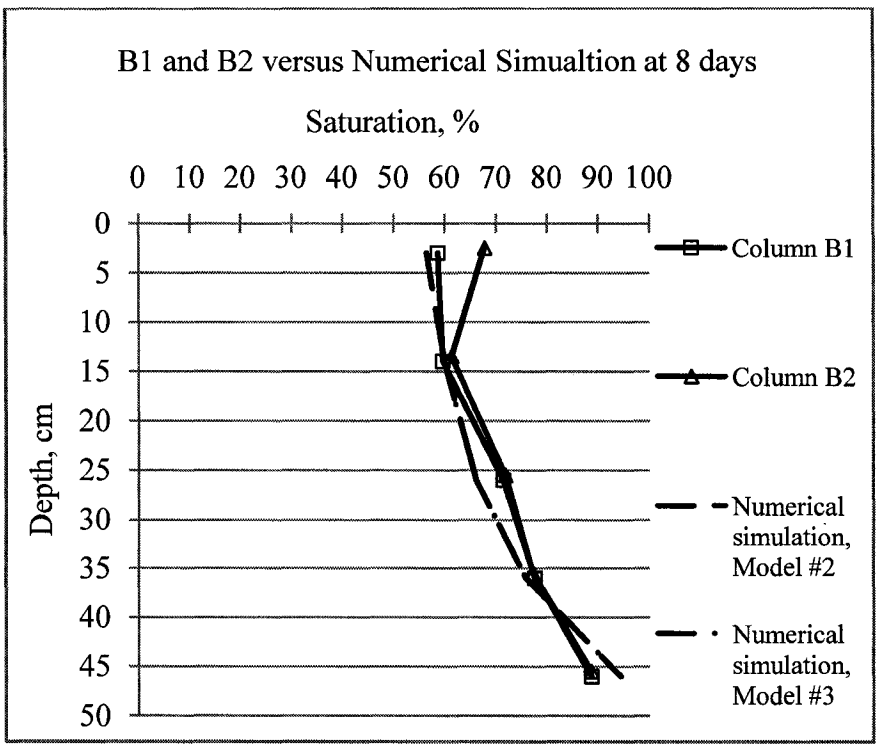

Figure 5.25- Total saturation for compacted peat columns versus numerical simulation at 8 days using Models #2 and #3

Reproduced with permission of the copyright owner. Further reproduction prohibited without permission.

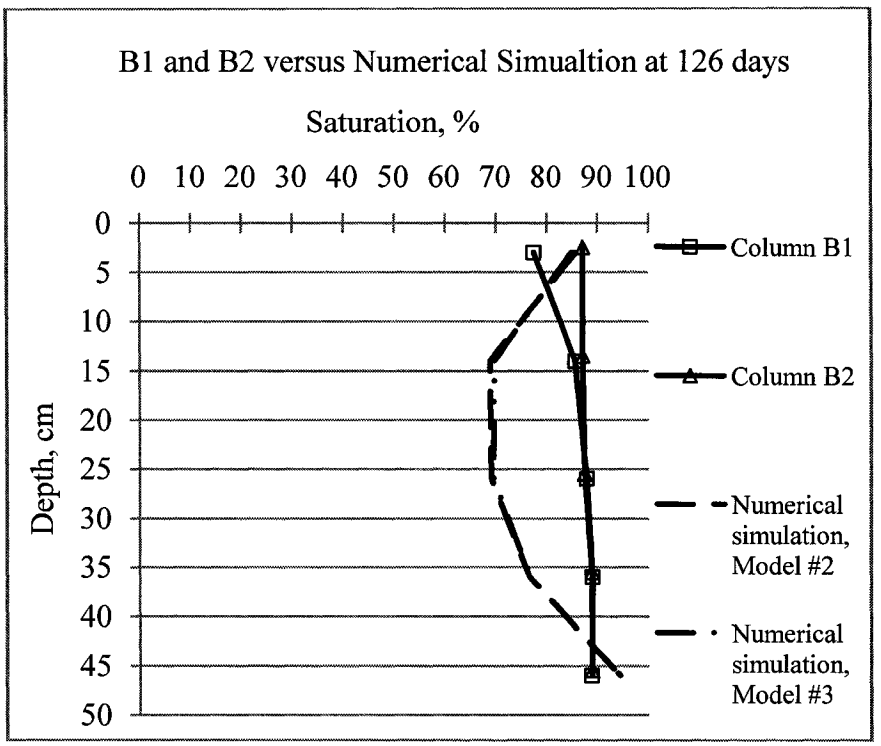

Figure 5.26- Total saturation for compacted peat columns versus numerical simulation at 126 days using Models #2 and #3

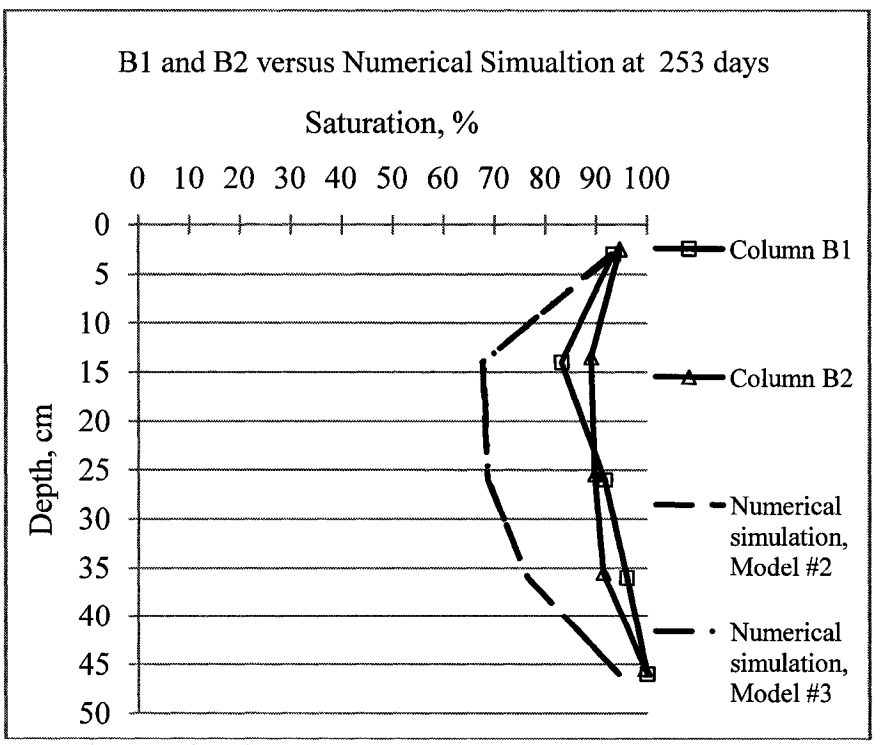

Figure 5.27- Total saturation for compacted peat columns versus numerical simulation at 253 days using Models #2 and #3

Reproduced with permission of the copyright owner. Further reproduction prohibited without permission.

The observation that saturation profiles shift in peat and sharply increase at the top few centimeters for sands was also noted in the loose peat and filter media bed sand, respectively. It is also related to the combination of porosity and saturated hydraulic conductivity for each soil. For example, although the saturated hydraulic conductivity in the filter media bed sand was higher than the compacted peat, the porosity of the filter media bed sand was approximately half that of the compacted peat soil. The latter resulted in the distribution of substrate further with depth in the compacted peat soil and resulted in the shift behavior noted in the entire saturation profile as the biomass is distributed over a greater depth in the soil.

5.5.4 Results for Filter Media Bed Sand and Loose Peat Soils

As discussed in the subsection that presented the control column results, both the filter media bed sand and loose peat soils were disregarded from the biological clogging simulations. The choice of the time and spatial discretizations to be 0.1 seconds and 10 cm will not reasonably simulate the biological clogging process because the entire soil column will be simulated by five grid blocks. As shown with the septic bed sand, concrete sand, and compacted peat soils, clogging occurred mainly in the top few centimetres and using a 10 cm grid block size will not capture the saturation increase due to biomass growth.

5.6 Summary of the Findings

Stage three was aimed to model the bioclogging process using the one-dimensional numerical developed earlier by Mostafa and Van Geel (2007). Three main challenges were faced during the numerical simulation process; adjustment of the input parameters

Reproduced with permission of the copyright owner. Further reproduction prohibited without permission.

to calibrate the model, the equations implemented in the numerical code and how well they represent the experimental data, and the selection of the appropriate conceptual model from the three conceptual models presented by Mostafa and Van Geel (2007).

Adjustment of the input parameters to calibrate the numerical code was conducted in two steps; the first step was used to adjust the soil parameters using the experimental data from the control columns to calibrate the hydraulic modeling component of the numerical code. The second step used the data from the remaining twenty columns to adjust the Monod kinetic parameters obtained from stage two to calibrate the clogging component of the numerical code. Table (5.2) summarizes the adjusted soil and Monod kinetic parameters used to simulate the biological clogging process in stage three. The italic/underlined numbers listed in Table (5.2) are the parameters that were adjusted from what was obtained by the separate experiments conducted in stage one and the experiment conducted in stage two.

A number of significant changes were made to the numerical code introduced by Mostafa and Van Geel (2007) to better simulate the experiment data obtained from stage one. A new top head boundary condition was added to allow a pulse to pond when the soil cannot conduct the flow due to microbial growth. With the new top head boundary condition, the code was able to simulate ponding conditions experienced by the experimental columns.

The microbial saturation introduced by Mostafa and Van Geel (2007) was replaced by a new term called biofilm saturation. This biofilm saturation accounts for three different components; active biomass, EPS, and an inert fraction. It is believed that bacteria cells alone do not physically clog the pores of a soil but rather the bacteria cells

Reproduced with permission of the copyright owner. Further reproduction prohibited without permission.

and their by-products contribute to the biological clogging process. A biofilm model was adapted in this research because visual inspection of the clogged experiment columns in stage one revealed that a biomat was developed on the surface of the columns which supported a biofilm model concept. Density values, adapted from the literature, for the three biofilm components were assumed to convert biomass into volume to calculate the corresponding saturations. Table (5.2) presents the density values assumed for the biofilm components.

Table 5.2- Summary of the soil properties and Monod kinetic parameters after they were adjusted and the additional input parameters to the numerical code

Soil Type	Irreducible saturation S_{wr}, %	van Genuchten parameters n	van Genuchten parameters α, cm^{-1}	K_{sat}, cm/s	Porosity	ρ_{dry}, g/cm^3	ρ_{bulk}, g/cm^3
Filter media bed sand, C	*0.00*	*1.691*	*0.617*	*0.427*	0.450	1.631	1.638
Concrete sand, D	*9.20*	*2.485*	*0.106*	*0.012*	0.387	1.753	1.820
Septic bed sand, E	6.89	*1.906*	*0.054*	*0.00225*	0.366	1.352	1.617
Peat, loose density, A	*15.09*	*1.405*	*0.366*	*1.250*	0.878	0.084	0.588
Peat, compacted density, B	37.36	*1.659*	*0.127*	0.035	0.824	0.150	0.763

Monod kinetic parameters	
Cell yield coefficient, Y, $mg_{cell}/mg_{substrate}$	0.0508
Maximum specific rate of substrate utilization, q_m, $mg_{substrate}/mg_{cell}$ s^{-1}	0.000521
Cell decay coefficient, b, s^{-1}	2.96×10^{-8}
Half-velocity constant, K_s, $mg_{substrate}/L$	540.128

Soil type/Parameter	Compacted peat	Concrete sand	Septic bed sand
Maximum relative permeability	0.50	0.85	0.70
Minimum relative permeability	0.0003	0.00007	0.002
Initial biomass concentration, mg/cm^3	0.005	0.05	0.00007

Parameter	Biofilm component: Active biomass	EPS	Inert
Density, g/cm^3	0.0175	0.05	0.055

Reproduced with permission of the copyright owner. Further reproduction prohibited without permission.

The modified code also adapted the concept of an initial maximum relative permeability at the beginning of a simulation and minimum relative permeability once a biomat layer is developed. This conceptual model is consistent with research presented by Beach and McCary (2003), White and West (2003), Beach et al. (2005), and others; which assigned hydraulic properties to biomat layers and treated them as soil layers. For the simulations presented in this chapter, a maximum relative permeability was calculated for the top block only based on an assumption of 1% biofilm saturation initially occupying the void space while a minimum relative permeability was calibrated based on a comparison between the hydraulic loading at later times and the pressure head at the surface of the simulated column. Table (5.2) lists the calculated/calibrated maximum and minimum relative permeability values used in the numerical simulations for septic bed sand, concrete sand, and compacted peat soils. By allowing a minimum relative permeability through a developed biomat layer, the modified code was capable of simulating the biomat layer that developed and extended further below the soil surface as noted from the column experiments.

It was clear from the numerical simulation results, and based on the discussion of Model #1 by Mostafa and Van Geel (2007), that Model #1 will not show any significant increase in the total saturation except when sufficient biomass is developed to significantly impact the relative permeability of the simulated soil. Both Models #2 and #3 were able to simulate an increase in the total saturation profiles at early times which reflected what was observed from the saturation profiles measured in stage one. It is believed that both Models #2 and #3 provide a better representation of what occurs in reality in comparison to Model #1.

Reproduced with permission of the copyright owner. Further reproduction prohibited without permission.

6. CONCLUSIONS, RECOMMENDATIONS AND SCIENTIFIC CONTRIBUTIONS

6.1 Conclusions

Literature presents different conceptual models for clogging in saturated soils but corresponding conceptual models for clogging in unsaturated soils are limited. Mostafa and Van Geel (2007) proposed three conceptual models that relate the relative permeability term to the microbial growth in unsaturated soils. The models were implemented in a one-dimensional numerical code and only hypothetical simulations were run with the code to verify the correctness of the implementation of the flow, contaminant transport, and Monod equations in the code. No experimental data were used to validate the three conceptual models.

The objectives of this research were to study the effect of different pore structures (peat versus sand soils) on biological clogging of unsaturated soils and to improve, if required, and validate the models proposed by Mostafa and Van Geel (2007) using experimental data. The research was divided into three stages. In stage one, experimental columns tests were conducted to determine the impact of soil properties on the clogging process. In stage two, experimental testing was conducted and a spreadsheet model was developed to estimate the Monod kinetic parameters needed to numerically simulate the biological clogging behavior observed from the experimental results of stage one. In stage three, the soil and Monod kinetic parameters obtained from stages one and two were used to simulate the clogging process for the column experiments. Also, several modifications were made to the conceptual model proposed by Mostafa and Van Geel

Reproduced with permission of the copyright owner. Further reproduction prohibited without permission.

(2007) to better simulate the experimental conditions observed during stage one of this research.

Saturation profiles measured in stage one using TDR illustrated a shifting pattern for the peat columns while they indicated a sharp increase in saturation over the top few centimetres for the sand columns. In general, it took longer for the peat columns to clog than the sand columns. Only the filter media bed sand demonstrated a similar clogging time as the peat soils due to its high saturated hydraulic conductivity and lower saturation profile due to its soil moisture curve.

In stage two, a continuously fed batch system was used to estimate the Monod kinetic parameters. A spreadsheet model was used to simulate the experimental conditions and estimate the Monod kinetic parameters. The best fit parameters were 0.0508 $mg_{cell}/mg_{substrate}$ for the cell yield coefficient (Y), 0.000521 $mg_{substrate}/mg_{cell}$. s for the maximum rate of substrate utilization (q_m), 2.96×10^{-8} s^{-1} for the decay coefficient (b), and 540.128 $mg_{substrate}/L$ for the half-velocity constant (K_s) and these fell within the range of values published in the literature.

Soil and Monod kinetic parameters obtained in stages one and two were used in stage three to simulate the column experiments. Also, a number of significant changes were made to the conceptual bioclogging model introduced by Mostafa and Van Geel (2007) to better simulate the experiment data obtained from stage one. The changes are summarized as follows;

- The specified head or flux boundary condition was replaced with a head-dependant boundary condition to better reflect the conditions in the column experiments. At the beginning of a pulse, an initial head equivalent to the total

Reproduced with permission of the copyright owner. Further reproduction prohibited without permission.

hydraulic load of a pulse is prescribed at the top of the column. After each time step, the flux into the column is calculated and the prescribed head, which represents the depth of ponded water, was adjusted accordingly. This allowed the top boundary condition to adjust as the biomat formed in the top layer of soil.

- Microbial saturation term proposed by Mostafa and Van Geel (2007) used a simple model to convert the microbial growth to a saturation term. Since the Monod equation only simulated a bacteria concentration, the biomass density needed to convert the bacteria concentration to a biomass volume was, at best, an estimate and was artificially lowered to account for the bacteria by-products that also form with the biomass. Hence, a modified conceptual model of the biofilm presented in the literature, which accounts for active biomass, EPS, and an inert fraction, was implemented to better represent the mass and volume of biomass generated.
- The modified code allows the biomat that forms to have a specified minimum relative permeability which allows flow through the developed biomat under ponding conditions. This conceptual model is consistent with the literature as reported by many researchers (e.g. Taylor and Jaffé (1990a); Beach and McCary (2003); Beach et al. (2005)). This minimum relative permeability allows the code to run even if the total saturation reaches 100% and hence the excess biomass generated at a clogged layer is redistributed to the downstream grid block and progressively clogs the pores increasing the depth of the biomat layer. Progressive clogging can be seen in some simulations where a column showed ponding at the top surface and pores were 100% clogged to 3-4 cm from the surface of the soil.

Reproduced with permission of the copyright owner. Further reproduction prohibited without permission.

This latter finding from the numerical simulations agreed with what was found from the column experiments in stage one.

After adjusting the soil and Monod kinetic parameters to calibrate the numerical code, biological clogging simulations were conducted on septic bed sand, concrete sand and compacted peat soils. The three conceptual models proposed by Mostafa and Van Geel (2007) that relate the relative permeability term to the biomass growth were compared to determine which model better reflected the clogging process. Model #1, which assumed clogging of the smallest pore first and used a modified form of Mualem's equation to account for this reduction, did not simulate the trends seen in the column experiments. Models #2 and #3, based on a simple reduction factor of one minus the biomass saturation and a flow reduction factor based on a biofilm model, respectively, were able to simulate the impact of biological clogging on the flow and saturation profiles measured for the column experiments.

6.2 Recommendations and Future Work

Future research should include experimental and numerical improvements to the current research. More experimental tests should be conducted on different commercial biofilter soil types or new soil types to check the behavior of the saturation profile due to biomass growth. Simulation of the data from these soils will increase the confidence in the current modified numerical code with all the modifications/changes proposed in this research. Also, inoculating the experimental columns with septic tank effluent at the beginning of the experiment in stage one would have been helpful and worth testing to study the differences between the sources of bacteria on the biological clogging process.

Reproduced with permission of the copyright owner. Further reproduction prohibited without permission.

Effect of suspended solids was not significant in this study and did not impact the time to clog. Testing with higher silica content or an alternate material should illustrate the impact of physical clogging on the saturation profile. Physical and biological clogging should significantly impact the clogging time.

The experimental setup used in stage two to obtain Monod kinetic parameters could be improved as well. More soil types could be used in the experimental setup and a comparison between the estimated Monod kinetic parameters with what was found in this research will increase the confidence in the parameters estimated in this research.

The numerical code could also be improved. Studying the oxygen utilization in the columns will help and provide more confidence and better understanding of the oxygen distribution in the columns. Also, since there was no other way of oxygen diffusion to the experimental columns except from the top and/or bottom surfaces, the ponded pulses may have resulted in depleting the oxygen and hence led to the development of anaerobic conditions. The current modified code does not simulate oxygen diffusion nor incorporate modeling of anaerobic conditions.

Microbial transport and filtration/straining of suspended solids are also two important features the code does not include. This study shows that progressive clogging may occur and a developed biomat could extend 3 to 4 cm below the soil surface and adding microbial transport to the code may better simulate this biomat development. Also, adding filtration/straining of suspended solids will help simulating physical clogging which is a feature the current modified code lacks.

Reproduced with permission of the copyright owner. Further reproduction prohibited without permission.

6.3 Scientific Contributions

There are two main significant contributions from this research work to science and engineering. They can be categorized under two areas; experimental and conceptual/numerical contributions.

The experimental contribution involves the generation of a detailed and valuable data set using four different soils. The different soils represent various pore size distributions, porosities, densities, as well as organic versus inorganic soils. The measured saturation and outflow profiles were used to monitor and study the biological clogging process that occurred in the soils under unsaturated conditions. This data set showed how different pore structures can affect the biological clogging behavior noted in the tested soils.

The conceptual and numerical models introduced in this research were also a significant contribution of this work. This model helped increase our understanding of biological clogging in unsaturated soils. From this main contribution, three major contributions can be further defined and they are summarized as follow;

- Introducing three conceptual models that relate the relative permeability term to biomass growth which were presented by Mostafa and Van Geel (2007) and were further investigated in this research work.
- Introducing a minimum relative permeability term to the conceptual model once a biomat is developed. This concept was discussed by other researchers (e.g. Beach and McCary (2003)). The addition of this minimum relative permeability term was a great benefit in explaining how the biomat layer behaves after the soil pores are filled with biomass.

Reproduced with permission of the copyright owner. Further reproduction prohibited without permission.

- Introducing a better representation of biomass growth by incorporating a multi-component biofilm model that includes three main components; microorganisms, EPS, and inert fraction. The incorporation of a biofilm model helped simulate and explain the bioclogging noted from the experimental data set generated using the experimental work of this research.

To the author's knowledge, the experimental and numerical investigation presented herein is one of the first attempts to develop and validate a conceptual model for biological clogging of unsaturated soils in which the unsaturated flow hydraulics and progressive clogging are simulated using the unsaturated flow equation, the Monod equation to simulate biomass growth, and a conceptual model to relate the unsaturated relative permeability term to the biomass growth within the pore space.

Reproduced with permission of the copyright owner. Further reproduction prohibited without permission.

7. REFERENCES

Allison, L.D., "*Effect of Microorganisms on Permeability of Soil under Prolonged Submergence*" Soil Science, Vol. 63, P. 439-450, 1947.

Alvarez, P.J., P.J. Anid and T.M. Vogel, "*Kinetics of Aerobic Biodegradation of Benzene and Toluene in Sandy Aquifer Material*", Biodegradation, Vol. 2, No. 1, P. 43-51, 1991.

American Society for Testing and Materials, "*Standard Test Methods for Moisture, Ash, and Organic Matter of Peat and Other Organic Soils*", ASTM D 2974-87, 1995.

Anderson, J.R. and J.M. Slinger, "*Europium Chelate and Fluorescent Brighteners Staining of Soil Propagules and their Photomicrographic Counting. 1. Methods*", Soil Biology and Biochemistry, Vol. 7, P. 205-209, 1975.

Baek, N.H., L.S. Clesceri and N.L. Clesceri, "*Modeling of Enhanced Biodegradation in Unsaturated Soil Zone*", Journal of Environmental Engineering Division, American Society of Civil Engineering, Vol. 115, No. 1, P. 150-172, 1989.

Bakke, R., "*Biofilm Detachment*", unpublished doctoral thesis, Montana State University, Bozeman, MT, 1986.

Balkwill, D.L., T.E. Rucinsky and L.E. Casida, "*Release of Microorganisms from Soil with Respect to Transmission Electron Microscopy Viewing and Plate Counts*", Antonie van Leeuwenhoek, Vol. 43, P. 73-87, 1977.

Balkwill, D.L., F.R. Leach, J.T. Wilson, J.F. McNabb and D.C. White, "*Equivalence of Microbial Biomass Measures Based on Membrane Lipid and Cell Wall Components, Adenosine Triphosphate, and Direct Counts in Subsurface Aquifer Sediments*", Microbial Ecology, Vol. 16, P. 73-84, 1988.

Baveye, P. and A. Valocchi, "*An Evaluation of Mathematical Models of the Transport of Biological Reacting Solutes in Saturated Soils and Aquifers*", American Geophysical Union, Water Resource Research, Vol. 25, No. 6, P. 1413-1421, 1989.

Beach, D.N. and J.E. McCary, "*Numerical Modeling of Unsaturated Flow in Wastewater Soil Absorption Systems*", Ground Water Monitoring Remediation, Vol. 23, No. 2, P. 64-72, 2003.

Beach, D.N.H., J.E. McCary, K.S. Lowe, and R.L. Siegrist, "*Temporal Changes in Hydraulic Conductivity of Sand Porous Media Biofilters during Wastewater Infiltration Due to Biomat Formation*", Journal of Hydrology, Vol. 311, P. 230-243, 2005.

Reproduced with permission of the copyright owner. Further reproduction prohibited without permission.

Beal, C.D., E.A. Gardner, G. Kirchhof, and N.W. Menzies, "*Long-Term Flow Rates and Biomat Zone Hydrology in Soil Columns Receiving Septic Tank Effluent*", Water Research, Vol. 40, P. 2327-2338, 2006.

Bishop, P.L., T.C. Zhang and Y. Fu, "*Effects of Biofilm Structure, Microbial Distribution and Mass Transport on Biodegradation Processes*", Water Science and Technology, Vol. 31, No. 1, P. 143-152, 1995.

Black, J.G., "*Microbiology, Principles and Explorations*", Marymount University, Prentice Hall, Upper Saddle River, NJ, 1999.

Boller, M., A. Schwager, J. Eugster and J. Mottier, "*Dynamic Behavior of Intermittent Buried Filters*", Water Science and Technology, Vol. 28, No. 10, P. 99-107, 1993.

Brooks, R.H. and A.T. Corey, "*Hydraulic Properties of Porous Media*", Hydrology Paper 3, Colorado State University, Fort Collins, Colorado, P. 22-27, 1964.

Burdine, N.T., "*Relative Permeability Calculations from Pore Size Distribution Data*", The American Institute of Mining, Metallurgical, and Petroleum Engineers, Vol. 198, P. 71-78, 1953.

Childs, E.C. and N. Collis-George, "*The Permeability of Porous Materials*", Proceedings of the Royal Society of London. Series A, Mathematical and Physical Sciences, Vol. 201, No. 1066, P. 392-405, 1950.

Christensen B.E. and W.G. Characklis, *"Physical and Chemical Properties of Biofilms, In Biofilm"*, Edited by Characklis W.G. and K.C. Marshall, P. 93-130, Wiley, New York, 1990.

Clement, T.P., B.S. Hooker and R.S. Skeen, "*Macroscopic Models for Predicting Changes in Saturated Porous Media Properties Caused by Microbial Growth*", Ground Water, Vol. 34, No. 5, P. 934-942, September-October 1996.

Dale, N.G., "*Bacteria in Intertidal Sediments: Factors Related to Their Distribution*", Limnology and Oceanography, Vol. 19, P. 509-518, 1974.

Davies, D.G., "*Regulation of Matrix Polymer in Biofilm Formation and Dispersion. In: Microbial Extracellular Polymeric Substances: Characterization, Structure and Function*", Edited by Wingender J., T.R., Neu and H-C. Flemming, Springer, Berlin, 1999.

Dennis, J.E. and R.B. Schnabel, "*Numerical Methods for Unconstrained Optimization and Nonlinear Equations*", Prentice-Hall, Inc., Englewood Cliffs, New Jersey, 1983.

Reproduced with permission of the copyright owner. Further reproduction prohibited without permission.

Droste, R.L., E. Andras and K.J. Kennedy, "*Initial Biofilm Formation of Acetoclastic Methanogenic Bacteria*", Biofouling, Vol. 2, P. 191–210, 1990.

Eaton, A.D., L.S. Clescei, E.W. Rice and A.E. Greenberg, "*Standard Methods for the Examination of Water and Wastewater*", American Public Health Association, 21th edition, 2005.

Premier Tech. Enviroment, Ecoflo® Biofilters, Residential Products, http://www.ecofloontario.com/biofilter_files/ecoflo_biofilter.htm, 2/2/2009.

Evans, E., M.R. Brown and P. Gilbert, "*Iron Chelator, Exopolysaccharide and Protease Production in Staphylococcus Epidermidis: A Comparative Study of the Effects of Specific Growth Rate in Biofilm and Planktonic Culture*" Microbiology, Vol. 140, P. 153-157, 1994.

Frankenberger, W.T., Jr. E.R. Troeh and L.C. Dumenil, "*Bacterial Effects on Hydraulic Conductivity of Soils*", Soil Science Society of American Journal, Vol. 43, P. 333-338, 1979.

Frind, E.O., "*Solution of the Advective-Dispersion Equation with Free Exit Boundary*", Numerical Method for Partial Differential Equations, Vol. 4, P. 301-313, 1988.

Hagedorn, C., E.L. McCoy and T.M. Rahe, "*The Potential for Ground Water Contamination from Septic Effluent*", Journal of Environmental Quality, Vol. 10, No. 1, P. 1-7, 1981.

Haverkamp, R. and M. Vauclin, "*A Note on Estimating Finite Difference Interblock Hydraulic Conductivity Values for Transient Unsaturated Flow Problems*", Water Resources Research, Vol. 15, No. 1, P. 181-187, 1979.

Hoehn, R.C. and A.D. Ray, "*Effects of Thickness on Bacterial Film*", Journal of the Water Pollution Control Federation, Vol. 45, P. 2302-2320, 1973.

Hsieh, Ke M., G.A. Murgel, L.W. Lion and M.L. Shuler, "*Interactions of Microbial Biofilms with Toxic Trace Metals: 1. Observation and Modeling of Cell Growth, Attachment, and Production of Extracellular Polymer*", Biotechnology and Bioengineering, Vol. 44, P. 219-231, 1994.

Jawson, M.D., "*Soil Clogging By Septic Tank Effluent: Causes, Methods of Correction*", M. S. Thesis, University of Wisconsin, Madison, United States, 1976.

Kennedy, P.L., "*Investigation of Flow through Peat Filters*" M. A. Sc. Thesis, Carleton University, Ottawa, Ontario, Canada, 1998.

Reproduced with permission of the copyright owner. Further reproduction prohibited without permission.

Kennedy, P.L. and P.J. Van Geel, *"Impact of Density on the Hydraulics of Peat Filters"*, Canadian Geotechnical Journal, Vol. 38, No. 6, P. 1213-1219, 2001.

Khammar, N., L. Malhautier, V. Degrange, R. Lensi and J.L. Fanlo, "*Evaluation of Dispersion Methods for Enumeration of Microorganisms from Peat and Activated Carbon Biofilters Treating Volatile Organic Compounds*", Chemosphere, Vol. 54, No. 3, P. 243-254, 2004.

Kristiansen, R., "*Sand-Filter Trenches for Purification of Septic Tank Effluent: I. The Clogging Mechanism and Soil Physical Environment*", Journal of Environmental Quality, Vol. 10, No. 3, P. 353-357, 1981a.

Kristiansen, R., "*Sand-Filter Trenches for Purification of Septic Tank Effluent: III. The Microflora*", Journal of Environmental Quality, Vol. 10, No. 3, P. 361-364, 1981b.

Kornegay, B.H. and J.F. Andrews, *"Characteristics and Kinetics of Fixed-Film Biological Reactors*", Final report, Grant WP-01181, Federal Water Pollution Control Administration, U.S. GPO, Washington, 1967.

Kreft, J-U and J.W.T. Wimpenny, "*Effect of EPS on Biofilm Structure and Function as Revealed by an Individual-Based Model of Biofilm Growth*", Water Science and Technology, Vol. 43, No. 6, P. 135–141, 2001.

Laspidou, C.S. and B.E. Rittmann, "*A Unified Theory for Extracellular Polymeric Substances, Soluble Microbial Products, and Active and Inert Biomass*", Water Research, Vol. 36, P. 2711–2720, 2002a.

Laspidou, C.S. and B.E. Rittmann, "*Non-Steady state Modeling of Extracellular Polymeric Substances, Soluble Microbial Products, and Active and Inert Biomass*", Water Research, Vol. 36, P. 1983–1992, 2002b.

Laspidou, C.S. and B.E. Rittmann, "*Modeling the Development of Biofilm Density Including Active Bacteria, Inert Biomass, and Extracellular Polymeric Substances*", Water Research, Vol. 38, P. 3349–3361, 2004a.

Laspidou, C.S. and B.E. Rittmann, "*Evaluating Trends in Biofilm Density Using the UMCCA Model*", Water Research, Vol. 38, P. 3362–3372, 2004b.

Laspidou, C.S. and B.E. Rittmann, "*Modeling Biofilm Complexity by Including Active and Inert Biomass and Extracellular Polymeric Substances*", Biofilm, Vol. 1, P. 285-291, 2004c.

Lenhard, R.J. and J.C. Parker, "*A Model for Hysteretic Constitutive Relations Governing Multiphase Flow 2. Permeability-Saturation Relations"*, Water Resources Research, Vol. 23, No. 21, P. 2197-2206, 1987.

Reproduced with permission of the copyright owner. Further reproduction prohibited without permission.

Lindahl, V. and L. Bakken, "*Evaluation of Methods for Extraction of Bacteria from Soil* ", Microbiology Ecology, Vol. 16, No. 2, P. 135-142, 1995.

Mattison, R.G., H. Taki and S. Harayama, "*The Bacterivorous Soil Flagellate Heteromita Globosa Reduces Bacterial Clogging Under Denitrifying Conditions in Sand-Filled Aquifer Columns*", Applied and Environmental Microbiology, Vol. 68, No. 9, P. 4539-4545, 2002.

McCalla, T.M., "*Studies on the Effect of Microorganisms on Rate of Percolation of Water through Soils*", Soil Science Society of American Proceedings, Vol. 15, P. 182-186, 1950.

Melo, L.F. and J.D. Pinheiro, "*Fouling Tests: Equipment and Methods. In: Fouling in Heat Exchange Equipment*", Edited by Suitor, J.W. and A.M. Pritchard, P. 43–49, New York: American Society of Mechanical Engineers, 1984.

Mian, F.A., T.R. Jarman and R.C. Righelato, "*Biosynthesis of Exopolysaccharide by Pseudomonas aeruginosa*", Journal of Bacteriology, Vol. 134, No. 2, P. 418-422, 1978.

Molz, F.J., M.A. Widdowson and L.D. Benefield, "*Simulation of Microbial Growth Dynamics Coupled to Nutrient and Oxygen Transport in Porous Media*", Water Resources Research, Vol. 22, No. 8, P. 1207-1216, 1986.

Monod, J., "*The Growth of Bacterial Cultures*", Annual Review of Microbiology, P. 371-394, 1949.

Mostafa, M., "*Conceptual Models for Biological Clogging of Unsaturated Soils*" M. A. Sc. Thesis, Carleton University, Ottawa, Ontario, Canada, 2004.

Mostafa, M. and P.J. Van Geel, "*Conceptual Models and Simulations for Biological Clogging in Unsaturated Soils*", Vadose Zone Journal, Vol. 6, P. 175–185, 2007.

Mualem, Y., "*A New Model for Predicting the Hydraulic Conductivity of Unsaturated Porous Media*", American Geophysical Union, Water Resource Research, Vol. 12, No. 3, P. 513-522, 1976.

NSF International, Waterloo Biofilter Systems, Inc., "*Environmental Technology Verification Report, Reduction of Nitrogen in Domestic Wastewater from Individual Residential Homes*", United States Environmental Protection Agency, http://www.nsf.org/business/water_quality_protection_center/pdf/Waterloo_Biofilter_EPAAcceptedFinalReport.pdf, April 2003, 2/2/2009.

Reproduced with permission of the copyright owner. Further reproduction prohibited without permission.

Oberdorfer, J.A. and F.L. Peterson, "*Waste-Water Injection: Geochemical and Biogeochemical Clogging Processes*", Ground Water, Vol. 23, P. 753-761, 1985.

Odencrantz, J.E., A.J. Valocchi and B.E. Rittmann, "*Modeling Two-Dimensional Solute Transport with Different Biodegradation Kinetics*", Paper presented at Petroleum Hydrocarbons and Organic Chemicals in Groundwater, Am. Pet. Inst., Houston, Tex., Oct. 31 to Nov. 2, 1990.

Okubo, T. and J. Matsumoto, "*Effect of Infiltration Rate on Biological Clogging and Water Quality Changes during Artificial Recharges*", Water Resources Research, Vol. 15, P. 1536-1542, 1979.

Okubo, T. and J. Matsumoto, "*Biological Clogging of Sand and Changes of Organic Constituents during Artificial Recharge*", Water Research, Vol. 17, P. 813-821, 1983.

Ontario Building Code, "*Division B - Part 8: Sewage Systems*", Ministry of Municipal Affairs and Housing, Building and Development Branch, Ontario Building Code, 2006.

Or, D., "*Physical Processes Affecting Microbial Habitats and Activity in Unsaturated Porous Media*", Agricultural Sciences, Vol. 2, No. 2, P. 39-45, 2002.

Picioreanu, C., M. C. M. van Loosdrecht, and J.J. Heijnen, "*A New Combined Differential-Discrete Cellular Automaton Approach for Biofilm Modeling: Application for Growth in Gel Beads*", Biotechnology and Bioengineering, Vol. 57, No. 6, P. 718-731, 1998.

Ramsay, A.J., "*Extraction of Bacteria from Soil: Efficiency of Shaking or Ultrasonication as Indicated by Direct Counts and Autoradiography*", Soil Biology and Biochemistry, Vol. 16, No. 5, P. 475-481, 1984.

Rice, R.C., "*Soil Clogging during Infiltration of Secondary Effluent*", Journal Water Pollution Control Federation, Vol. 46, P. 708-716, 1974.

Rittmann, B.E., "*The Significance of Biofilms in Porous Media*", Water Resources Research, Vol. 29, No. 7, P. 2195-2202, 1993.

Rittmann, B.E. and P.L. McCarty, "*Variable-Order Model of Bacterial-Film Kinetics*", Journal of Environmental Engineering Division, Vol. 104, P. 889-899, 1978.

Rittmann, B.E. and P.L. McCarty, "*Evaluation of Steady-State-Biofilm Kinetics*", Biotechnology and Bioengineering, Vol. 22, P. 2343-2357, 1980.

Rittmann, B.E. and P.L. McCarty, "*Substrate Flux into Biofilms of Any Thickness*", Journal of Environmental Division, American Society of Civil Engineering, Vol. 107, (EE4), P. 831-849, 1981.

Reproduced with permission of the copyright owner. Further reproduction prohibited without permission.

Rittmann B.E., P.L. McCarty, "*Environmental Biotechnology: Principles and Applications*", NY: Mc-Graw Hill, New York, 2001.

Robertson, B.R., D.K. Button, and A.L. Koch, "*Determination of the Biomasses of Small Bacteria at Low Concentrations in a Mixture of Species with Forward Light Scatter Measurements by Flow Cytometry*", Applied and Environmental Microbiology, Vol. 64, No. 10, P. 3900–3909, 1998.

Robinson J.A., M.G. Trulear and W.G. Characklis, "*Cellular Reproduction and Extracellular Polymer Formation by Pseudomonas Aeruginosa in Continuous Culture*", Biotechnology and Bioengineering, Vol. 26, P. 1409–1417, 1984.

Rockhold, M.L., R.R. Yarwood, M.R. Niemet, P.J. Bottomley and J.S. Selker, "*Considerations for Modeling Bacterial-Induced Changes in Hydraulic Properties of Variably Saturated Porous Media*", Advances in Water Resources, Vol. 25, P. 477-495, 2002.

Seki, K., T. Miyazaki and M. Nakano, "*Reduction of Hydraulic Conductivity due to Microbial Effects*", European Journal of Soil Science, Vol. 181, P. 137-144, 1996.

Seki, K., T. Miyazaki and M. Nakano, "*Effects of Microorganisms on Hydraulic Conductivity Decrease in Infiltration*", European Journal of Soil Science, Vol. 49, P. 231-236, 1998.

Seki, K., T. Suko and T. Miyazaki, "*Bioclogging of Glass Beads by Bacteria and Fungi*", Transactions of World Congress of Soil Science, Symposium No. 51, P. 1244-1 - 1244-8, 2002.

Schirmer, M., B.J. Bulter, J.W. Roy, E.O. Frind and J.F. Barker, "*A Relative-Least-Squares Technique to Determine Unique Monod Kinetic Parameters of BTEX Compounds Using Batch Experiments*", Journal of Contaminant Hydrology, Vol. 37, No. 1-2, P. 69-86, 1999.

Schwager, A., and M. Boller, "*Transport Phenomena in Intermittent Filters*", Water Science Technology, Vol. 35, No. 6, P. 13-20, 1997.

Shibchurn, A. "*Water content Measurement on Peat Using Time Domain Reflectometry*" M.Eng. Thesis, Carleton University, Ottawa, Ontario, Canada, 2001.

Shibchurn, A., P.J. Van Geel and P.L. Kennedy, "*Impact of Density on the Hydraulic Properties of Peat and the Time Domain Reflectometry (TDR) Moisture Calibration Curve*", Canadian Geotechnical Journal, Vol. 42, No. 1, P. 279-286, 2005.

Reproduced with permission of the copyright owner. Further reproduction prohibited without permission.

Siegrist, R.L., J.E. McCray and K.S. Lowe, "*Wastewater Infiltration into Soil and the Effect of Infiltrative Surface Architecture*", Small Flows Quarterly Journal, Vol. 5, No. 1, P. 29-39, 2004.

Siegrist, R.L., "*Evolving a Rational Design Approach for Sizing Soil Treatment Units: Design for Wastewater Effluent Infiltration*", Small Flows Quarterly Journal, Vol. 7, No. 3, P. 16-24, 2006.

Simunek, J., M. Sejna, and M.Th. van Genuchten, "*The HYDRUS-2D Software Package for Simulating Water Flow and Solute Transport in Two–Dimensional Variably Saturated Media*", Version 2.0 IGWMC-TPS-53C, Golden, Colorado: International Groundwater Modeling Center, Colorado School of Mines, 1999.

Spychata, M. and R. Blazejewski, "*Sand Filter Clogging by Septic Tank Effluent*", Water Science and Technology, Vol. 48, No. 11-12, P. 153-159, 2003.

Supplementary Standard SB-5, "*Approved Sewage Treatment Units*", Ministry of Municipal Affairs and Housing, Building and Development Branch, Ontario Building Code, 2006.

Sutherland, I.W., "*Biofilm Polysaccharides. In: Microbial Extracellular Polymeric Substances: Characterization, Structure and Function*", Edited by Wingender J., T.R., Neu and H-C. Flemming, Springer, Berlin, 1999.

Taylor, S.W. and P.R. Jaffé, "*Biofilm Growth and the Related Changes in the Physical Properties of a Porous Medium. 1. Experimental Investigation*", Water Resources Research, Vol. 26, No. 9, P. 2153-2159, 1990a.

Taylor, S.W., P.C.D. Milly and P. R. Jaffé, "*Biofilm Growth and the Related Changes in the Physical Properties of a Porous Medium. 2. Permeability*", Water Resources Research, Vol. 26, No. 9, P. 2161-2169, 1990.

Taylor, S.W. and P.R. Jaffé, "*Substrate and Biomass Transport in a Porous Medium*", Water Resources Research, Vol. 26, No. 9, P. 2181-2194, 1990b.

Tchobanoglous, G. and F.L. Burton, "*Wastewater Engineering Treatment, Disposal, and Reuse 3rd Edn*", P. 775-776, Metcalf & Eddy McGraw-Hill, New York, 1991.

Trulear, M.G., "*Cellular Reproduction and Extracellular Polymer Formation in the Development of Biofilm*", unpublished doctoral thesis, Montana State University, Bozeman, MT, 1983.

Trulear, M.G. and W.G. Characklis, "*Dynamics of Biofilm Processes*", Journal of the Water Pollution Control Federation, Vol. 9, P. 1288-1301, 1982.

Reproduced with permission of the copyright owner. Further reproduction prohibited without permission.

Turakhia, M.H. and W.G. Characklis, "*Activity of Pseudomonas Aeruginosa in Biofilms: Effect of Calcium*", Biotechnology and Bioengineering, Vol. 33, P. 406–414, 1989.

Van Genuchten, M.Th., "*A Closed-form Equation for Predicting the Hydraulic Conductivity of Unsaturated Soils*", Soil Science Society of American Journal, Vol. 44, P. 892-898, 1980.

Van Veen, J.A., and E.A. Paul, "*Conversion of Biovolume Measurements of Soil Organisms, Grown Under Various Moisture Tensions, to Biomass and Their Nutrient Content*", Applied and Environmental Microbiology, Vol. 37, No. 4, P. 686-692, 1979.

Vieira, M.J., L.P. Melo and M.M. Pinheiro, "*Biofilm Formations: Hydrodynamic Effects on Internal Diffusion and Structure*", Biofouling, Vol. 7, P. 67–80, 1993.

Wastewater Virtual Trade Show Technologies, United States Environmental Protection Agency, http://www.epa.gov/boston/assistance/ceitts/wastewater/techs.html,2/2/2009.

Waterloo Biofitlers, Waterloo Biofitlers Systems Inc., On-Site Wastewater Treatment, http://www.waterloo-biofilter.com, 2/2/2009.

Weise, W. and G. Rheinheimer, "*Fluoreszenzmikroskopische Untersuchungen uber die Bakterienbesiedlung mariner Sandsedimente*", Botanica Marina, Vol. 22, P. 99-106, 1979.

White, K.D., and L.T. West, "*In-ground Dispersal of Wastewater Effluent: The Science of Getting Water into the Ground*", Small Flows Quarterly Journal, Vol. 4, No. 2, P. 28-35, 2003.

Williams, A.G., Ph.D. thesis, University of Wales, Scotland, 1974.

Williams, A.G. and J.W.T. Wimpenny, "*Exo-polysaccharide Production by Pseudomonas NCIBl1264 Grown in Batch Culture*", Journal of General Microbiology, Vol. 102, P. 13-21, 1977.

Williamson, K. and P.L. McCarty, "*A Model of Substrate Utilization by Bacterial Films*", Journal Water Pollution Control Federation, Vol. 48, No. 1, P. 9-24, 1976a.

Williamson, K. and P.L. McCarty, "*Verification Studies of the Biofilm Model for Bacterial Substrate Utilization*", Journal of the Water Pollution Control Federation, Vol. 48, P. 281-296, 1976b.

Zhang, T.C. and P.L. Bishop, "*Density, Porosity, and Pore Structure of Biofilms*", Water Research, Vol. 28, No. 11, P. 2267-2277, 1994.

Reproduced with permission of the copyright owner. Further reproduction prohibited without permission.

Zheng, C. and G.D. Bennett, "*Applied Contaminant Transport Modeling, Theory and Practice*", Van Nostrand Reinhold, ITP™ A Division of International Thomson Publishing Inc., 1995.

Reproduced with permission of the copyright owner. Further reproduction prohibited without permission.

Appendix A- Stage One Data

Appendix A provides raw data collected in stage one. It also provides analyses conducted on the raw data which helped deliberating the results discussed in the body of the thesis.

A.1 Data Collected from the Separate Experiments

A.1.1 Particle Size Analysis Data

Table A.1- Particle size analysis for the filter media bed sand soil conducted in the lab

Mass of the sample = 1271.9 g				Empty tray weight = 108.36 g	
Sieve, mm	Weight of empty sieve, g	Sample+ tray of 108.36, g	Mass retained, g	Cumulative mass passed, g	Total percent passed, %
11.20	583.44	583.44	0.00	1271.90	100.00
8.00	563.20	563.20	0.00	1271.90	100.00
6.35	564.99	564.99	0.00	1271.90	100.00
4.76	608.32	608.72	0.40	1271.50	99.97
2.38	482.07	940.48	458.41	813.09	63.93
2.00	487.34	651.27	163.93	649.16	51.04
1.19	427.71	741.27	313.56	335.60	26.39
0.212	317.96	639.13	321.17	14.43	1.13
0.15	311.34	318.83	7.49	6.94	0.55
0.125	306.41	307.22	0.81	6.13	0.48
0.075	305.00	307.60	2.60	3.53	0.28
Pan	291.82	292.71	0.89	2.64	0.21
		Sum	1269.26		

Mass lost = 2.64 g
% Lost = 0.21 %

Table A.2- Particle size analysis for the filter media bed sand soil provided by the manufacture

Sieve, mm	Total percent passed, %
9.50	100.00
4.75	99.60
2.36	51.20
1.15	21.10
0.60	9.40
0.30	3.60
0.15	1.70
0.075	1.00

Reproduced with permission of the copyright owner. Further reproduction prohibited without permission.

Table A.3- Particle size analysis for the concrete sand soil conducted in the lab

Mass of the sample = 710.51 g				Empty tray weight 107.99 g	
Sieve, mm	Weight of empty sieve, g	sample+ tray of 107.99 g	Mass retained, g	Cumulative mass Passed, g	Total percent passed, %
11.2	583.44	583.44	0.00	710.51	100.00
8.00	563.30	563.30	0.00	710.51	100.00
6.35	565.42	567.46	2.04	708.47	99.71
4.76	608.55	615.80	7.25	701.22	98.69
2.38	484.08	563.90	79.82	621.40	87.46
2.00	488.74	516.26	27.52	593.88	83.59
1.19	428.38	513.43	85.05	508.83	71.61
0.212	318.33	755.12	436.79	72.04	10.14
0.15	311.28	352.69	41.41	30.63	4.31
0.125	306.31	315.14	8.83	21.80	3.07
0.075	304.87	316.90	12.03	9.77	1.38
Pan	291.75	300.19	8.44	1.33	0.19
		Sum	709.18		

Mass lost = 1.33 g
% Lost = 0.19 %

Table A.4- Particle size analysis for the concrete sand soil provided by the manufacture

Sieve, mm	Total percent passed, %
9.50	100.00
4.75	96.70
2.36	84.20
1.18	70.40
0.60	50.20
0.30	21.60
0.15	4.10
0.075	1.70

Reproduced with permission of the copyright owner. Further reproduction prohibited without permission.

Table A.5- Particle size analysis for the septic bed sand soil conducted in the lab

Mass of the sample = 628.43 g				Empty tray weight 127.60 g	
Sieve, mm	Weight of empty sieve, g	sample+ tray of 127.60 g	Mass retained, g	Cumulative mass Passed, g	Total percent passed, %
11.20	583.44	583.44	0.00	628.43	100.00
8.00	563.32	563.32	0.00	628.43	100.00
6.35	565.28	565.28	0.00	628.43	100.00
4.76	608.47	608.68	0.21	628.22	99.97
2.38	482.88	488.76	5.88	622.34	99.03
2.00	487.83	490.30	2.47	619.87	98.64
1.19	427.96	432.48	4.52	615.35	97.92
0.212	318.36	537.26	218.90	396.45	63.09
0.15	311.47	469.21	157.74	238.71	37.99
0.125	306.41	356.19	49.78	188.93	30.06
0.075	304.89	398.69	93.80	95.13	15.14
Pan	291.74	386.87	95.13	0.00	0.00
		Sum	628.43		
Mass lost = 0.0g					
% Lost = 0.00 %					

Table A.6- Particle size analysis for the septic bed sand soil provided by the manufacture

Sieve, mm	Total percent passed, %
4.75	100.00
2.36	100.00
1.15	99.70
0.60	98.70
0.30	92.70
0.15	38.70
0.075	13.80

Reproduced with permission of the copyright owner. Further reproduction prohibited without permission.

Table A.7- Particle size analysis for the peat soil conducted in the lab

Sample 1, Mass of the sample = 121.57 g				Empty tray weight = 107.94 g	
Sieve, mm	Weight of empty sieve, g	sample+ tray of 229.51, g	Mass retained, g	Cumulative mass Passed, g	Total percent passed, %
38.1	531.85	0.00	0.00	121.57	100.00
25.4	538.70	0.00	0.00	121.57	100.00
22.6	581.04	0.00	0.00	121.57	100.00
19.00	499.96	0.00	0.00	121.57	100.00
13.5	546.40	556.06	9.66	111.91	92.05
12.7	558.77	562.13	3.36	108.55	89.29
11.2	586.53	594.40	7.87	100.68	82.82
8.00	564.31	592.42	28.11	72.57	59.69
6.35	565.97	582.86	16.89	55.68	45.80
4.76	522.40	536.05	13.65	42.03	34.57
2.38	483.55	496.15	12.60	29.43	24.21
2.00	488.15	490.02	1.87	27.56	22.67
0.212	318.18	331.90	13.72	3.27	2.69
0.15	311.88	312.53	0.65	2.62	2.16
0.125	308.85	309.09	0.24	2.38	1.96
0.075	305.05	305.78	0.73	1.65	1.36
Pan	291.81	293.10	1.29	0.36	0.30

Sample 2, Mass of the sample = 128.52 g				Empty tray weight = 107.94 g	
Sieve, mm	Weight of empty sieve, g	sample+ tray of 236.46, g	Mass retained, g	Cumulative mass Passed, g	Total percent passed, %
38.10	531.85	0.00	0.00	128.52	100.00
25.40	538.70	0.00	0.00	128.52	100.00
22.60	581.04	0.00	0.00	128.52	100.00
19.00	499.96	0.00	0.00	128.52	100.00
13.50	546.40	547.10	0.70	127.82	99.46
12.70	558.77	559.49	0.72	127.10	98.90
11.20	586.53	588.07	1.54	125.56	97.70
8.00	564.31	583.97	19.66	105.90	82.40
6.35	565.97	580.31	14.34	91.56	71.24
4.76	522.40	536.01	13.61	77.95	60.65
2.38	483.55	499.98	16.43	50.91	39.61
2.00	488.15	491.17	3.02	47.89	37.26
0.212	318.18	352.73	34.55	13.34	10.38
0.15	311.88	315.08	3.20	10.14	7.89
0.125	308.85	310.15	1.30	8.84	6.88
0.075	305.05	308.15	3.10	5.74	4.47
Pan	291.81	294.41	2.60	3.14	2.44

Reproduced with permission of the copyright owner. Further reproduction prohibited without permission.

Reproduced with permission of the copyright owner. Further reproduction prohibited without permission.

A.1.2 Fiber Content for Peat Soil

Table A.8- Fiber content measured in the lab for the peat soil

Sample number	Mass of peat sample, g	Mass of $NaPo_3$, g	Mass of empty tray, g	Mass of tray + sample before oven dry, g	Mass of tray + sample after oven dry at 105 °C, g	Mass of dried fibers, g	Fiber Content, %	Average, %	Std. Dev.
1	100.00	25.07	40.10	564.90	106.80	66.70	66.70		
2	100.00	25.04	40.00	537.40	104.20	64.20	64.20		
3	100.00	25.04	39.40	542.30	100.10	60.70	60.70	64.00	2.14
4	100.00	25.04	39.20	568.80	101.90	62.70	62.70		
5	100.00	25.01	40.20	637.70	105.90	65.70	65.70		

A.1.3 pH for Peat Soil

Table A.9- pH measured in the lab for the peat soil

Sample number	Mass of empty tray, g	Mass of tray + peat, g	Mass of peat sample, g	pH with DI water	Measuring cup, g	Measuring cup + peat sample + $CaCl_2$, g	pH with $CaCl_2$	Difference between pH with DI water and with $CaCl_2$
1	24.50	42.70	18.20	3.65	0.547	1.659	2.33	1.32
2	23.50	39.60	16.10	3.28	0.5255	1.6388	2.37	0.91
3	23.50	41.70	18.20	3.60	0.5264	1.6363	2.40	1.20
4	23.40	42.70	19.30	3.50	0.5329	1.6434	2.37	1.13
5	23.40	42.20	18.80	3.31	0.5223	1.6339	2.37	0.94
6	23.40	41.00	17.60	3.55	0.5372	1.646	2.36	1.19
			Average	3.48		Average	2.37	1.12
			Std. Dev.	0.140		Std. Dev.	0.021	0.146

A.1.4 Saturated Hydraulic Conductivity Values for the Sand Soils

Data listed in this subsection was measured using the permeability test. It should be noted that the measured saturated hydraulic conductivity values were adjusted while calibrating the numerical code in stage three. Comparison between the measured outflow profiles and numerical simulations were used to obtain the saturated hydraulic conductivity values that best represents the experimental data collected in stage one.

Table A.10- Saturated hydraulic conductivity for filter media bed sand soil

Diameter, cm	7.5		Surface area, cm^2	44.18		
Test 1						
Height of soil, cm	21.9		Total head, cm	124.9	Gradient	5.70
Collected vol., mL	Time, sec	K_{sat}, cm/s	Time, sec	K_{sat}, cm/s		
500	9	0.2205	9	0.2205	Average	Std. Dev.
1000	17	0.2335	17	0.2335	0.227	0.0056
1500	26	0.2290	26	0.2290		
2000	35	0.2268	36	0.2205		
Test 2						
Height of soil, cm	21.9		Total head, cm	103.2	Gradient	4.71
Collected vol., mL	Time, sec	K_{sat}, cm/s	Time, sec	K_{sat}, cm/s		
500	11	0.2184	11	0.2184	Average	Std. Dev.
1000	22	0.2184	23	0.2089	0.215	0.0045
1500	33	0.2184	34	0.2119		
2000	44	0.2184	46	0.2089		
Test 3						
Height of soil, cm	21.9		Total head, cm	83.0	Gradient	3.79
Collected vol., mL	Time, sec	K_{sat}, cm/s	Time, sec	K_{sat}, cm/s		
500	15	0.1991	15	0.1991	Average	Std. Dev.
1000	30	0.1991	31	0.1927	0.195	0.0048
1500	45	0.1991	47	0.1906		
2000	61	0.1958	64	0.1866		
					Average	Std. Dev.
					0.212	0.0141

Reproduced with permission of the copyright owner. Further reproduction prohibited without permission.

Reproduced with permission of the copyright owner. Further reproduction prohibited without permission.

Table A.11- Saturated hydraulic conductivity for concrete sand soil

Diameter, cm	7.5		Surface area, cm^2	44.18				
Test 1								
Height of soil, cm	22.1		Total head, cm	124.9			Gradient	5.65
Collected vol., mL	Time, sec	K_{sat}, cm/s	Collected vol., mL	Time, sec	K_{sat}, cm/s			
10	19	0.00211	5	9	0.00223			
15	29	0.00207	10	19	0.00211			
16	32	0.00200	15	29	0.00207			
23	46	0.00200	20	39	0.00205			
30	60	0.00200	25	49	0.00204			
35	69	0.00203	30	59	0.00204			
41	81	0.00203	35	69	0.00203			
45	89	0.00203	40	79	0.00203			
50	99	0.00202	45	89	0.00203			
			50	99	0.00202			
Test 2								
Height of soil, cm	22.1		Total head, cm	103.2			Gradient	4.67
Collected vol., mL	Time, sec	K_{sat}, cm/s	Collected vol., mL	Time, sec	K_{sat}, cm/s	Collected vol., mL	Time, sec	K_{sat}, cm/s
10	22	0.00220	5	12	0.00202	5	12	0.00202
15	34	0.00214	10	23	0.00211	10	23	0.00211
20	45	0.00215	15	35	0.00208	15	35	0.00208
25	58	0.00209	20	46	0.00211	20	46	0.00211
30	72	0.00202	25	58	0.00209	25	59	0.00205
35	83	0.00204	30	70	0.00208	30	71	0.00205
40	94	0.00206	35	82	0.00207	35	84	0.00202
45	105	0.00208	40	94	0.00206	40	96	0.00202
50	117	0.00207	45	106	0.00206	45	109	0.00200
			50	118	0.00205	50	121	0.00200

Average	Std. Dev.
0.00205	0.00005

Average	Std. Dev.
0.00206	0.00005

Average	Std. Dev.
0.00207	0.00005

Reproduced with permission of the copyright owner. Further reproduction prohibited without permission.

Table A.12- Saturated hydraulic conductivity for septic bed sand soil

Diameter, cm	7.5		Surface area, cm^2		44.18					
Test 1										
Height of soil, cm	22.2		Total head, cm		124.9		Gradient	5.63		
Collected vol., mL	Time, sec	K_{sat}, cm/s	Time, sec	K_{sat}, cm/s	Time, sec	K_{sat}, cm/s	Time, sec	K_{sat}, cm/s		
5	16	0.00126	16	0.00126	16	0.00126	15	0.00134		
10	32	0.00126	31	0.00130	31	0.00130	31	0.00130		
15	48	0.00126	47	0.00128	48	0.00126	48	0.00126		
20	65	0.00124	64	0.00126	64	0.00126	65	0.00124		
25	81	0.00124	80	0.00126	80	0.00126	81	0.00124	Average	Std. Dev.
30	97	0.00124	96	0.00126	97	0.00124	97	0.00124	0.00125	0.00002
35	113	0.00125	112	0.00126	113	0.00125	113	0.00125		
40	129	0.00125	129	0.00125	130	0.00124	130	0.00124		
45	146	0.00124	145	0.00125	146	0.00124	146	0.00124		
50	162	0.00124	162	0.00124	164	0.00123	164	0.00123	Average	Std. Dev.
Test 2									0.00124	0.00002
Height of soil, cm	22.2		Total head, cm		103.0		Gradient	4.64		
Collected vol., mL	Time, sec	K_{sat}, cm/s	Time, sec	K_{sat}, cm/s	Time, sec	K_{sat}, cm/s	Time, sec	K_{sat}, cm/s		
5	20	0.00122	20	0.00122	19	0.00128	20	0.00122		
10	39	0.00125	38	0.00128	39	0.00125	39	0.00125		
15	59	0.00124	58	0.00126	59	0.00124	59	0.00124		
20	80	0.00122	79	0.00124	80	0.00122	80	0.00122		
25	100	0.00122	99	0.00123	99	0.00123	100	0.00122	Average	Std. Dev.
30	120	0.00122	119	0.00123	120	0.00122	120	0.00122	0.00123	0.00002
35	140	0.00122	139	0.00123	140	0.00122	140	0.00122		
40	160	0.00122	159	0.00123	160	0.00122	160	0.00122		
45	181	0.00121	180	0.00122	180	0.00122	181	0.00121		
50	202	0.00121	201	0.00121	202	0.00121	202	0.00121		

A.1.5 Measured Porosity Value for the Sand Soils

Separate experiment was conducted to measure the porosity of the sand soils. The measured porosity values were approximately similar to the moisture content values measured for the sand columns at 100% saturation (i.e. before gravity drainage) using TDR. The data measured in the lab is presented in Table (A.13).

Table A.13- Porosity test for sand soils

Soil	W empty crucible (1), g	W after adding water to the mark level(2), g	W of soil and water added till the mark level (3), g	W after oven dry (4), g	V_1 = (3)-(4), g	V_2 = (2)-(1), g	Porosity	Avg. porosity	Std. Dev.
Filter media bed sand soil	62.6	137.9	197.9	165.3	32.6	75.3	0.433	0.450	0.022
	55.1	135.2	199.0	165.0	34.0	80.1	0.424		
	62.5	131.2	198.6	168.5	30.1	68.7	0.438		
	55.1	117.8	199.2	169.0	30.2	62.7	0.482		
	62.6	134.5	215.8	182.3	33.5	71.9	0.466		
	55.1	119.2	195.1	165.8	29.3	64.1	0.457		
Concrete sand soil	67.5	138.5	223.5	195.4	28.1	71.0	0.396	0.388	0.006
	67.0	131.5	212.1	187.3	24.8	64.5	0.385		
	56.6	118.9	200.7	176.6	24.1	62.3	0.387		
	57.4	119.3	204.8	180.5	24.3	61.9	0.393		
	57.4	119.2	204.3	180.8	23.5	61.8	0.380		
	54.0	118.3	207.6	183.1	24.5	64.3	0.381		
	56.6	115.8	199.0	176.2	22.8	59.2	0.385		
	54.0	116.7	209.3	184.7	24.6	62.7	0.392		
	66.6	125.3	215.3	192.3	23.0	58.7	0.392		
Septic bed sand soil	56.6	122.7	197.6	172.7	24.9	66.1	0.377	0.362	0.016
	66.0	134.8	209.8	184.8	25.0	68.8	0.363		
	66.8	128.9	223.7	200.1	23.6	62.1	0.380		
	67.3	134.3	212.6	189.4	23.2	67.0	0.346		
	59.1	135.2	211.9	186.9	25.0	76.1	0.329		
	59.1	123.8	206.8	182.8	24.0	64.7	0.371		
	66.8	131.0	216.1	193.2	22.9	64.2	0.357		
	67.3	127.1	206.1	183.9	22.2	59.8	0.371		
	59.2	119.2	198.2	176.6	21.6	60.0	0.360		

Reproduced with permission of the copyright owner. Further reproduction prohibited without permission.

A.1.6 Soil Moisture Curves for the Soils used in Stage One

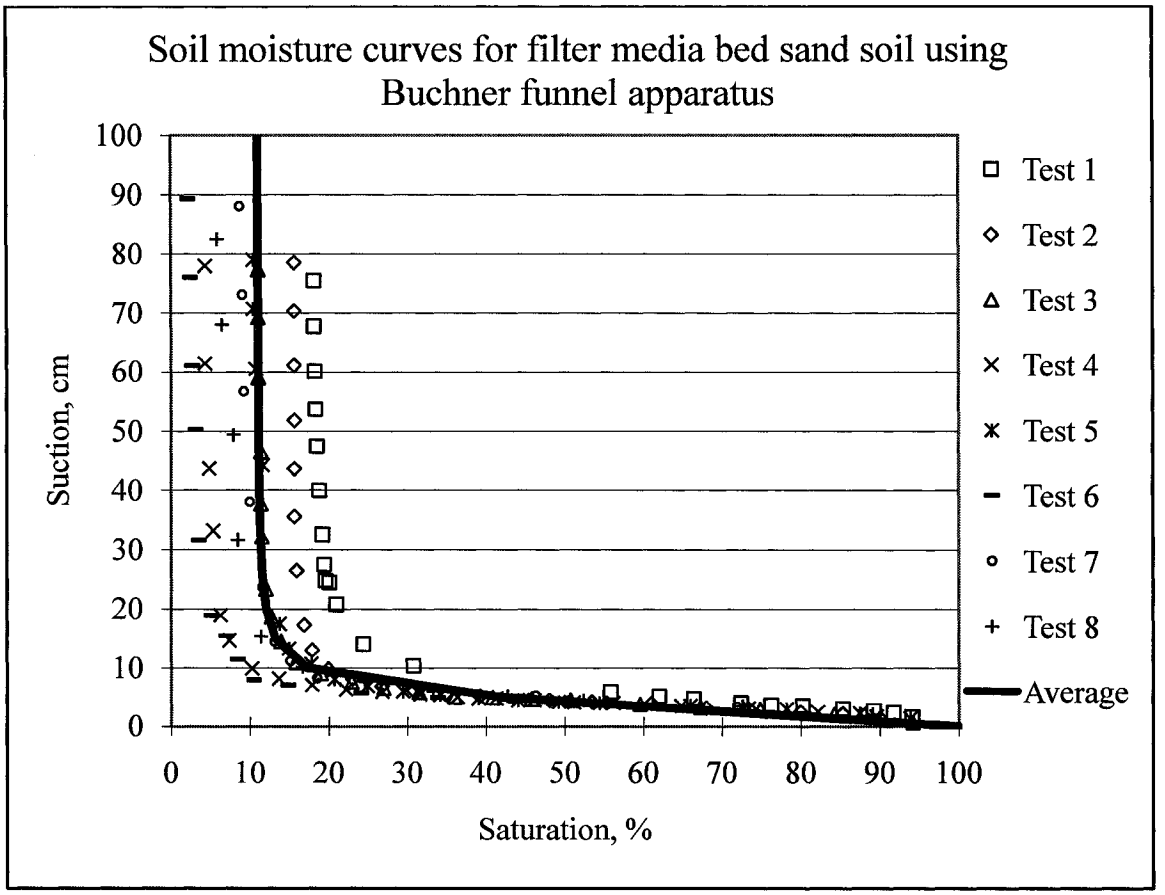

Figure A.1- Soil moisture curves for filter media bed sand soil using Buchner funnel apparatus

Reproduced with permission of the copyright owner. Further reproduction prohibited without permission.

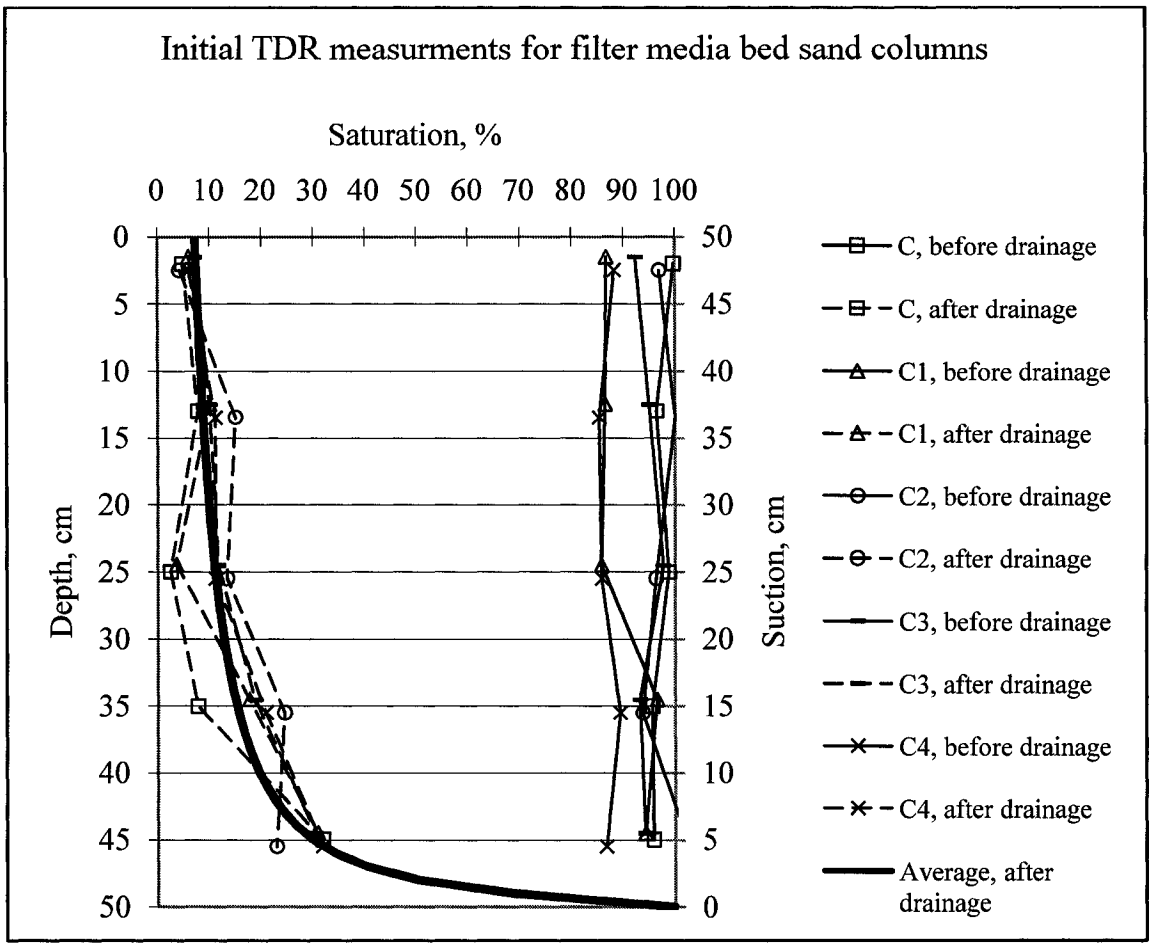

Figure A.2- TDR measurements recorded after filter media bed sand columns were initially saturated and then gravity drained for one day

Reproduced with permission of the copyright owner. Further reproduction prohibited without permission.

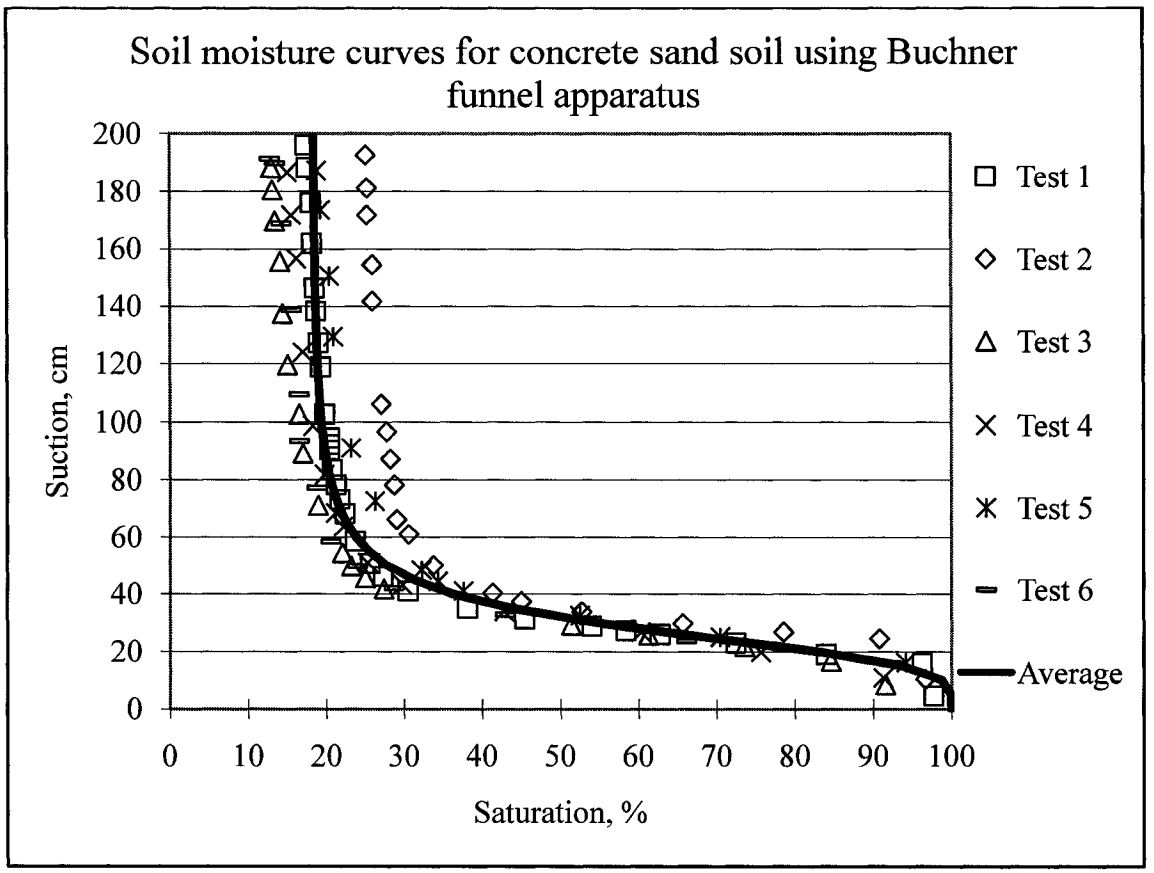

Figure A.3- Soil moisture curves for concrete sand soil using Buchner funnel apparatus

Reproduced with permission of the copyright owner. Further reproduction prohibited without permission.

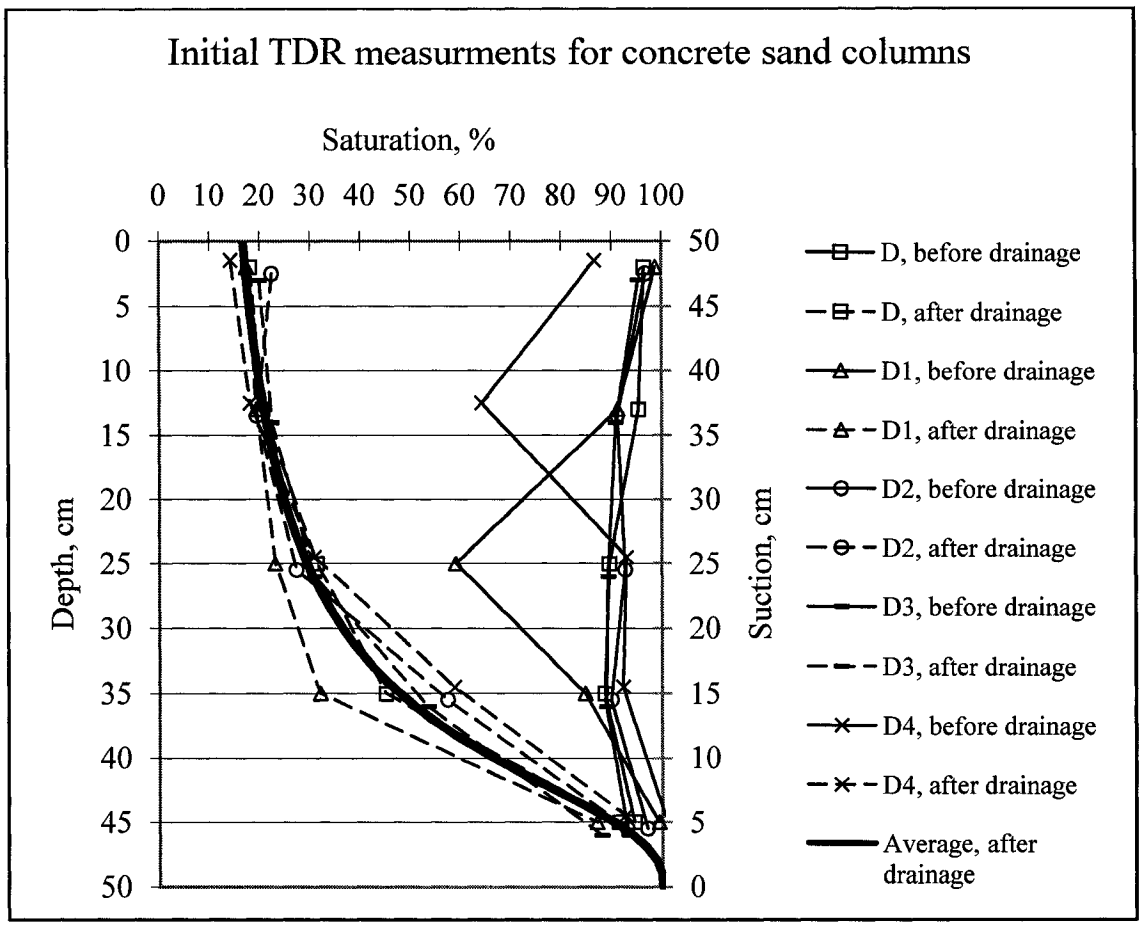

Figure A.4- TDR measurements recorded after concrete sand columns were initially saturated and then gravity drained for one day

Reproduced with permission of the copyright owner. Further reproduction prohibited without permission.

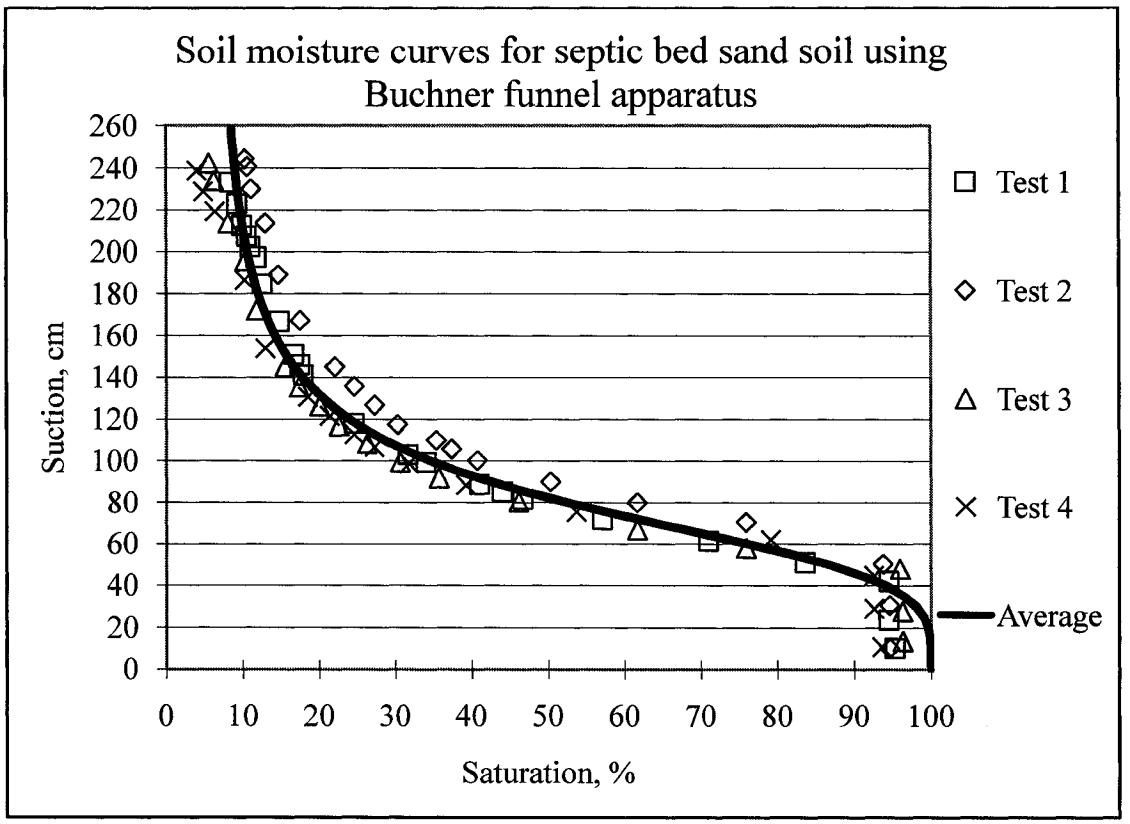

Figure A.5- Soil moisture curves for septic bed sand soil using Buchner funnel apparatus

Reproduced with permission of the copyright owner. Further reproduction prohibited without permission.

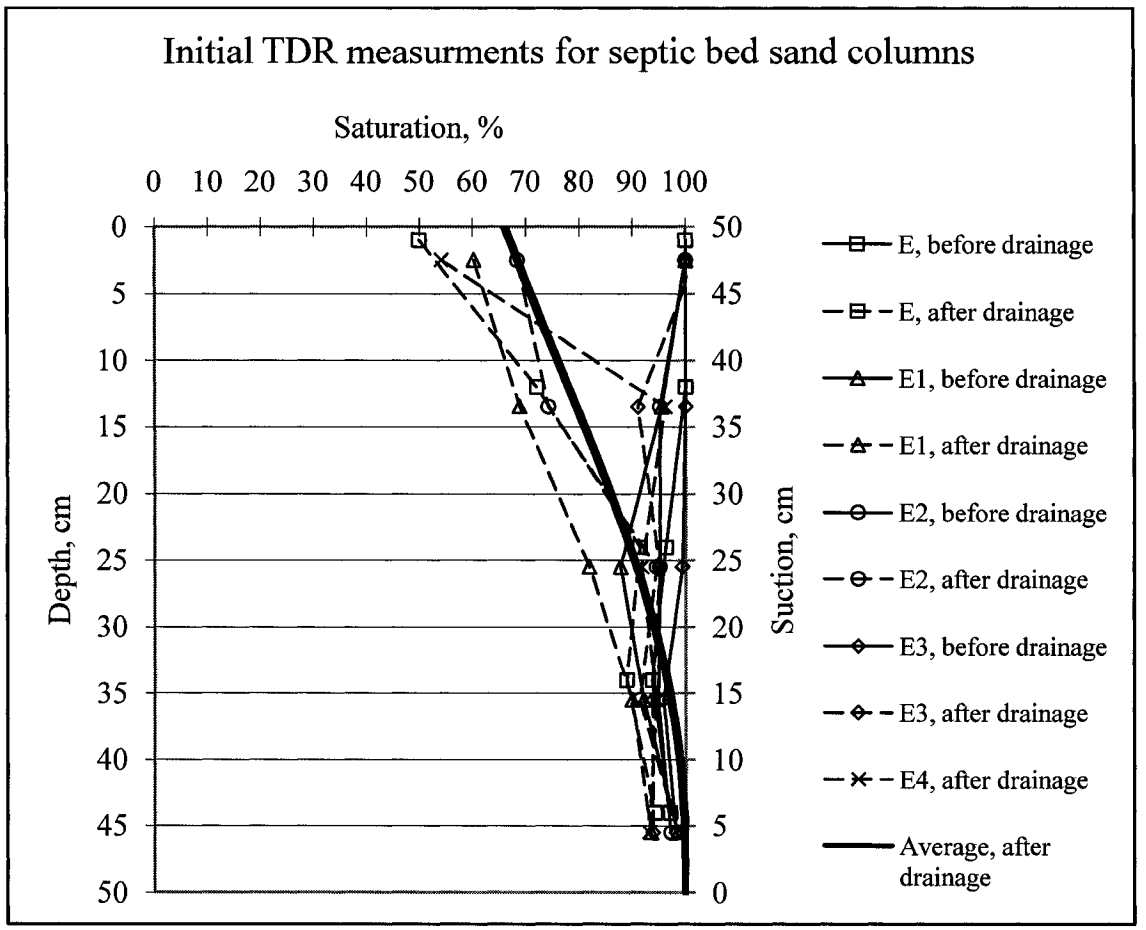

Figure A.6- TDR measurements recorded after septic bed sand columns were initially saturated and then gravity drained for one day

Reproduced with permission of the copyright owner. Further reproduction prohibited without permission.

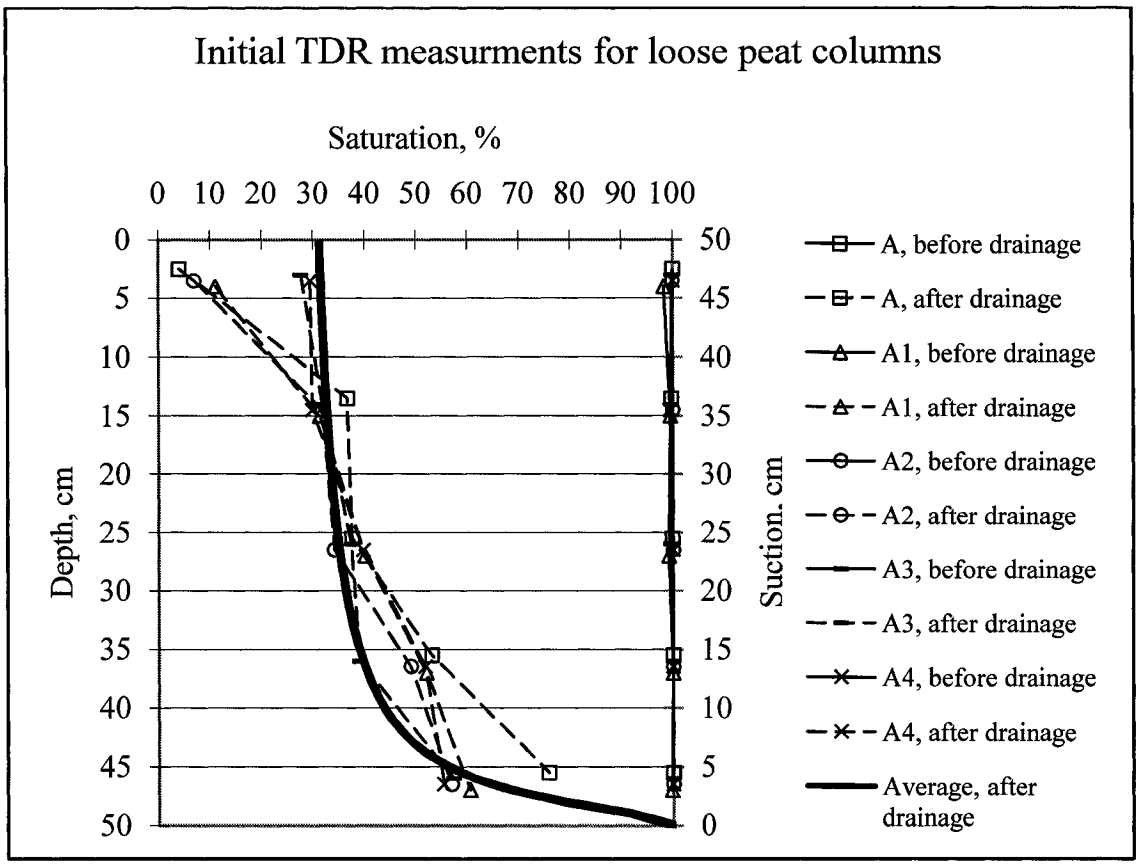

Figure A.7- TDR measurements recorded after loose peat columns were initially saturated and then gravity drained for one day

Reproduced with permission of the copyright owner. Further reproduction prohibited without permission.

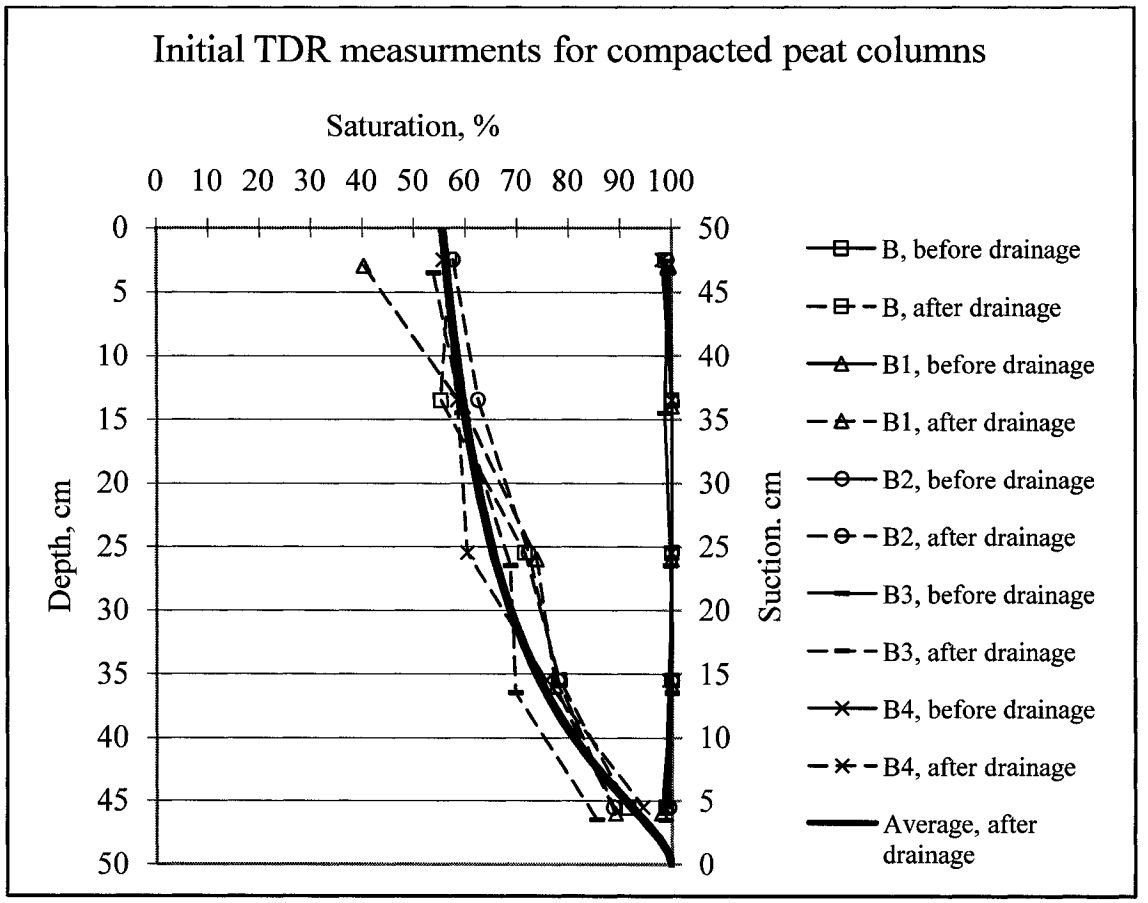

Figure A.8- TDR measurements recorded after compacted peat columns were initially saturated and then gravity drained for one day

Reproduced with permission of the copyright owner. Further reproduction prohibited without permission.

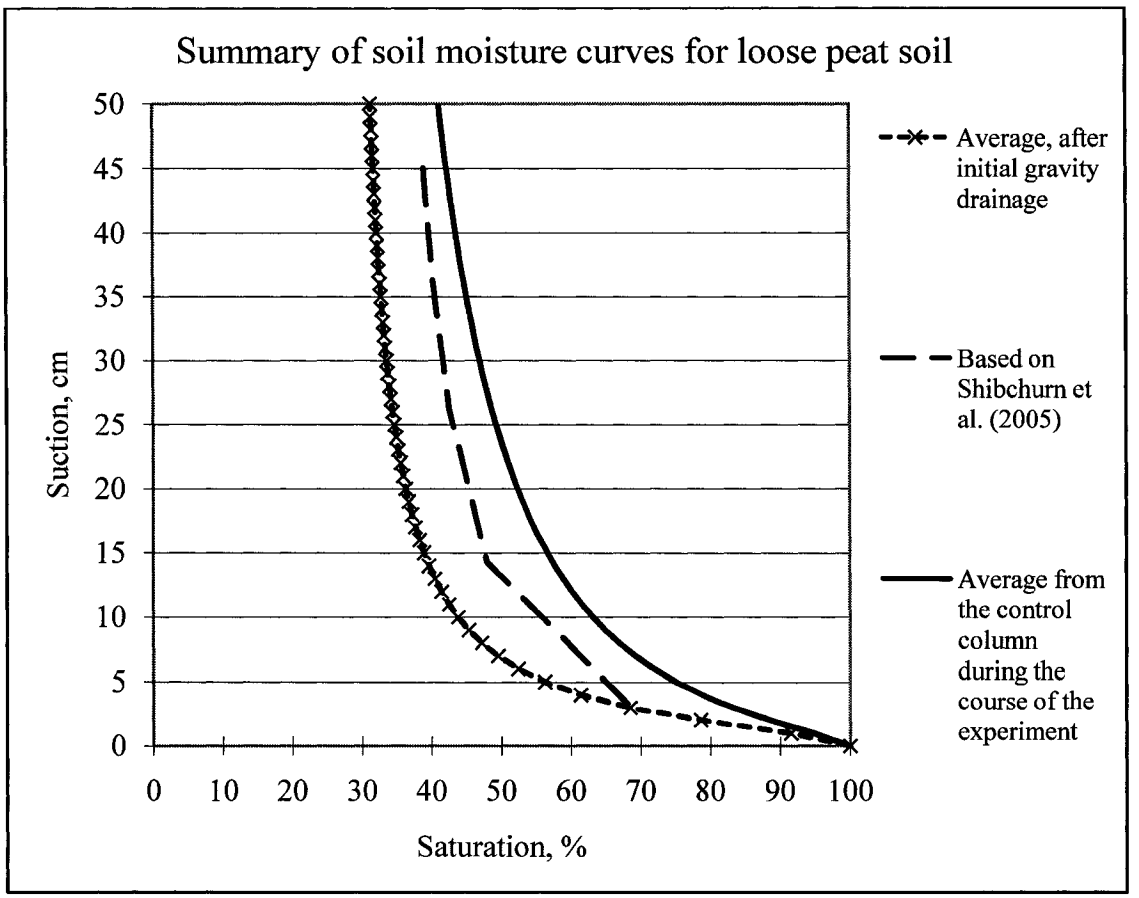

Figure A.9- Comparison between the three methods used to estimate the soil moisture curve for loose peat soil

Reproduced with permission of the copyright owner. Further reproduction prohibited without permission.

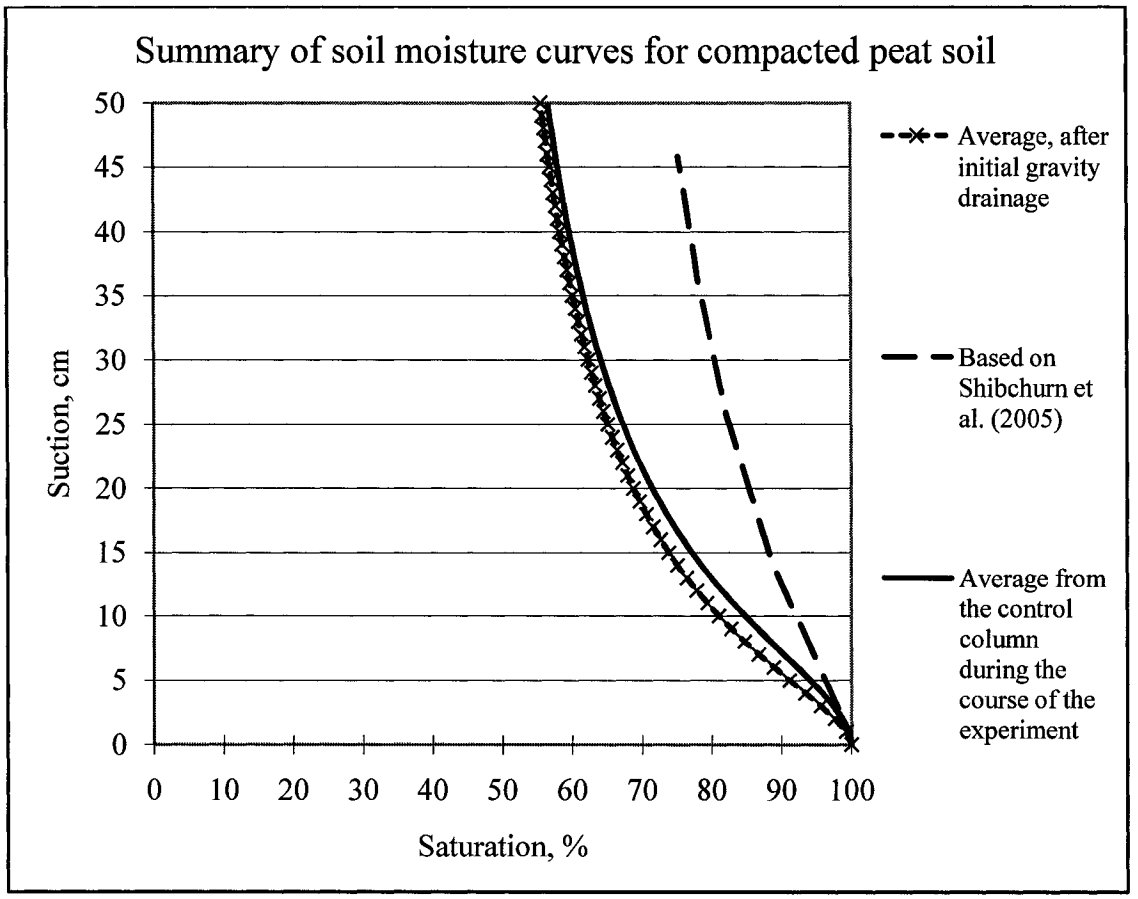

Figure A.10- Comparison between three methods used to estimate the soil moisture curve for compacted peat soil

Reproduced with permission of the copyright owner. Further reproduction prohibited without permission.

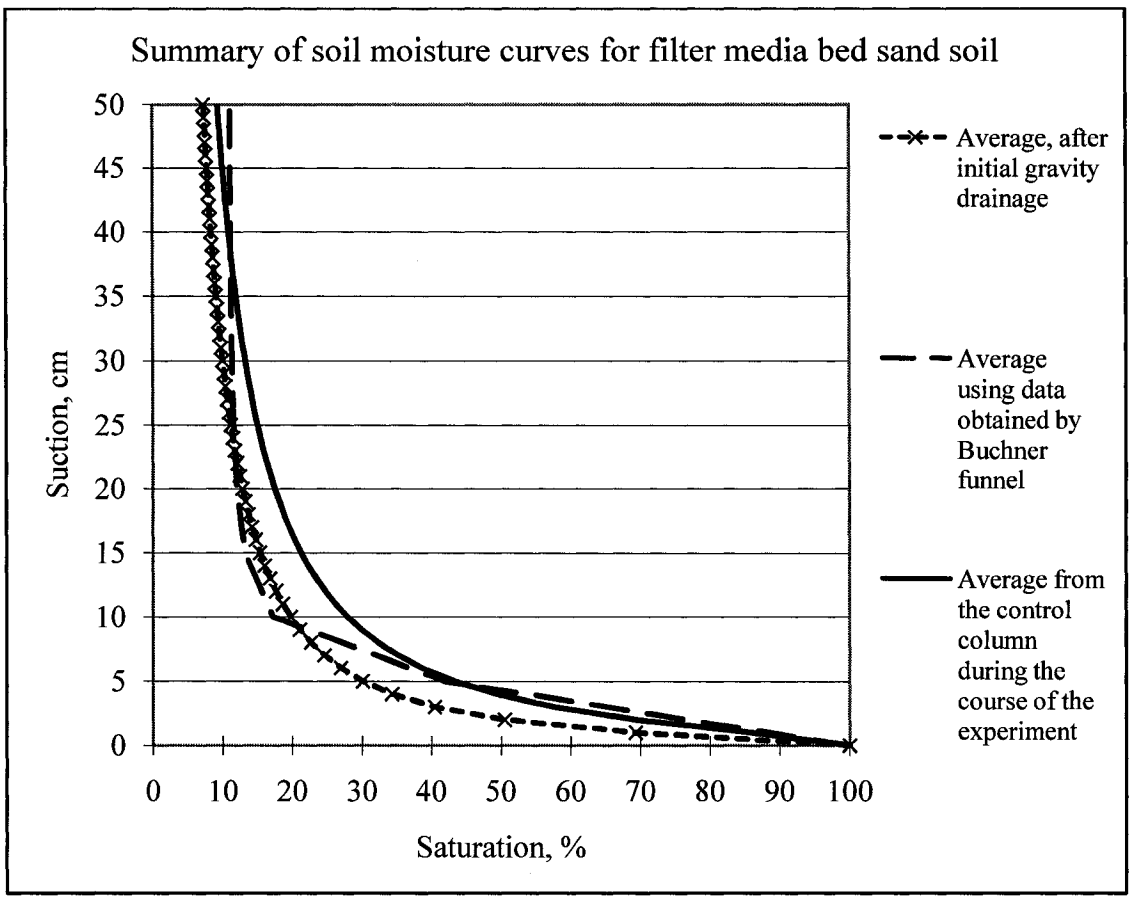

Figure A.11- Comparison between the three methods used to estimate the soil moisture curve for filter media bed sand soil

Reproduced with permission of the copyright owner. Further reproduction prohibited without permission.

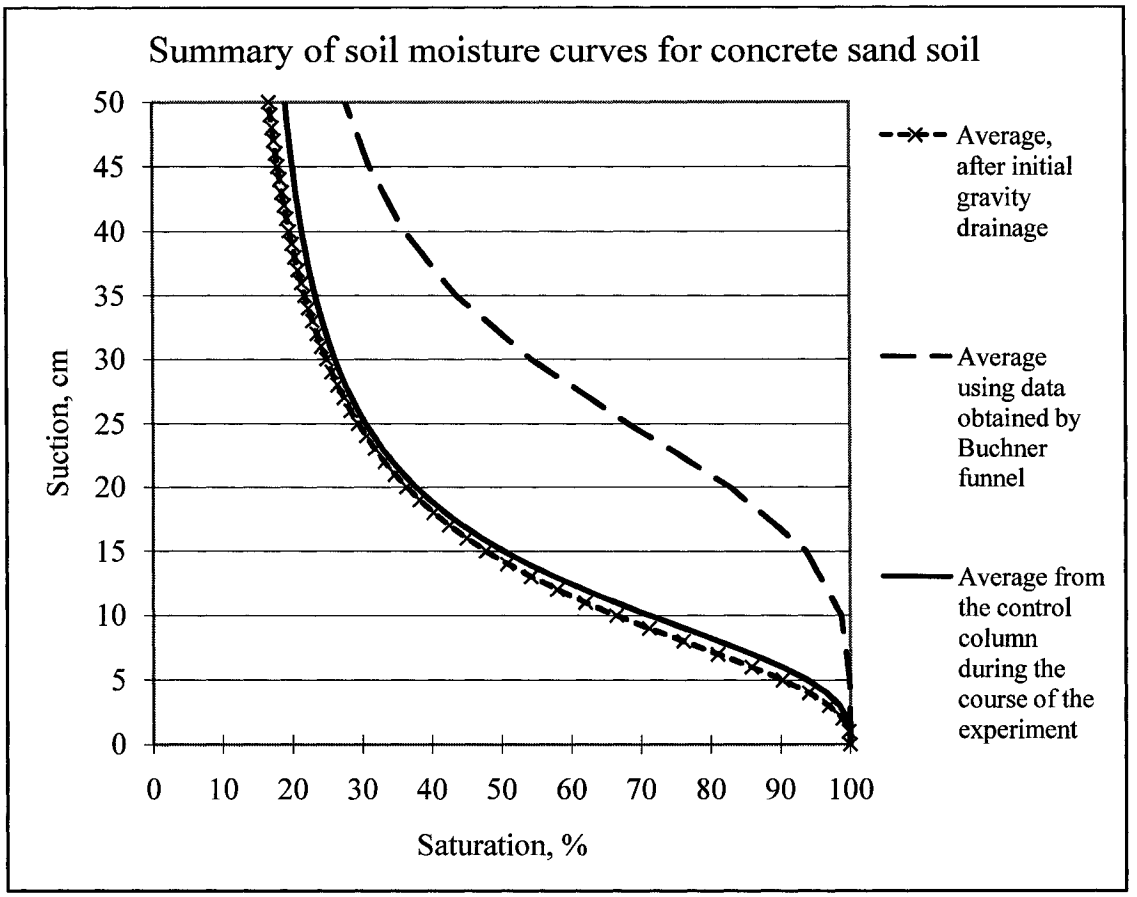

Figure A.12- Comparison between the three methods used to estimate the soil moisture curve for concrete sand soil

Reproduced with permission of the copyright owner. Further reproduction prohibited without permission.

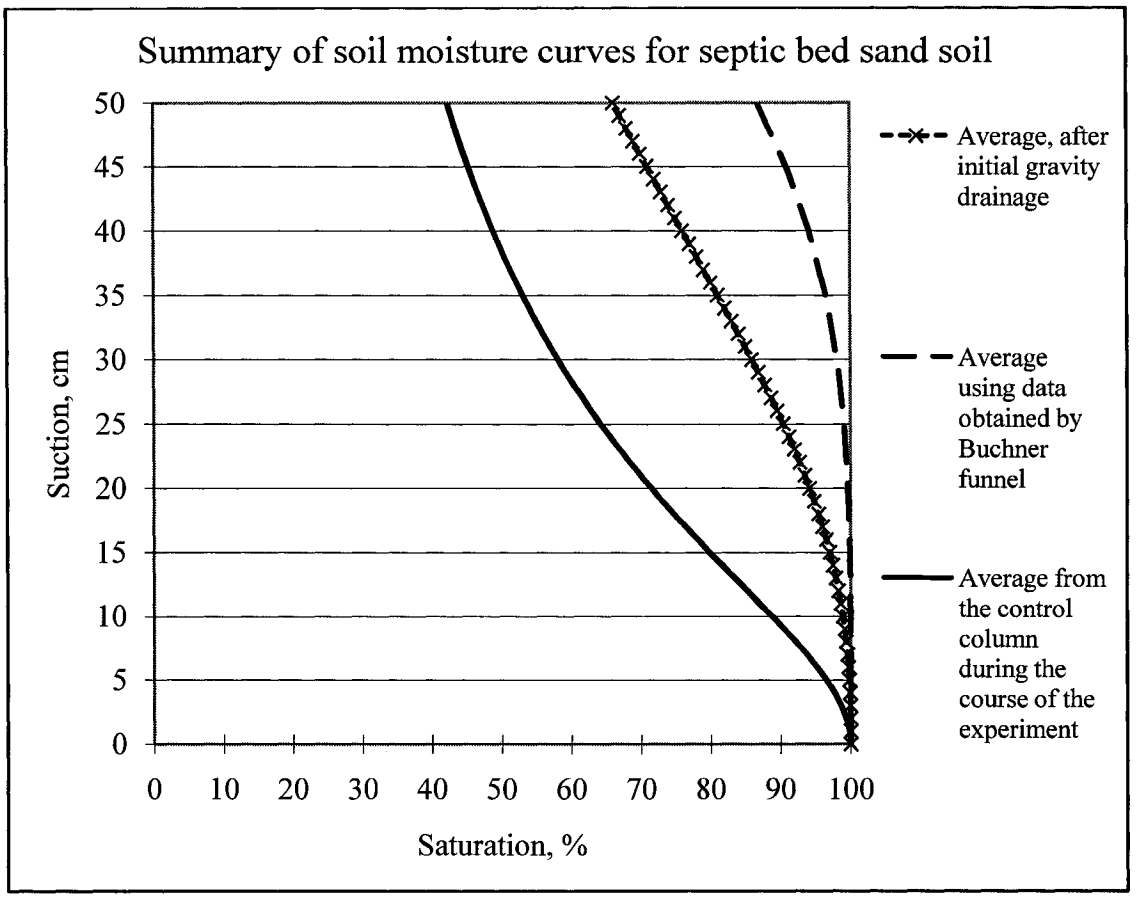

Figure A.13- Comparison between the three methods used to estimate the soil moisture curve for septic bed sand soil

Table A.14- Comparison between soil parameters obtained using the three methods discussed in chapter three

Soil type	After gravity drainage for one day			From Buchner funnel apparatus			From averaging the saturation profiles for control column during the course of the experiment		
	n	α, cm^{-1}	S_{wr}	n	α, cm^{-1}	S_{wr}	n	α, cm^{-1}	S_{wr}
A	1.871	0.528	27.02	1.499	0.841	27.02	***1.405***	***0.366***	***15.09***
B	***1.659***	***0.127***	***37.36***	1.369	0.076	37.36	1.823	0.096	40.75
C	1.624	1.334	0.00	3.562	0.281	10.99	***1.691***	***0.617***	***0.00***
D	***2.485***	***0.106***	***9.20***	4.128	0.039	18.22	2.862	0.096	14.51
E	2.504	0.021	6.89	4.134	0.014	6.89	***1.906***	***0.054***	***6.89***

Reproduced with permission of the copyright owner. Further reproduction prohibited without permission.

Table (A.14) shows parameters in bold and italic. These parameters were the soil parameters used in stage three in the modeling process.

A.2 Calculation of Available Void Space for Each Soil at Steady State

Table A.15- Available void space for each soil at steady state

Loose peat soil, A			Compacted peat Soil, B		
Soil height, cm = 50			Soil height, cm = 50		
Diameter of the x-sectional area, cm = 15.24			Diameter of the x-sectional area, cm = 15.24		
Area of the x-section, cm^2 = 182.41			Area of the x-section, cm^2 = 182.41		
Porosity = 0.878			Porosity = 0.824		
Suction, cm	Sat. %	Vol. of water, cm^3	Suction, cm	Sat. %	Vol. of water, cm^3
0	100.0		0	100.00	
1	94.84	156.08	1	99.21	149.79
2	88.65	146.99	2	97.61	147.99
3	83.28	137.73	3	95.59	145.27
4	78.80	129.84	4	93.37	142.09
5	75.08	123.28	5	91.10	138.71
6	71.95	117.79	6	88.86	135.32
7	69.28	113.14	7	86.71	132.02
8	66.97	109.15	8	84.68	128.87
9	64.95	105.68	9	82.77	125.90
10	63.17	102.64	10	80.98	123.13
11	61.59	99.95	11	79.33	120.54
12	60.16	97.54	12	77.79	118.14
13	58.88	95.36	13	76.36	115.91
14	57.70	93.39	14	75.03	113.83
15	56.63	91.59	15	73.79	111.91
16	55.64	89.94	16	72.64	110.11
17	54.73	88.42	17	71.57	108.44
18	53.89	87.02	18	70.57	106.88
19	53.10	85.71	19	69.63	105.42
20	52.36	84.49	20	68.75	104.05
21	51.67	83.35	21	67.92	102.77
22	51.03	82.28	22	67.15	101.56
23	50.42	81.27	23	66.41	100.43
24	49.84	80.32	24	65.72	99.36
25	49.30	79.42	25	65.07	98.34
26	48.78	78.57	26	64.45	97.38
27	48.29	77.76	27	63.86	96.48
28	47.82	76.99	28	63.30	95.62
29	47.38	76.26	29	62.77	94.80
30	46.95	75.57	30	62.26	94.02
31	46.54	74.90	31	61.78	93.28
32	46.15	74.26	32	61.32	92.57
33	45.78	73.65	33	60.88	91.89
34	45.42	73.06	34	60.46	91.24

Reproduced with permission of the copyright owner. Further reproduction prohibited without permission.

35	45.09	72.50	35	60.06	90.63
36	44.75	71.96	36	59.67	90.03
37	44.43	71.44	37	59.30	89.46
38	44.12	70.94	38	58.95	88.92
39	43.82	70.45	39	58.61	88.39
40	43.54	69.99	40	58.28	87.89
41	43.26	69.53	41	57.96	87.40
42	42.99	69.10	42	57.66	86.94
43	42.73	68.68	43	57.36	86.48
44	42.48	68.27	44	57.08	86.05
45	42.24	67.87	45	56.80	85.63
46	42.00	67.49	46	56.54	85.22
47	41.77	67.11	47	56.28	84.83
48	41.55	66.75	48	56.03	84.45
49	41.33	66.40	49	55.79	84.08
50	41.12	66.06	50	55.56	83.73

Vol. of water under the initial soil moisture curve, cm^3 = 4347.91
Total vol. of voids, cm^3 = 8011.17
Available voids vol., cm^3 = 3663.26

Vol. of water under the initial soil moisture curve, cm^3 = 5224.21
Total vol. of voids, cm^3 = 7519.39
Available voids vol., cm^3 = 2295.18

Filter media bed sand soil, C
Soil column height, cm = 50
Diameter of the x-sectional area, cm = 15.24
Area of the x-section, cm^2 = 182.41
Porosity = 0.450

Suction, cm	Sat. %	Vol. of water, cm^3
0	100.00	
1	86.11	76.38
2	69.60	63.91
3	57.74	52.26
4	49.42	43.98
5	43.37	38.08
6	38.78	33.72
7	35.19	30.36
8	32.29	27.70
9	29.91	25.53
10	27.90	23.73
11	26.19	22.20
12	24.72	20.90
13	23.43	19.76
14	22.29	18.76
15	21.27	17.88
16	20.37	17.09
17	19.55	16.38
18	18.80	15.74
19	18.12	15.15
20	17.50	14.62
21	16.93	14.13

Concrete sand soil, D
Soil column height, cm =50
Diameter of the x-sectional area, cm = 15.24
Area of the x-section, cm^2 = 182.41
Porosity = 0.387

Suction, cm	Sat. %	Vol. of water, cm^3
0	100.00	
1	99.80	70.49
2	98.86	70.09
3	96.97	69.09
4	94.08	67.40
5	90.39	65.05
6	85.87	62.16
7	81.04	58.89
8	76.07	55.43
9	71.16	51.94
10	66.45	48.55
11	62.03	45.33
12	57.95	42.33
13	54.23	39.58
14	50.84	37.07
15	47.78	34.79
16	45.02	32.74
17	42.53	30.89
18	40.28	29.21
19	38.24	27.70
20	36.40	26.33
21	34.73	25.10

Reproduced with permission of the copyright owner. Further reproduction prohibited without permission.

22	16.40	13.68	22	33.22	23.97
23	15.91	13.26	23	31.84	22.95
24	15.45	12.87	24	30.58	22.02
25	15.03	12.51	25	29.42	21.17
26	14.63	12.17	26	28.36	20.39
27	14.25	11.85	27	27.39	19.67
28	13.90	11.56	28	26.50	19.01
29	13.57	11.28	29	25.67	18.40
30	13.26	11.01	30	24.90	17.84
31	12.96	10.76	31	24.19	17.32
32	12.69	10.53	32	23.54	16.84
33	12.42	10.30	33	22.92	16.39
34	12.17	10.09	34	22.35	15.97
35	11.93	9.89	35	21.82	15.58
36	11.70	9.70	36	21.32	15.22
37	11.48	9.51	37	20.85	14.88
38	11.27	9.34	38	20.41	14.56
39	11.07	9.17	39	20.00	14.26
40	10.88	9.01	40	19.61	13.98
41	10.70	8.86	41	19.25	13.71
42	10.52	8.71	42	18.90	13.46
43	10.35	8.57	43	18.58	13.22
44	10.19	8.43	44	18.27	13.00
45	10.03	8.30	45	17.98	12.79
46	9.88	8.17	46	17.70	12.59
47	9.74	8.05	47	17.44	12.40
48	9.60	7.93	48	17.19	12.22
49	9.46	7.82	49	16.95	12.05
50	9.33	7.71	50	16.73	11.88

Vol. of water under the initial soil moisture curve, cm^3 = 899.29
Total vol. of voids, cm^3 = 4104.33
Available voids vol., cm^3 = 3205.04

Vol. of water under the initial soil moisture curve, cm^3 = 1457.86
Total vol. of voids, cm^3 = 3528.00
Available voids vol., cm^3 = 2070.14

Septic bed sand soil, E
Soil column height, cm = 50
Diameter of the x-sectional area, cm = 15.24
Area of the x-section, cm^2 = 182.41
Porosity 0.366

Suction, cm	Sat. %	Vol. of water, cm^3
0	100.00	
1	99.83	66.63
2	99.37	66.42
3	98.65	66.03
4	97.71	65.48
5	96.56	64.78
6	95.24	63.96
7	93.78	63.03
8	92.21	62.02

Reproduced with permission of the copyright owner. Further reproduction prohibited without permission.

9	90.54	60.94
10	88.81	59.81
11	87.04	58.64
12	85.25	57.45
13	83.45	56.25
14	81.65	55.05
15	79.87	53.86
16	78.12	52.68
17	76.40	51.52
18	74.72	50.39
19	73.08	49.28
20	71.49	48.21
21	69.94	47.16
22	68.44	46.14
23	66.99	45.16
24	65.59	44.21
25	64.24	43.29
26	62.94	42.41
27	61.68	41.55
28	60.46	40.73
29	59.29	39.93
30	58.17	39.17
31	57.08	38.43
32	56.03	37.72
33	55.02	37.03
34	54.05	36.37
35	53.11	35.73
36	52.20	35.11
37	51.33	34.52
38	50.48	33.95
39	49.67	33.40
40	48.88	32.86
41	48.12	32.35
42	47.39	31.85
43	46.68	31.37
44	45.99	30.90
45	45.33	30.45
46	44.68	30.01
47	44.06	29.59
48	43.46	29.18
49	42.87	28.79
50	42.31	28.40

Vol. of water under the initial soil moisture curve, cm^3 = 2260.18
Total vol. of voids, cm^3 = 3334.48
Available voids vol., cm^3 = 1074.30

Reproduced with permission of the copyright owner. Further reproduction prohibited without permission.

A.3 Cumulative Influent Load for the Experimental Columns with Time

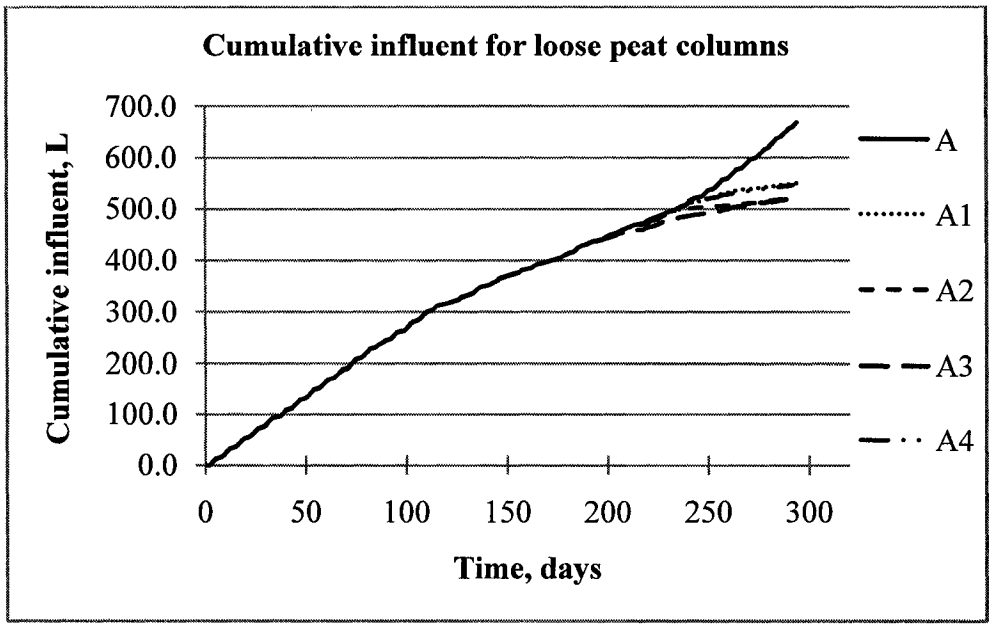

Figure A.14- Cumulative influent load for loose peat columns

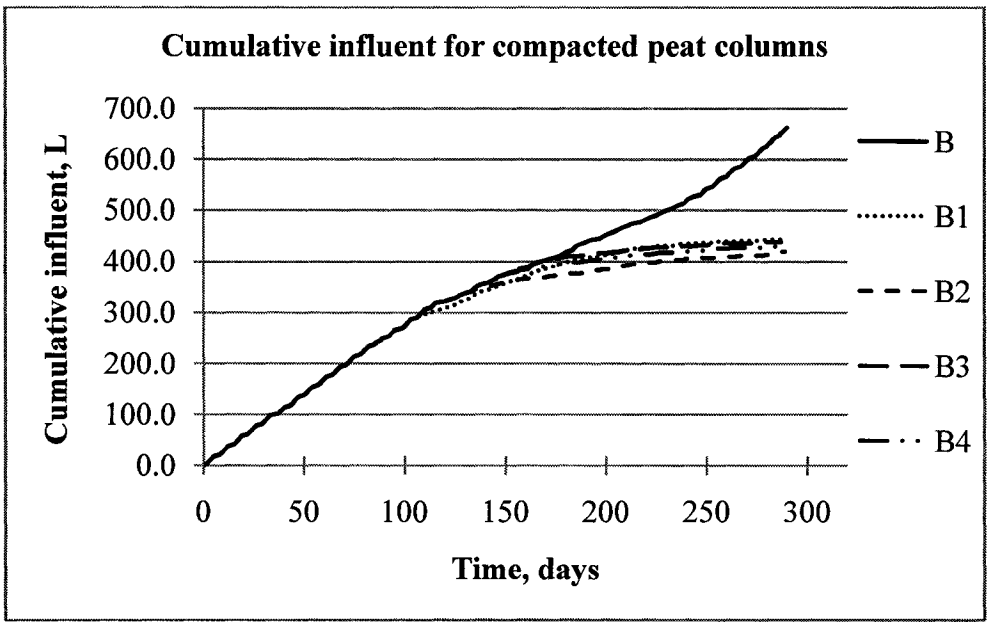

Figure A.15- Cumulative influent load for compacted peat columns

Reproduced with permission of the copyright owner. Further reproduction prohibited without permission.

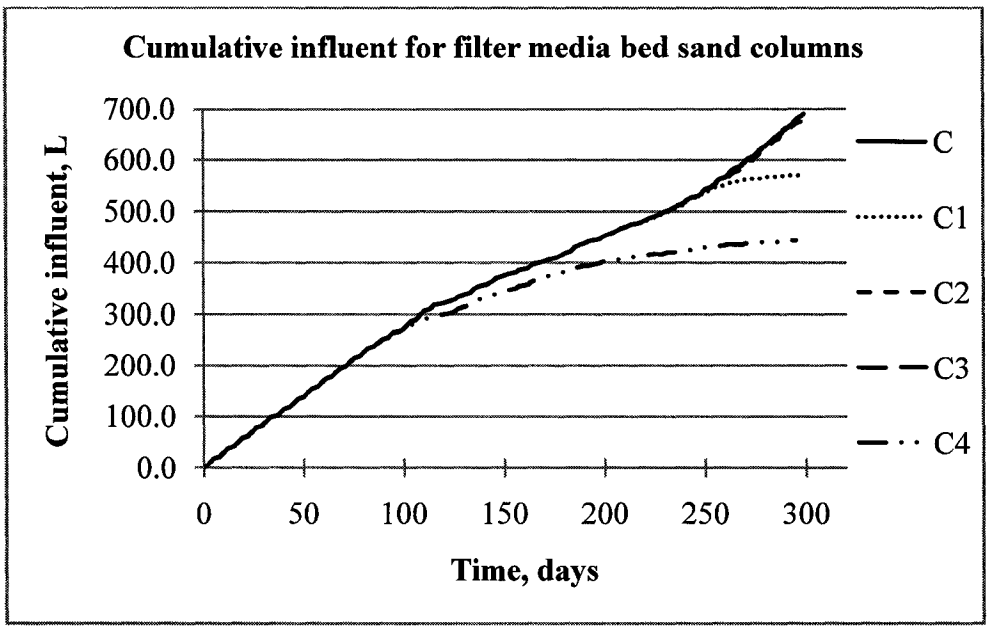

Figure A.16- Cumulative influent load for filter media bed sand columns

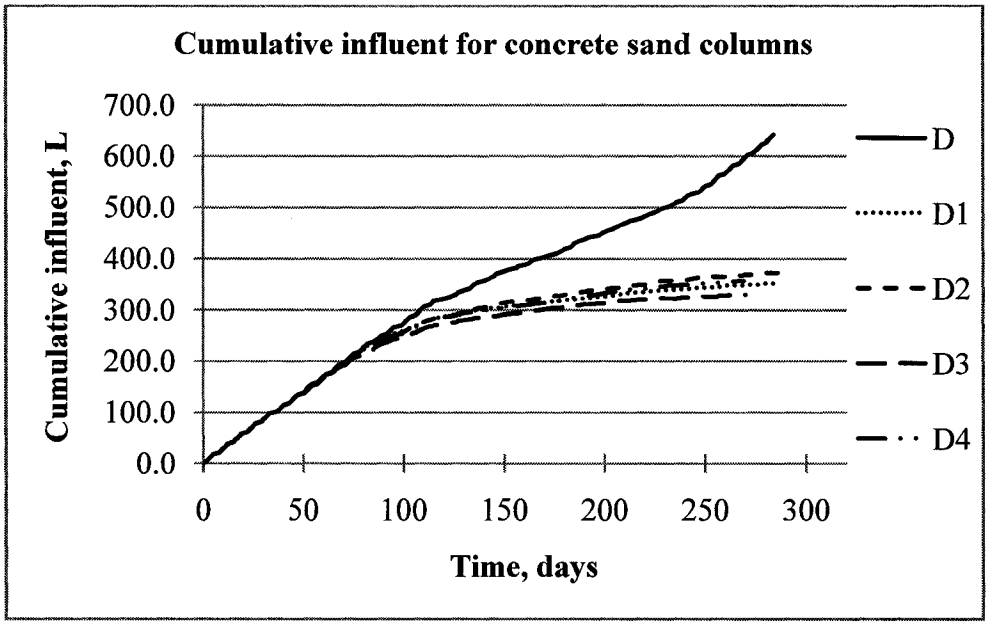

Figure A.17- Cumulative influent load for concrete sand columns

Reproduced with permission of the copyright owner. Further reproduction prohibited without permission.

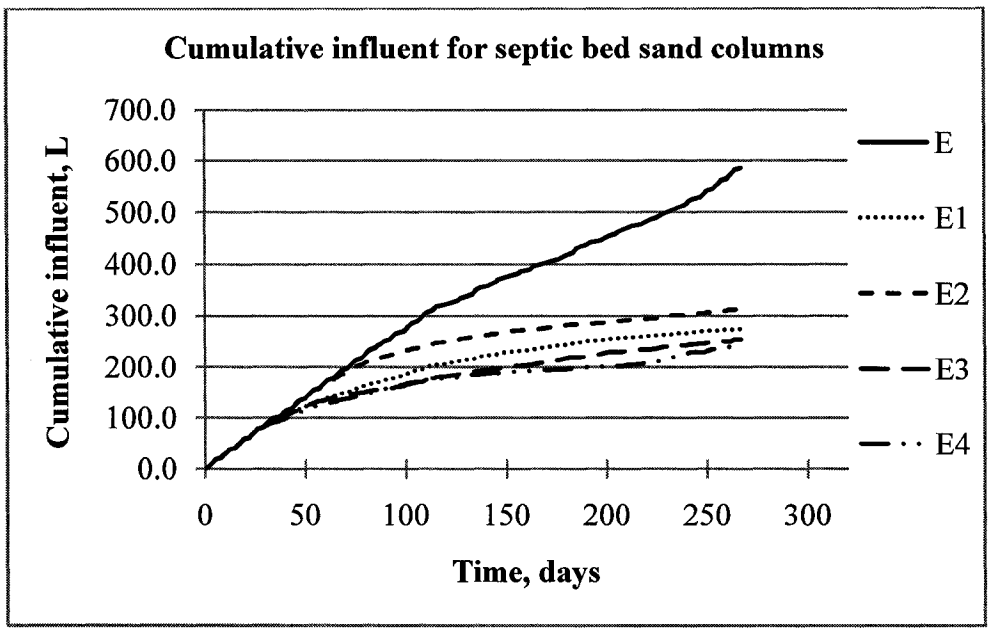

Figure A.18- Cumulative influent load for septic bed sand columns

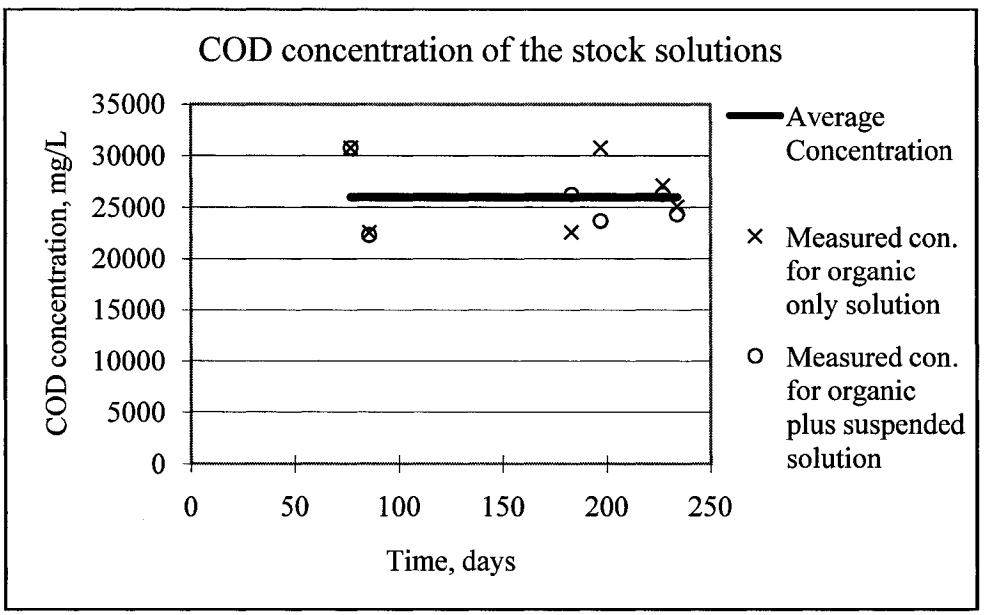

Figure A.19- COD concentration of the stock solutions; organic only and organic plus suspended

Reproduced with permission of the copyright owner. Further reproduction prohibited without permission.

Table A.16- Time to reduce loading/clogging for the experimental columns

Soil type	Column label	Time from day one, days		
		a[1]	b[2]	c[3]
Loose peat	A	295	295	295
	A1	240	267	295
	A2	232	239	294
	A3	192	274	294
	A4	213	274	293
Compacted peat	B	292	292	292
	B1	107	218	290
	B2	134	232	290
	B3	157	183	288
	B4	156	183	288
Filter media bed sand	C	300	300	300
	C1	248	274	299
	C2	299	299	299
	C3	296	296	296
	C4	94	253	296
Concrete sand	D	286	286	286
	D1	81	204	287
	D2	80	204	287
	D3	65	183	271
	D4	61	211	270
Septic bed sand	E	268	268	268
	E1	38	190	269
	E2	53	183	269
	E3	32	183	268
	E4	30	133	267

[1]a, After this day, hydraulic loading reduced to less than 20 L per week due to clogging
[2]b, After this day, hydraulic loading reduced to less than or equal to 4 L per week due to clogging
[3]c, Time when column was dismantled

Reproduced with permission of the copyright owner. Further reproduction prohibited without permission.

A.4 Measured Weight of the Experimental Columns

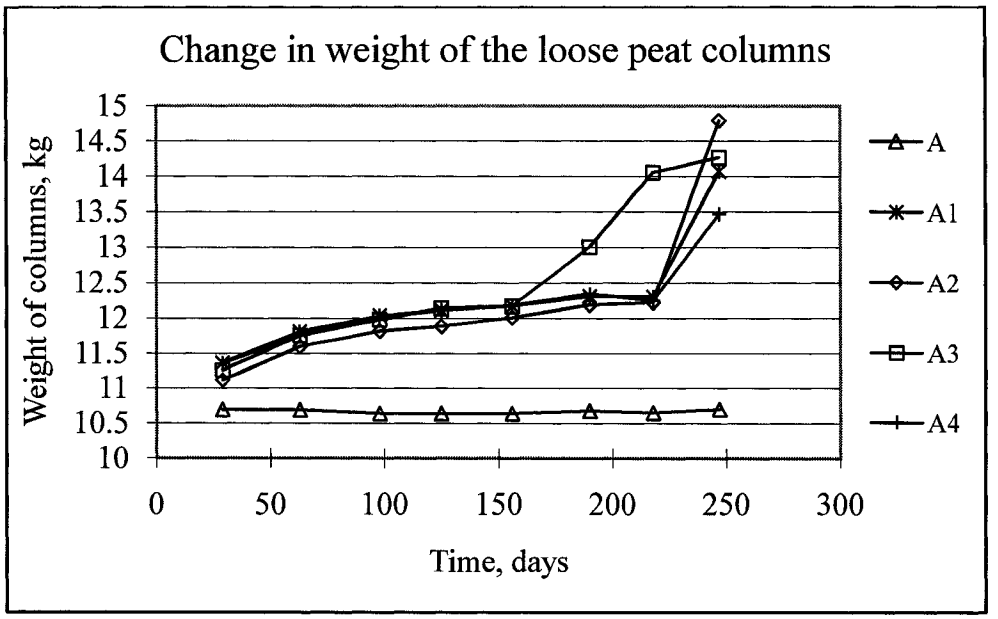

Figure A.20- Change in weight of the loose peat columns with time

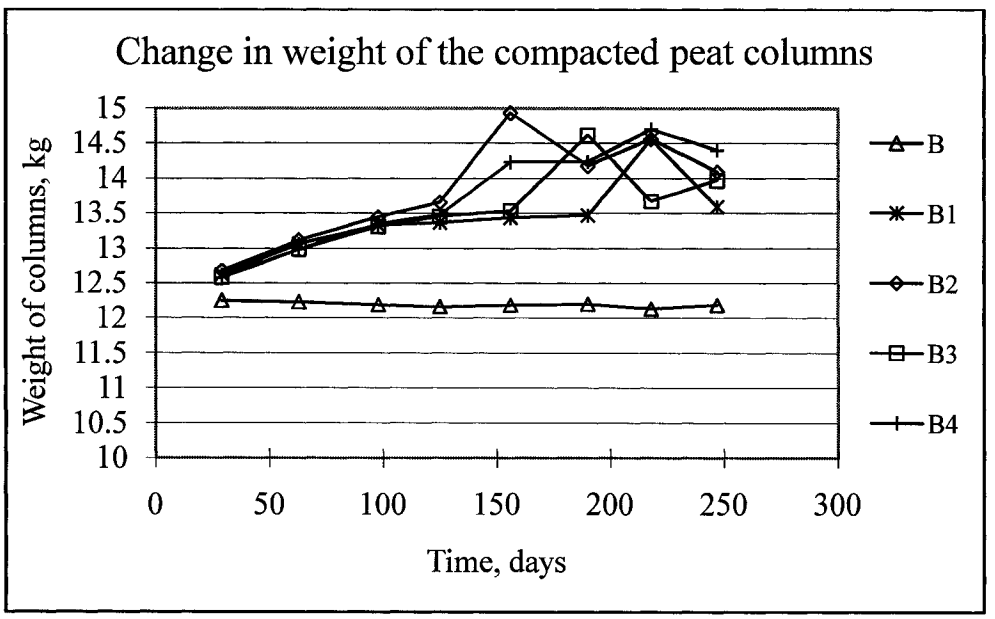

Figure A.21- Change in weight of the compacted peat columns with time

Reproduced with permission of the copyright owner. Further reproduction prohibited without permission.

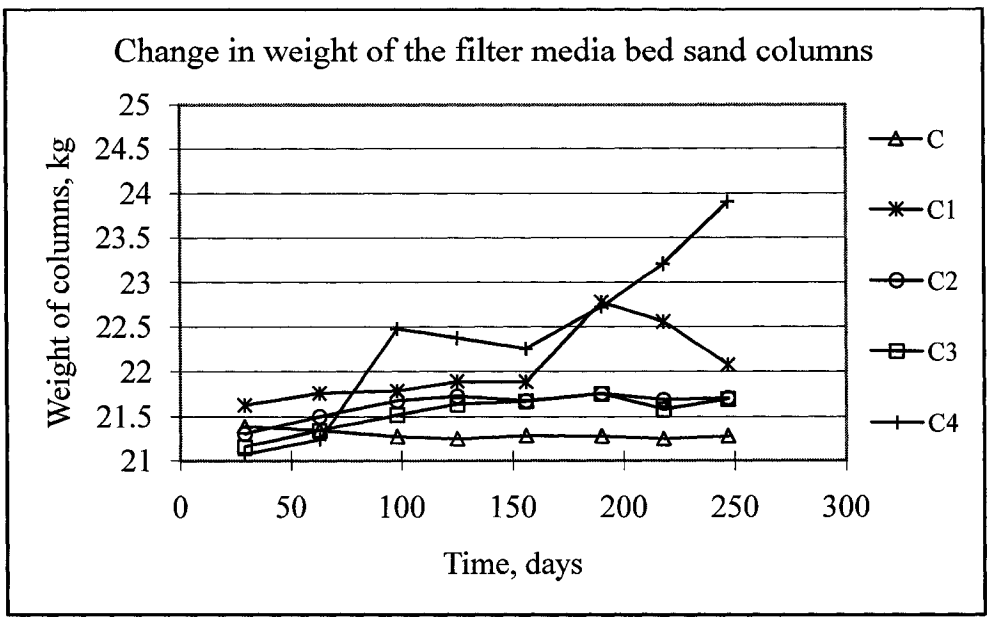

Figure A.22- Change in weight of the filter media bed sand columns with time

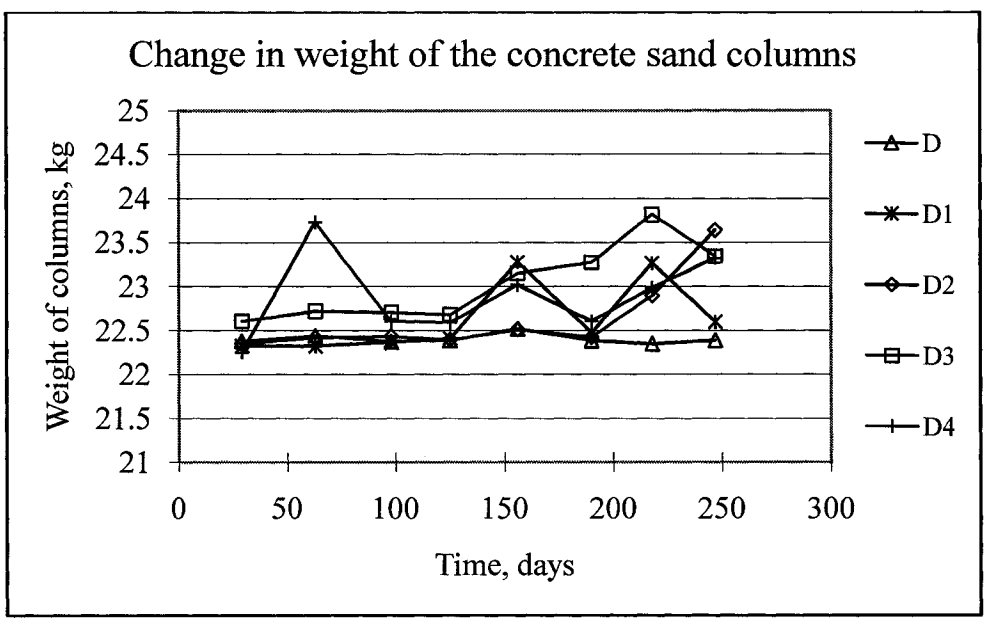

Figure A.23- Change in weight of the concrete sand columns with time

Reproduced with permission of the copyright owner. Further reproduction prohibited without permission.

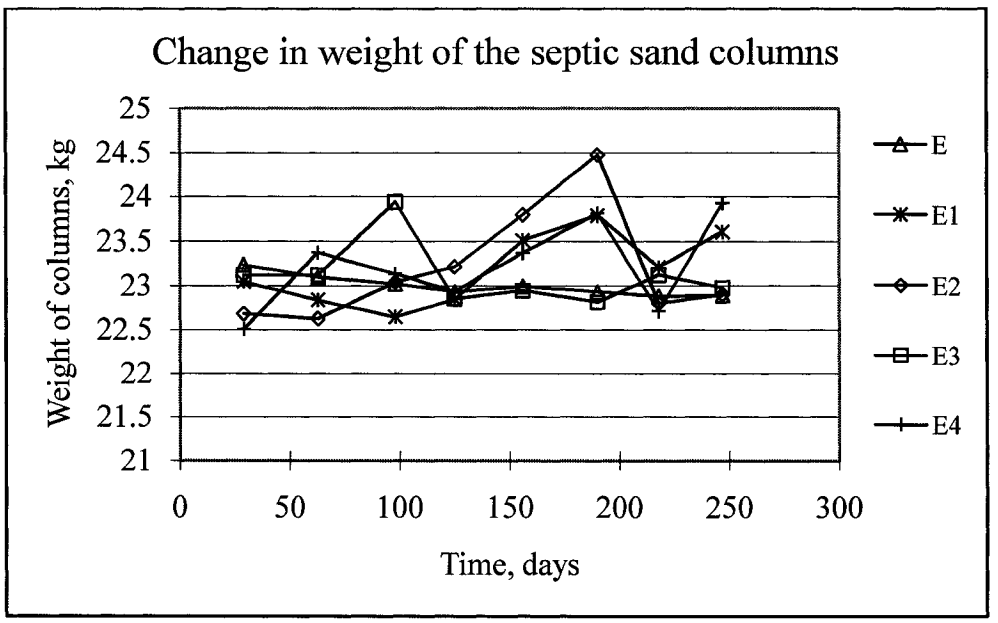

Figure A.24- Change in weight of the septic bed sand columns with time

A.5 Outflow from the Experimental Columns

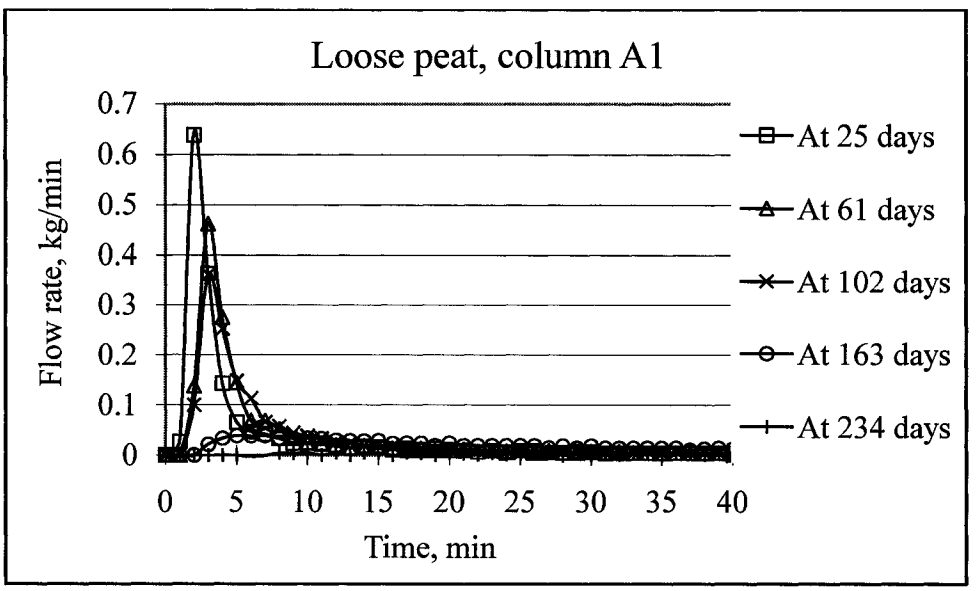

Figure A.25- Outflow from loose peat column A1

Reproduced with permission of the copyright owner. Further reproduction prohibited without permission.

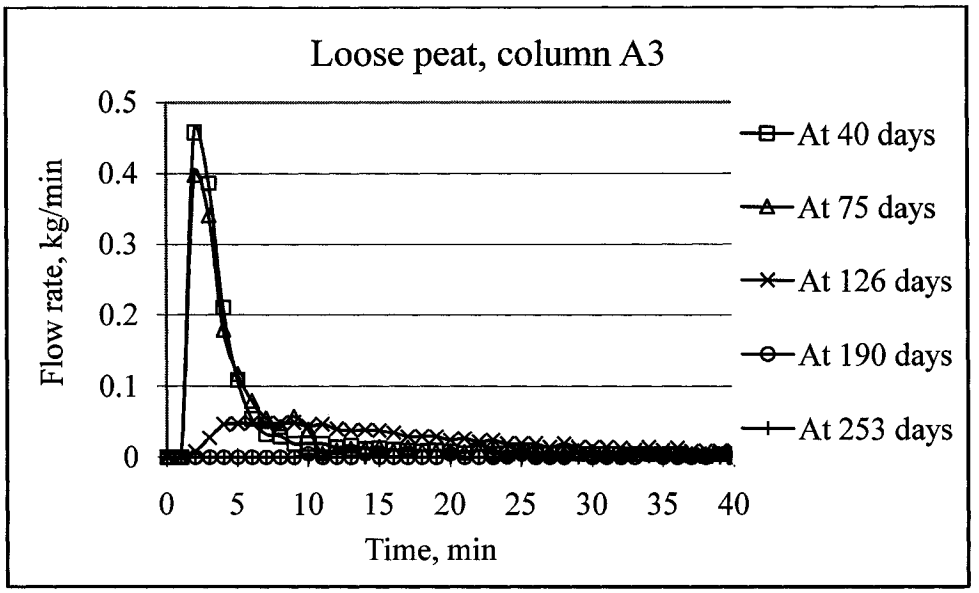

Figure A.26- Outflow from loose peat column A3

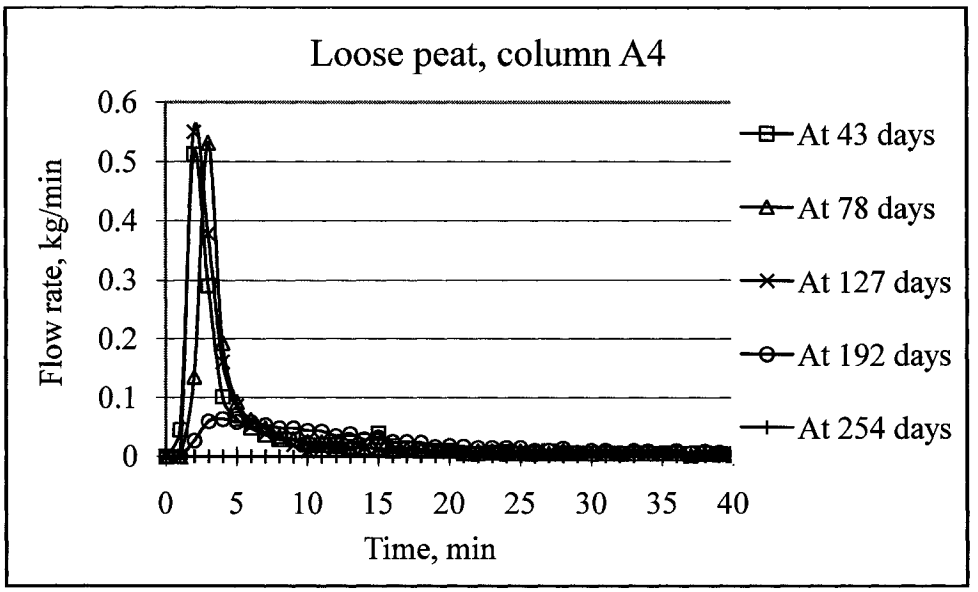

Figure A.27- Outflow from loose peat column A4

Reproduced with permission of the copyright owner. Further reproduction prohibited without permission.

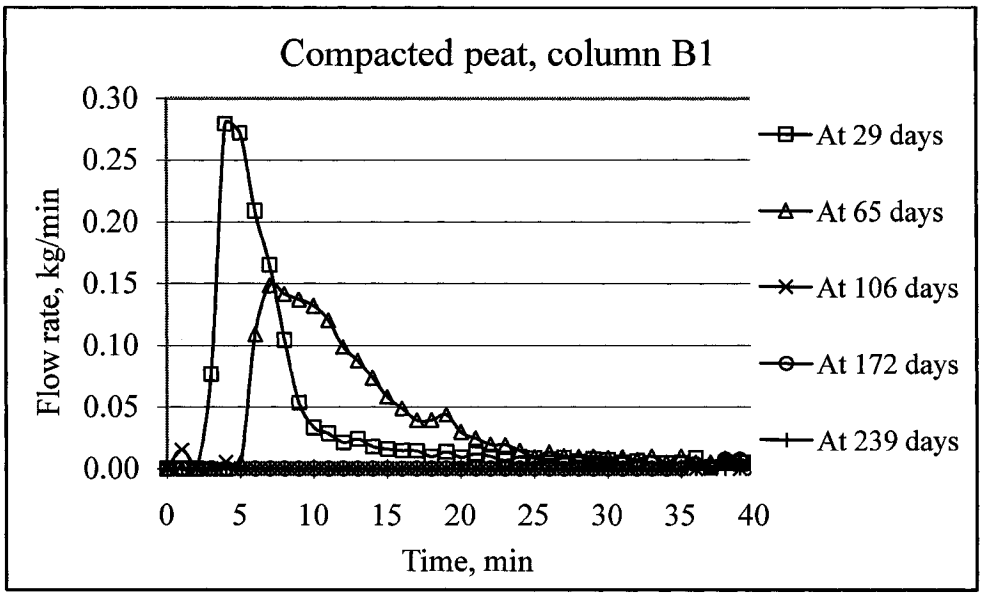

Figure A.28- Outflow from compacted peat column B1

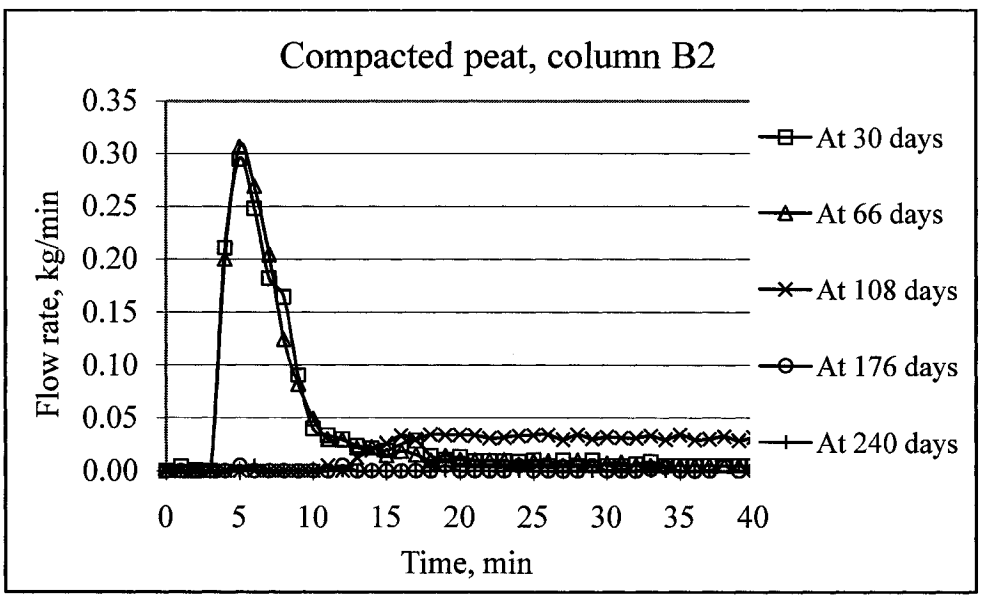

Figure A.29- Outflow from compacted peat column B2

Reproduced with permission of the copyright owner. Further reproduction prohibited without permission.

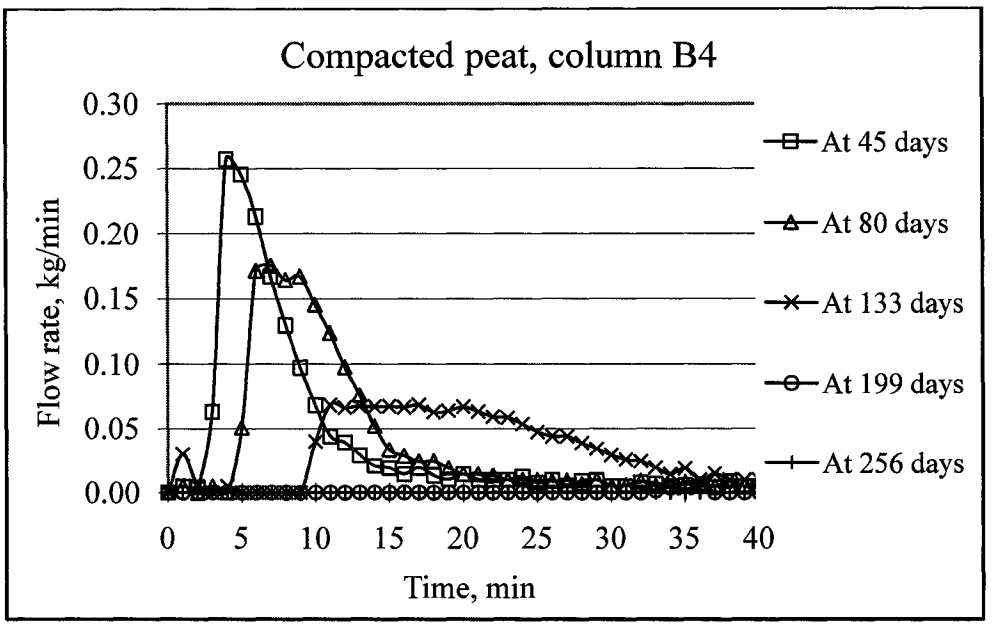

Figure A.30- Outflow from compacted peat column B4

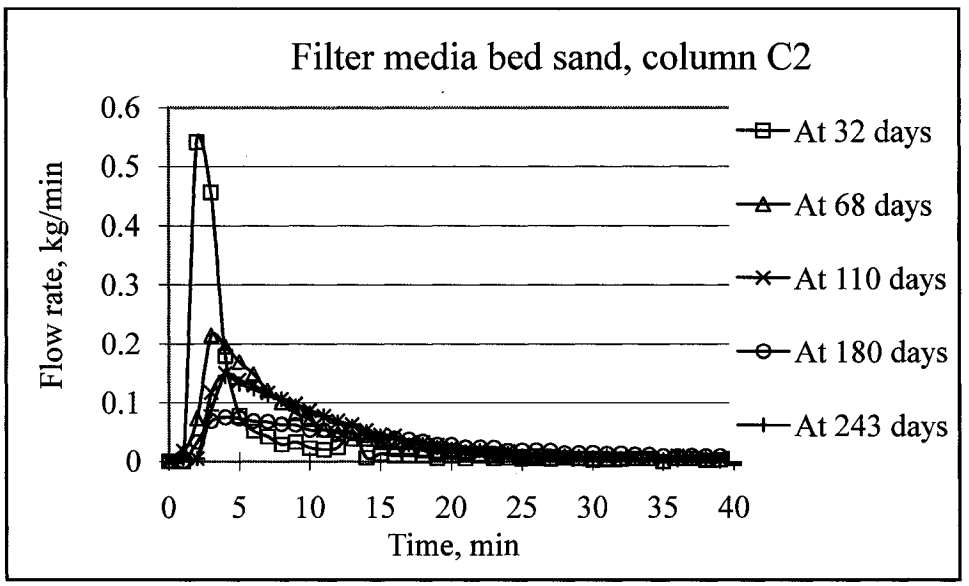

Figure A.31- Outflow from filter media bed sand column C2

Reproduced with permission of the copyright owner. Further reproduction prohibited without permission.

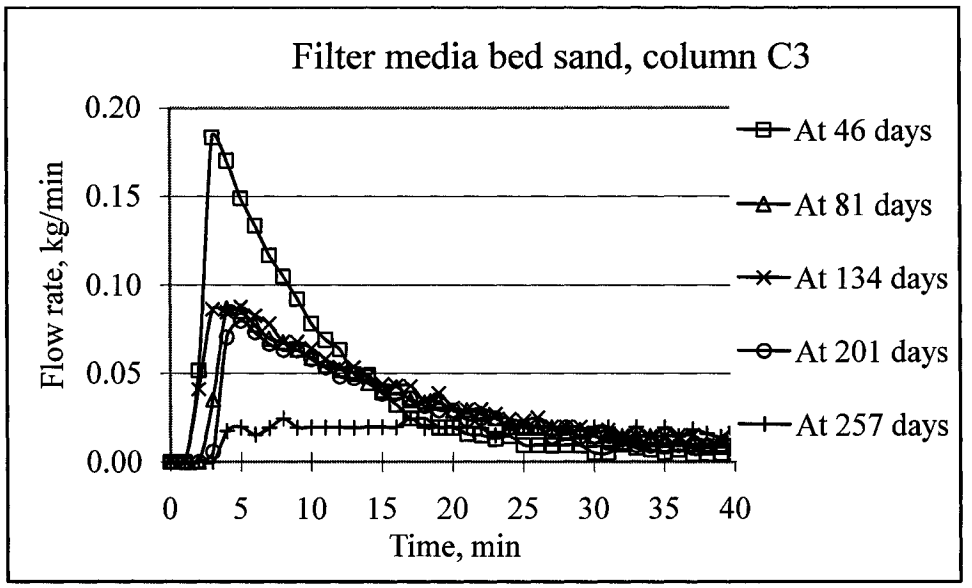

Figure A.32- Outflow from filter media bed sand column C3

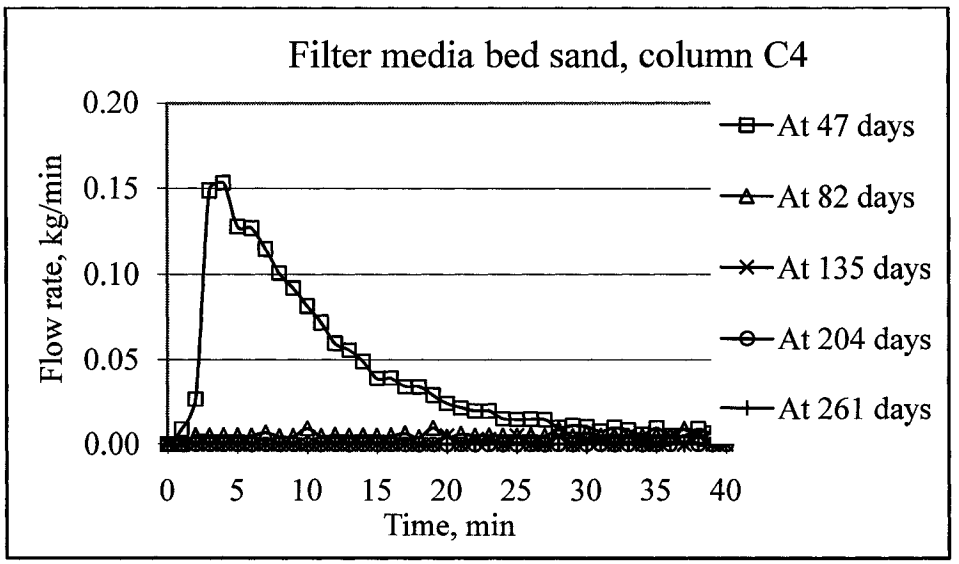

Figure A.33- Outflow from filter media bed sand column C4

Reproduced with permission of the copyright owner. Further reproduction prohibited without permission.

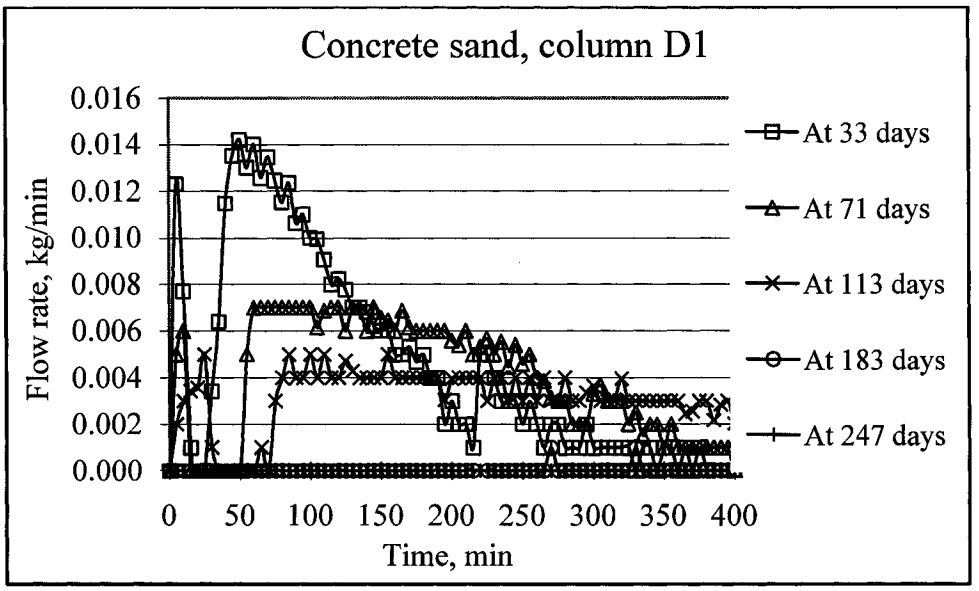

Figure A.34- Outflow from concrete sand column D1

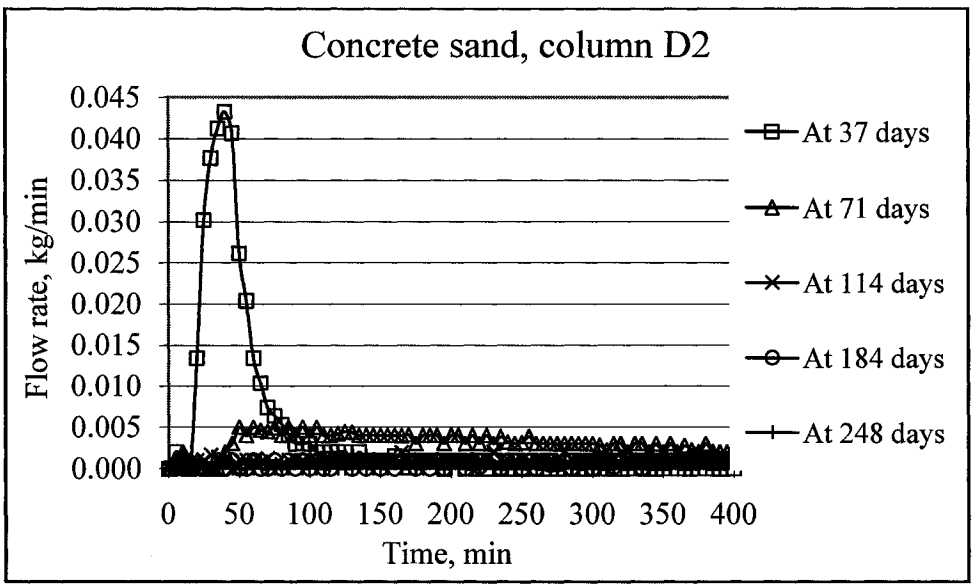

Figure A.35- Outflow from concrete sand column D2

Reproduced with permission of the copyright owner. Further reproduction prohibited without permission.

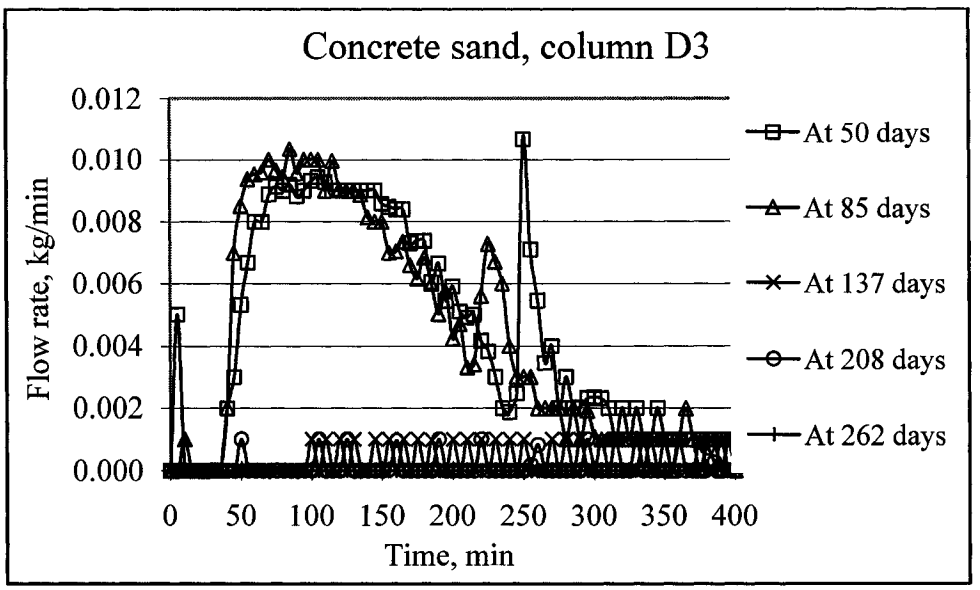

Figure A.36- Outflow from concrete sand column D3

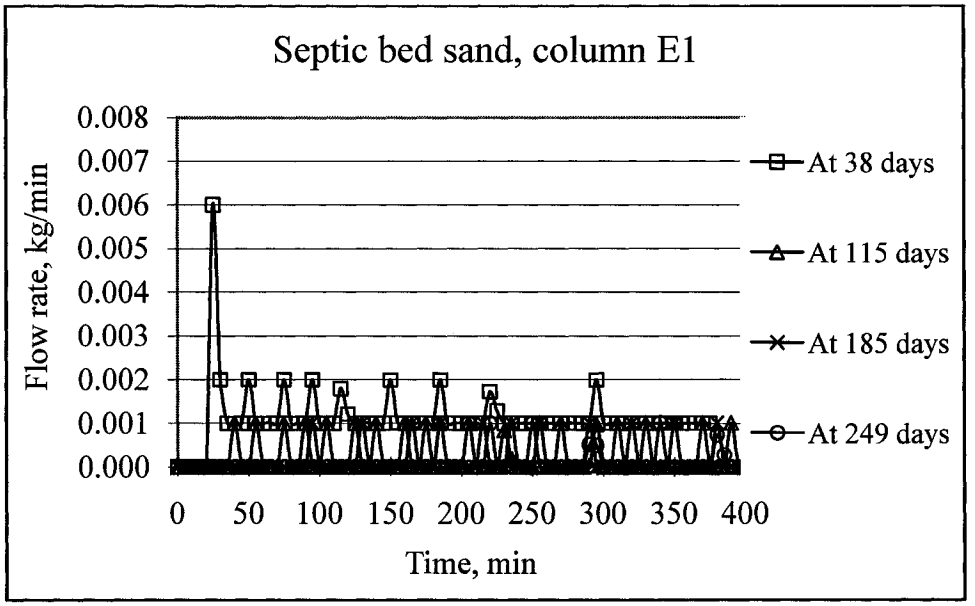

Figure A.37- Outflow from septic bed sand column E1

Reproduced with permission of the copyright owner. Further reproduction prohibited without permission.

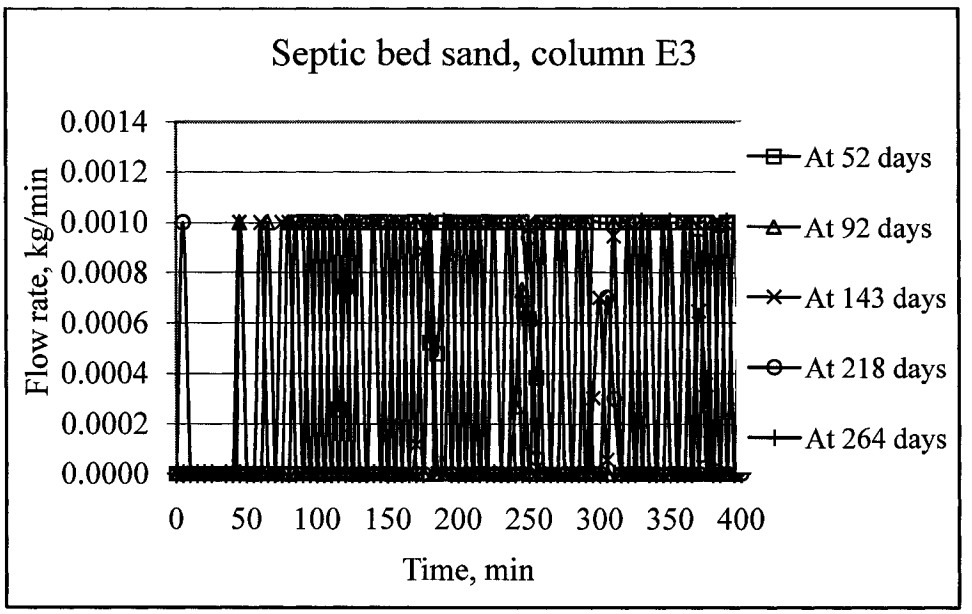

Figure A.38- Outflow from septic bed sand column E3

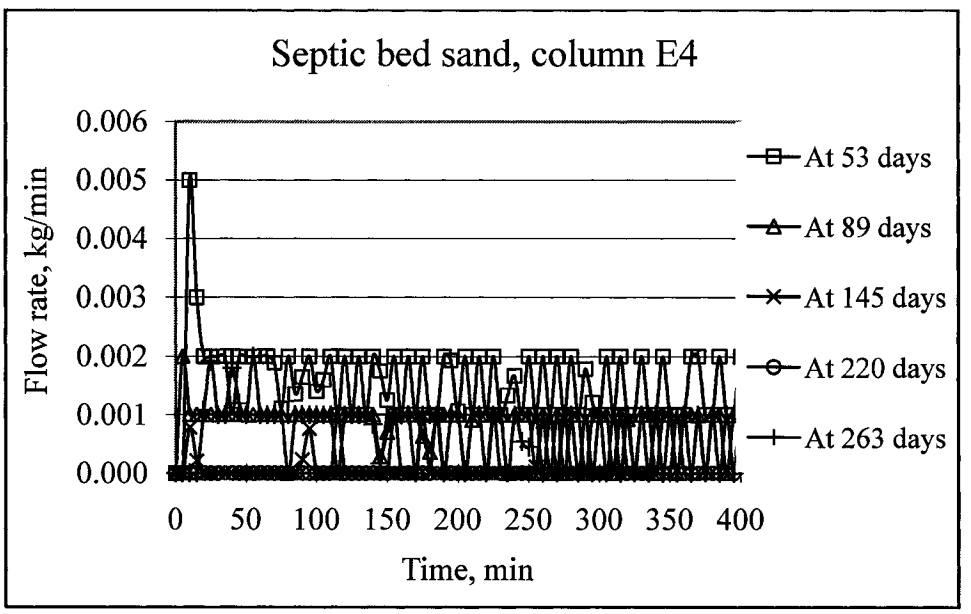

Figure A.39- Outflow from septic bed sand column E4

Reproduced with permission of the copyright owner. Further reproduction prohibited without permission.

A.6 Visual Images for the Experimental Columns

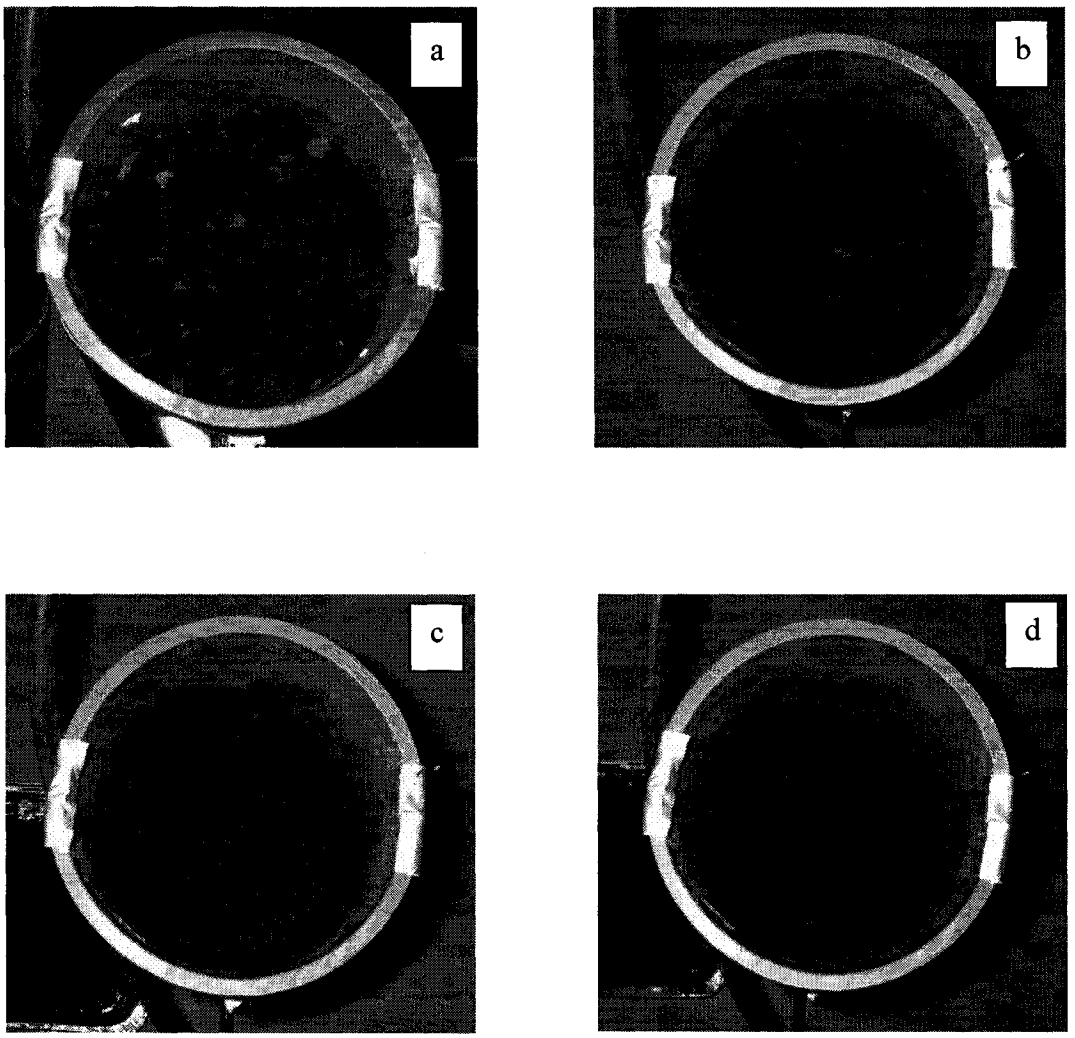

Figure A.40- Visual images of loose peat column A at dismantle time: (a) at the top surface of the column; (b) at a depth of 3 cm from the top surface; (c) at a depth of 8 cm from the top surface; and (d) at a depth of 17 cm from the top surface.

Reproduced with permission of the copyright owner. Further reproduction prohibited without permission.

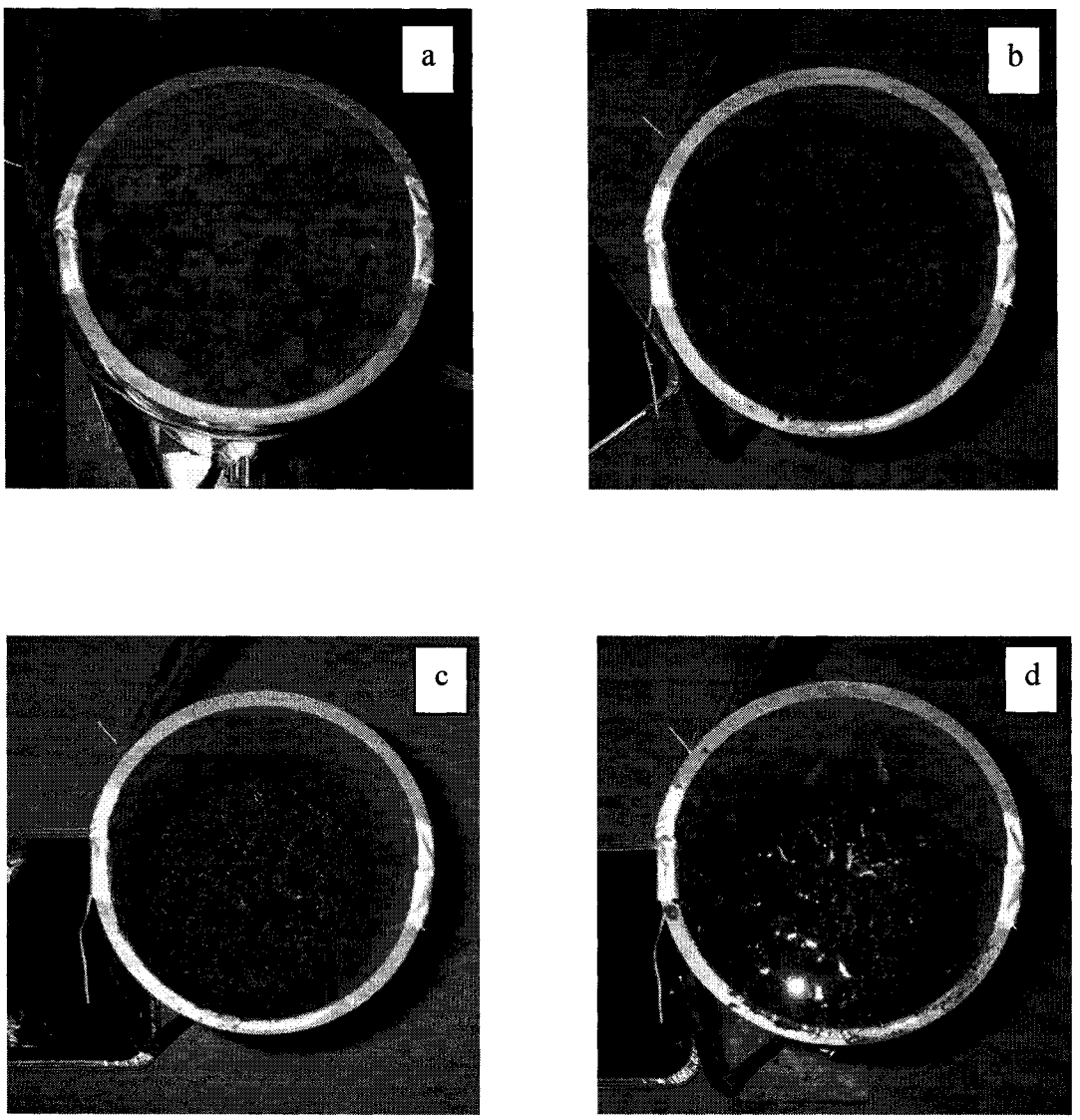

Figure A.41- Visual images of loose peat column A1 at dismantle time: (a) at the top surface of the column; (b) at a depth of 4.5 cm from the top surface; (c) at a depth of 10.5 cm from the top surface; and (d) at a depth of 18 cm from the top surface

Reproduced with permission of the copyright owner. Further reproduction prohibited without permission.

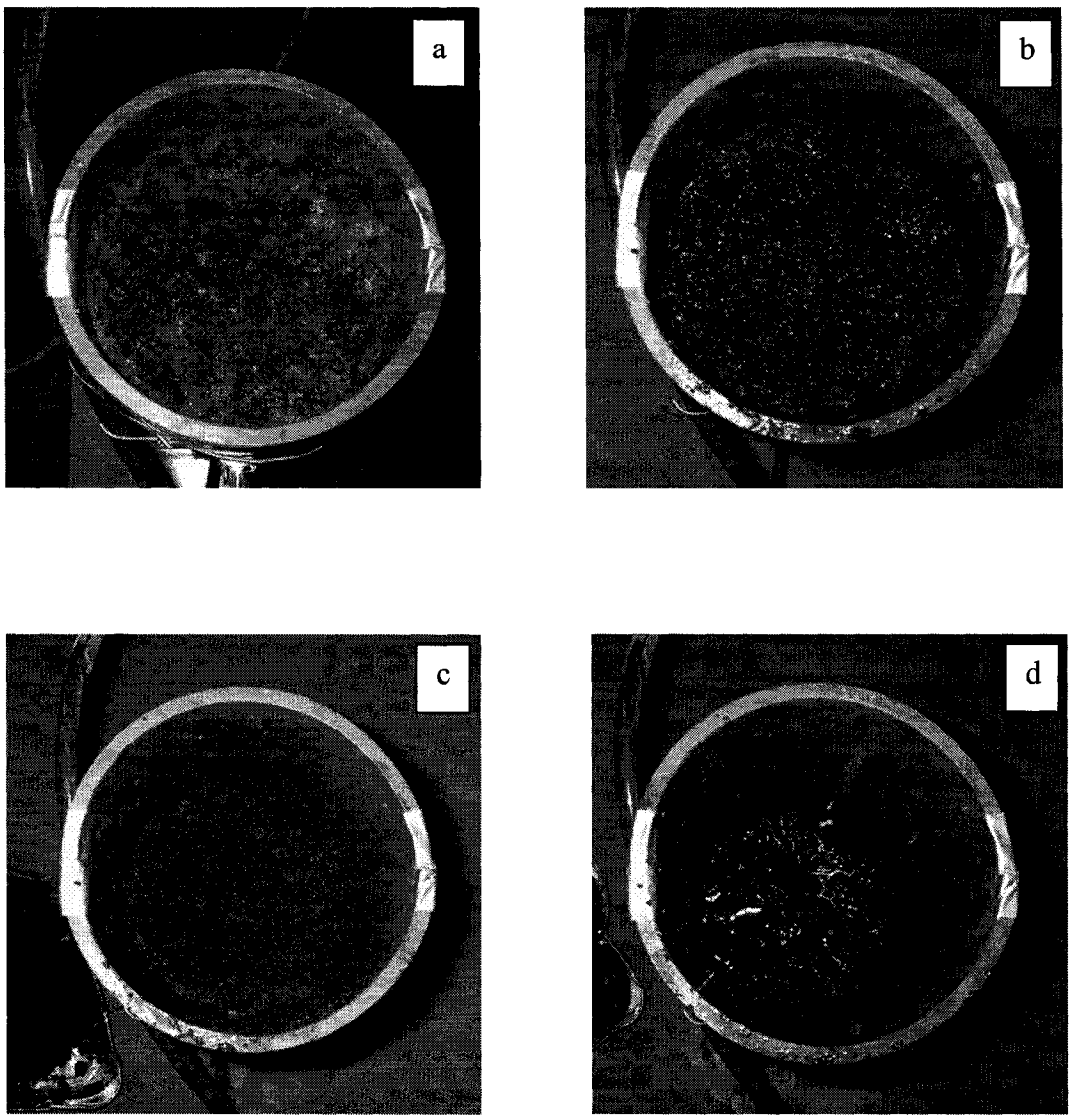

Figure A.42- Visual images of loose peat column A2 at dismantle time: (a) at the top surface of the column; (b) at a depth of 3.5 cm from the top surface; (c) at a depth of 8.5 cm from the top surface; and (d) at a depth of 18.5 cm from the top surface

Reproduced with permission of the copyright owner. Further reproduction prohibited without permission.

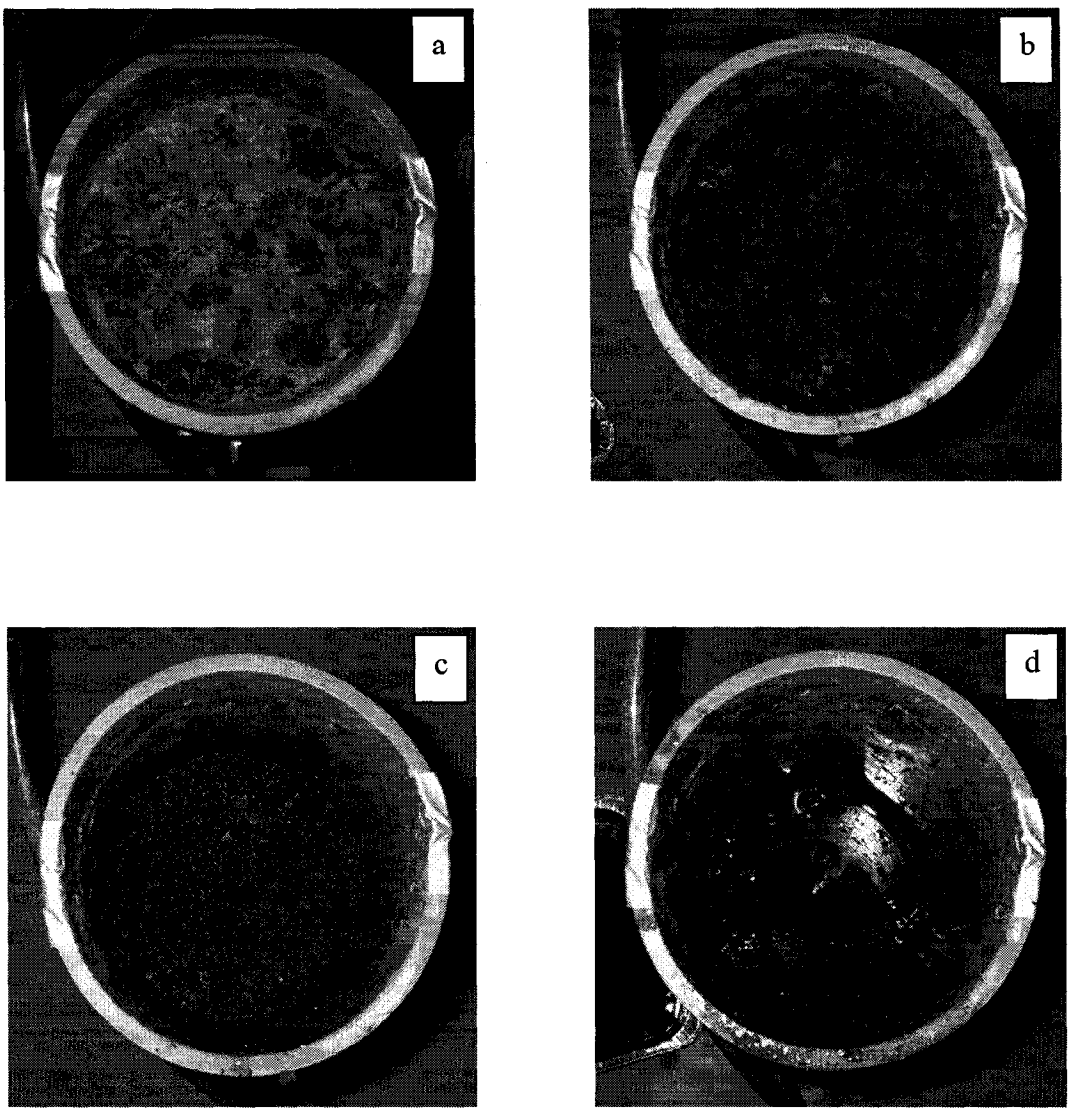

Figure A.43- Visual images of loose peat column A3 at dismantle time: (a) at the top surface of the column; (b) at a depth of 3 cm from the top surface; (c) at a depth of 8.5 cm from the top surface; and (d) at a depth of 17.5 cm from the top surface

Reproduced with permission of the copyright owner. Further reproduction prohibited without permission.

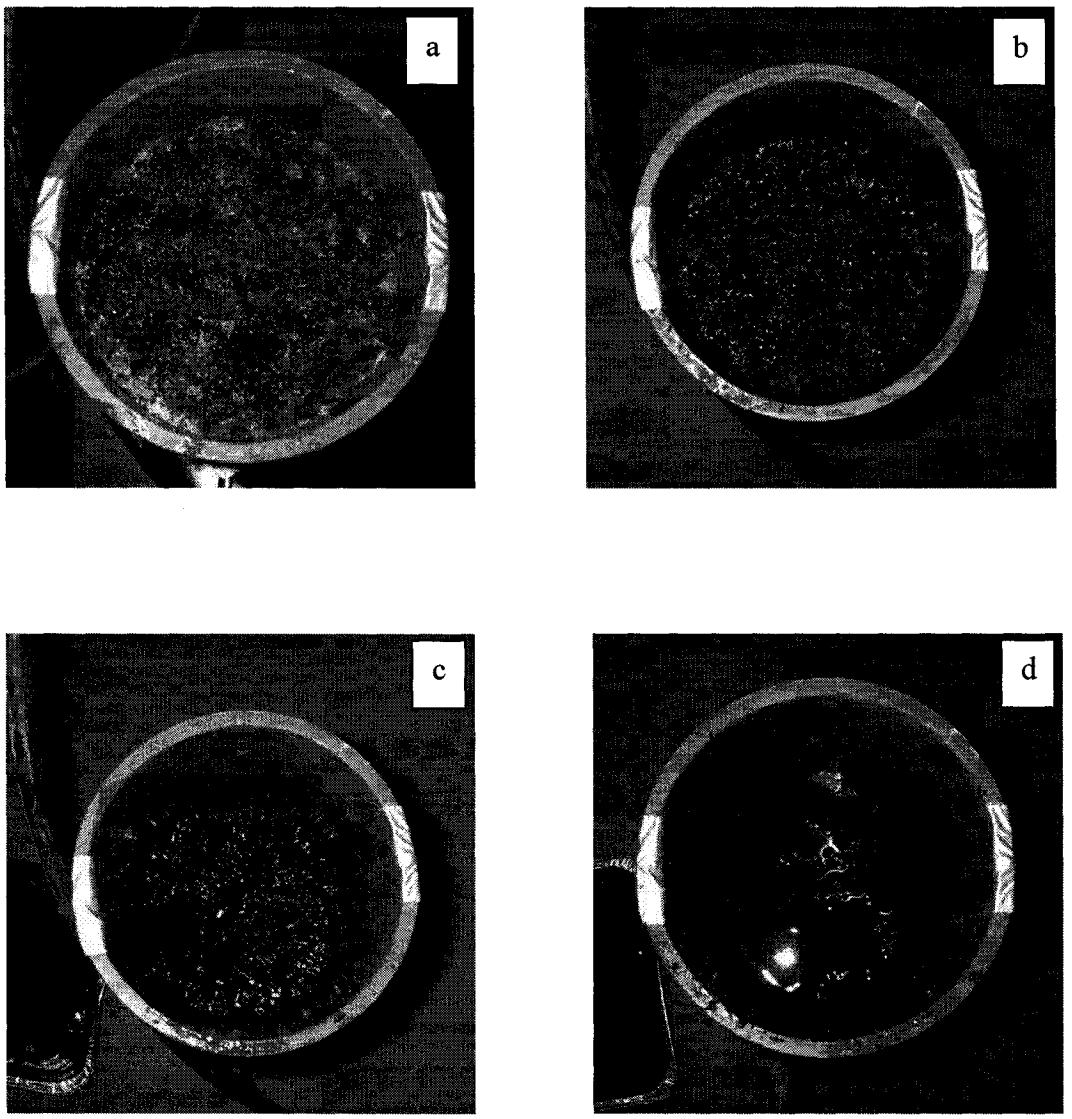

Figure A.44- Visual images of loose peat column A4 at dismantle time: (a) at the top surface of the column; (b) at a depth of 3.5 cm from the top surface; (c) at a depth of 10 cm from the top surface; and (d) at a depth of 22 cm from the top surface

Reproduced with permission of the copyright owner. Further reproduction prohibited without permission.

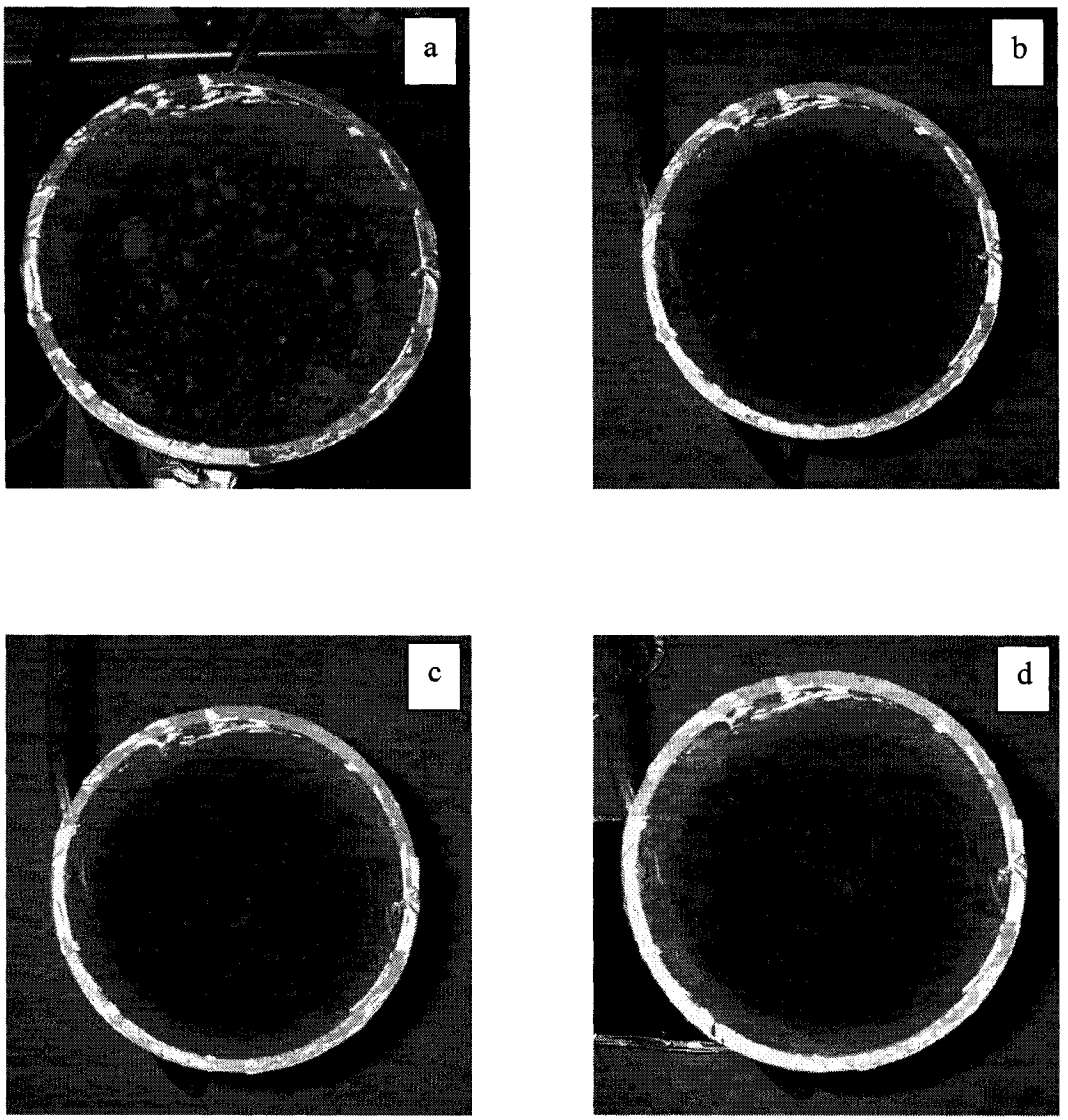

Figure A.45- Visual images of compacted peat column B at dismantle time: (a) at the top surface of the column; (b) at a depth of 2.5 cm from the top surface; (c) at a depth of 8 cm from the top surface; and (d) at a depth of 17 cm from the top surface

Reproduced with permission of the copyright owner. Further reproduction prohibited without permission.

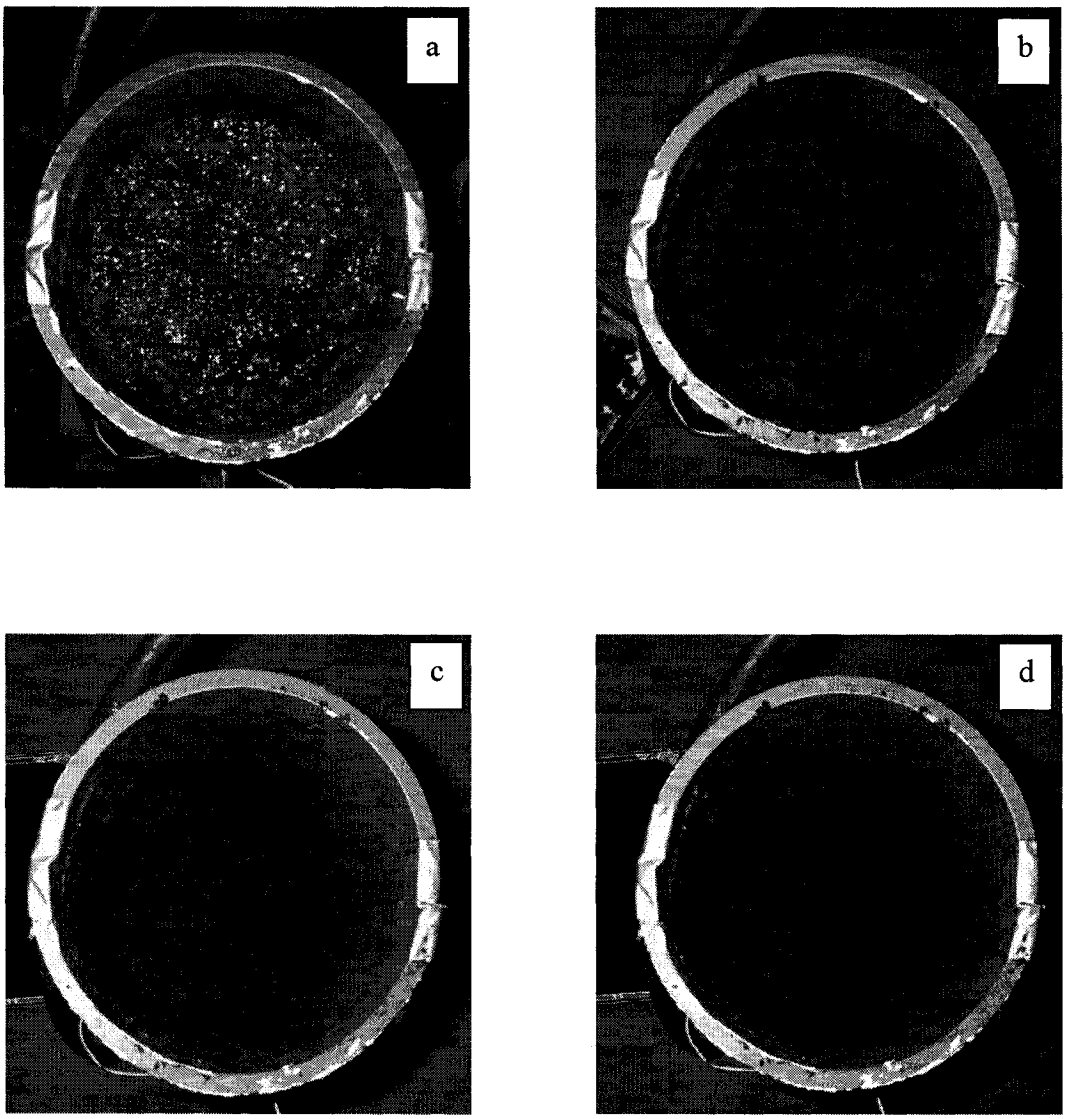

Figure A.46- Visual images of compacted peat column B1 at dismantle time: (a) at the top surface of the column; (b) at a depth of 2 cm from the top surface; (c) at a depth of 8.5 cm from the top surface; and (d) at a depth of 17 cm from the top surface

Reproduced with permission of the copyright owner. Further reproduction prohibited without permission.

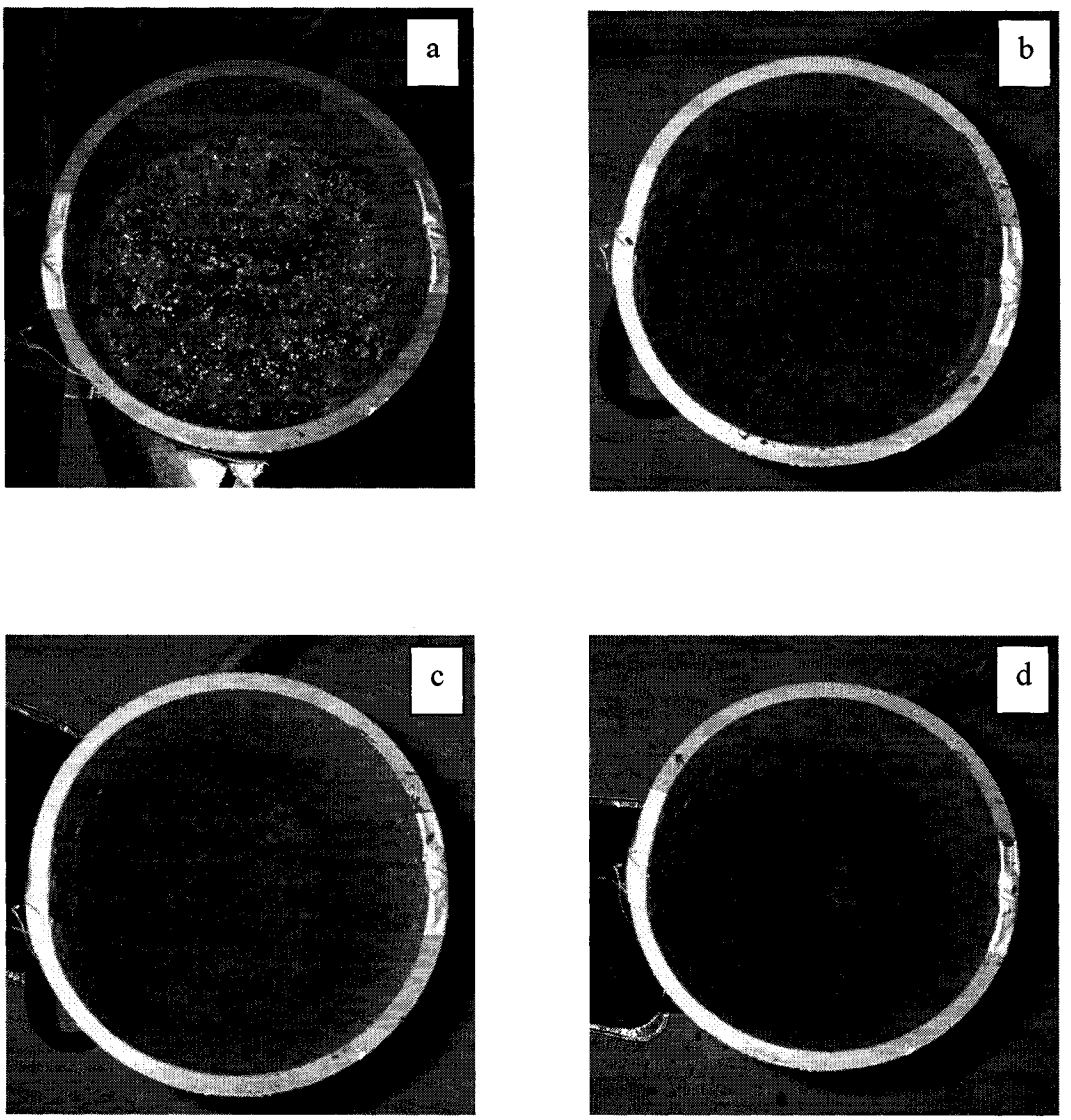

Figure A.47- Visual images of compacted peat column B2 at dismantle time: (a) at the top surface of the column; (b) at a depth of 2.5 cm from the top surface; (c) at a depth of 8.5 cm from the top surface; and (d) at a depth of 16.5 cm from the top surface

Reproduced with permission of the copyright owner. Further reproduction prohibited without permission.

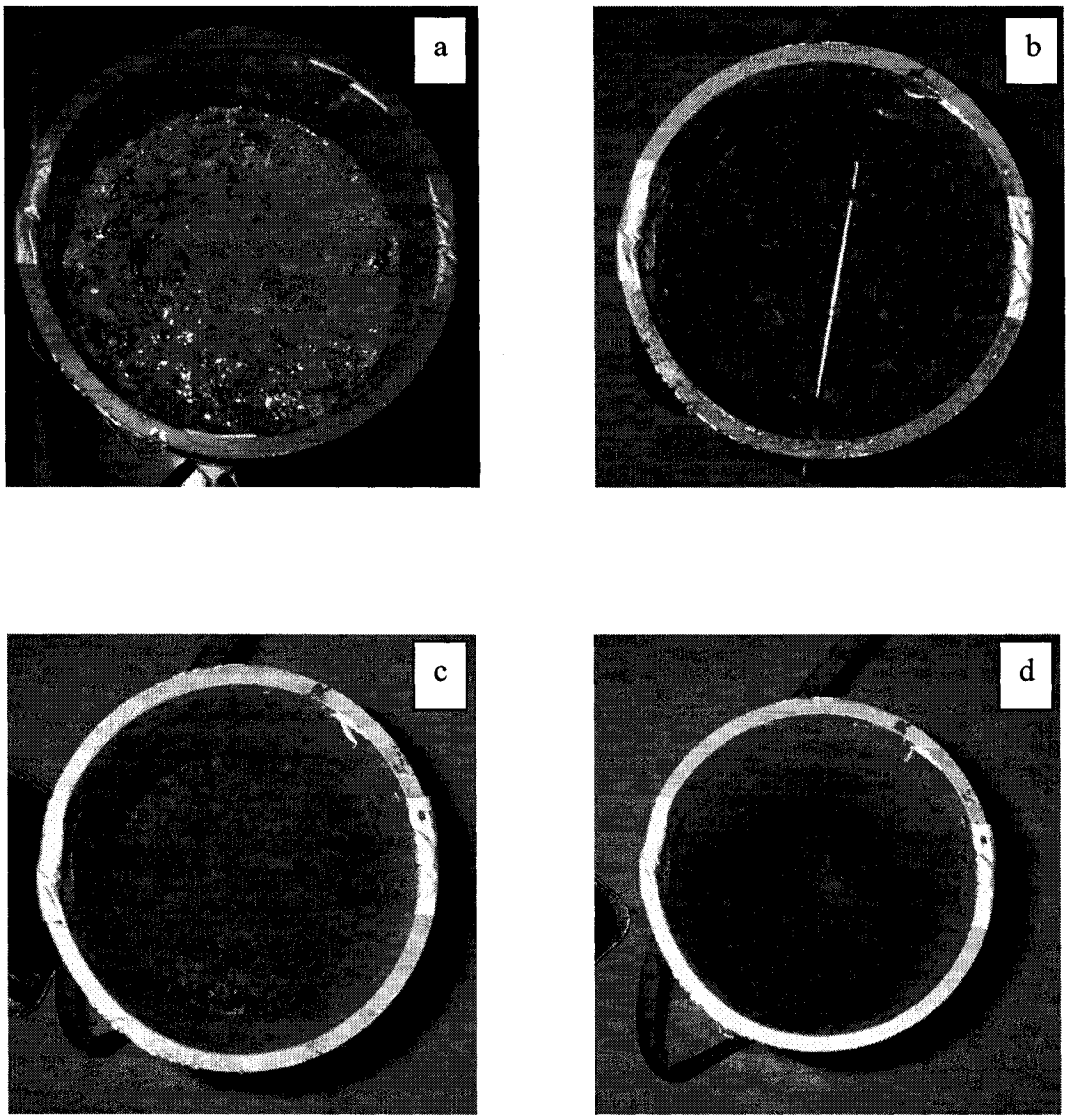

Figure A.48- Visual images of compacted peat column B3 at dismantle time: (a) at the top surface of the column; (b) at a depth of 2.5 cm from the top surface; (c) at a depth of 8.5 cm from the top surface; and (d) at a depth of 18.5 cm from the top surface

Reproduced with permission of the copyright owner. Further reproduction prohibited without permission.

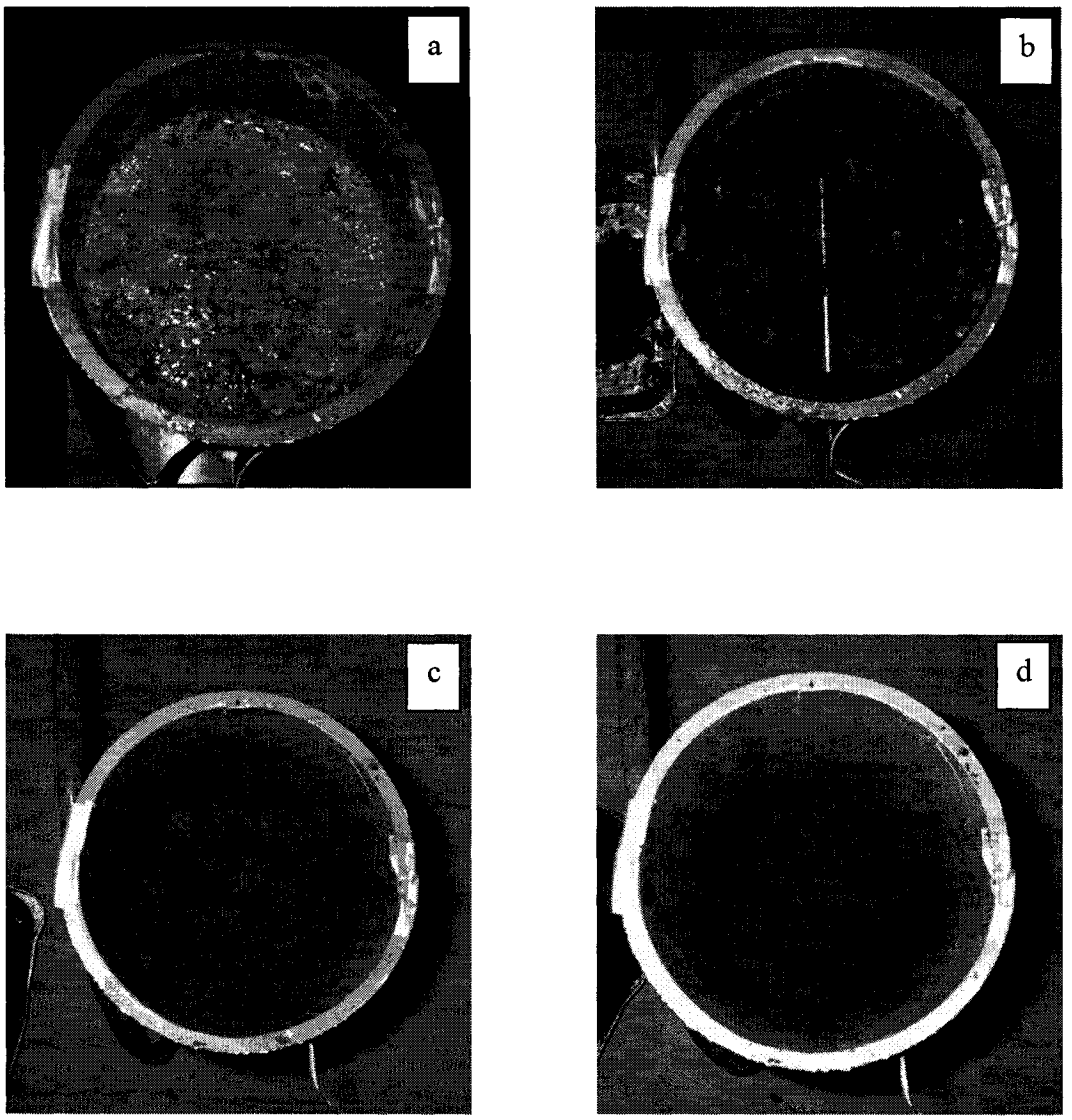

Figure A.49- Visual images of compacted peat column B4 at dismantle time: (a) at the top surface of the column; (b) at a depth of 2.5 cm from the top surface; (c) at a depth of 8 cm from the top surface; and (d) at a depth of 16.5 cm from the top surface

Reproduced with permission of the copyright owner. Further reproduction prohibited without permission.

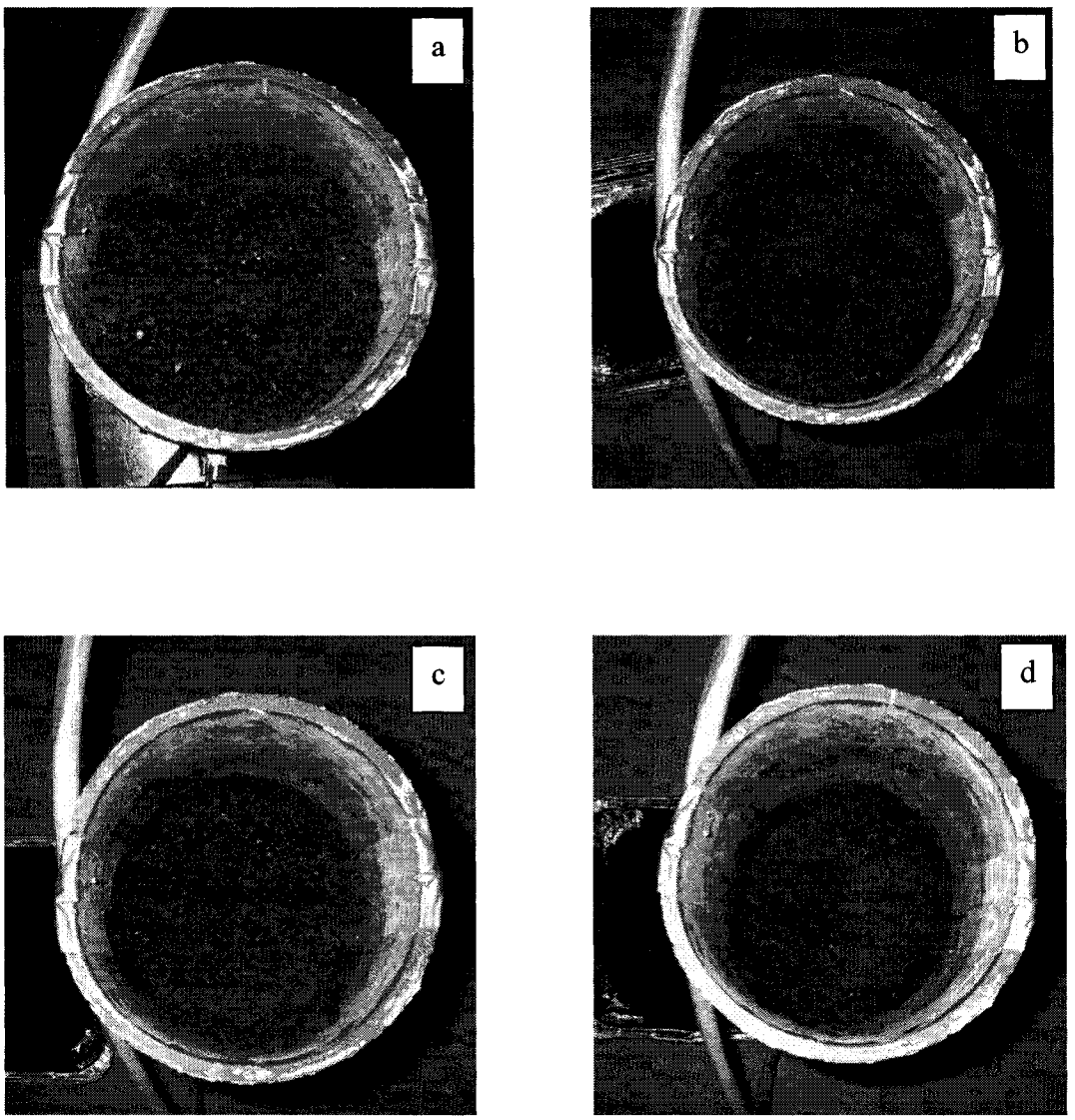

Figure A.50- Visual images of filter media bed sand column C at dismantle time: (a) at the top surface of the column; (b) at a depth of 3 cm from the top surface; (c) at a depth of 9.5 cm from the top surface; and (d) at a depth of 17 cm from the top surface

Reproduced with permission of the copyright owner. Further reproduction prohibited without permission.

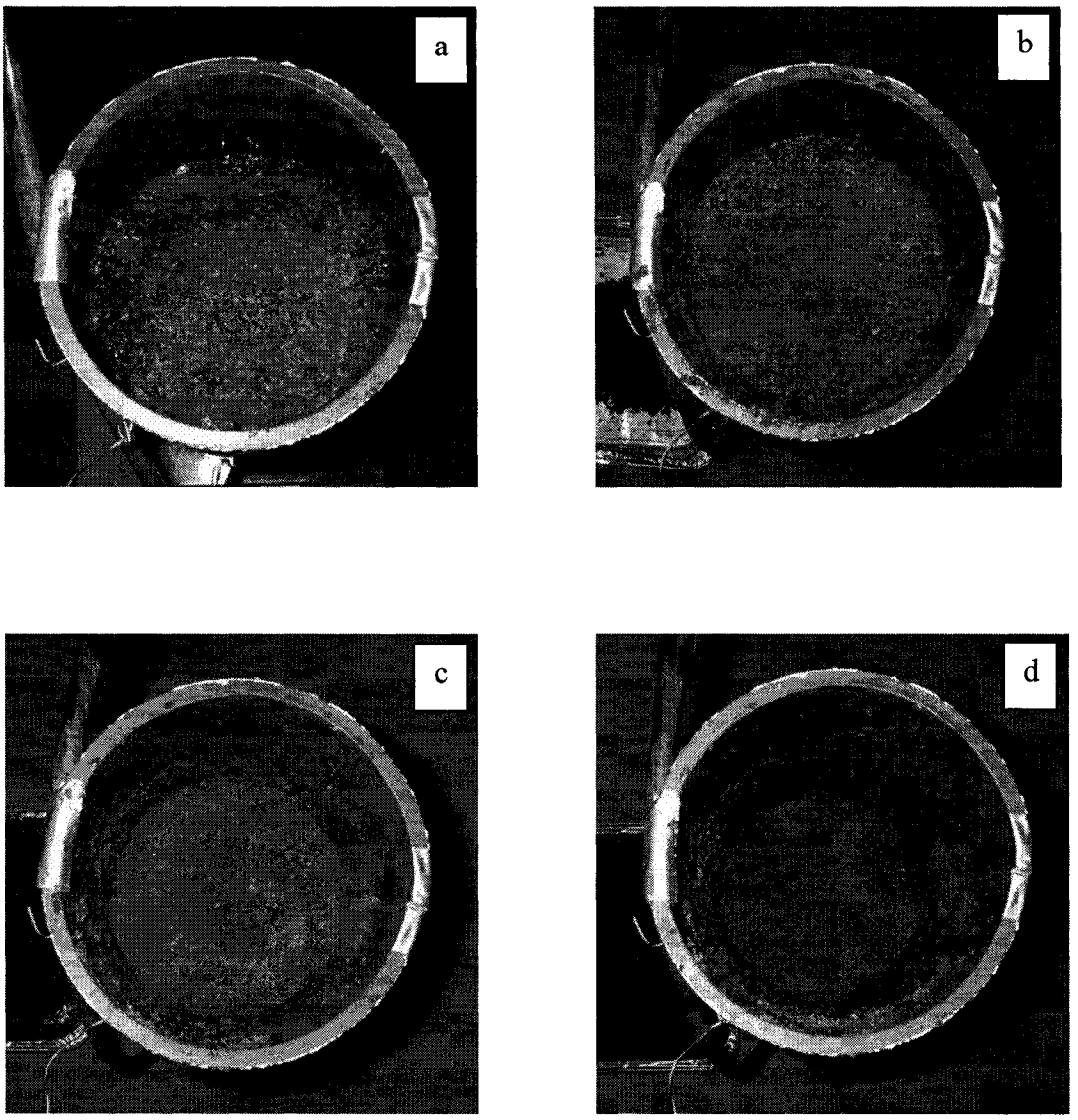

Figure A.51- Visual images of filter media bed sand column C1 at dismantle time: (a) at the top surface of the column; (b) at a depth of 1.5 cm from the top surface; (c) at a depth of 7.5 cm from the top surface; and (d) at a depth of 16 cm from the top surface

Reproduced with permission of the copyright owner. Further reproduction prohibited without permission.

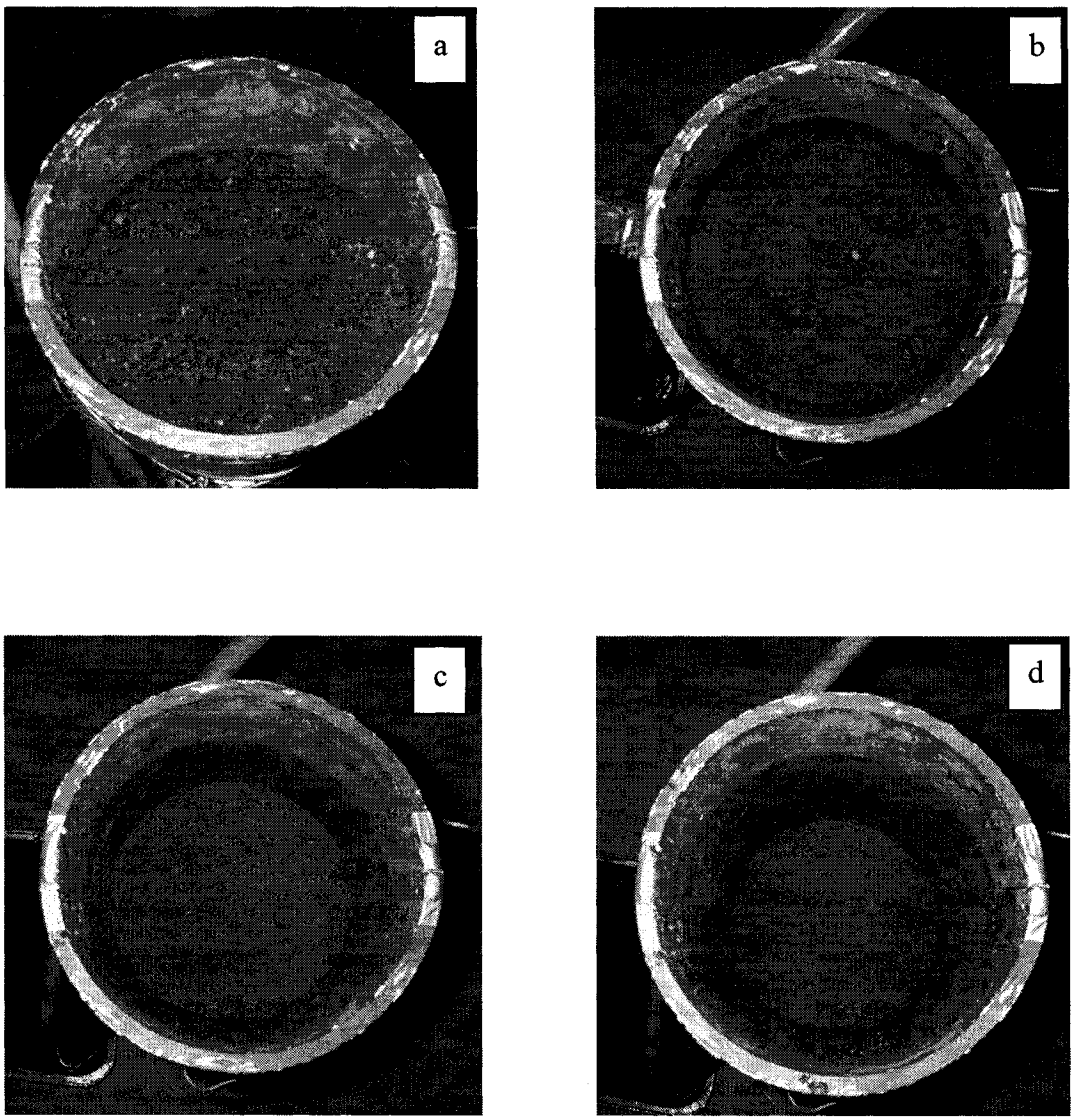

Figure A.52- Visual images of filter media bed sand column C2 at dismantle time: (a) at the top surface of the column; (b) at a depth of 2.5 cm from the top surface; (c) at a depth of 9 cm from the top surface; and (d) at a depth of 17 cm from the top surface

Reproduced with permission of the copyright owner. Further reproduction prohibited without permission.

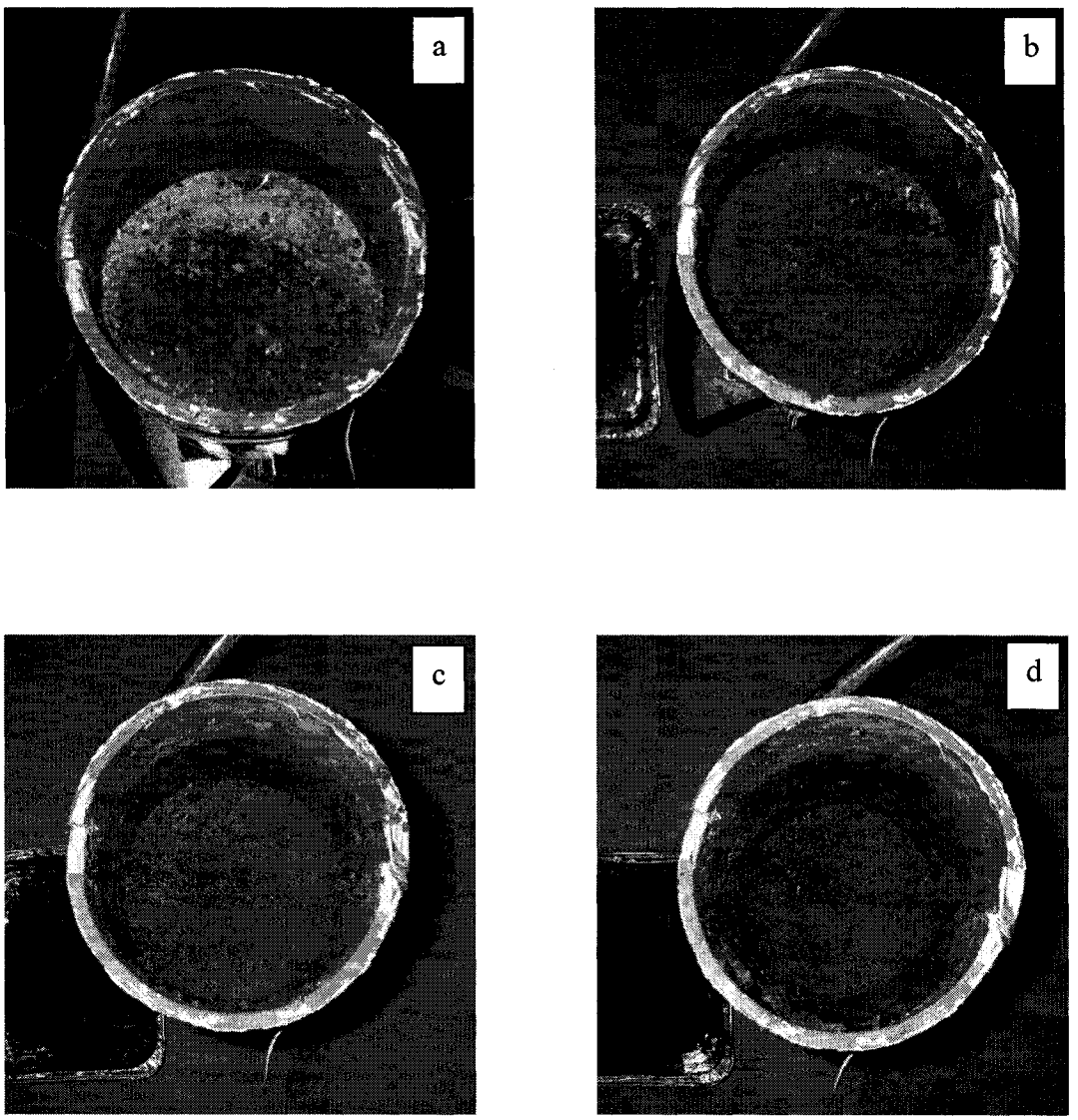

Figure A.53- Visual images of filter media bed sand column C3 at dismantle time: (a) at the top surface of the column; (b) at a depth of 2 cm from the top surface; (c) at a depth of 7.5 cm from the top surface; and (d) at a depth of 15.5 cm from the top surface

Reproduced with permission of the copyright owner. Further reproduction prohibited without permission.

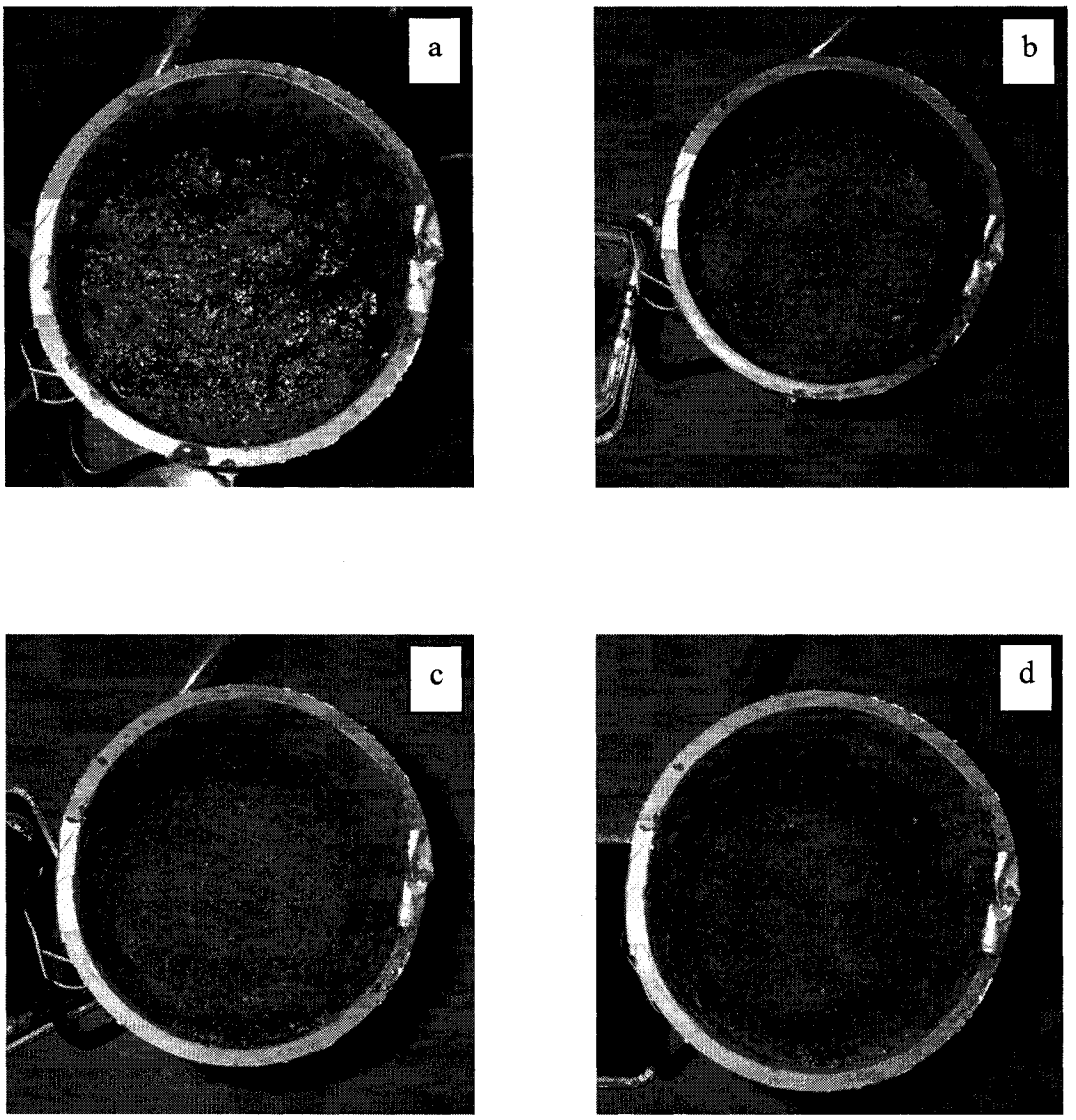

Figure A.54- Visual images of filter media bed sand column C4 at dismantle time: (a) at the top surface of the column; (b) at a depth of 2.5 cm from the top surface; (c) at a depth of 8 cm from the top surface; and (d) at a depth of 16 cm from the top surface

Reproduced with permission of the copyright owner. Further reproduction prohibited without permission.

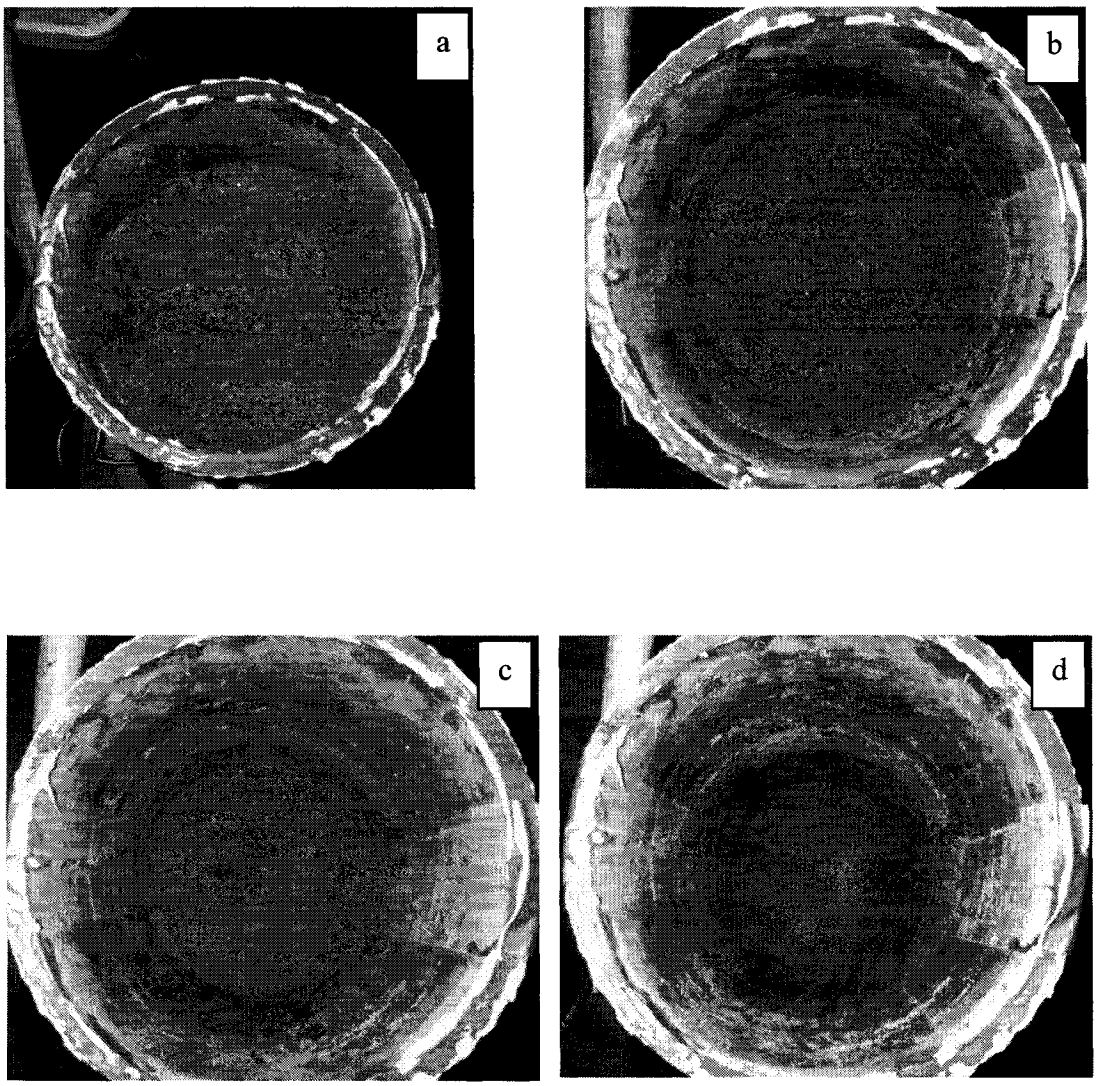

Figure A.55- Visual images of concrete sand column D at dismantle time: (a) at the top surface of the column; (b) at a depth of 8.5 cm from the top surface; (c) at a depth of 16.5 cm from the top surface; and (d) at a depth of 26 cm from the top surface

Reproduced with permission of the copyright owner. Further reproduction prohibited without permission.

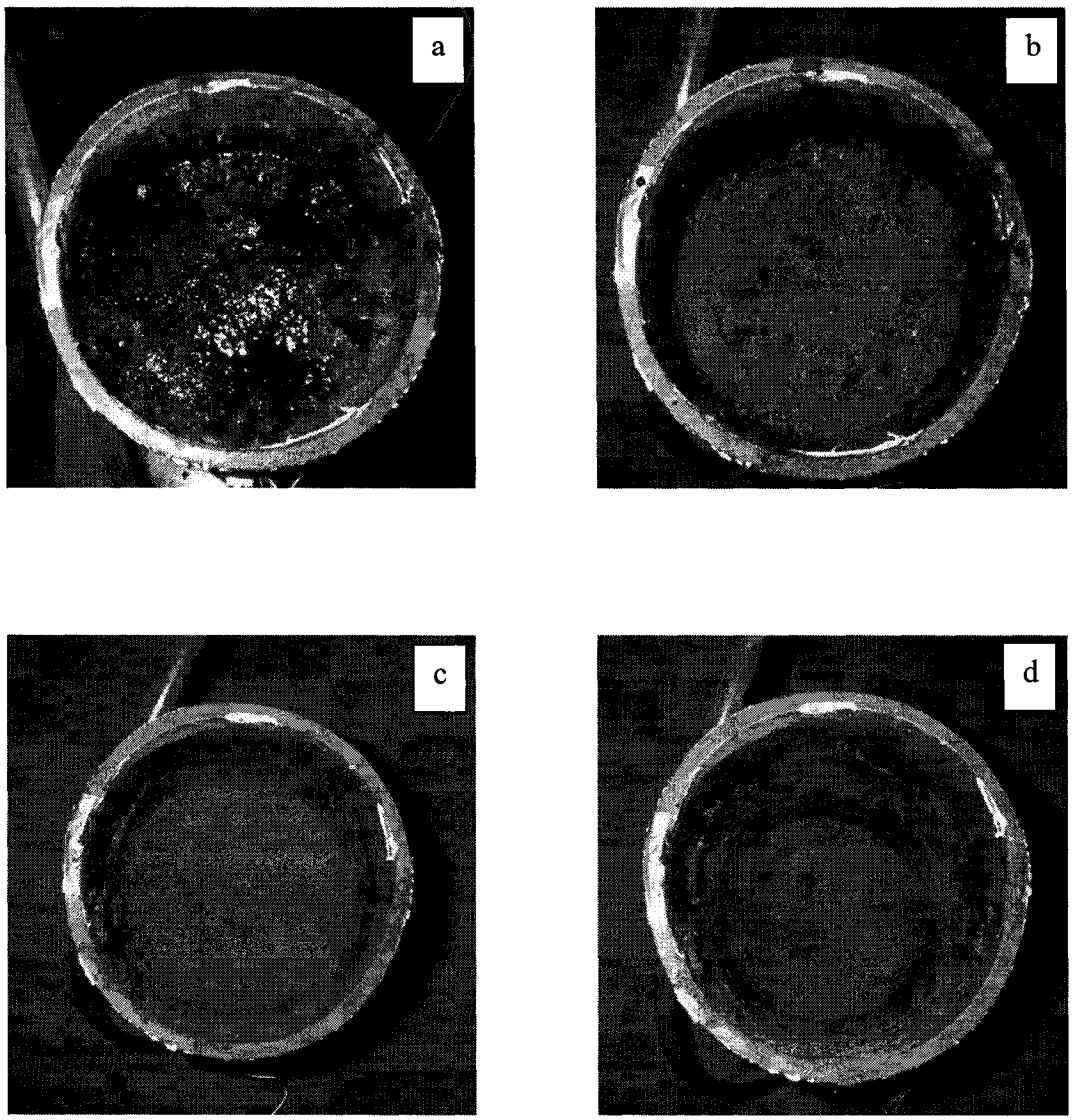

Figure A.56- Visual images of concrete sand column D1 at dismantle time: (a) at the top surface of the column; (b) at a depth of 2 cm from the top surface; (c) at a depth of 8 cm from the top surface; and (d) at a depth of 17 cm from the top surface

Reproduced with permission of the copyright owner. Further reproduction prohibited without permission.

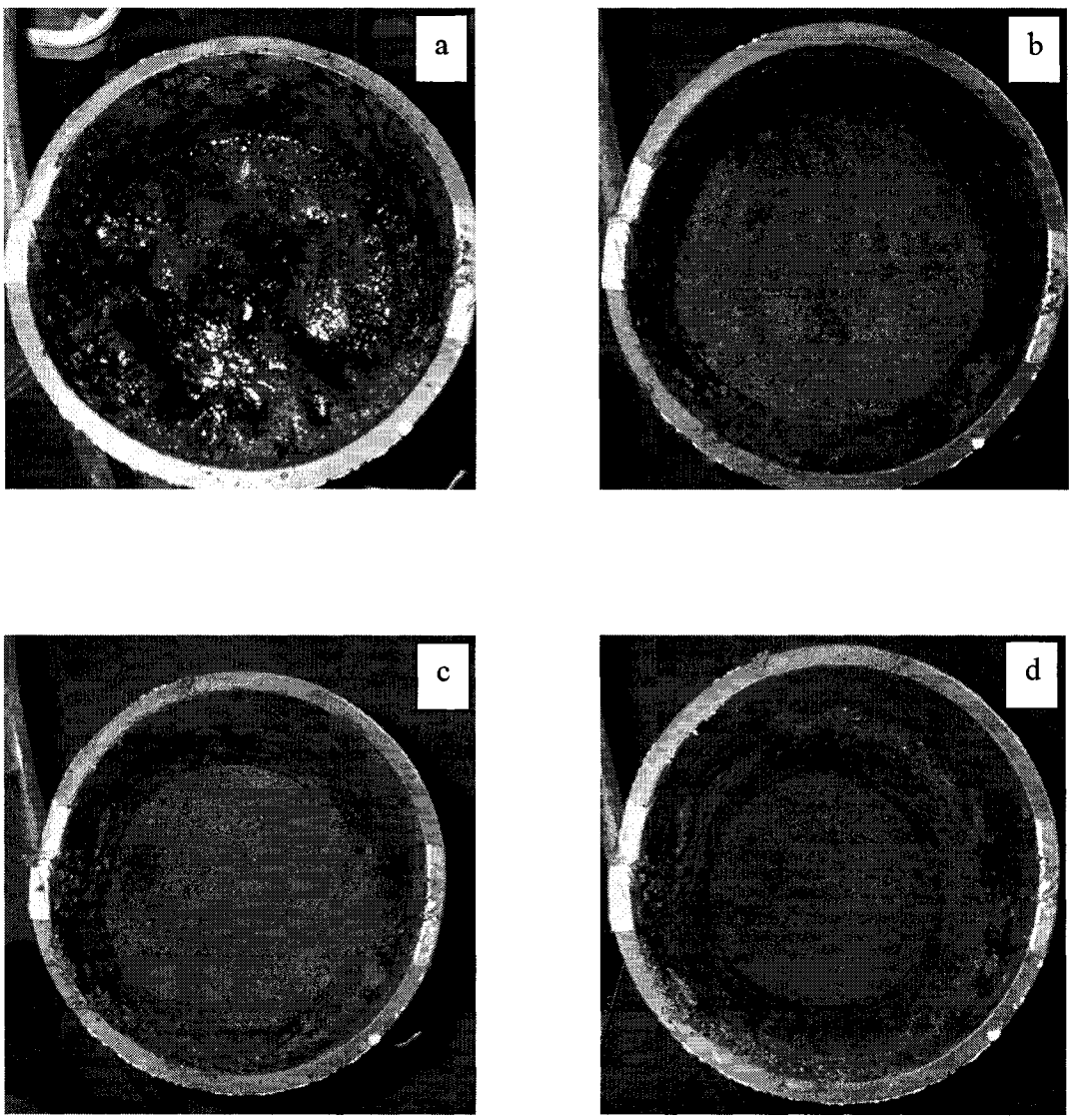

Figure A.57- Visual images of concrete sand column D2 at dismantle time: (a) at the top surface of the column; (b) at a depth of 3 cm from the top surface; (c) at a depth of 7.5 cm from the top surface; and (d) at a depth of 15.5 cm from the top surface

Reproduced with permission of the copyright owner. Further reproduction prohibited without permission.

Figure A.58- Visual image at the top surface of concrete sand column D3 at dismantle time

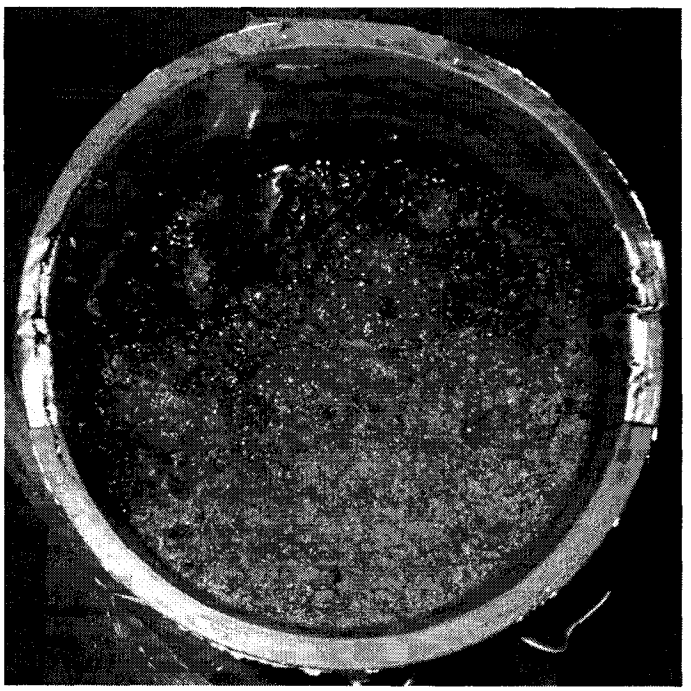

Figure A.59- Visual image at the top surface of concrete sand column D4 at dismantle time

Reproduced with permission of the copyright owner. Further reproduction prohibited without permission.

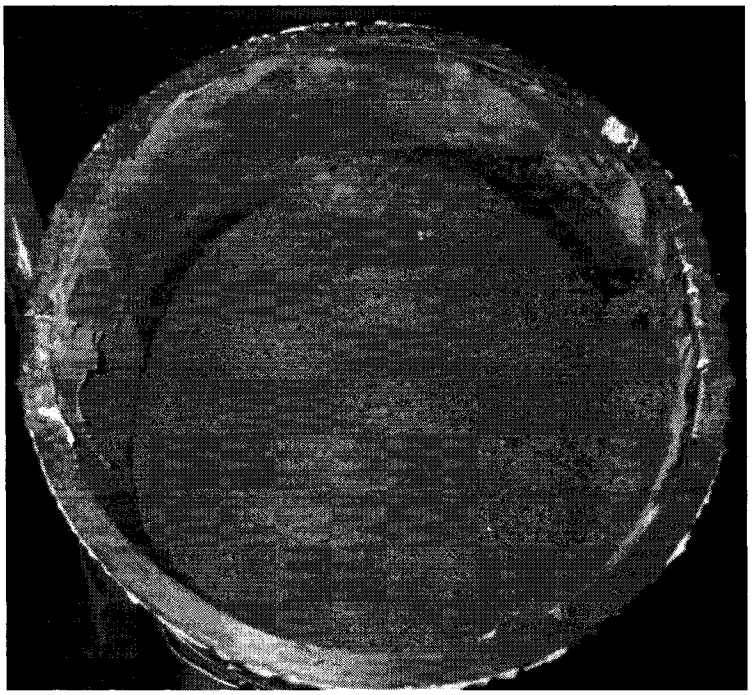

Figure A.60- Visual image at the top surface of septic bed sand column E at dismantle time

Figure A.61- Visual image at the top surface of septic bed sand column E1 at dismantle time

Reproduced with permission of the copyright owner. Further reproduction prohibited without permission.

Figure A.62- Visual image at the top surface of septic bed sand column E2 at dismantle time

Figure A.63- Visual image at the top surface of septic bed sand column E3 at dismantle time

Reproduced with permission of the copyright owner. Further reproduction prohibited without permission.

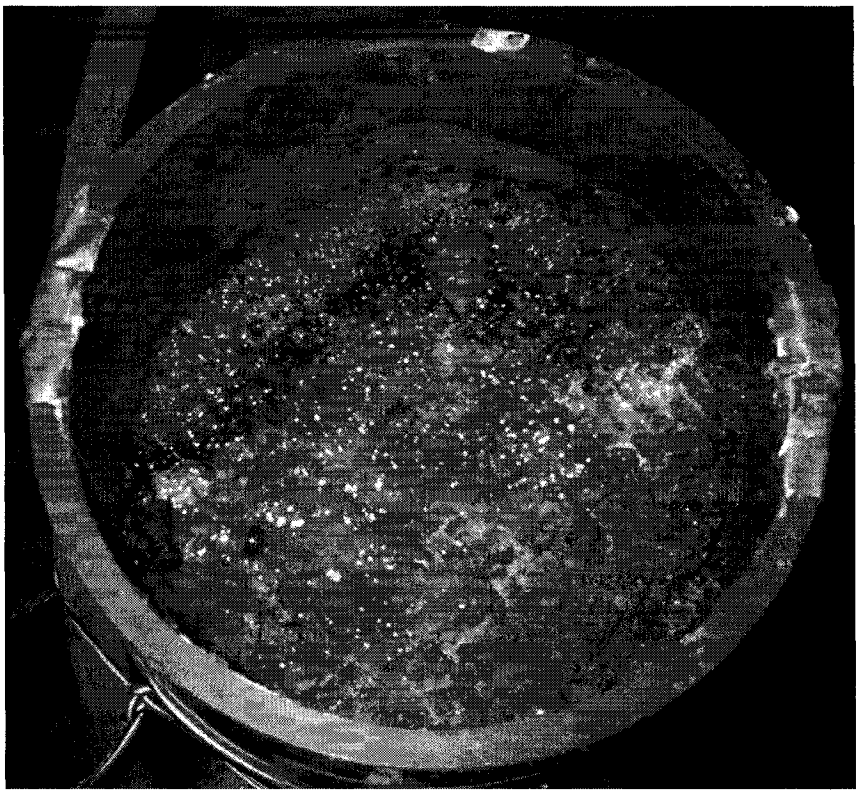

Figure A.64- Visual image at the top surface of septic bed sand column E4 at dismantle time

Reproduced with permission of the copyright owner. Further reproduction prohibited without permission.

Appendix B- Stage Two Data

Appendix B provides raw data collected in stage two. It also provides a comparison between the effluent concentrations measured from the test cells and the corresponding results from the spreadsheet model developed in stage two after using the decay rate value adjusted in stage three.

B.1 Raw Data Collected In Stage Two from the Test Cells

Table B.1- Data collected from test cell 12

Dismantle date: 29/6/2007
Porosity = 0.387
Density, g/cm^3 = 1.677
Volume of voids in the mass used for the MC calculations, mL = 195.474
Volume of water in the voids at dismantle time, mL = 61.56

Bacteria Analysis for Cell 12:
Analysis on samples taken from the tray containing the soil from the test cell

Weight of sample 1, g	Weight of sample 2, g	Weight of sample 3, g
4.079	4.05	4.076

Liquid TC and TOC for Cell 12:
Analysis on liquid samples

Sample	TC liquid, mg/L	Sample	TOC, mg/L	IC, mg/L
Tap water	1.737	Tap water	1.084	
Outflow, cell	87.62	Outflow, cell	56.41	31.21

Moisture Content Cell 12:
Analysis on tray containing the rest of the cell soil after taking all the samples for the other analyses

Weight of empty tray, g	Tray + soil before the oven dry, g	Tray + soil after the oven dry, g	MC%	WC%	Sat%
38.5	947.3	885.7	7.27	12.19	31.49

Reproduced with permission of the copyright owner. Further reproduction prohibited without permission.

Table B.2- Data collected from test cell 11

Dismantle date: 3/7/2007
Porosity = 0.387
Density, g/cm^3 = 1.686
Volume of voids in the mass used for the MC calculations, mL = 181.642
Volume of water in the voids at dismantle time, mL = 46.40

Bacteria Analysis for Cell 11:
Analysis on samples taken from the tray containing the soil from the test cell

Weight of sample 1, g	Weight of sample 2, g	Weight of sample 3, g
4.12	4.04	4.02

Liquid TC and TOC for Cell 11:
Analysis on liquid samples

Sample	TC liquid, mg/L	Sample	TOC, mg/L	IC, mg/L
Tap Water	8.793	Tap Water	4.536	
Outflow, cell	70.91	Outflow, cell	37.43	33.48

Moisture Content Cell 11:
Analysis on tray containing the rest of the cell soil after taking all the samples for the other analyses

Weight of empty tray, g	Tray + soil before the oven dry, g	Tray + soil after the oven dry, g	MC%	WC%	Sat%
38.5	876.4	830.0	5.86	9.89	25.54

Table B.3- Data collected from test cell 10

Dismantle date: 11/7/2007
Porosity = 0.387
Density, g/cm^3 = 1.669
Volume of voids in the mass used for the MC calculations, mL = 165.718
Volume of water in the voids at dismantle time, mL = 36.51

Bacteria Analysis for Cell 10:
Analysis on samples taken from the tray containing the soil from the test cell

Weight of sample 1, g	Weight of sample 2, g	Weight of sample 3, g
4.08	4.03	4.05

Liquid TC and TOC for Cell 10:
Analysis on liquid samples

Sample	TC liquid, mg/L	Sample	TOC, mg/L	IC, mg/L
Tap Water	9.09	Tap Water	4.63	
Outflow, cell	70.79	Outflow, cell	16.55	54.24

Moisture Content Cell 10:
Analysis on tray containing the rest of the cell soil after taking all the samples for the other analyses

Weight of empty tray, g	Tray + soil before the oven dry, g	Tray + soil after the oven dry, g	MC%	WC%	Sat%
37.40	788.3	751.8	5.11	8.53	22.03

Reproduced with permission of the copyright owner. Further reproduction prohibited without permission.

Table B.4- Data collected from test cell 9

Dismantle date: 13/7/2007
Porosity = 0.387
Density, g/cm^3 = 1.678
Volume of voids in the mass used for the MC calculations, mL = 163.910
Volume of water in the voids at dismantle time, mL = 43.21

Bacteria Analysis for Cell 9:
Analysis on samples taken from the tray containing the soil from the test cell

Weight of sample 1, g	Weight of sample 2, g	Weight of sample 3, g
4.02	4.01	4.04

Liquid TC and TOC for Cell 9:
Analysis on liquid samples

Sample	TC liquid, mg/L	Sample	TOC, mg/L	IC, mg/L
Tap Water	8.92	Tap Water	4.59	
Outflow, cell	67.24	Outflow, cell	12.73	54.51

Moisture Content Cell 9:
Analysis on tray containing the rest of the cell soil after taking all the samples for the other analyses

Weight of empty tray, g	Tray + soil before the oven dry, g	Tray + soil after the oven dry, g	MC%	WC%	Sat%
37.80	791.4	748.2	6.08	10.20	26.36

Table B.5- Data collected from test cell 8

Dismantle date: 17/7/2007
Porosity = 0.387
Density, g/cm^3 = 1.669
Volume of voids in the mass used for the MC calculations, mL = 175.870
Volume of water in the voids at dismantle time, mL = 74.19

Bacteria Analysis for Cell 8:
Analysis on samples taken from the tray containing the soil from the test cell

Weight of sample 1, g	Weight of sample 2, g	Weight of sample 3, g
4.04	4.03	4.05

Liquid TC and TOC for Cell 8:
Analysis on liquid samples

Sample	TC liquid, mg/L	Sample	TOC, mg/L	IC, mg/L
Tap Water	8.99	Tap Water	4.68	
Outflow, cell	87.62	Outflow, cell	27.08	60.54

Moisture Content Cell 8:
Analysis on tray containing the rest of the cell soil after taking all the samples for the other analyses

Weight of empty tray, g	Tray + soil before the oven dry, g	Tray + soil after the oven dry, g	MC%	WC%	Sat%
37.80	870.80	796.60	9.78	16.32	42.18

Reproduced with permission of the copyright owner. Further reproduction prohibited without permission.

Table B.6- Data collected from test cell 7

Dismantle date: 19/7/2007
Porosity = 0.387
Density, g/cm^3 = 1.681
Volume of voids in the mass used for the MC calculations, mL = 163.304
Volume of water in the voids at dismantle time, mL = 61.54

Bacteria Analysis for Cell 7:
Analysis on samples taken from the tray containing the soil from the test cell

Weight of sample 1, g	Weight of sample 2, g	Weight of sample 3, g
4.05	4.06	4.03

Liquid TC and TOC for Cell 7:
Analysis on liquid samples

Sample	TC liquid, mg/L	Sample	TOC, mg/L	IC, mg/L
Tap Water	8.87	Tap Water	4.78	
Outflow, cell	118.90	Outflow, cell	69.06	49.84

Moisture Content Cell 7:
Analysis on tray containing the rest of the cell soil after taking all the samples for the other analyses

Weight of empty tray, g	Tray + soil before the oven dry, g	Tray + soil after the oven dry, g	MC%	WC%	Sat%
37.70	808.42	746.90	8.67	14.58	37.68

Table B.7- Data collected from test cell 6

Dismantle date: 24/7/2007
Porosity = 0.387
Density, g/cm^3 = 1.684
Volume of voids in the mass used for the MC calculations, mL = 153.455
Volume of water in the voids at dismantle time, mL = 81.38

Bacteria Analysis for Cell 6:
Analysis on samples taken from the tray containing the soil from the test cell

Weight of sample 1, g	Weight of sample 2, g	Weight of sample 3, g
4.06	4.03	4.07

Liquid TC and TOC for Cell 6:
Analysis on liquid samples

Sample	TC liquid, mg/L	Sample	TOC, mg/L	IC, mg/L
Tap Water	9.88	Tap Water	4.53	
Outflow, cell	113.90	Outflow, cell	69.65	44.25

Moisture Content Cell 6:
Analysis on tray containing the rest of the cell soil after taking all the samples for the other analyses

Weight of empty tray, g	Tray + soil before the oven dry, g	Tray + soil after the oven dry, g	MC%	WC%	Sat%
33.90	783.30	701.90	12.19	20.52	53.03

Reproduced with permission of the copyright owner. Further reproduction prohibited without permission.

Table B.8- Data collected from test cell 5

Dismantle date: 26/7/2007
Porosity = 0.387
Density, g/cm^3 = 1.671
Volume of voids in the mass used for the MC calculations, mL = 168.114
Volume of water in the voids at dismantle time, mL = 50.60

Bacteria Analysis for Cell 5:
Analysis on samples taken from the tray containing the soil from the test cell

Weight of sample 1, g	Weight of sample 2, g	Weight of sample 3, g
4.06	4.07	4.06

Liquid TC and TOC for Cell 5:
Analysis on liquid samples

Sample	TC liquid, mg/L	Sample	TOC, mg/L	IC, mg/L
Tap Water	9.32	Tap Water	4.52	
Outflow, cell	85.30	Outflow, cell	42.38	42.92

Moisture Content Cell 5:
Analysis on tray containing the rest of the cell soil after taking all the samples for the other analyses

Weight of empty tray, g	Tray + soil before the oven dry, g	Tray + soil after the oven dry, g	MC%	WC%	Sat%
37.00	813.30	762.70	6.97	11.65	30.10

Table B.9- Data collected from test cell 4

Dismantle date: 31/7/2007
Porosity = 0.387
Density, g/cm^3 = 1.671
Volume of voids in the mass used for the MC calculations, mL = 177.206
Volume of water in the voids at dismantle time, mL = 101.40

Bacteria Analysis for Cell 4:
Analysis on samples taken from the tray containing the soil from the test cell

Weight of sample 1, g	Weight of sample 2, g	Weight of sample 3, g
4.07	4.07	4.10

Liquid TC and TOC for Cell 4:
Analysis on liquid samples

Sample	TC liquid, mg/L	Sample	TOC, mg/L	IC, mg/L
Tap Water	9.06	Tap Water	4.86	
Outflow, cell	142.60	Outflow, cell	100.40	42.20

Moisture Content Cell 4:
Analysis on tray containing the rest of the cell soil after taking all the samples for the other analyses

Weight of empty tray, g	Tray + soil before the oven dry, g	Tray + soil after the oven dry, g	MC%	WC%	Sat%
33.70	900.30	798.9	13.25	22.14	**57.22**

Reproduced with permission of the copyright owner. Further reproduction prohibited without permission.

Table B.10- Data collected from test cell 3

Dismantle date: 2/8/2007
Porosity = 0.387
Density, g/cm^3 = 1.668
Volume of voids in the mass used for the MC calculations, mL = 172.467
Volume of water in the voids at dismantle time, mL = 91.92

Bacteria Analysis for Cell 3:
Analysis on samples taken from the tray containing the soil from the test cell

Weight of sample 1, g	Weight of sample 2, g	Weight of sample 3, g
4.03	4.06	4.08

Liquid TC and TOC for Cell 3:
Analysis on liquid samples

Sample	TC liquid, mg/L	Sample	TOC, mg/L	IC, mg/L
Tap Water	8.85	Tap Water	4.66	
Outflow, cell	104.00	Outflow, cell	68.90	35.10

Moisture Content Cell 3:
Analysis on tray containing the rest of the cell soil after taking all the samples for the other analyses

Weight of empty tray, g	Tray + soil before the oven dry, g	Tray + soil after the oven dry, g	MC%	WC%	Sat%
36.80	871.70	779.80	12.37	20.63	53.30

Table B.11- Data collected from test cell 2

Dismantle date: 7/8/2007
Porosity = 0.387
Density, g/cm^3 = 1.668
Volume of voids in the mass used for the MC calculations, mL = 176.811
Volume of water in the voids at dismantle time, mL = 103.54

Bacteria Analysis for Cell 3:
Analysis on samples taken from the tray containing the soil from the test cell

Weight of sample 1, g	Weight of sample 2, g	Weight of sample 3, g
4.07	4.07	4.07

Liquid TC and TOC for Cell 3:
Analysis on liquid samples

Sample	TC liquid, mg/L	Sample	TOC, mg/L	IC, mg/L
Tap Water	9.30	Tap Water	3.69	
Outflow, cell	84.90	Outflow, cell	53.83	31.07

Moisture Content Cell 3:
Analysis on tray containing the rest of the cell soil after taking all the samples for the other analyses

Weight of empty tray, g	Tray + soil before the oven dry, g	Tray + soil after the oven dry, g	MC%	WC%	Sat%
33.90	904.8	800.5	13.59	22.66	58.56

Reproduced with permission of the copyright owner. Further reproduction prohibited without permission.

Table B.12- Data collected from test cell 1

Dismantle date: 9/8/2007
Porosity = 0.387
Density, g/cm^3 = 1.683
Volume of voids in the mass used for the MC calculations, mL = 165.431
Volume of water in the voids at dismantle time, mL = 72.94

Bacteria Analysis for Cell 3:
Analysis on samples taken from the tray containing the soil from the test cell

Weight of sample 1, g	Weight of sample 2, g	Weight of sample 3, g
4.03	4.05	4.05

Liquid TC and TOC for Cell 3:
Analysis on liquid samples

Sample	TC liquid, mg/L	Sample	TOC, mg/L	IC, mg/L
Tap Water	7.10	Tap Water	4.84	
Outflow, cell	97.15	Outflow, cell	47.70	49.45

Moisture Content Cell 3:
Analysis on tray containing the rest of the cell soil after taking all the samples for the other analyses

Weight of empty tray, g	Tray + soil before the oven dry, g	Tray + soil after the oven dry, g	MC%	WC%	Sat%
37.00	828.70	755.80	10.14	17.06	44.09

B.2 Comparison between the Results of the Model Developed in Stage Two and the Experimental Data Using the Calibrated Decay Rate Used in Stage Three

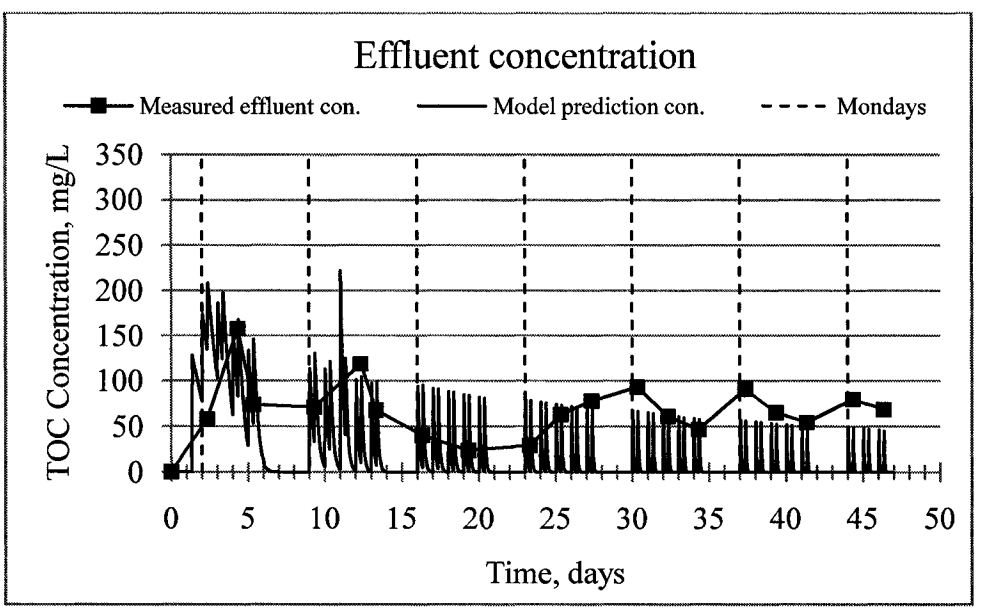

Figure B.1- Comparison between the measured effluent concentrations from the test cells and the results from the spreadsheet model at time step of 1 hour after using the decay rate adjusted in stage three

Reproduced with permission of the copyright owner. Further reproduction prohibited without permission.

Appendix C- Stage Three – Numerical Code

Appendix C provides description of the equations and initial/boundary conditions used in the original code developed by Mostafa and Van Geel (2007). Mostafa and Van Geel (2007) proposed a one-dimensional C++ code that solves the unsaturated flow and contaminant transport equations. The code includes the Monod kinetics equation to simulate the biodegradation of an organic substrate. The three conceptual models explained earlier were implemented in the code to relate the relative permeability to the microbial growth term in the unsaturated flow equation. A mass balance was incorporated into the code for the flow and contaminant transport equations to ensure that the solution conserves mass. The control volume approach and finite difference approximation were chosen as the numerical techniques to solve both the flow and contaminant transport equations, respectively. The code assumed a constant grid size, constant temperature and constant fluid density. The coordinate system used was positive upwards with an assumed datum at the base of the model domain.

The code was used to illustrate the impact of microbial growth on the biological clogging of unsaturated soils but was not validated against experimental data from the lab or the field. Appendix C is used to present the equations used in the code and the method of solution for each equation.

C.1 Flow Equation

Mostafa and Van Geel (2007) used the control volume approach in the unsaturated flow calculations. By using the control volume approach, the code solves for two unknowns sequentially; pressure head and saturation. This code uses the soil moisture

Reproduced with permission of the copyright owner. Further reproduction prohibited without permission.

curve that relates the pressure head to saturation for soils (e.g. Brooks and Corey (1964) or van Genuchten (1980)) along with the unsaturated flow equation derived from a control volume approach to solve for both pressure head and saturation.

The control volume approach involves conducting a mass balance for fluid flow on a certain volume or grid block. As shown in Figure (C.1), for any block, the mass balance is as follows,

$$Accumulation = Mass\ in - Mass\ out \tag{C.1}$$

where the accumulation term can be expressed as,

$$Accumulation = \left(\frac{\rho_w \ \phi_i}{\Delta t} \left(S_{w,i}^{t+\Delta t} - S_{w,i}^{t} \right) \right) \Delta x \ \Delta y \ \Delta z \tag{C.2}$$

where ρ_w is the water density, ϕ_i is the porosity at block i, Δt is the size of time step , Δx, Δy, and Δz are the size of the grid blocks in the x, y, and z directions, respectively.

Since the code is one-dimensional, the values of Δx and Δy are assumed to be unity and Δz is the size of the grid block in the vertical direction which is assumed constant for this code.

The porosity ϕ_i is assumed constant throughout the column. $S_{w,i}^{t+\Delta t}$ and $S_{w,i}^{t}$ are the water saturations of the ith block at times t+Δt and t, respectively.

Mostafa and Van Geel (2007) calculated the Mass in and Mass out using Darcy's Law for unsaturated flow. The equation for the mass in and out can be written as follows,

$$Mass\ in = \rho_w \ K(\theta)_{i+1/2} \left(\frac{h_{w,i+1} - h_{w,i}}{\Delta z} \right) \tag{C.3}$$

$$Mass\ out = \rho_w \ K(\theta)_{i-1/2} \left(\frac{h_{w,i} - h_{w,i-1}}{\Delta z} \right) \tag{C.4}$$

Reproduced with permission of the copyright owner. Further reproduction prohibited without permission.

where $K(\theta)_{i\pm1/2}$ is the unsaturated hydraulic conductivity, i+1/2 and i–1/2 indicate the grid block interface as shown in Figure (C.1) and h_w is the hydraulic head.

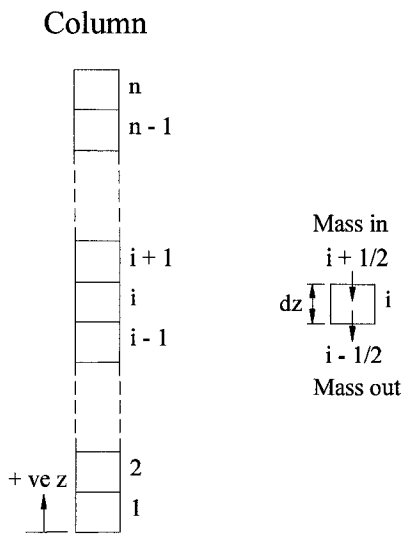

Figure C.1- General layout for the modeled column

Haverkamp and Vauclin (1979) investigated different ways to calculate the unsaturated hydraulic conductivity at the interface between blocks. They found that when,

$$K(\theta)_{i\pm1/2} = \left(K(\theta)_i \; K(\theta)_{i\pm1}\right)^{\frac{1}{2}} \tag{C.5}$$

the associated error from the geometric mean of the surrounding blocks is minimal. Therefore, Equation (C.5) was used to calculate K(θ) at the interfaces.

The final form of the flow equation that Mostafa and Van Geel (2007) used in the code was as follows,

$$\frac{\partial(\phi S_w)}{\partial t} = \frac{\partial}{\partial z}\left(K(S_w)\frac{\partial h_w}{\partial z}\right) \pm q \tag{C.6}$$

Reproduced with permission of the copyright owner. Further reproduction prohibited without permission.

C.2 Contaminant Transport Equation

Mostafa and Van Geel (2007) used the contaminant transport equation used by Baek et al. (1989) to simulate contaminant transport in the unsaturated zone with a source/sink term. This equation can be written as follows,

$$\frac{\partial(\phi S_w C)}{\partial t} = \frac{\partial}{\partial z}\left(\phi S_w D_S \frac{\partial C}{\partial z}\right) - \frac{\partial(q C)}{\partial z} - \phi S_w R_S \qquad \text{(C.7)}$$

where C is the concentration of the substrate (mg/L), D_s is the dispersion coefficient (cm^2/s) and R_S is the source/sink term which will be discussed in detail in the following subsections.

C.3 Numerical Solution

In the numerical code, Mostafa and Van Geel (2007) used the finite difference technique to solve for the contaminant transport equation. To solve the equation using finite difference, the domain has to be divided into a series of vertical grid blocks. As per the flow equation, the code assumes the domain is divided into equal size grid blocks. Figure (C.2) shows layout of three grid blocks equally divided. The concentration is assigned at the center of each block.

Due to the well known problem of sharp front while dealing with the contaminant transport problems, Mostafa and Van Geel (2007) considered two spatial weighting schemes; the upstream and central weighting. Upstream weighting is used at the beginning of the simulation to handle the sharp front problem. At later times central weighting or upstream weighting can be used to continue the simulation. The user has the flexibility to select the upstream or central weighing for each assigned stress period.

Reproduced with permission of the copyright owner. Further reproduction prohibited without permission.

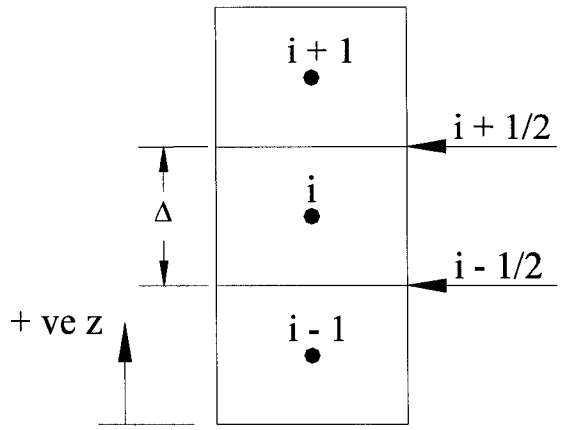

Figure C.2- Block-centered finite difference discretization of a one-dimensional problem domain, adapted from Zheng and Bennett (1995)

Mostafa and Van Geel (2007) used an explicit numerical scheme to solve for the unknowns, which are the concentration values in this case. In the explicit scheme, we are seeking $C_i^{t+\Delta t}$ with the knowledge of the concentrations at the previous time step (i.e. C_{i+1}^t, C_i^t, and C_{i-1}^t, Figure (C.3)). For the explicit scheme there is no matrix involved and the solution can be done easily.

Mostafa and Van Geel (2007) highlighted that dealing with contaminant transport in the unsaturated zone can generate a double sharp front problem. The first sharp front is generated by an infiltration event for the flow equation. As the saturation moves in the unsaturated soil, the saturation varies almost from 100% to the irreducible saturation and this generates a numerical stability problem when solving the flow equation. Also, as mentioned previously, there is a sharp front generated by the introduction of a contaminant where at the front the concentration varies sharply from C/C_o of 1.0 to zero. Hence, it can be considered a double sharp front problem and it may generate oscillation behaviour. Mostafa and Van Geel (2007) suggested that the upstream weighting scheme

Reproduced with permission of the copyright owner. Further reproduction prohibited without permission.

is the best solution for this problem as it gives more weight on the upstream nodes in the direction of the flow. In addition, the oscillation problem depends on the degree to which the dispersion term governs the solute transport. When the dispersion dominates, the oscillation problem disappears because the sharp front is dispersed.

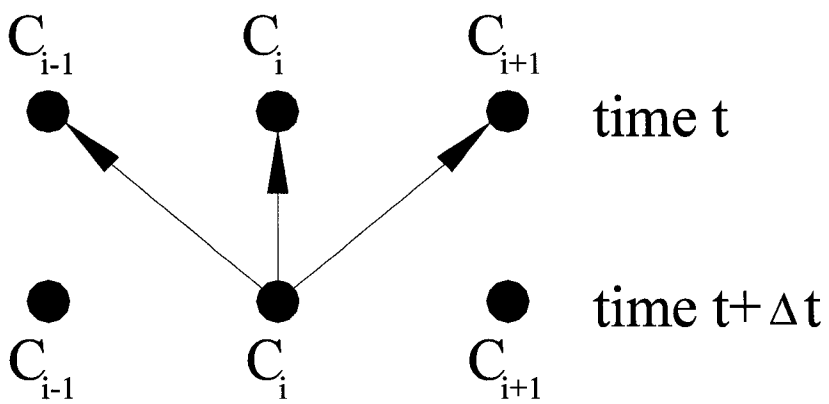

Figure C.3- Explicit scheme

C.4 Boundary and Initial Conditions

C.4.1 For the Flow Equation

For the initial condition, Mostafa and Van Geel (2007) assigned specified values for the total head, at time t = 0.0, as shown in Equation (C.8).

$$hw(z) = hw,i \qquad \text{from } z = 0 \text{ to } z = L,\ t = 0 \qquad (C.8)$$

where L is the column length.

For the boundary conditions (BCs), Mostafa and Van Geel (2007) implemented two different types of boundary conditions in the code; Dirichlet BC (Type 1 BC or specified total head) and Neuman BC (Type 2 BC or specified flux). One of these two boundary conditions must be assigned for the first and last grid blocks (block number 1 and block number n). In addition, the code allows the user to specify a flux for any block.

Reproduced with permission of the copyright owner. Further reproduction prohibited without permission.

The boundary conditions can be written in equation form as follows,

$h_w = h_{w,1}$ or $q = q_1$ for $z = 0$ and $t \geq 0$ (C.9)

$h_w = h_{w,n}$ or $q = q_n$ for $z = L$ and $t \geq 0$ (C.10)

Also, the code can solve for different stress periods where the values for the total heads and fluxes at any grid block can be changed from one stress period to the next. The user has the ability to specify the number of the stress periods and the appropriate boundary conditions for each stress period. This feature is in a great benefit when trying to simulate inflow that varies with time (e.g. pulse loading).

C.4.2 For the Contaminant Transport Equation

For the initial conditions, a concentration of zero mg/L is assigned to each grid block as the initial concentration (Equation (C.11)).

$$C = 0 \qquad 0 > z \geq L,\ t = 0 \qquad \text{(C.11)}$$

The boundary condition is assigned to an imaginary grid block upstream the top grid block which can be either a prescribed concentration, C_o, or a prescribed flux, qC_o.

For the bottom grid block, Mostafa and Van Geel (2007) allowed the concentration to be calculated according to a control volume approach which just allows the mass to leave the grid block via advection only. This is commonly referred to as a free exit boundary (Frind (1988)). The code also assumes contaminant mass can enter or leave the domain at any location via a flux term. Moreover, the code can solve for different boundary concentration values at different stress periods where the values for C_o can be changed. The user can specify a value for C_o during one stress period and this value can be changed in the next stress period, if needed.

Reproduced with permission of the copyright owner. Further reproduction prohibited without permission.

Figure (C.4) shows graphically the approach used to calculate the concentration at the first, last, and intermediate grid blocks.

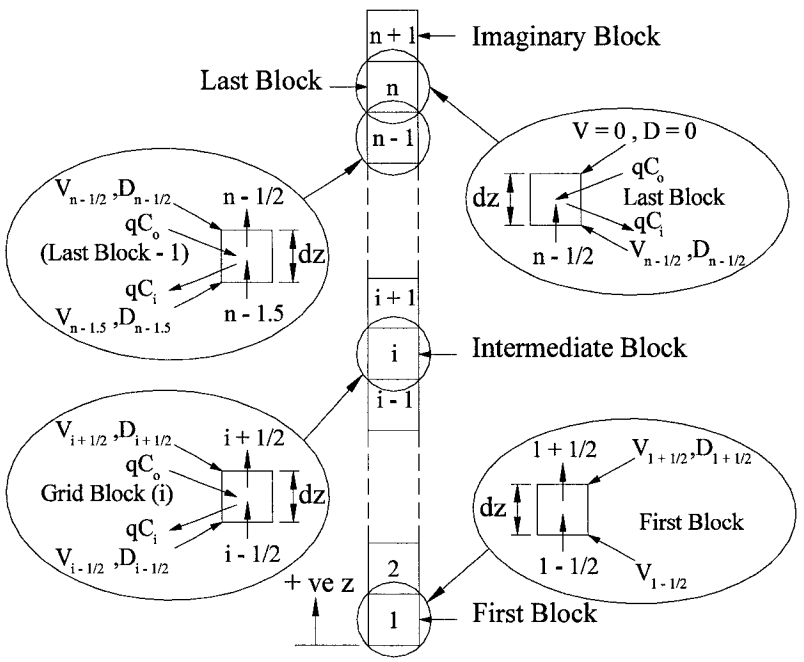

Figure C.4- Graphical representation for the initial and boundary concentrations.

C.5 Source/Sink Terms and Monod Kinetics

Mostafa and Van Geel (2007) chose Monod kinetics to simulate the biodegradation of a certain contaminant and the corresponding growth and decay of the microbial mass. In considering Monod kinetics, the source/sink term in the one-dimensional advection-dispersion equation (R_s) can be calculated as follows,

$$\frac{\partial C}{\partial t} = -R_s = -\frac{q_{\max}\, M\, C}{K_S + C} \tag{C.12}$$

and the complete one-dimensional transport equation can be written as,

$$\frac{\partial(\phi S_w C)}{\partial t} = \frac{\partial}{\partial z}\left(\phi\, S_w\, D_S\, \frac{\partial C}{\partial z}\right) - \frac{\partial(q\, C)}{\partial z} - (\phi)(S_w)\left(\frac{q_m\, M\, C}{K_s + C}\right) \tag{C.13}$$

Reproduced with permission of the copyright owner. Further reproduction prohibited without permission.

where M is the microbial concentration (mg/L), q_m is the maximum specific rate of substrate utilization ($mg_{substrate}/mg_{cell}\ s^{-1}$), K_s is the half-velocity constant (mg/L), and C is the substrate concentration as mentioned before (mg/L).

The change in microbial concentration with time can be calculated as follows,

$$\overbrace{\frac{\partial M}{\partial t}}^{\text{Change in microbial concentraion with time}} = \overbrace{(Y)\left(\frac{q_m M C}{K_s + C}\right)}^{\text{Growth rate}} - \overbrace{(b)(M)}^{\text{Decay rate}} \qquad \text{(C.14)}$$

where Y is the cell yield coefficient (mg cell / mg substrate) and b is the cell decay coefficient (s^{-1}).

C.5.1 Solution Procedure

Mostafa and Van Geel (2007) discussed the complexity of having two unknowns in one partial differential equation (Equation (C.13)). The two unknowns are the substrate concentration, C and the microbial concentration, M. Mostafa and Van Geel (2007) showed how Equation (C.13) can be organized simultaneously with the ordinary differential equation (i.e. Equation (C.14)) to solve for the contaminant and microbial concentrations at each time step.

Reproduced with permission of the copyright owner. Further reproduction prohibited without permission.

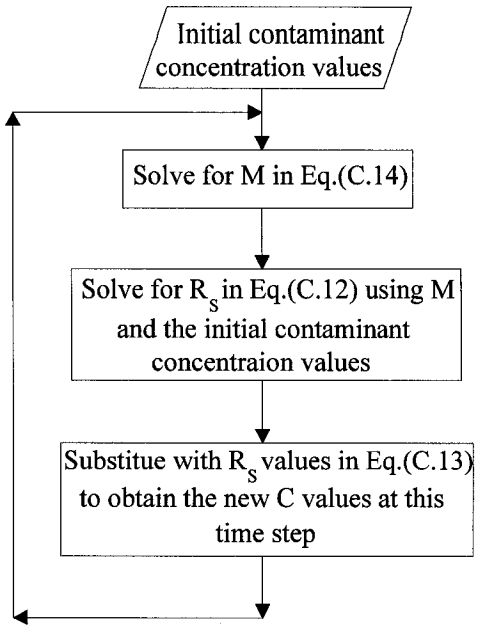

Figure C.5- Flow chart shows solution sequence of the contaminant and the microbial equations.

As shown in Figure (C.5), the initial concentrations are used as an initial value to determine microbial concentration, M (Equation (C.14)). After obtaining M, the source/sink term, R_S, is calculated based on the concentration values and M (Equation (C.12)). Then R_S is substituted into the advection-dispersion equation (Equation (C.13)) which is solved explicitly.

C.5.2 Operator-Splitting and Runge-Kutta Method to Solve Ordinary Differential Equations

Due to the complexity of Equation (C.7), Mostafa and Van Geel (2007) used an operator-splitting approach to solve for the substrate concentration and the microbial concentrations. Using operator splitting, one can divide the solution of the equation into two parts, solving the advection-dispersion part first (Equation (C.15)) then solving the reaction or biodegradation part (Equation (C.16)) as follows,

Reproduced with permission of the copyright owner. Further reproduction prohibited without permission.

$$\frac{\partial(\phi S_w C)}{\partial t} = \frac{\partial}{\partial z}\left(\phi S_w D_S \frac{\partial C}{\partial z}\right) - \frac{\partial(q C)}{\partial z} \tag{C.15}$$

$$\frac{\partial(\phi S_w C)}{\partial t} = -\phi S_w R_S \tag{C.16}$$

where R_S represents the reaction of interest. This decoupling is an efficient way to deal with complex reactions where the reaction time maybe much smaller than the advection – dispersion time step. Figure (C.6) shows graphically one operator-split cycle as shown by Odencrantz et al. (1990).

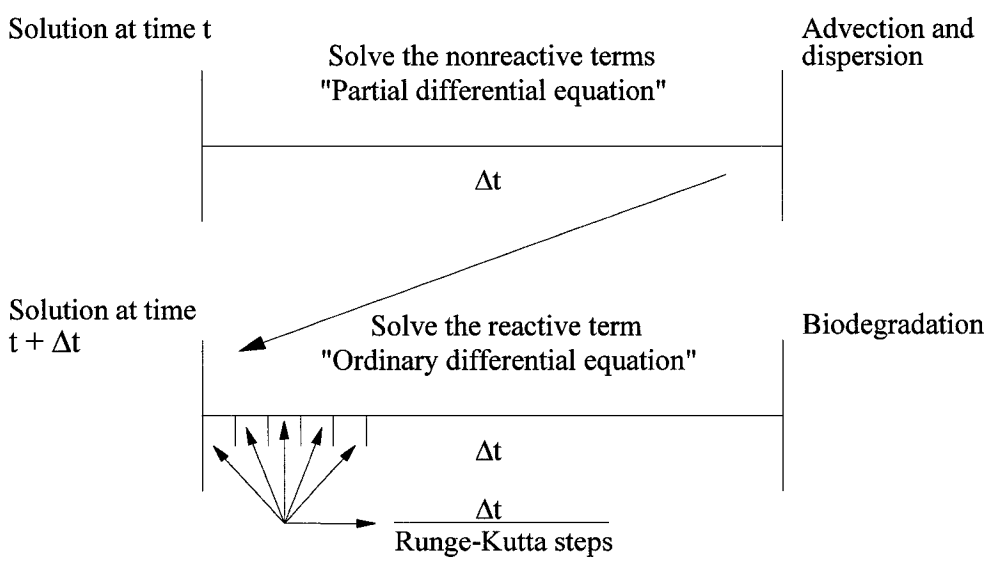

Figure C.6- Graphical representation of one complete operator- split cycle, adapted from Odencrantz et al. (1990)

After splitting the contaminant transport equation into advection–dispersion and biodegradation components, a method is needed to solve the system of nonlinear ordinary differential equations for the biodegradation equation (Equation (C.16)). The Runge-Kutta method is the technique used to solve the system of nonlinear ordinary differential equations (Dennis and Schnabel (1983); Odencrantz et al. (1990)). A fourth-order Runge-

Reproduced with permission of the copyright owner. Further reproduction prohibited without permission.

Kutta method is used because it is fifth order accurate in time (Dennis and Schnabel (1983); Odencrantz et al. (1990)). Further mathematical explanation of Runge-Kutta method can be found in Mostafa (2004).

Reproduced with permission of the copyright owner. Further reproduction prohibited without permission.